DISSERTATION

SIMULATION-BASED TSUNAMI EVACUATION RISK ASSESSMENT AND RISK-INFORMED MITIGATION

Submitted by

Zhenqiang Wang

Department of Civil and Environmental Engineering

In partial fulfillment of the requirements

For the Degree of Doctor of Philosophy

Colorado State University

Fort Collins, Colorado

Summer 2021

Doctoral Committee:

Advisor: Gaofeng Jia

Bruce R. Ellingwood
Hussam N. Mahmoud
Jason C. Quinn

Copyright by Zhenqiang Wang 2021

All Rights Reserved

ABSTRACT

SIMULATION-BASED TSUNAMI EVACUATION RISK ASSESSMENT AND RISK-INFORMED MITIGATION

Earthquake-induced tsunami can be very destructive involving significant loss of life. Evacuation to safety zones is regarded as one of the most effective ways to save lives from the tsunami strike due to the limited effectiveness of structural countermeasures. However, it is extremely challenging to successfully evacuate many people under the multi-hazard environment within a condensed time frame, especially under the near-field tsunami. Proper evacuation planning is crucial to support effective evacuation and reduce casualty. For effective evacuation planning, it is important to better understand the complex evacuation behavior for recommending proper response and behavior in an emergency. Also, it is important to have a clear picture of evacuation risk (e.g., measured in terms of expected casualty rate within a certain time frame) for informing policy and decision-making. Furthermore, it is important to identify effective pre-event mitigation strategies for effective risk reduction.

Important limitations exist in current research on the above aspects. Tsunami evacuation simulation using the agent-based model has been used to investigate the complex evacuation behavior; however, existing agent-based evacuation models usually neglect or simplify many important factors and/or mechanisms associated with the evacuation. The neglect or simplification would make the evacuation simulation less realistic and hence a good understanding of evacuation behavior challenging. For the quantification of tsunami evacuation risk, a systematic framework that can address complex evacuation models and uncertainty (including aleatory and epistemic uncertainties) models is needed; however, no such framework has been developed for the quantification of tsunami evacuation risk. Also, some important uncertainties such as that in the seismic damage to the bridge are usually neglected or the uncertainty quantification is simplified. In this case, it would

be difficult to assess the evacuation risk accurately and provide a clear picture of the evacuation risk. For effective pre-event evacuation risk mitigation, the effectiveness of different mitigation strategies needs to be quantitatively evaluated to identify more effective strategies. However, the effectiveness of the mitigation strategy is usually evaluated more qualitatively than quantitatively. Furthermore, the evaluation is typically conducted without systematically considering various uncertainties, which makes the identified strategies not robust to uncertainties. In tsunami evacuation risk assessment and mitigation, risk evaluation using general stochastic simulation techniques (e.g., Monte Carlo simulation) typically entails significant computational challenges. Efficient algorithms are needed to alleviate such computational challenges and facilitate such tasks.

To bridge the above knowledge gaps, this research proposes a generalized framework for simulation-based tsunami evacuation risk assessment and risk-informed mitigation. The framework is built layer by layer through integrating tsunami evacuation simulation using agent-based modeling (ABM) technique, simulation-based evacuation risk assessment, sensitivity analysis of evacuation risk, and risk-informed evaluation of mitigation strategies. An improved agent-based tsunami evacuation model is developed for more realistic tsunami evacuation simulation by incorporating many of the typically neglected or simplified but important factors and/or mechanisms in the evacuation. Using the proposed agent-based evacuation model, a simulation-based framework is proposed to quantify the evacuation risk, in which various uncertainties (including aleatory and epistemic uncertainties) associated with the evacuation are explicitly considered and modeled by proper selection of probability distribution models. Sensitivity analysis of evacuation risk with respect to the epistemic uncertainty is performed, and the sensitivity information can be used to guide effective epistemic uncertainty reduction and hence for more accurate risk assessment. Also, sensitivity analysis is performed to identify critical risk factors, and the sensitivity information can be used to guide effective evacuation modeling and selection of candidate risk mitigation strategies. Risk-informed evaluation of different types of candidate mitigation strategies (including infrastructural and non-infrastructural strategies) is conducted to identify more effective strategies that are robust to uncertainties. Efficient sample-based approaches are developed to alleviate the computa-

tional challenges in evacuation risk assessment, sensitivity analysis, and risk-informed evaluation of mitigation strategies. As an illustrative example, the proposed framework is applied to tsunami evacuation risk assessment and risk-informed mitigation for the coastal community of Seaside, Oregon.

ACKNOWLEDGEMENTS

I would first like to express my sincerest gratitude to my advisor, Dr. Gaofeng Jia, for his guidance and help in the pursuit of my Ph.D., either in research or in life. His patience, guidance, and motivation in research have significantly improved my research skills and way of thinking and behaving. His care, support, and help in life have made my journey of Ph.D. enjoyable. I will forever appreciate all the things he has done, and words cannot express my gratitude.

I would also like to express my thanks to my additional committee members, Dr. Bruce Ellingwood, Dr. Hussam Mahmoud, and Dr. Jason Quinn for serving on my committee, and providing support and contributions to this research. I would also like to express my gratitude to Dr. Bruce Ellingwood for his courses, from which I learned a lot.

I would also like to thank my friends at Colorado State University, and in Fort Collins for their friendship, support, and help during my graduate study in the U.S. I have enjoyed my time with them, making not only a lot of good memories but good friendships as well.

Most importantly, I would like to thank my family and family-in-law for their endless support and reassurance in this endeavor. I am truly fortunate to have my wife, Xinfang in my life who has been supporting me in pursuit of my dream, and to have my daughter, Anna who brings me joy every day.

DEDICATION

I dedicate this dissertation to my family.

TABLE OF CONTENTS

ABSTRACT ii
ACKNOWLEDGEMENTS v
DEDICATION vi
LIST OF TABLES x
LIST OF FIGURES xi

Chapter 1 Introduction 1
1.1 Motivation 1
1.1.1 Tsunami evacuation simulation 3
1.1.2 Tsunami evacuation risk assessment 6
1.1.3 Tsunami evacuation risk mitigation 8
1.1.4 Summary: Knowledge gaps in tsunami evacuation risk assessment and mitigation 9
1.2 Objectives and scope of research 10
1.3 Organization of research 11

Chapter 2 Framework for simulation-based tsunami evacuation risk assessment and risk-informed mitigation 13

Chapter 3 Tsunami evacuation simulation using ABM 16
3.1 Introduction 16
3.1.1 Existing models for tsunami evacuation simulation 17
3.1.2 Comparison of different models for tsunami evacuation simulation . . . 25
3.1.3 Limitations in existing agent-based tsunami evacuation models 27
3.2 Proposed agent-based tsunami evacuation model 31
3.3 Modeling details 33
3.3.1 Evacuation environment model (EEM) 34
3.3.2 Evacuation decision and behavior model (EBM) 36
3.3.3 Evacuation performance model (EPM) 42
3.3.4 General applicability of the proposed agent-based model for tsunami evacuation simulation 43
3.4 Illustrative example: Simulation of tsunami evacuation in Seaside, Oregon using the proposed agent-based model 43
3.4.1 Study area 44
3.4.2 Agent-based tsunami evacuation model details 44
3.4.3 Evacuation simulation 51
3.4.4 General tsunami evacuation process simulated using the proposed agent-based tsunami evacuation model 53
3.5 Summary 54

Chapter 4 Simulation-based tsunami evacuation risk assessment . . . 56
4.1 Introduction . . . 56
4.2 Proposed simulation-based framework for tsunami evacuation risk quantification . . . 58
4.2.1 Uncertainty quantification . . . 59
4.2.2 Risk consequence measure . . . 59
4.2.3 Risk quantification . . . 59
4.3 Tsunami evacuation risk assessment . . . 60
4.4 Illustrative example: Simulation-based tsunami evacuation risk assessment for Seaside, Oregon . . . 61
4.4.1 Overall evacuation risk under different cases . . . 64
4.4.2 The impact of considered factors and mechanisms on tsunami evacuation risk . . . 66
4.4.3 The impact of population size on tsunami evacuation risk . . . 70
4.4.4 The impact of the time of day on tsunami evacuation risk . . . 72
4.5 Summary . . . 76

Chapter 5 Sensitivity analysis of tsunami evacuation risk with respect to epistemic uncertainty . . . 78
5.1 Introduction . . . 78
5.2 Sensitivity analysis of tsunami evacuation risk with respect to epistemic uncertainty . . . 80
5.2.1 Sensitivity of tsunami evacuation risk to epistemic uncertainty . . . 80
5.2.2 Global sensitivity measure: Sobol' index . . . 81
5.2.3 Computational challenges in the calculation of risk-based Sobol' indices 82
5.3 Efficient sensitivity analysis of tsunami evacuation risk using the augmented sample-based approach . . . 83
5.3.1 Calculation of first-order Sobol' indices . . . 84
5.3.2 Calculation of higher-order Sobol' indices . . . 88
5.4 Illustrative example: Sensitivity analysis of tsunami evacuation risk with respect to epistemic uncertainty for Seaside, Oregon . . . 89
5.4.1 Results and discussions: Case 1 . . . 91
5.4.2 Results and discussions: Case 2 . . . 93
5.5 Summary . . . 97

Chapter 6 Identification of critical risk factors using sensitivity analysis . . . 99
6.1 Introduction . . . 99
6.2 Sensitivity analysis for identifying critical risk factors . . . 101
6.3 Variation of the sensitivity of risk factors with key distribution parameters . 102
6.4 Illustrative example: Identification of critical risk factors using sensitivity analysis for Seaside, Oregon . . . 105
6.4.1 Sensitivity analysis . . . 106
6.4.2 Variation of sensitivity of risk factors with the key distribution parameter 112
6.5 Summary . . . 115

Chapter 7 Risk-informed evaluation of mitigation strategies . . . 116
7.1 Introduction . . . 116
7.2 Sensitivity-based effective selection of candidate evacuation risk mitigation strategies . . . 119
7.3 Risk-informed evaluation of mitigation strategies . . . 121
7.3.1 Calculation of evacuation risk under the mitigation strategy by modifying the tsunami evacuation model . . . 122
7.3.2 Calculation of evacuation risk under the mitigation strategy using existing simulations . . . 122
7.4 Illustrative example: Risk-informed evaluation of different mitigation strategies for Seaside, Oregon . . . 126
7.4.1 Candidate infrastructural mitigation strategies . . . 128
7.4.2 Candidate non-infrastructural mitigation strategies . . . 130
7.5 Result and discussions . . . 131
7.5.1 Risk mitigation by each candidate strategy . . . 131
7.5.2 Comparison of evacuation risk reductions for different strategies . . . 138
7.6 Summary . . . 140

Chapter 8 Conclusions and future directions . . . 141
8.1 Conclusions . . . 141
8.2 Future directions . . . 144

Bibliography . . . 146

Appendix A Stochastic sampling . . . 171

Appendix B Kernel density estimation . . . 173
B.1 Regular KDE . . . 173
B.2 Boundary corrected KDE . . . 173

LIST OF TABLES

1.1 Casualties in the ten worst tsunamis in history (Australian Geographic 2011). 2

3.1 Important factors or mechanisms that are usually neglected or simplified in existing agent-based evacuation models. 29
3.2 The parameters used to determine the road widths occupied by the car and pedestrian for the existing road network. 45
3.3 Key continuous uncertain model inputs in the tsunami evacuation simulation. 52

4.1 Definition of simulation cases. 62
4.2 The comparison of the daytime and nighttime scenarios. 73

5.1 Continuous input random variables and associated parameters in tsunami evacuation. . 90
5.2 Sensitivity indices for the tsunami evacuation risk: Case 1. 92
5.3 Sensitivity indices for the tsunami evacuation risk: Case 2. 94

6.1 Relative entropy values for continuous input random variables and the damage states of the top five ranked bridges under the daytime scenario with 15,000 evacuees. 107
6.2 Relative entropy values for continuous input random variables and the damage states of the top five ranked bridges under the daytime scenario with 5000 evacuees. 109
6.3 Relative entropy values for continuous input random variables and the damage states of the top five ranked bridges under the nighttime scenario (Nighttime1) with 15,000 evacuees. 111
6.4 The link IDs for the top five ranked bridges corresponding to different μ_c values. 114

7.1 The parameters used to determine the road widths of the evacuation routes occupied by the car and pedestrian after widening evacuation routes (shown based on the functional class of the evacuation route). 129
7.2 The thresholds used to determine the traffic stage on widened evacuation routes. 129

LIST OF FIGURES

1.1 A tsunami historical outlook around the globe (SMS Tsunami Warning 2018). 1
1.2 Illustration of (a) the condensed time frame to evacuate under the near-field tsunami (adapted from USGS (2020b)), and (b) the damaged evacuation environment due to the earthquake. 3
1.3 Illustration of sources of uncertainty associated with tsunami evacuation. The sources of the figures are: "Multiple hazards" adapted from USGS (2020b), and "Tsunami evacuation" (Vallarta Daily News 2017). 7
1.4 Illustration of (a) infrastructural mitigation strategy, bridge retrofit (Buckle et al. 2006), and (b) non-infrastructural mitigation strategy, tsunami preparedness education using the evacuation map (The Oregon Department of Geology and Mineral Industries 2013). 9

2.1 Framework for simulation-based tsunami risk assessment and risk-informed mitigation. 14

3.1 Identified evacuation shelters and routes using GIS-based model (Dewi 2012). 18
3.2 Illustration of (a) the forces acting on each particle, and (b) spring-dashpot model (Abustan 2013) in DEM-based model. 19
3.3 Simulation of building evacuation due to fire using the CA model with (a) the room on fire, and (b) one time step of the evacuation. 21
3.4 Illustration of (a) the interactions between different variables, and (b) dynamic change of populations over time tracked by the SD model. 22
3.5 Illustration of tsunami evacuation simulation in Seaside, Oregon using the agent-based model. 24
3.6 Illustration of the proposed agent-based tsunami evacuation model. 32
3.7 The agent-based tsunami evacuation model interface. 33
3.8 The relationship between the pedestrian speed and pedestrian density ahead (adjusted from Goto et al. (2012)). 39
3.9 Illustration of (a) Cascadia Subduction Zone (CSZ) (USGS 2020a), and (b) Seaside, Oregon. 44
3.10 The existing road network in Seaside, Oregon. 46
3.11 Tsunami evacuation routes and zones in Seaside, Oregon. 47
3.12 Population distribution in Seaside, Oregon at the noontime of some weekends in the summer. 50
3.13 The general tsunami evacuation process simulated using the proposed agent-based tsunami evacuation model at (a) $t = 0$ min, (b) $t = 12$ min, (c) $t = 28$ min, (d) $t = 38$ min, (e) $t = 45$ min, and (f) $t = 55$ min. 53

4.1 Framework for quantification of tsunami evacuation risk. 58
4.2 The variations of evacuation risk in terms of danger rate, safety rate, casualty rate over time under different cases, where (a) shows the expected pedestrian rate, (b) shows the expected car rate, and (c) shows the expected total rate. 64
4.3 The variations of evacuation risk in terms of casualty rate for (a) pedestrian, (b) car, and (c) total over time under different cases. 67

4.4 The variations of evacuation risk in terms of casualty rate for (a) pedestrian, (b) car, and (c) total over time under different population sizes. 71
4.5 The variations of evacuation risk in terms of casualty rate for (a) pedestrian, (b) car, and (c) total over time under the daytime and two nighttime scenarios. 74

5.1 Illustration of sensitivity analysis of tsunami evacuation risk with respect to epistemic uncertainty. 81
5.2 The steps to efficiently calculate the first-order Sobol' index using the augmented sample-based approach. 88
5.3 Illustration of (a) samples from $\pi(\mu_c)$, (b) samples from $\pi(\mu_e)$, (c) $\pi(\mu_c)$ estimated using boundary corrected KDE, (d) $\pi(\mu_e)$ estimated using boundary corrected KDE, (e) variation of the integrand $\pi^2(\mu_c)/p(\mu_c)$ in calculation of S_i for μ_c, and (f) variation of the integrand $\pi^2(\mu_e)/p(\mu_e)$ in calculation of S_i for μ_e. All results are for Case 2. . . 96

6.1 Relative entropy ranking for the damage state of bridges under the daytime scenario with 15,000 evacuees. 107
6.2 Relative entropy of the damage state of bridges under the daytime scenario with 15,000 evacuees. 109
6.3 Relative entropy ranking for the damage state of bridges under the daytime scenario with 5000 evacuees. 110
6.4 Relative entropy ranking for the damage state of bridges under the nighttime scenario (Nighttime1) with 15,000 evacuees. 111
6.5 Relative entropy values for p_c conditional on different values of μ_c. 112
6.6 Relative entropy values for continuous input random variables of interest, and the damage state of the top five ranked bridges conditional on different values of μ_c. 114

7.1 Illustration of risk-informed evaluation of candidate mitigation strategies. The sources of the figures are: S_1 (City of Seaside 2010), S_2 (Buckle et al. 2006), S_3 (Applied Technology Council 2019), S_4 (The Oregon Department of Geology and Mineral Industries 2013), and S_5 (Banse 2012). 121
7.2 Illustration of the candidate evacuation risk mitigation strategies selected based on critical risk factors. 127
7.3 The variations of evacuation risk in terms of casualty rate for (a) pedestrian, (b) car, and (c) total over time before and after widening evacuation routes. 133
7.4 The evacuation risk in terms of casualty rate for the pedestrian, car, and total using the optimal bridge retrofit strategy with different m values. 134
7.5 The variations of evacuation risk in terms of casualty rate for (a) pedestrian, (b) car, and (c) total over time before and after building vertical shelters. 135
7.6 The variations of evacuation risk $H(p_r)$ as a function of p_r for the pedestrian, car, and total. 136
7.7 The variations of evacuation risk $H(p_c)$ as a function of p_c for the pedestrian, car, and total. 138
7.8 Comparison of evacuation risk reductions for considered mitigation strategies. 139

A.1 Integration of stochastic sampling with risk assessment to generate samples from $\pi(\mathbf{x}, \boldsymbol{\theta})$. 172

B.1 Illustration of KDE and boundary corrected KDE (Jia 2014) 174

Chapter 1

Introduction

1.1 Motivation

Earthquake-induced tsunamis are disasters that threaten coastal communities all over the world. A tsunami historical outlook around the globe since the year 1600 BC is shown in Fig. 1.1, in which a larger circle indicates a greater earthquake and the color of the circle represents the tsunami intensity. An earthquake-induced tsunami occurs with relatively low frequency but is usually very destructive causing extensive damages to infrastructure and enormous loss of life worldwide (Aguirre-Ayerbe et al. 2018; Løvholt et al. 2019), especially for the low-lying coastal communities threatened by near-field tsunamis. Extreme numbers of casualties have been demonstrated in the ten worst tsunamis in history, as shown in Table 1.1.

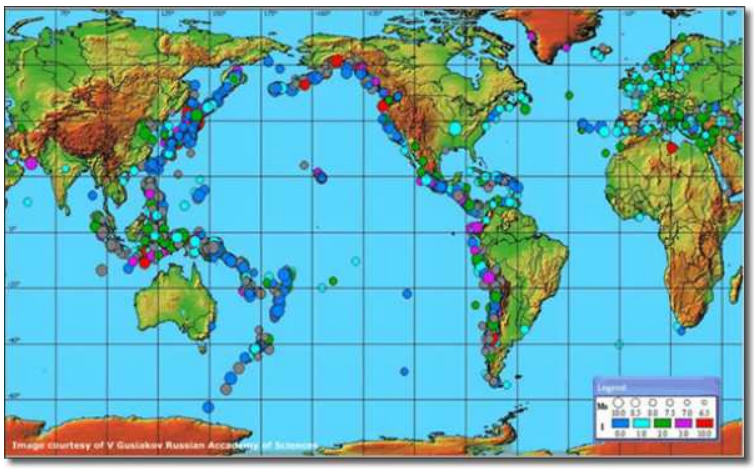


Figure 1.1: A tsunami historical outlook around the globe (SMS Tsunami Warning 2018).

The significant loss of life caused by the earthquake-induced tsunami mainly results from (1) limited effectiveness of structural countermeasures to protect the coastal community from extreme tsunamis. Structural countermeasures (e.g., breakwaters, seawalls, etc.) might be used to reduce the loss of life; however, such countermeasures have not been widely used outside Japan (León

Table 1.1: Casualties in the ten worst tsunamis in history (Australian Geographic 2011).

Date	Location	Casualties
December 26, 2004	Sumatra, Indonesia	230,000
March 11, 2011	North Pacific Coast, Japan	18,000
November 1, 1755	Lisbon, Portugal	60,000
August 27, 1883	Krakatau, Indonesia	40,000
September 20, 1498	Enshunada Sea, Japan	31,000
October 28, 1707	Nankaido, Japan	30,000
June 15, 1896	Sanriku, Japan	22,000
August 13, 1868	Northern Chile	25,000
April 24, 1771	Ryuku Islands, Japan	12,000
January 18, 1586	Ise Bay, Japan	8,000

and March 2016). More importantly, it is difficult to save human life from devastating tsunamis using only structural countermeasures (Cabinet Office 2011; Suppasri et al. 2013; Takabatake et al. 2017); (2) condensed time frame to evacuate to the safety zone (illustrated in Fig. 1.2(a)). Due to the destructive power of the earthquake-induced tsunami, evacuation to safety zones is regarded as one of the most effective ways to save lives from the tsunami strike (Takabatake et al. 2017). However, the tsunami is expected to arrive in a very short time after the earthquake, especially the near-field tsunami (within minutes, e.g., 10 to 30 minutes) (Applied Technology Council 2009; Raskin et al. 2011). It is very challenging to successfully evacuate a large number of people in such a short time frame; (3) evacuation delays due to damaged evacuation environment caused by the earthquake (illustrated in Fig. 1.2(b)). The destructive tsunami is typically produced by a large-magnitude earthquake (i.e., magnitude 7.6 and greater) (USGS 2020c). The destructive earthquake can cause severe damage to bridges (Mostafizi et al. 2019b) or buildings, and the debris from damaged buildings might block nearby roads (Stern and Sinuany-Stern 1989). The traffic capacity of a transportation network may be significantly reduced due to the bridge damage (Jacob et al. 2014) or the road blockage (Stern and Sinuany-Stern 1989; Murakami et al. 2014; Jacob et al. 2014). The reduction in traffic capacity could delay the evacuation and ultimately lead to more casualties.

Proper evacuation planning is crucial to support effective evacuation and reduce casualty. To produce an effective evacuation plan, many issues need to be taken into account and several impor-

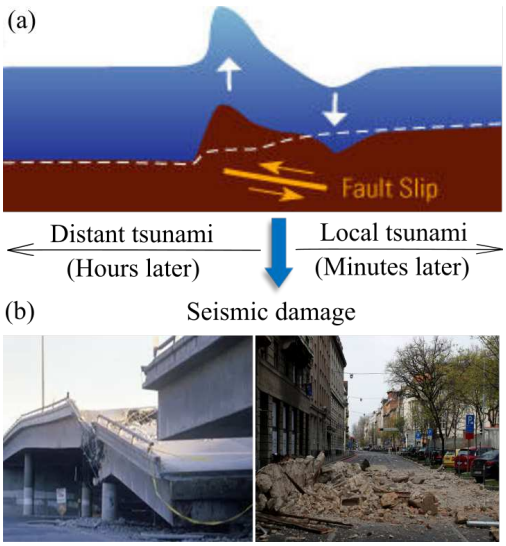


Figure 1.2: Illustration of (a) the condensed time frame to evacuate under the near-field tsunami (adapted from USGS (2020b)), and (b) the damaged evacuation environment due to the earthquake.

tant ones must be well addressed, including (1) a good understanding of the evacuation behavior. The complex evacuation behaviors need to be investigated (typically through evacuation simulation) and well understood such that proper response and behavior can be recommended for effective evacuation planning; (2) accurate quantification of evacuation risk (e.g., the expected proportion of the number of casualties to the population within a given time frame). The level of risk can be used to inform policy and decision-making for effective risk management within the evacuation plan (UNESCO 2007); (3) identification of effective risk mitigation strategies for more effective risk reduction.

1.1.1 Tsunami evacuation simulation

For effective tsunami evacuation planning, the evacuation process (especially the evacuation behavior) needs to be well investigated. Evacuation simulation is commonly used to investigate the evacuation behavior due to the difficulty of conducting evacuation drills (Takabatake et al. 2017). Many evacuation modeling techniques have been applied to tsunami (or flood) evacuation simulation, such as geographic information system (GIS)-based model (CRATER 2005; Dewi 2012; Wood et al. 2016; Benchekroun and El Mouraouah 2018), distinct element method (DEM)-based

model (Gotoh et al. 2004, 2009; Rahman et al. 2014; Abustan 2013), cellular automata (CA) model (Li et al. 2019b), and agent-based model (Usuzawa et al. 1997; Fujioka et al. 2002; Lämmel 2011; Wijerathne et al. 2013). In addition, the system dynamics (SD) model (Ahmad and Simonovic 2000a; Simonovic and Ahmad 2005; Berariu et al. 2016) that has been used for flood management might also be applied to tsunami evacuation simulation.

An proper evacuation model needs to be selected to capture the complex and dynamic evacuation process (especially the evacuation behavior). In particular, the evacuation decision and behavior would be very complex (e.g., irrational behavior such as the following behavior) in the damaged evacuation environment due to the large earthquake as well as within the condensed time frame, especially under the near-field tsunami. In this context, out of these models, the models other than the agent-based model typically lack the capacity to capture the complexity of evacuees' decision and behavior and hence the dynamics of emergency evacuation (Mas et al. 2015). More specifically, the GIS approach uses a static setting and does not simulate the dynamic evacuation process and complex evacuation behaviors (Benchekroun and El Mouraouah 2018). The DEM employs physical laws such as Newton's second law of motion to simulate the evacuee's motion in a crowd, which makes it difficult to model the evacuation behavior involving psychological factors such as a sudden change in moving direction (Mas et al. 2015). In the CA model, many components are not described accurately because the model is built on discrete space-time and relatively simple motion rules (Li et al. 2019a). Therefore, applying the CA model to tsunami evacuation simulation would entail challenges such as how to accurately describe the environment under the seismic and tsunami hazards. The SD model lacks spatial complexity (e.g., the population distribution) and requires many assumptions about the evacuation system when being applied to simulate the evacuation process (Mas et al. 2015).

As an alternative, the agent-based model is preferred for tsunami evacuation simulation due to its capability of capturing the emergent phenomena through characterizing the natural and human system dynamics and modeling the individual-level interactions among agents as well as the agent's interactions with the environment (Mas et al. 2012; Wang et al. 2016). Agent-based evacu-

ation modeling (ABM) is an evacuation modeling technique to simulate the behaviors of a system of autonomous decision-making entities named agents as well as the interactions between them and with the environment (Bonabeau 2002). Since one of the first agent-based tsunami evacuation models was introduced using a network evacuation modeling approach that is widely used for evacuation simulations of other natural hazards such as hurricanes, floods, nuclear disasters, and fires in buildings (Usuzawa et al. 1997), many tsunami evacuation models have been developed using ABM (Mas et al. 2015).

In existing agent-based evacuation models, however, many important factors or mechanisms associated with the tsunami evacuation are usually neglected or simplified for modeling convenience or due to computational challenges. For instance, modeling of seismic damages to bridges is typically simplified as fail or safe rather than modeling different damage states and reducing the traffic capacity accordingly. Similarly, the impact of debris caused by damaged infrastructure on the traffic capacity of the road is usually neglected. In the modeling of evacuation behaviors, some important interactions such as the pedestrian-vehicle interaction in the multimodal evacuation (e.g., evacuation on foot and by car) are typically neglected (Takabatake et al. 2017). However, the pedestrian and vehicle might interact with each other (Jacob et al. 2014), e.g., share the path between the walkway and lane. Also, some interactions between individuals (pedestrians or cars) such as the following behavior are usually neglected, although some evacuees may panic and simply follow others in an emergency. In addition, usually only a small population (i.e., maybe much smaller than the actual population) is considered in evacuation due to increasing computational effort as the population size (and accordingly the number of agents) increases (Mostafizi et al. 2019b). Considering the highly nonlinear nature of the evacuation, results from simulations using a smaller than actual population may not be able to give a good indication of the actual evacuation performance. The above neglects or simplifications would make it difficult to better understand the complex evacuation behavior and also may lead to inaccurate estimation of evacuation risk.

1.1.2 Tsunami evacuation risk assessment

Tsunami evacuation risk assessment is vital to policy-making, determining the nature and level of response for risk mitigation within the evacuation planning (UNESCO 2007). The risk needs to be accurately assessed to provide valuable information for effective planning such as enhancing the public awareness of the risk and improving the preparedness for potential disaster, promoting effective evacuation risk mitigation to reduce the casualty, etc.

To accurately assess the tsunami evacuation risk, various uncertainties associated with the evacuation need to be considered and properly quantified. The uncertainties may be the aleatory uncertainty that corresponds to the natural and inherent variability of the evacuation process and is irreducible (Der Kiureghian and Ditlevsen 2009; González et al. 2009). The uncertainties may be the epistemic uncertainty which corresponds to a lack of knowledge and is reducible when more data is collected (Der Kiureghian and Ditlevsen 2009; González et al. 2009). In terms of sources, various uncertainties exist in tsunami evacuation (illustrated in Fig. 1.3), related to the seismic and tsunami hazards (Wood and Schmidtlein 2013; Park and Cox 2016; Muhammad et al. 2017), the population size and spatial distribution (Fraser et al. 2014; Mostafizi et al. 2017), the evacuation decision and behavior (Wang et al. 2016; Mostafizi et al. 2017), etc.

For existing research on tsunami evacuation risk quantification, many important uncertainties are either neglected or considered in a simplified way. For example, the uncertainty in the seismic damage to the bridge is usually not probabilistically considered (e.g., by simply removing the damaged bridges from the network, essentially assuming complete damage all the time while neglecting the uncertainty in the damage states and residual traffic capacity of bridges) (Jacob et al. 2014; Mostafizi et al. 2017). Also, some of the uncertainties in the evacuation decision and behavior are usually neglected. Also, usually epistemic uncertainties are not incorporated in the risk quantification (i.e., only consider the aleatory uncertainty but neglect the epistemic uncertainty) (Wang and Jia 2021). The neglect of uncertainty and/or simplification of uncertainty quantification might result in inaccurate evacuation risk quantification. In addition, a systematic framework that can address complex evacuation models and uncertainty models is needed for the quantification of

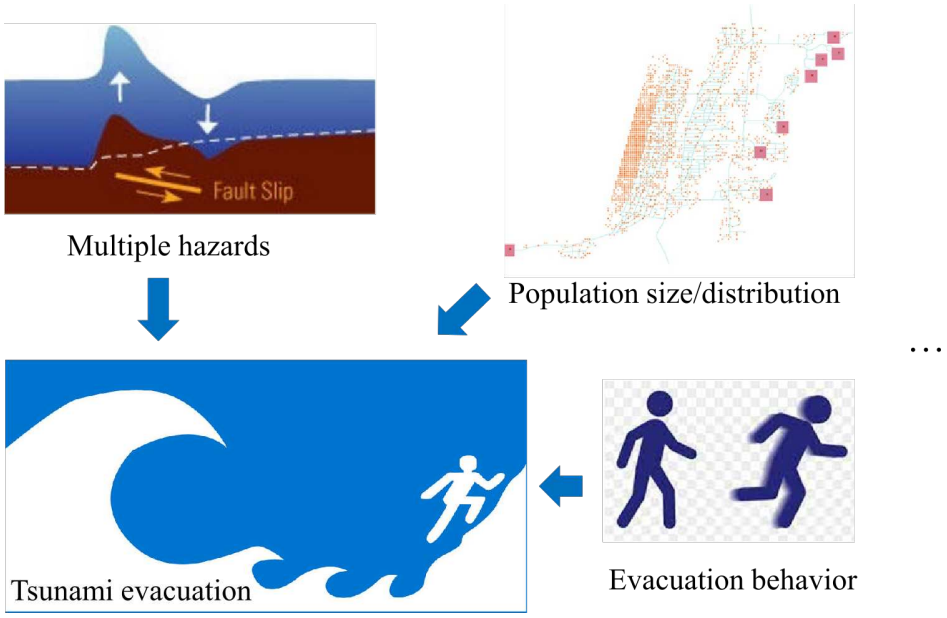


Figure 1.3: Illustration of sources of uncertainty associated with tsunami evacuation. The sources of the figures are: "Multiple hazards" adapted from USGS (2020b), and "Tsunami evacuation" (Vallarta Daily News 2017).

tsunami evacuation risk. However, no such framework has been developed for tsunami evacuation risk quantification.

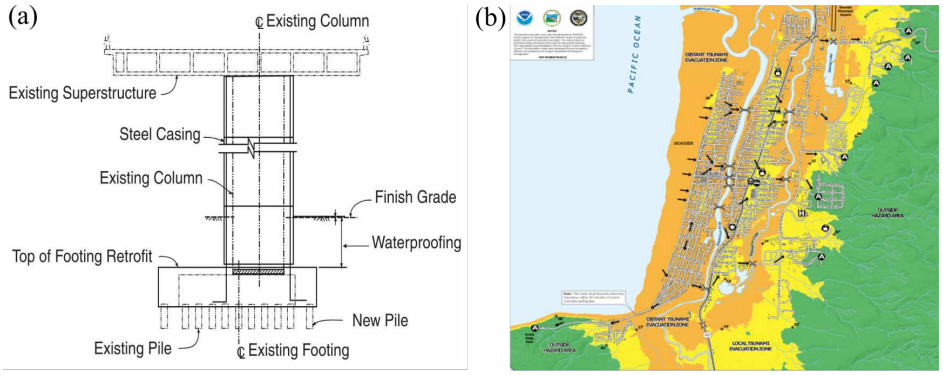
Furthermore, the evacuation risk could be more accurately assessed by reducing the epistemic uncertainties (Post et al. 2009; Jelínek et al. 2012) (e.g., through collecting more data (Der Kiureghian and Ditlevsen 2009; González et al. 2009)). To prioritize such data collection, it is critical to identify the epistemic uncertainties that have a high impact on the variability in the evacuation risk. Sensitivity analysis could be used for such a task. To the best of our knowledge, however, no sensitivity analysis of tsunami evacuation risk has been performed to evaluate the impact of various epistemic uncertainties on the variability in the evacuation risk and identify those having relatively high impacts.

In risk assessment and sensitivity analysis, typically many simulations are required. Direct use of general stochastic simulation techniques such as Monte Carlo simulation (MCS) (Robert and Casella 2004) for risk assessment and sensitivity analysis would entail significant computational challenges, especially in the context of tsunami evacuation since the tsunami evacuation model

could be expensive to run. To alleviate the computational challenges, efficient algorithms are needed.

1.1.3 Tsunami evacuation risk mitigation

The pre-event mitigation is regarded as an effective way to reduce evacuation risk (UNESCO 2007). Both infrastructural and non-infrastructural strategies have been considered. For example, Fig. 1.4 shows one infrastructural strategy, bridge retrofit, and one non-infrastructural strategy, tsunami preparedness education using the evacuation map. For an effective evacuation risk reduction, more effective (or optimal) mitigation strategies need to be identified out of all candidate strategies. In this context, the effectiveness of different mitigation strategies needs to be quantitatively evaluated for comparison. For the limited research on the evaluation of different types of evacuation risk mitigation strategies, most of them evaluate the strategies qualitatively (Priest et al. 2016) or semi-quantitatively (Aguirre-Ayerbe et al. 2018) rather than quantitatively. As for the candidate mitigation strategies for evaluation, typically they are selected based on feasibility but not necessarily based on quantitative analysis of whether they are promising or not in reducing the evacuation risk (Okumura et al. 2017; Aguirre-Ayerbe et al. 2018). Moreover, the mitigation strategy should be robust to various uncertainties associated with the evacuation. However, in existing research, the effectiveness of mitigation is typically not evaluated based on risk with systematic consideration of various uncertainties, and hence the identified mitigation strategies may not be robust to uncertainty. Furthermore, the effective strategy is usually identified by exhaustive enumeration (e.g., identify critical links by repetitive removal of each link and comparing the impacts of the failure of each link (Mostafizi et al. 2017)), which typically entails significant computational challenges. To devise more effective or optimal mitigation strategies, efficient algorithms are needed.



Bridge retrofit Tsunami preparedness education

Figure 1.4: Illustration of (a) infrastructural mitigation strategy, bridge retrofit (Buckle et al. 2006), and (b) non-infrastructural mitigation strategy, tsunami preparedness education using the evacuation map (The Oregon Department of Geology and Mineral Industries 2013).

1.1.4 Summary: Knowledge gaps in tsunami evacuation risk assessment and mitigation

Overall, there are several knowledge gaps in tsunami evacuation risk assessment and mitigation in existing research. The tsunami evacuation needs to be simulated more realistically to better understand the complex evacuation behavior, and provide the basis for risk assessment and mitigation. The agent-based model is preferred for tsunami evacuation simulation; however, existing agent-based tsunami evacuation models usually neglect or simplify many important factors and/or mechanisms associated with the evacuation process. In tsunami evacuation, various uncertainties (including aleatory and epistemic uncertainties) exist, e.g., related to multiple hazards, evacuation behavior, etc. These uncertainties need to be considered and properly quantified for risk assessment. In existing research, however, some important uncertainties are usually neglected or the uncertainty quantification is simplified. Overall, a systematic framework that can address complex evacuation models and uncertainty models is needed for risk quantification; however, no such framework has been developed for the quantification of tsunami evacuation risk. For effective evacuation risk mitigation, the effectiveness of different mitigation strategies needs to be evaluated. However, existing evaluations of the mitigation strategies are usually more qualitative than quantitative. Also, the effectiveness of mitigation strategies is typically not evaluated with sys-

tematic consideration of various uncertainties (e.g., not risk-based) and the identified mitigation strategies may not be robust to uncertainty. Approaches for quantitative evaluation of different mitigation strategies with consideration of various uncertainties are needed. In risk assessment and mitigation, risk evaluation using general stochastic simulation techniques (e.g., MCS) typically requires huge computational efforts. Efficient algorithms are needed to alleviate the computational challenge and facilitate the assessment of tsunami evacuation risk and the evaluation and selection of risk mitigation strategies.

1.2 Objectives and scope of research

Motivated by the above knowledge gaps in tsunami evacuation risk assessment and mitigation for effective evacuation planning, this research develops a generalized framework and uses it to perform simulation-based tsunami evacuation risk assessment and risk-informed mitigation. The framework is built layer by layer through integrating tsunami evacuation simulation, simulation-based evacuation risk assessment, sensitivity analysis of evacuation risk, and risk-informed evaluation of mitigation strategies. In particular, the following four objectives will be accomplished.

- **Objective 1: Simulate tsunami evacuation using ABM**

  Develop an improved agent-based tsunami evacuation model for a more realistic simulation of the tsunami evacuation by incorporating many of the important factors and mechanisms associated with evacuation. Apply the developed model to a coastal community subject to near-field earthquake-induced tsunami to better understand the complex evacuation process and evacuation performance.

- **Objective 2: Develop a generalized simulation-based framework for tsunami evacuation risk assessment**

  Develop a simulation-based framework for tsunami evacuation risk quantification that is capable of addressing complex evacuation models and uncertainty models (for quantification of various uncertainties, including aleatory and epistemic uncertainties).

- **Objective 3: Sensitivity analysis of tsunami evacuation risk**

  Use probabilistic sensitivity analysis to investigate the impacts of various risk factors and associated uncertainties on the evacuation risk. Sensitivity analysis with respect to epistemic uncertainty will also be carried out. Efficient augmented sample-based approaches will be developed to facilitate the sensitivity analysis.

- **Objective 4: Risk-informed evaluation of different mitigation strategies**

  Use sensitivity analysis results to guide the selection of candidate mitigation strategies, and evaluate the effectiveness of the different candidate mitigation strategies (including infrastructural and non-infrastructural strategies) based on tsunami evacuation risk reduction.

1.3 Organization of research

The remainder of this dissertation is to accomplish the above objectives for simulation-based tsunami evacuation risk assessment and risk-informed mitigation. Chapter 2 presents the proposed overall framework for simulation-based tsunami evacuation risk assessment and risk-informed mitigation, which integrates tsunami evacuation simulation, evacuation risk assessment, sensitivity analysis, and evacuation risk mitigation. In later chapters, the components of the proposed framework are presented and the use of each component is illustrated by taking the tsunami evacuation in Seaside, Oregon as an example. Chapter 3 develops an improved agent-based model for tsunami evacuation simulation by incorporating many of the important factors and mechanisms associated with evacuation. The developed model is used to better understand the complex evacuation process and evacuation performance. Chapter 4 develops a generalized simulation-based framework for the quantification of tsunami evacuation risk. The improved agent-based evacuation model is used within the framework for tsunami evacuation simulation. Various uncertainties (including aleatory and epistemic uncertainties) related to the evacuation process are considered and quantified by the proper selection of probability models. The evacuation risk under different scenarios (e.g., different population sizes, different times of the day, etc.) is comprehensively investigated. Chapter 5

conducts sensitivity analysis of evacuation risk with respect to the epistemic uncertainty to investigate the impacts of various epistemic uncertainties on the variability in the risk. An augmented sample-based approach is developed to efficiently perform the sensitivity analysis. The sensitivity analysis results can be used to prioritize the data collection for epistemic uncertainty reduction and further for more accurate risk assessment. Chapter 6 performs probabilistic sensitivity analysis to identify critical risk factors associated with evacuation that have high impacts on the evacuation risk. The sensitivity analysis is efficiently performed using an augmented sample-based approach extending from the one proposed in Chapter 5. Based on the critical risk factors identified by the probabilistic sensitivity analysis in Chapter 6, candidate risk mitigation strategies (including infrastructural and non-infrastructural strategies) are effectively selected in Chapter 7. Then the risk-informed evaluation of different candidate mitigation strategies is conducted to identify more effective strategies that are robust to uncertainties. The risk-informed evaluation of mitigation strategies is illustrated through an example, in which strategies including route widening, bridge retrofit, building vertical shelters, preparedness education, and evacuation drills are evaluated and compared quantitatively based on evacuation risk reduction. Chapter 8 concludes this research work and discusses future directions.

Chapter 2

Framework for simulation-based tsunami evacuation risk assessment and risk-informed mitigation

This chapter provides an overview of the overall proposed framework for simulation-based tsunami evacuation risk assessment and risk-informed mitigation (shown in Fig. 2.1). The framework consists of four major components: tsunami evacuation simulation, simulation-based evacuation risk assessment, sensitivity analysis, and risk-informed mitigation.

An improved agent-based model is developed for more realistic tsunami evacuation simulation by incorporating many important factors and mechanisms that are usually neglected and/or simplified in existing agent-based models. The proposed evacuation model consists of three sub-models, i.e., evacuation environment model (EEM), evacuation decision and behavior model (EBM), and evacuation performance model (EPM). In the EEM, the evacuation environment is modeled, including the multiple hazards (i.e., earthquake and earthquake-induced tsunami) as well as seismic damages to the bridge, etc. The EBM includes models for the individual decision and behavior, individual-level interactions among evacuees, and the evacuees' interactions with the environment. The probabilistic evacuation performance is modeled in the EPM. The proposed agent-based model is used to simulate the tsunami evacuation and better understand the complex evacuation process and evacuation performance. The evacuation simulation is used to support evacuation risk assessment, sensitivity analysis, and risk-informed evaluation of mitigation strategies.

The improved agent-based evacuation model is used within the proposed simulation-based framework to quantify tsunami evacuation risk. Various uncertainties associated with the evacuation (including aleatory and epistemic uncertainties) are explicitly considered. Probability models are used to quantify the aleatory uncertainty in input random variables in the evacuation simulation while the epistemic uncertainty is quantified through modeling the uncertainty in the distribution parameters of the selected probability models. The evacuation risk (e.g., the expected proportion

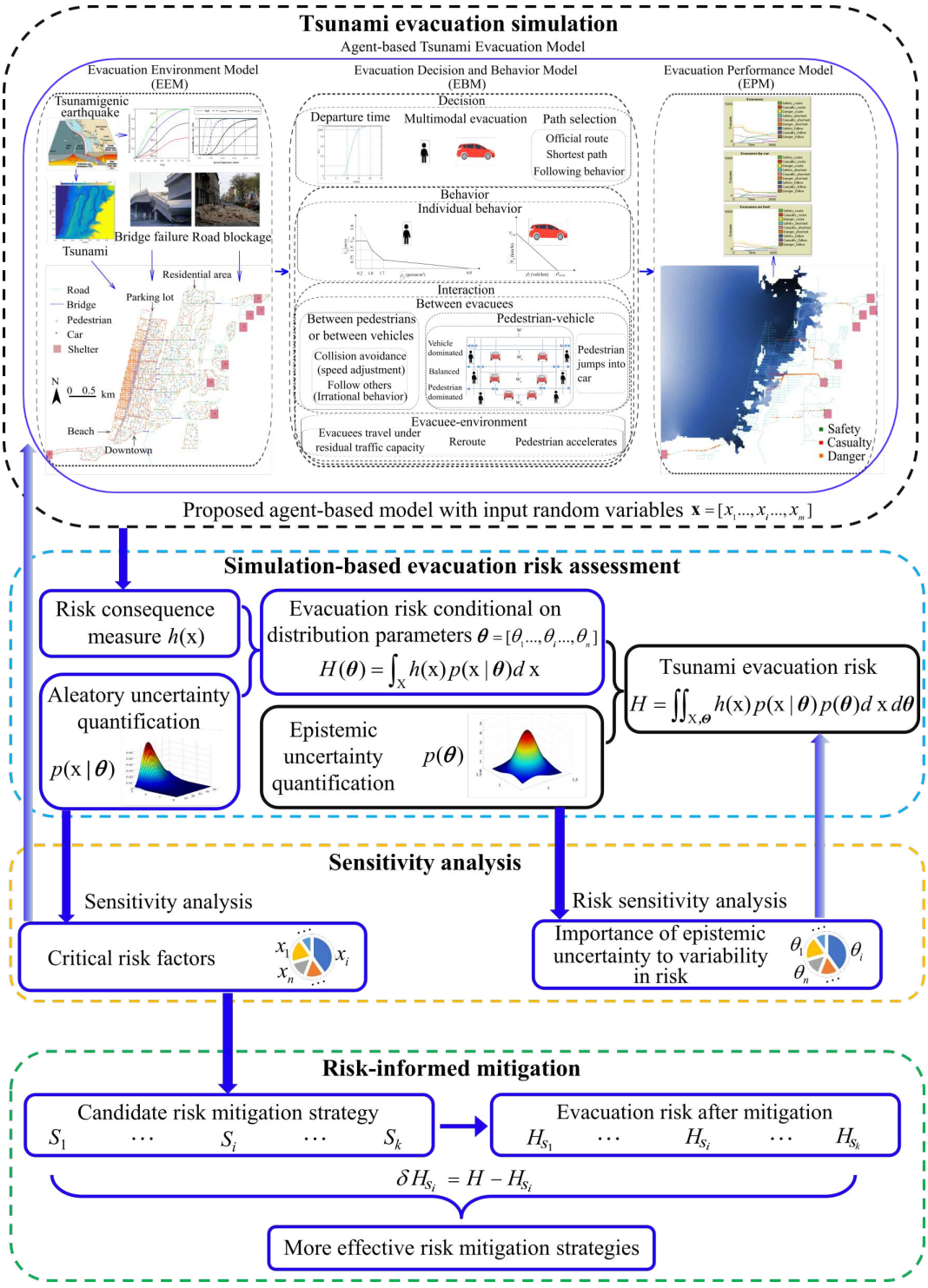


Figure 2.1: Framework for simulation-based tsunami risk assessment and risk-informed mitigation.

of the number of casualties to the population within a given time frame) is then quantified by propagating all the uncertainties.

For more accurate risk assessment, epistemic uncertainty can be reduced by additional data collection, and to support this, risk sensitivity analysis is performed to identify the impacts of the epistemic uncertainties on the variability in the evacuation risk. In addition, sensitivity analysis is performed to identify the critical risk factors with aleatory uncertainties (i.e., input random variables) that contribute more to the evacuation risk. The sensitivity results can be used to guide effective evacuation modeling and effective selection of candidate risk mitigation strategies. The above sensitivity analyses are efficiently performed using the proposed augmented sample-based approach based on the simulations/samples for evacuation risk assessment. So there is a seamless integration between evacuation risk assessment and the sensitivity analyses.

Then the simulation-based evacuation risk assessment framework is used to quantitatively evaluate the evacuation risk under different mitigation strategies to enable risk-informed mitigation. The critical risk factors identified in the sensitivity analysis are used to guide the selection of candidate risk mitigation strategies. Efficient simulation-based approaches are developed to enable efficient evacuation risk assessment under different infrastructural and non-infrastructural mitigation strategies. Based on the level of risk reduction, the effectiveness of each candidate mitigation strategy is evaluated and ultimately more effective strategies are identified.

The overall proposed framework can be used to support tsunami evacuation risk assessment and risk-informed mitigation for effective evacuation planning.

Chapter 3

Tsunami evacuation simulation using ABM

3.1 Introduction

It is extremely difficult to successfully evacuate a large population from a disaster in a short time. Proper planning such as pre-event evacuation risk mitigation is crucial for a successful evacuation. To make effective plans, it is vital to better understand the evacuation process, especially the evacuation behavior (e.g., evacuate on foot or by car under tsunami). An evacuation drill might be conducted to investigate the evacuation behavior. However, it is challenging, resource-intensive, and even dangerous to realistically conduct evacuation drills due to the complexity, which requires multi-agency coordination involving physical, psychological, and socioeconomic factors (Takabatake et al. 2017). Due to various uncertainties associated with the disaster, evacuation decision and behavior, etc., it is even more challenging or infeasible to repeat evacuation drills multiple times under different scenarios. As an alternative, evacuation simulation can comprehensively investigate the evacuation behavior under different scenarios, which is much cheaper and safer compared to evacuation drills (Helton et al. 2013; Abustan 2013; Zsifkovits and Pham 2017; Jumadi et al. 2017).

Many modeling techniques have been employed in evacuation simulation (Hu 2017; Li et al. 2019a). Here, five candidate models are summarized that either have been applied or have the potential to be applied to tsunami evacuation simulation, including geographic information system (GIS)-based model, distinct element method (DEM)-based model, cellular automata (CA) model, system dynamics (SD) model, and agent-based model.

3.1.1 Existing models for tsunami evacuation simulation

Geographic information system (GIS)-based model

GIS is a computer-based technology and methodology that is capable of capturing and analyzing spatial and geographic data for a wide range of applications. One important application is to evaluate, display, send, and receive the spatial information for crisis response (e.g., evacuation from disaster) through integration with the simulation model for an emergency.

GIS has been widely applied in evacuation simulation, particularly associated with: (1) shelters such as evaluating the site suitability (Dalal et al. 2007; Kar and Hodgson 2008; Elheishy et al. 2013), and assessing the coverage area (Mallick 2014); (2) routes such as route selection (Dunn and Newton 1992; Wilson and Cales 2008; Ma et al. 2012; Billah et al. 2018); (3) decision-support systems for evacuation planning (De Silva and Eglese 2000; De Silva 2001; Kwan and Lee 2005). For example, a GIS-based model was proposed to select suitable shelters based on distance, capacity, and the availability of life requirements (Elheishy et al. 2013). A GIS-based model was developed for evacuation route planning with the shortest route to shelters for a coastal community (Billah et al. 2018). GIS was integrated with a simulation model to develop a spatial decision-support system for evacuation planning (De Silva and Eglese 2000).

In recent years, GIS has been used in tsunami evacuation simulation. Several programs were developed to select evacuation routes. For example, ETR (Evacuation Route Tools) was developed and applied in Thailand (CRATER 2005). "Route Finder" was developed in MapInfo GIS platform and has been widely applied such as in French Riviera (Sahal et al. 2013) and Martinique (Péroche et al. 2014). "CASPER" (Capacity Aware Shortest Path Evacuation Routing) was developed for ArcGIS Network Analyst (Shahabi and Wilson 2014). A method using GIS tools was developed to select the most effective evacuation routes in a tsunami-prone area (Dewi 2012). Network analysis and various GIS techniques were used to determine the location and capacity of potentially suitable evacuation shelters and the most effective evacuation routes. The least-cost-distance (LCD) model implemented in ArcMap by taking into account the slope and land cover of an area was developed and applied in the U.S. Pacific Northwest (Wood et al. 2016). GIS-based evacuation modeling was

applied to find the most effective routes taking into account the shortest travel time to evacuate out of hazard zones under tsunami (Benchekroun and El Mouraouah 2018). Fig. 3.1 illustrates the selected locations of shelters and the most effective evacuation routes in a tsunami-prone area using the GIS-based model. The red cross represents the identified shelter and the black arrow is the most effective evacuation route.

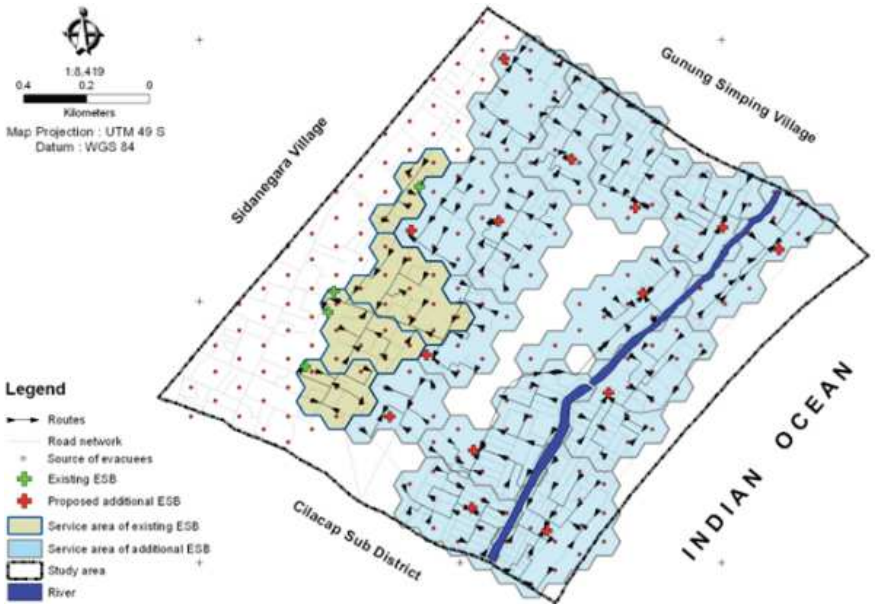


Figure 3.1: Identified evacuation shelters and routes using GIS-based model (Dewi 2012).

Distinct element method (DEM)-based model

DEM is a numerical modeling approach to simulate a large number of rigid or deformable bodies or particles. In DEM, particles are first assigned spatial orientations and initial velocities. Then, the forces (e.g., physical repulsive force and psychological repulsive force, shown in Fig. 3.2(a)) acting on each particle are calculated based on initial data, relevant physical laws, and contact models (e.g., spring-dashpot model shown in Fig. 3.2(b)). The forces acting on each particle are summed up and Newton's equation of motion is used to compute the acceleration, velocity, and displacement of each particle. The new positions are used to update the forces for the next time step (Abustan 2013). The pioneer of DEM was originally developed to solve problems in rock

mechanics (Cundall and Strack 1979). Today DEM is becoming extensively accepted in various research areas such as geology, chemistry, and engineering, etc..

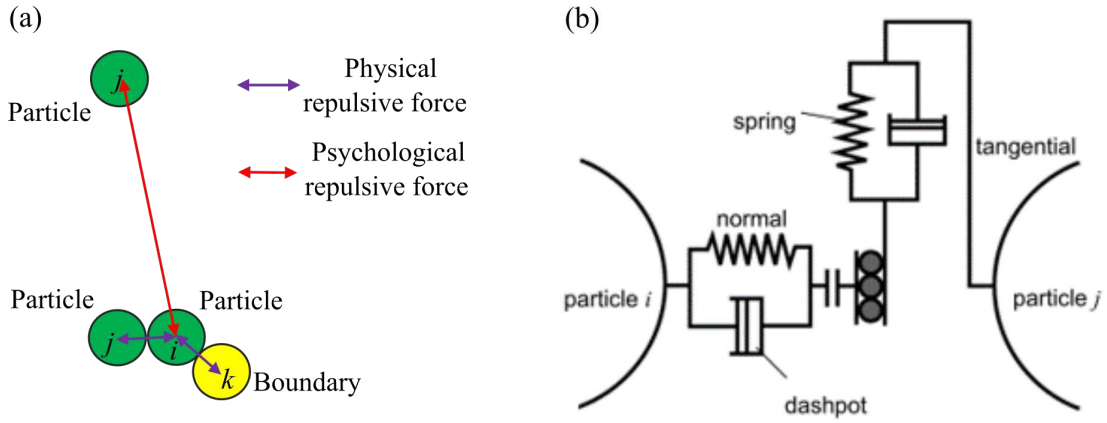


Figure 3.2: Illustration of (a) the forces acting on each particle, and (b) spring-dashpot model (Abustan 2013) in DEM-based model.

One of the first research on evacuation simulation integrated with DEM can be found in Kiyono et al. (1996), where the DEM-based model was used to simulate the behavior of a crowd evacuation during an emergency disaster. The proposed DEM-based model was modified such that it can simulate collision avoidance (Kiyono et al. 1998). A crowd modeling program named CrowdDMX was developed based on DEM for crowd dynamic simulation (Langston et al. 2006). The CrowdDMX was further developed to tackle the contraflow problem (Smith and Mccarty 2009). Also, the CrowdDMX was extended to study the subgroup behavior in crowd dynamics simulation (Singh et al. 2009). A DEM-based crowd evacuation simulator developed in Gotoh et al. (2004) was improved by introducing the self-evasive action to study the contraflow of pedestrian movement (Gotoh et al. 2012), in which collision avoidance or the alignment behavior between adjacent pedestrians are considered.

In recent years, the DEM has been applied in tsunami evacuation simulation. An evacuation process simulator was developed based on DEM to investigate the crowd evacuation process from tsunami attack (Gotoh et al. 2004). The DEM-based crowd evacuation simulator was used to a town planning against tsunami inundation (Gotoh et al. 2008). The DEM-based simulator was

further used to select appropriate evacuation places for tsunami evacuation planning (Gotoh et al. 2009). The DEM-based crowd evacuation simulator introduced in Gotoh et al. (2004) was extended to incorporate group behavior by introducing in-group and out-group interactions (Rahman et al. 2014). The DEM-based crowd evacuation simulator developed in Gotoh et al. (2004, 2012) was used to investigate how the accumulative population that complete evacuation changes over time under different scenarios (Abustan 2013).

Cellular automata (CA) model

CA are dynamic systems with discrete space and time. The space of CA is divided into a regular grid of cells with initial states. The states of all cells (or behaviors) are updated synchronously in a discrete-time step according to some local, identical interaction rules (Sipper and Tomassini 1998). The state of each cell is determined by adjacent cells at the previous time step (Yuan and Tan 2009, 2011). The first system of CA was developed for calculating liquid motion in the late 1950s (Bialynicki-Birula and Bialynicka-Birula 2005), in which a liquid was considered as a group of discrete units and the motion of each unit was calculated based on its neighbors' behaviors. Nowadays CA is being applied in various areas such as physics, theoretical biology, and engineering, etc.

Various CA models have been developed to simulate crowd evacuation under different situations (Zheng et al. 2009). These CA models are based on interactions either among pedestrians or between pedestrians and environments. For the CA models based on the interaction among pedestrians, they are typically used to study friction effects of pedestrian behavior (Kirchner et al. 2003a,b; Schultz et al. 2007) or the bi-direction pedestrian behavior (Fang et al. 2003; Li et al. 2005) or herding behavior (Nishinari et al. 2006). For instance, a CA model was proposed for pedestrian dynamics with friction to simulate competitive behavior in emergency egress from an aircraft (Kirchner et al. 2003a). A CA model was presented to simulate the bi-direction pedestrian movement in a corridor (Li et al. 2005). A stochastic CA model was proposed to investigate the following behaviors of pedestrians in building evacuation (Nishinari et al. 2006). For the CA models based on interactions between pedestrians and environments, they are usually used to investigate

the impact of the exit width or obstacle on pedestrian movement. For example, a two-dimensional CA model was proposed to study the exit dynamics of occupant evacuation (Zhao et al. 2006). A two-dimensional CA model was used to simulate the pedestrian evacuation in a room with fixed obstacles (Varas et al. 2007). A CA model without step back was presented to simulate the pedestrian counter flow in a channel (Yu and Song 2007). Fig. 3.3 illustrates the simulation of building evacuation due to fire using the CA model, where (a) shows the room on fire and (b) demonstrates one time step of the evacuation.

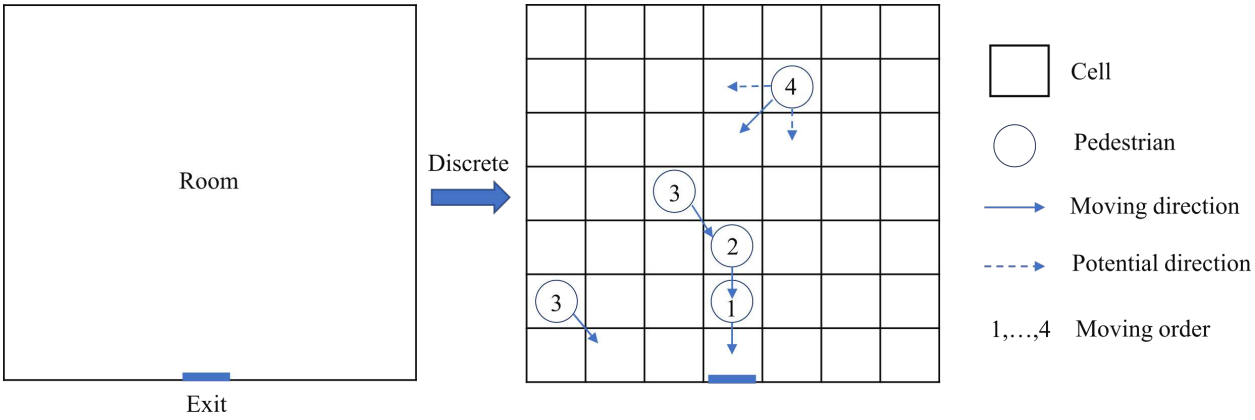


Figure 3.3: Simulation of building evacuation due to fire using the CA model with (a) the room on fire, and (b) one time step of the evacuation.

Although a lot of CA models exist for the building evacuation simulation, few CA models have been developed to simulate flood evacuation or tsunami evacuation. A model was proposed to simulate crowd evacuations in flood disasters by combining CA and a multi-agent system (Li et al. 2019b). When an earthquake occurs, many people have to leave the coast as soon as possible for avoiding the tsunami. The traffic network is not designed well for such a situation. To improve network performance for tsunami evacuation, a CA model for traffic network optimization developed in Tamaki et al. (2004) was applied to perform the traffic network design (Kita et al. 2015).

System dynamics (SD) model

SD is a methodology and mathematical modeling technique to understand the dynamic behavior of complex systems. The SD model solves the problem of simultaneity by updating all

variables in small time increments with positive and negative feedback and time delays structuring the interactions and control. SD was first introduced to understand strategic problems in complex dynamic systems (Forrester 1961). Since then, SD has been widely used to model social, natural, management, and engineered systems (Ahmad and Simonovic 2001). Some engineering applications of SD are river basin planning (Palmer et al. 1993), long-term water resources planning and policy analysis (Simonovic et al. 1997; Simonovic and Fahmy 1999), management of scarce water resources (Fletcher 1998), and reservoir operation (Ahmad and Simonovic 2000b).

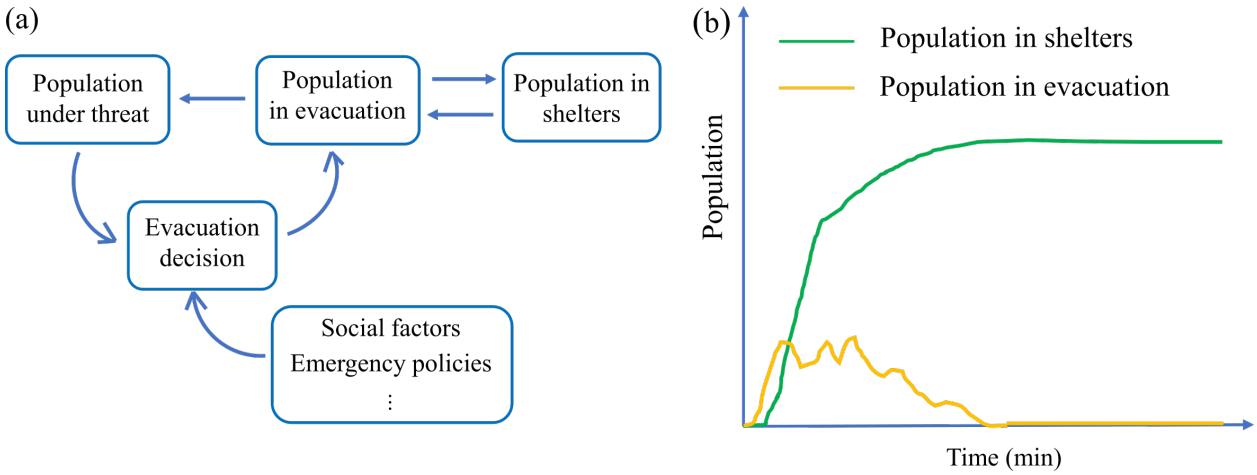


Figure 3.4: Illustration of (a) the interactions between different variables, and (b) dynamic change of populations over time tracked by the SD model.

In recent years, the SD model has been used for disaster management. For example, an SD model that captures dynamic interactions between different components of the flood management system was presented in Ahmad and Simonovic (2000a). The model was used to evaluate the consequences of various policy alternatives for flood management. SD was used in Gillespie et al. (2004) to understand the natural and social systems involved in disasters for designing safe systems. An SD model was developed in Simonovic and Ahmad (2005) to capture human behavior during flood emergency evacuation. The interactions between different variables are modeled (shown in Fig. 3.4(a)) and the dynamic behavior of evacuation system is tracked (illustrated in Fig. 3.4(b)). Ultimately, the model is able to evaluate the effectiveness of different flood emer-

gency management procedures. In Peng et al. (2014), an SD model was proposed to analyze the behaviors of disrupted disaster relief supply chains for post-seismic supply chain risk management. An SD model that covers the complexity of decision-making processes in times of floods was developed for training decision-makers in flood response (Berariu et al. 2016).

Agent-based model

Agent-based modeling (ABM) is a modeling technique to simulate the behaviors of a system of autonomous decision-making entities named agents as well as the interactions between them and with the environment (Bonabeau 2002). One of the earliest agent-based models in concept was a segregation model (Schelling 1971), which presented the basic concept of agent-based models as autonomous agents interacting with an observed aggregate, the emergent outcome in a shared environment. However, the agent-based model did not become widespread until the appearance of modeling software such as NetLogo in the 1990s because the agent-based model is computation-intensive. The agent-based model has found wide applications in many areas such as biology, business, and engineering, etc.

Due to the capability of capturing emergent phenomena, providing a natural description of a system, and being flexible (Munadi et al. 2012), the agent-based model has been used to simulate various evacuation processes. For example, an agent-based model was used to emulate human movement patterns in the built environment based on Gibson's approach (Turner and Penn 2002). An agent-based model was used to investigate the impact of individual actions and their interdependence on the performance of a metro system under a tunnel fire (Zarboutis and Marmaras 2004). An agent-based model based on CA was proposed to simulate pedestrian dynamics, in which different pedestrian characteristics such as gender, speed, herding behavior, and obstacle avoidance behavior are considered (Toyama et al. 2006). A multi-agent-based framework was presented to simulate human and social behaviors such as competitive behavior, queuing behavior, and herding behavior during emergency evacuations (Pan et al. 2007). The crowded evacuation process under terrorist bomb attacks was simulated by introducing the Virtual Reality (VR)-based Belief, Desire, and Intention (BDI) software agent (Shendarkar et al. 2008). An agent-based crowd simulation

system was developed to investigate the impact of intra-group structure and inter-group relationships on crowd behavior (Qiu and Hu 2010). An agent-based public decision support system was presented to model emergency evacuation of individuals with disabilities in terms of speed, ability to negotiate the environment, etc. (Manley and Kim 2012). The impact of a hurricane storm surge flooding on the number of fatalities was evaluated using a dynamic agent-based model (Lumbroso et al. 2017). Integrating building information modeling (BIM) technology and ABM, a simulation model for offshore oil and gas platforms were proposed to evaluate different evacuation plans (Cheng et al. 2018).

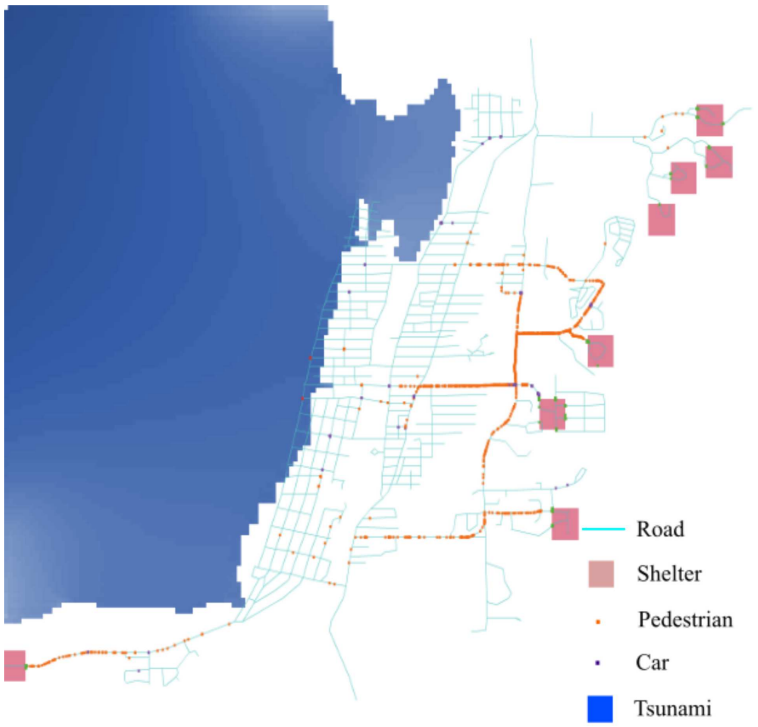


Figure 3.5: Illustration of tsunami evacuation simulation in Seaside, Oregon using the agent-based model.

One of the first agent-based tsunami evacuation models was introduced in Usuzawa et al. (1997) using a network modeling approach that is widely used for evacuation simulations of other natural hazards such as hurricanes, floods, nuclear disasters, and fires in buildings. Since then, many tsunami evacuation models have been developed using ABM (Mas et al. 2015). For example, a multi-agent-based tsunami evacuation model was introduced to simulate more complex human be-

haviors in tsunami evacuation (Fujioka et al. 2002). The agent-based tsunami evacuation model presented in Katada et al. (2004) started the application of tsunami evacuation simulations for tsunami mitigation, particularly for disaster education. The tsunami evacuation model used Multi-Agent Transport Simulation (MATSim) to implement large-scale agent-based simulation (Lämmel 2011). The tsunami evacuation model was developed with finer levels of details with the development of high-performance computing (HPC) (Wijerathne et al. 2013). An agent-based modeling framework was developed for a multimodal near-field tsunami evacuation simulation (Wang et al. 2016). Fig. 3.5 illustrates one tsunami evacuation simulation in Seaside, Oregon using the agent-based model, where different types of agents are modeled, including the road, shelter, pedestrian, car, tsunami, etc.

3.1.2 Comparison of different models for tsunami evacuation simulation

Each of the above five models has its advantages and limitations in the application. A key to select the proper model for tsunami evacuation simulation is whether the model can simulate the tsunami evacuation as expected. In this research, the model is expected to be capable of capturing the tsunami evacuation in an uncertain situation, especially the complex evacuation behavior in the multi-hazard environment within the condensed time frame (e.g., irrational behavior). Also, the model should be able to naturally describe the evacuation system such as the multi-hazard environment, individual behaviors of evacuees, and interactions among agents as well as between agents and the environment. Furthermore, the model should be flexible enough such that it adjusts to different factors and mechanisms in evacuation such as the population size, evacuation behaviors, etc.

GIS approach is a top–down method that uses aggregate descriptions of a system. It has a static setting and the advantage of not dealing with the dynamics of the evacuation process and the complexity of evacuation behaviors (Benchekroun and El Mouraouah 2018). However, this also means the GIS-based model is not well suited to track the dynamics of the evacuation process and the diversity of evacuation behaviors (Astle and Crooks 2006) unless it incorporates micro-scale

components provided by other simulation models such as agent-based model (Johnston 2013). Therefore, the GIS-based model is typically used to identify the optimal location of the shelter and/or select the most effective evacuation route for the aggregated population in each block of the coastal community under a tsunami. Generally, it is unable to track the change of the populations that are under threat, become the casualty, and reach shelters over time because the limit of tsunami run-up rather than the time-history of inundation is typically used in the simulation.

DEM applies physical laws (e.g., Newton's second law of motion) to the evacuees who evacuate in a crowd. The DEM-based model may provide a good description of crowd behavior through tracking individual behaviors and the interactions between individuals as well as between individuals and the obstacle. However, it is not suitable to simulate the herding or queuing behavior that is common in tsunami evacuation. Also, using physical laws such as Newton's second law of motion is difficult to model some important evacuation behaviors such as a sudden change in moving direction due to psychological factors (Mas et al. 2015).

In the CA model, the time, space, and state are discrete, and the spatial interaction only exists between adjacent cells. Due to these characteristics, the CA model can simulate the evacuation process with a small computational effort and especially suitable for simulating the crowd evacuation process (Li et al. 2019a). However, the description of the environment, human behavior, and human position and velocity are typically inaccurate because the CA model is based on discrete space-time and relatively simple motion rules are set (Li et al. 2019a). It would pose significant challenges when applying the CA model to simulate tsunami evacuation, e.g., how to accurately describe the environment subject to earthquake and tsunami, capture complex human behaviors, and characterize the human position and velocity. Therefore, the CA model is typically used to simulate crowd behaviors in building evacuation rather than in tsunami evacuation.

The SD model allows to track the dynamic behavior of the evacuation system as well as understand the interactions between different variables. However, it lacks spatial complexity and requires many assumptions about the system when being applied to simulate the evacuation process (Mas et al. 2015). Therefore, the SD model is typically used to evaluate different emergency

policies for disaster management, e.g., flooding evacuation planning. Generally, it is not used to simulate the complex evacuation process, especially complex evacuation behaviors.

The agent-based model typically consists of sub-models that are capable of simulating the environment, agents, decision-making, learning rules, and interactions between agents as well as between agents and the environment. The agent-based model has been widely applied to simulate the evacuation process due to multiple benefits it provides: (1) it captures emergent phenomena; (2) it provides a natural description of a system; and (3) it is flexible (Bonabeau 2002; Mas et al. 2015). For tsunami evacuation simulation, the agent-based model can model irrational behaviors such as following others (herding behavior). The agent-based model can naturally describe the evacuation system including the environment under seismic and tsunami hazards, numerous agents with complex evacuation decisions and behaviors, and the individual-level interactions among agents and the agents' interactions with the environment. The agent-based model is capable of tuning the complexity of agents associated with population size, evacuation behavior, degree of rationality, and rules of interactions (Abustan 2013). Note that the agent-based model is generally more computationally intensive than the other four models (Zheng et al. 2009); however, such a challenge can be addressed by HPC.

3.1.3 Limitations in existing agent-based tsunami evacuation models

Each agent-based tsunami evacuation model has its characteristics, while a sophisticated one typically models the evacuation environment (including modeling of seismic and tsunami hazards, transportation network, tsunami shelters, and population distribution), the evacuation decision and behavior (e.g., departure time, evacuation mode, evacuation behavior, etc.), and the evacuation performance (e.g., the casualty rate) (Mostafizi et al. 2019b). Different agent-based models might have different focuses; however, it is critical to understand the nature of earthquake-induced tsunami as well as the complexity of the evacuation decision and behavior such that the evacuation environment, evacuation decision and behavior, and evacuation performance could be modeled realistically.

For the earthquake-induced tsunami, especially the near-field one, two important characteristics in terms of time and space need to be better understood for evacuation simulation (illustrated in Fig. 1.2), i.e., (1) the condensed time frame to evacuate (i.e., time), and (2) the damaged evacuation environment due to the earthquake (i.e., space). As for (1), under the near-field tsunami with a condensed time frame for evacuation (only minutes of forewarning and to evacuate), the appropriate evacuation decision and behavior is crucial for the successful evacuation (León and March 2016; Nakaya et al. 2018). However, the evacuation decision and behavior would be very complex within the condensed time frame (Tsushima et al. 2011; Priest et al. 2016). Before evacuation, evacuees need to decide when to evacuate (i.e., departure time), how to evacuate (i.e., evacuation mode, on foot or by car), and where to evacuate (i.e., use evacuation routes or search the shortest path). In the evacuation, evacuees would have complex individual behaviors as well as interactions with each other and with the hazardous environment. For the individual behavior, evacuation speed would adjust according to the traffic density some distance ahead. For interactions, (1) some pedestrians (or cars) might have the following behavior in emergency (Takabatake et al. 2017) and collision is avoided with each other by adjusting the speed; (2) for multimodal evacuation on foot and by car, the pedestrian-vehicle interaction would exist, e.g., use the shared path between the sidewalk and lane, or pedestrians can jump into cars in the evacuation; (3) evacuees would change the direction (re-route) when the road is blocked or the bridge collapses or the road/bridge is congested; pedestrians would accelerate when the inundation comes closer. Furthermore, some evacuees might behave irrationally such as simply following others in a panic (Takabatake et al. 2017). As for (2), people evacuate under a hazardous environment. The large-magnitude earthquake can severely damage bridges and buildings, and building debris may block nearby roads (León and March 2016; Mostafizi et al. 2019b). The traffic capacity of a transportation network would reduce due to the seismic damage to the bridge (Jacob et al. 2014) or due to the road blockage caused by the debris from damaged infrastructure (Stern and Sinuany-Stern 1989; Murakami et al. 2014; Jacob et al. 2014). The reduction in traffic capacity could lead to a significant increase in evacuation time and thus life loss (Jacob et al. 2014; Mostafizi et al. 2017). Moreover, the traffic

information on the seismic damage to bridges and debris on roads may be available or unavailable, which would impact the evacuation behavior (e.g., the selection of evacuation path) and hence the evacuation performance.

Besides the above considerations about the multi-hazard evacuation environment and evacuation decision and behavior under a short time, some other important factors or mechanisms need to be considered realistically in the simulation. For instance, the variability in pedestrian speed would exist due to the different characteristics of pedestrians. The population size might be much larger than the residential population in the peak season when a large number of tourists visit the coastal community (Mostafizi et al. 2019b). All of these may have a high impact on the evacuation performance and therefore need to be taken into account in the simulation.

Table 3.1: Important factors or mechanisms that are usually neglected or simplified in existing agent-based evacuation models.

Simulation	Typically neglected or simplified factors or mechanisms in evacuation
Environment	Uncertain seismic damages to bridges and debris effect on roads
	Traffic information such as the accessibility of the bridge and road
	Population mobility (i.e., change of population due to factors such as tourism)
Behavior	Evacuation path selection, e.g., the shortest path, the evacuation route, etc.
	Variability in the pedestrian speed
	Speed adjustment according to traffic density ahead
	Interaction between evacuees, e.g., following behavior, pedestrian-vehicle interaction, etc.
	Interaction between evacuees and the environment, e.g., reroute behavior

However, existing agent-based evacuation models usually neglect or simplify many of the above important factors or mechanisms, which are summarized in Table 3.1. In the simulation of the evacuation environment, (1) the seismic damage to bridges is usually neglected or the quantification of the uncertainty in seismic damages is simplified by removing damaged bridges from the network (e.g., in Jacob et al. (2014); Mostafizi et al. (2017)), which is unrealistic. Moreover, the impact of debris from damaged infrastructure on road traffic is usually neglected; (2) it is typically assumed that the above traffic information (i.e., the accessibility of the bridge and road) is available in the simulation. However, the traffic information might be unavailable within a short time after the earthquake; (3) usually a relatively small number of evacuees (e.g., smaller than the

actual population) are considered while the population mobility is neglected (Goto et al. 2012; Imamura et al. 2012; Takabatake et al. 2017; Mostafizi et al. 2019b). The number of evacuees might be much larger in some peak seasons. Considering the highly nonlinear nature of the evacuation, results from simulations using a smaller than actual population may not give a good indication of the results under more realistic, large populations.

In the simulation of the evacuation decision and behavior using existing agent-based evacuation models, (1) it is usually assumed that evacuees search the shortest path in terms of distance or time and follow the shortest path to shelters in evacuation; however, some evacuees might follow evacuation routes to evacuate when such routes exist or some evacuees might behave irrationally such as simply follow others in a panic (Takabatake et al. 2018), especially for those who are unfamiliar with the evacuation (e.g., tourists); however, such irrational behavior is typically neglected in evacuation simulation, which is unrealistic because many people might not respond rationally within a short time frame, and evacuation simulation with bounded rationality such as evacuating only through the evacuation route or shortest path may not be able to capture the complex evacuation behavior; (2) for the evacuation on foot, usually all pedestrians are assigned the same pedestrian speed or they are classified into several groups based on the characteristics such as age and each group is assigned a certain pedestrian speed (Takabatake et al. 2017, 2018). However, variability exists in the pedestrian speed due to different characteristics of pedestrians; (3) the pedestrian speed is usually assumed to be constant throughout the evacuation while the speed adjustment according to the traffic density is neglected (Takabatake et al. 2017); (4) the interaction between individuals (pedestrians or cars) such as the following behavior is typically neglected. In the multimodal evacuation on foot and by car, usually, no interaction is considered between the pedestrian and car (Takabatake et al. 2017; Mostafizi et al. 2019b). This neglect is unrealistic because the pedestrian and nearby car might interact with each other (Jacob et al. 2014), e.g., both the pedestrian and car can use the shared path between the walkway and lane while it is usually assumed that they just travel within their own road spaces. Another type of interaction between the pedestrian and car is the pedestrian can jump into the nearby car in the evacuation, which is

typically not simulated; (5) the interactions between evacuees and the multi-hazard environment are usually neglected. For example, the traffic capacity reduction of the damaged bridge may cause traffic congestion and then slow down the evacuee's traveling speed, which would in turn impact the traffic congestion level of the damaged bridge. Moreover, typically evacuees would reroute if there is traffic congestion ahead (Goto et al. 2012; Takabatake et al. 2017), which would in turn impact the traffic congestion level. In addition, pedestrians would accelerate when they are told the inundation reaches the shoreline or when they see that the water comes closer, which would in turn impact the traffic congestion level of the link.

Also, various uncertainties associated with the evacuation need to be incorporated in simulation for a realistic simulation (Mostafizi et al. 2019b) and a more accurate evacuation risk assessment. However, many of them are usually neglected. For example, one approach to model the departure time is to assume an "all together" evacuation in which all evacuees start evacuating at a certain time (e.g., 0 min or 5 min) after the tsunami warning (Post et al. 2009); however, such a scenario has never occurred in past tsunami events.

3.2 Proposed agent-based tsunami evacuation model

To address the above limitations in the tsunami evacuation simulation, an improved agent-based tsunami evacuation model is developed by extending an agent-based modeling framework for a multimodal near-field tsunami evacuation simulation proposed in Wang et al. (2016) through incorporating the typically neglected or simplified but important factors and mechanisms. These improvements would better characterize the nature and dynamics of the evacuation system. Also, the improvements enable better modeling of the evacuee's decision and behavior, individual-level interactions among evacuees, and the evacuees' interactions with the damaged environment under the condensed time frame, especially under the near-field tsunami.

The proposed model (shown in Fig. 3.6) consists of the evacuation environment model (EEM), evacuation decision and behavior model (EBM), and evacuation performance model (EPM). In the EEM, (1) The uncertainties in the seismic damage to bridges and the road blockage due to debris

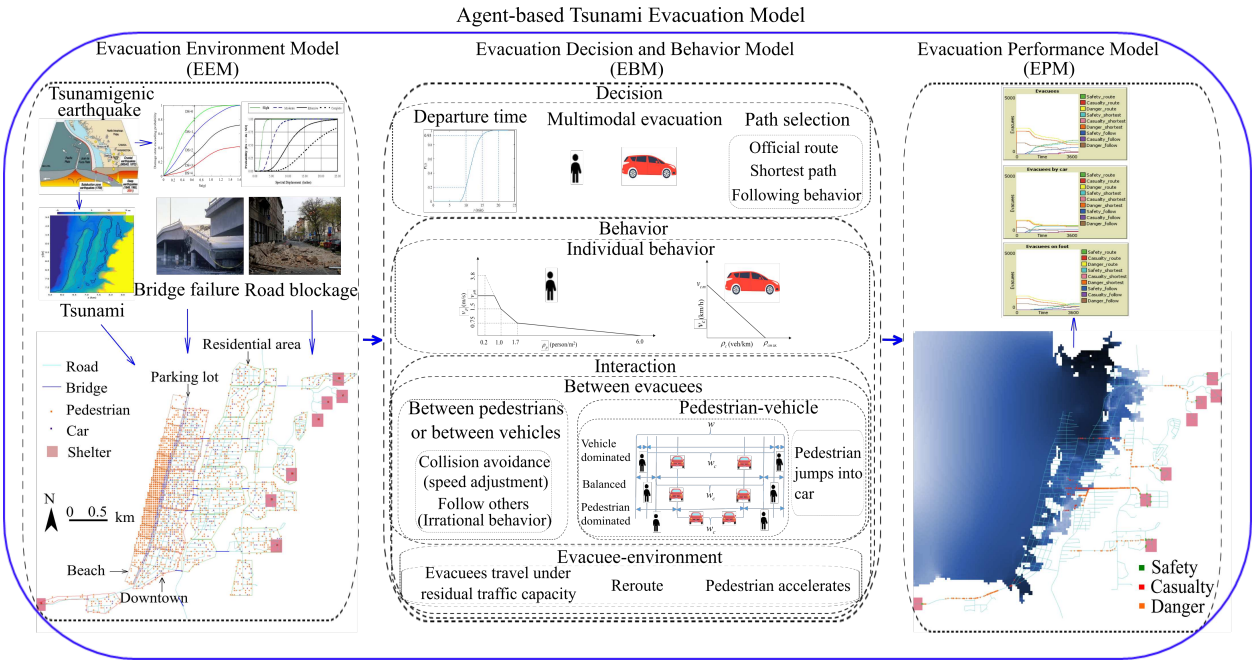


Figure 3.6: Illustration of the proposed agent-based tsunami evacuation model.

from damaged buildings are modeled; (2) the traffic information on the bridge damage due to the earthquake and road blockage caused by debris is considered to be available since such information is important and needs to be collected for guiding effective evacuation; (3) different population sizes are used to model the population mobility and capture the non-linearity of a tsunami evacuation. In the EBM, (1) the pedestrian speed variability, and speed adjustment for both the pedestrian and car according to traffic density are concurrently considered in the multimodal evacuation (i.e., evacuation on foot and by car); (2) different selections of evacuation path are considered, including following the evacuation route, searching the shortest path, and following behavior that is used to model the irrational behavior in the condensed time frame as well as the interaction between individuals (pedestrians or cars); (3) besides the speed adjustment and following behavior, two other interactions between evacuees are modeled, i.e., the pedestrian-vehicle interaction that is modeled by traffic stage transition determined by the volume ratio of the pedestrian and vehicle, and the pedestrian could jump into the nearby car in an evacuation; (4) the interactions between evacuees and the multi-hazard environment are modeled. The traffic capacity reduction of the damaged bridge would cause traffic congestion and hence slow down the evacuee's traveling speed, which

would in turn impact the traffic congestion level of the damaged bridge. Evacuees may change direction when the traffic congestion occurs ahead, which in turn impacts the traffic congestion and hence evacuees' traveling speeds. Pedestrians are expected to accelerate when they are told the inundation reaches the shoreline as well as when they see the inundation from some distance away, which would in turn impact the traffic congestion of the link and hence the pedestrian speed; (5) besides the uncertainty in seismic damages to bridges and road blockage due to debris from damaged buildings, various other uncertainties associated with the evacuation are explicitly taken into account.

To better use modern data with a high level of detail, capture the emergent phenomena, and tune the complexity of the agent's behavior, the agent-based tsunami evacuation model is developed in an integrated agent-based modeling environment (NetLogo) (Wilensky 2001). Fig. 3.7 shows a snapshot of the agent-based tsunami evacuation model interface in NetLogo.

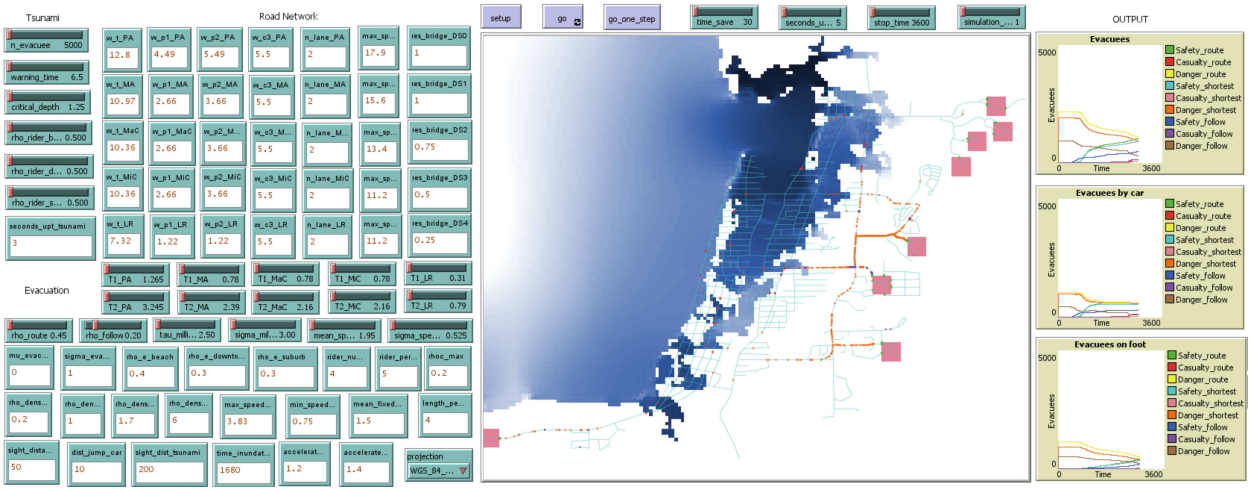


Figure 3.7: The agent-based tsunami evacuation model interface.

3.3 Modeling details

This section discusses the modeling details for EEM, EBM, and EPM as well as the general applicability of the proposed model.

3.3.1 Evacuation environment model (EEM)

The EEM simulates the earthquake-induced tsunami, transportation network, tsunami shelters, and population distribution.

Modeling earthquake-induced tsunami

For earthquake-induced tsunami, multiple hazards are considered, including the seismic and resulting tsunami hazards. As for the seismic hazard, either probabilistic or scenario earthquake can be considered (McGuire 2001; Adachi and Ellingwood 2010). The spatially distributed ground-motion intensities can be estimated by using proper ground-motion models (Campbell and Bozorgnia 2008; Abrahamson et al. 2018) and correlation models for the intensity measures (Loth and Baker 2013; Weatherill et al. 2015). The predicted intensity measures at each site will be used as inputs to estimate the probability of damage states for the corresponding bridges and buildings (FEMA 2009). As for the earthquake-induced tsunami, either probabilistic or scenario tsunami can be considered (Park and Cox 2016). The tsunami inundation is simulated using ComMIT/MOST, which is the tsunami model of NOAA Center for Tsunami Research (NCTR) and capable of simulating three processes of tsunami evolution: generation, propagation, and inundation (Titov and González 1997). In the model, three series of nested grids (A, B, and C) can be used to optimize the simulation for the three tsunami processes. The inundation model provides time histories of flow depth and speed at different locations of the area under investigation.

Transportation network

The transportation network used for evacuation is extracted from OpenStreetMap and saved as a shapefile in which intersections and road segments (or bridges) are represented by nodes and links (the number of the link is denoted as n), respectively. The characteristics of the transportation network such as the coordinates of intersections, cross-sections of roads, bridge types are included in the shapefiles.

The traffic capacity of the damaged link would reduce due to the seismic damage to the bridge as well as the road blockage caused by the debris from damaged buildings. Instead of simply

removing the damaged bridge from the network, its residual capacity is modeled and used for evacuation simulation. In particular, the fragility functions of bridges and buildings are used to estimate the corresponding probability of damage states (e.g., none, slight, moderate, extensive, and complete) (FEMA 2009). For bridges, different residual rates can be defined and used to estimate the residual traffic capacity based on different levels of seismic damage (Wang and Jia 2019a, 2020b), e.g., 100% (none/slight), 75% (moderate), 50% (extensive), and 25% (complete).

For roads, the debris effect is considered and simulated based on the study in Feng et al. (2020). The main ideas in Feng et al. (2020) are: (1) the debris effect is only considered when the roadway is within 10 m of a building which is higher than 25 m and severely damaged (e.g., complete damage in FEMA (2009)) by the earthquake; (2) the probability of road blockage on one lane due to debris increases linearly with the height of the building: 0% and 100% for the height of 25 m and over 75 m, respectively; (3) the length of the debris-affected region of the roadway is considered to be equal to the frontage of the building along the road. Then, the residual traffic capacity of the debris-affected road is calculated by (Feng et al. 2020)

$$C_w = C_0 \cdot \frac{r_s \cdot l_w + N_L \cdot (l - l_w)}{l} \cdot r_{VR} \tag{3.1}$$

where C_0 is the traffic capacity of the road without debris effect; l is the road length and l_w is the total length of the weaving area; N_L represents the number of lanes; r_s denotes the lane correction coefficient, i.e., 0.3, 1.8, 2.6, 3.4 and 4.0 for the road with 1, 2, 3, 4, and 5 lanes, respectively; r_{VR} is the volume ratio correction coefficient (Roess et al. 2011). Ultimately, the residual rate of the traffic capacity of the debris-affected road (i.e., C_w/C_0)) is obtained. Based on C_w/C_0, here the traffic capacity reduction is simulated by proportionally reducing the road width used by pedestrians and the traffic jam density for the pedestrian and car, respectively.

Considering the importance and feasibility of collecting the traffic information on the bridge damage due to the earthquake and road blockage caused by damaged buildings, it is assumed that this information is available for evacuees in the evacuation.

Tsunami shelter

Both horizontal and vertical evacuation shelters are regarded as effective to reduce the number of casualties (Mostafizi et al. 2019b). Typically, all the shelters are assumed to be capable of withstanding earthquake and tsunami hazard (Applied Technology Council 2019). For the capacity of the shelter, either a limited or an unlimited capacity can be used depending on the shelters (Mostafizi et al. 2019b; Goto et al. 2012).

Population distribution

The population distribution throughout the community can be of high spatiotemporal variability in terms of types (e.g., residents and tourists), genders, or ages (Mostafizi et al. 2017). Existing research usually considers a relatively small population in evacuation simulation (e.g., in Mostafizi et al. (2017); Priest et al. (2016)), which might be unrealistic. We consider population mobility and use different populations in simulation to investigate the impact of the population size (denoted n_e) on evacuation risk. For the evacuation by car, the evacuees are usually assumed to be in cars when evacuation starts (Mas et al. 2012), or change their classifications to cars after reaching the link of the transportation network (Wang et al. 2016), which might also be unrealistic. To simulate the evacuation by car more realistically, some parking lots are placed in the areas where cars are not likely to be accessed in seconds and simulate the process of evacuees reaching their cars on foot first and then evacuating by car. For the distribution scenario, normal and uniform distributions are used to simulate the uncertainty in the population distribution over the study regions.

3.3.2 Evacuation decision and behavior model (EBM)

In the EBM, the evacuation decision and behavior are simulated. The evacuation decision includes the departure time, evacuation mode, and evacuation path selection. The evacuation behavior consists of individual behavior, interactions between evacuees and between the evacuee and environment, and irrational behavior.

Evacuation decision-Departure time

The Rayleigh distribution suggested in Wang et al. (2016) is adjusted to characterize the uncertainty in departure time in which the probability of action for each evacuee is considered by

$$P(t) = \begin{cases} 0, & 0 < t < t_0 + \tau \\ 1 - e^{-(t-\tau)^2/(2\sigma_t^2)}, & t \geq t_0 + \tau \end{cases} \tag{3.2}$$

where t is the departure time after receiving the tsunami warning (unit: min); t_0 is the time when being notified the tsunami warning after the earthquake ground shaking (unit: min); τ is the delay time after receiving the tsunami warning (unit: min); σ_t is the scale parameter.

Evacuation decision-Multimodal evacuation

In the modeling of the multimodal evacuation (including on foot and by car), the proportion of evacuation by car (denoted p_c) is treated as uncertain considering that in an emergency the individual selection of evacuation mode (i.e., choose to evacuate on foot or by car) may vary for each evacuee. It is assumed that p_c follows the normal distribution with uncertain mean μ_c and constant standard deviation σ_c, and lies within some selected range.

In the simulation, variability is assigned to the pedestrian speed v_p to consider the uncertainty in the pedestrian's characteristics such as age and physical condition (Wang et al. 2016). v_p is assumed to follow a truncated within (0.75, 3.83) (unit: m/s) normal distribution with mean μ_p and standard deviation σ_p (Wang et al. 2016; Goto et al. 2012). Here, $v_p = 0.75$ m/s is considered as the lowest pedestrian speed (slow walk) and 3.83 m/s is considered as the highest pedestrian speed (fast run) (Web Marketing Associates 2010). Note that the pedestrian speed could be modeled using the probability distribution based on the actual age groups (including residents and tourists) when such data is available.

Evacuation decision-Evacuation path selection

Three types of evacuation path selection are considered, i.e., using the evacuation route, searching the shortest path, and following behavior. Considering the selection of the evacuation path might vary in an emergency, the proportion of each type is modeled as uncertain.

As for the evacuation using the evacuation route, evacuation routes are typically identified based on the evacuation map and verified by Google Street View imagery (Lonergan et al. 2015). Evacuation zones throughout the community are created such that the evacuees in the same evacuation zone can use the same evacuation route to evacuate. Some considerations about the creation and use of evacuation zones are: (1) the centroids of the two zones on opposite sides of some route almost have the same distance to the route; (2) in each evacuation zone, the evacuees who decide to use evacuation routes would first move to the closest route and then follow the route to the shelter; (3) if the bridge on the route collapses, the evacuees who plan to use the route directly search the shortest path rather than use the route.

For the evacuation using the shortest path, the closest shelter in terms of distance is searched using the shortest path algorithm such as the A* algorithm (Anguelov 2011).

Some evacuees may panic and have the following behavior in evacuation under the condensed time frame, especially for those who are unfamiliar with the tsunami evacuation (e.g., tourist) (Takabatake et al. 2017). It is assumed that a small percentage of evacuees (both on foot and by car) respond in this manner, i.e., the pedestrian and car would simply follow the pedestrian and car ahead, respectively. The details of this irrational behavior will be presented later.

Evacuation behavior-Individual behavior

Speed adjustment for both the pedestrian and car according to the traffic density ahead is incorporated in the multimodal evacuation model. The pedestrian speed v_p adjusts according to the surrounding pedestrian density ρ_p (Goto et al. 2012). Based on the speed-density relationship in Goto et al. (2012), we introduce a pedestrian speed adjustment model which is shown in Fig. 3.8. Unlike Goto et al. (2012) where the pedestrian speed ranges from the slow walk (i.e., 0.75 m/s) to normal walk (i.e., 1.5 m/s), here the pedestrian speed covers slow walk, normal walk, and fast

run (i.e., 3.83 m/s). Also, here the speed-density relationship is considered to be linear rather than nonlinear due to the lack of data.

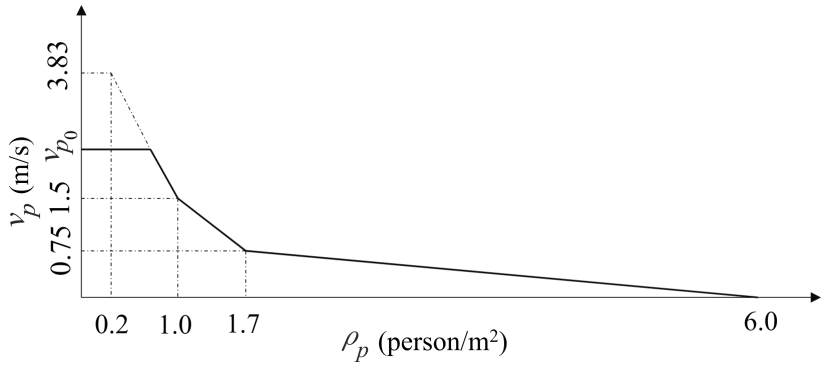


Figure 3.8: The relationship between the pedestrian speed and pedestrian density ahead (adjusted from Goto et al. (2012)).

In the model, v_{p_0} represents the preferred pedestrian speed, and ρ_p denotes the pedestrian density 4 m ahead along the evacuation path. According to the model, the pedestrian speed will reduce as the pedestrian density increases.

Car speed v_c is adjusted according to the car density ρ_c within the free run-length ahead of it. Here, the well-known Greenshields' model of speed and density (Greenshields 1935) is used to approximate the car speed adjustment

$$v_c = v_{cm}\left(1 - \frac{\rho_c}{\rho_{cm}}\right) \tag{3.3}$$

where v_{cm} is the maximum speed limit and ρ_{cm} is the maximum density (i.e., jam density).

Evacuation behavior-Interaction

Interactions between evacuees The interaction between pedestrians or cars is simulated by the speed adjustment, which was discussed in the individual behavior, and by the irrational behavior (i.e., following behavior), which will be presented later.

Two types of interactions between the pedestrian and car are simulated in the EBM. One type is explicitly simulated by introducing dynamic traffic stage transitions based on the volume ratio of

the pedestrian and car. Here the dynamic traffic stage transition model is established by adjusting the model in Mauro et al. (2014) to make it more general. Compared to the model in Mauro et al. (2014), which only uses one variable to represent the total road width, the adjusted model introduces several other variables to represent the different widths and the number of lanes to make the model applicable to different types of roads. The adjusted model has the following form

$$\begin{aligned} V_p/V_v \leq T_1 \quad &\rightarrow \quad w_p = w_{wmin}\,; \quad w_v = w - w_{wmin} \\ T_1 < V_p/V_v \leq T_2 \quad &\rightarrow \quad w_p = w_w\,; \quad w_v = w - w_w \\ V_p/V_v > T_2 \quad &\rightarrow \quad w_p = w - w_r \times n_l\,; \quad w_v = w_r \times n_l \end{aligned} \tag{3.4}$$

where V_p and V_v represent the pedestrian volume and vehicle volume (unit: person) on the same link, respectively; for comparison, one vehicle can be assumed to be equivalent to some number of pedestrians based on the average space occupied; w_p and w_v represent the road widths occupied by the pedestrian and vehicle (unit: m), respectively; w is the total road width (unit: m); w_{wmin} is the minimum road width used by the pedestrian (unit: m); w_w is the road width that can be used by the pedestrian, including sidewalks, multi-use path, and roadway shoulders (unit: m); w_r is the width of vehicle lane (unit: m); n_l is the number of vehicle lanes occupied by the vehicle, which are typically smaller than the total number of vehicle lanes in the car-dominated stage; T_1 and T_2 are the thresholds for different traffic stages.

The other type of pedestrian-vehicle interaction is the pedestrian jumps into the nearby car (e.g., within 10 m) after walking and then evacuates by car. This interaction is considered to occur when: (1) the pedestrian dominates the traffic; (2) no traffic congestion exists for the car; (3) there is at least one car traveling on the road link. It is assumed that no more than one pedestrian can jump into the same car.

Interactions between the evacuee and the environment Under the multi-hazard environment, evacuees would interact with the environment. Here, three types of such interactions are modeled, i.e., (1) the traffic capacity reduction of the damaged bridge due to seismic damage or the road

blockage would cause traffic congestion and hence slow down the evacuee's traveling speed, which in turn impacts the traffic congestion level of the damaged bridge; (2) evacuees would change direction (reroute) when the bridge collapses due to the seismic damage, the road is blocked by debris from the damaged building, or the road/bridge is congested (it is assumed that the sight distance is 50 m during daytime based on the study in Jacob et al. (2014); Aguilar et al. (2017, 2019)). The reroute behavior due to the traffic congestion would in turn change the nearby traffic congestion level and further impact evacuees' traveling speeds; (3) pedestrians are considered to accelerate when the tsunami inundation comes closer. The pedestrian acceleration would impact the traffic such as the congestion level of the link, which would in turn impact the pedestrian speed. For (2), the evacuees that use the evacuation route or the shortest path would search the new evacuation path which excludes the collapsed bridge, the blocked road, and the congested links. Once the evacuation path is determined, they would evacuate following the new path. The evacuees with the following behavior would reroute to other passable links and continue following others to evacuate. For (3), pedestrians are considered to accelerate when the inundation reaches the shoreline and further accelerate when they see the inundation from 200 m far away if they evacuate in the daytime. The acceleration is simulated by scaling the preferred pedestrian speed (i.e., v_{p_0}) by a constant that is greater than 1 (denoted ρ_a) in the pedestrian speed-density model. It is assumed that the scaling factor is 1.2 (denoted $\rho_{a_1} = 1.2$) and 1.4 (denoted $\rho_{a_2} = 1.4$) for the above two accelerations, respectively.

Evacuation behavior-Irrational behavior

As mentioned in the evacuation path selection, some evacuees may behave irrationally and have the following behavior to evacuate rather than evacuate with purposeful behaviors (i.e., using the evacuation route or the shortest path) in the condensed time frame. Considering the tsunami evacuation program and/or evacuation drill are commonly held for the residents in the tsunami-prone community and the tsunami evacuation knowledge (e.g., evacuation map) is typically provided to the tourists, it is assumed a small uncertain proportion of evacuees (including residents and tourist) evacuate by simply following others. As for the following behavior, two rules are adjusted and

used in our model based on the study in Takabatake et al. (2017). The evacuees with the following behavior would count the number of evacuees of the same type (evacuation on foot or by car) on each road when they reach an intersection and choose the road taken by the largest number of evacuees of the same type (no congestion), i.e., "following other individuals". When no evacuee exists on each road, the evacuees with the following behavior would choose the road that can lead them inland, i.e., "going inland". Note that, the evacuees with the following behavior might actually follow the evacuees using the evacuation route or the shortest path or follow each other, or just follow the road that can lead them to the inland. Ultimately, the evacuees with the following behavior might reach the shelter or higher land.

3.3.3 Evacuation performance model (EPM)

The evacuation performance can be measured using different quantities of interest such as casualty, evacuation time, etc. Typically, the evacuation performance indicator associated with the loss of life such as the casualty rate (i.e., the proportion of casualties to the total number of evacuees) is used. The flow characteristics such as depth and velocity determine the casualty through impacting the human body (Lind et al. 2004; Jonkman et al. 2008), while many other factors including evacuee's age, gender, and mental and physical state also have an impact on the casualty in tsunami inundation (Yeh 2010). Usually, critical water depth is used to approximate the casualty without considering other factors (Wang et al. 2016; Mostafizi et al. 2017), or the casualty probability is estimated as a function of depth and velocity, which are limited to given intervals (Mas et al. 2012). In this research, the evacuee is considered to be a casualty when the water depth is larger than the given critical depth of h_c. The uncertainty in h_c is modeled to consider the varied characteristics of evacuees.

3.3.4 General applicability of the proposed agent-based model for tsunami evacuation simulation

The proposed agent-based tsunami evacuation model is developed with a modular programming paradigm and sub-models (i.e., the EEM, EBM, and EPM) including components in each sub-model. These components are general and can capture the nature of tsunami evacuation through characterizing the evacuation system dynamics and modeling the individual-level interactions among evacuees and the evacuees' interactions with the multi-hazard environment. Due to the above characteristics, the proposed agent-based evacuation model is general, and each sub-model can be adapted to different settings by changing/updating the EEM, EBM, and EPM accordingly. For example, for a different site, we can update the EEM by using the seismic hazard model for the site to simulate the earthquake, using numerical models such as ComMIT/MOST along with topography for the site to simulate tsunami generation and propagation, by using the corresponding ground motion prediction equations and fragility functions of roads and bridges to estimate and update the seismic damages, and by updating the transportation network, shelters, and the population distribution throughout the community. When modeling the departure time, evacuation mode, and evacuation speed in the EBM, different distributions of evacuation model parameters could be updated to model the uncertainties in the evacuation decision and behavior based on the characteristics of the population. In the EPM, depending on the performance of interest, besides the casualty rate, other performance quantities could be also used to measure the evacuation performance. Therefore, the proposed agent-based tsunami evacuation model can be used in different geographic locations for tsunami evacuation simulation.

3.4 Illustrative example: Simulation of tsunami evacuation in Seaside, Oregon using the proposed agent-based model

The proposed agent-based evacuation model is applied to tsunami evacuation simulation for Seaside, Oregon.

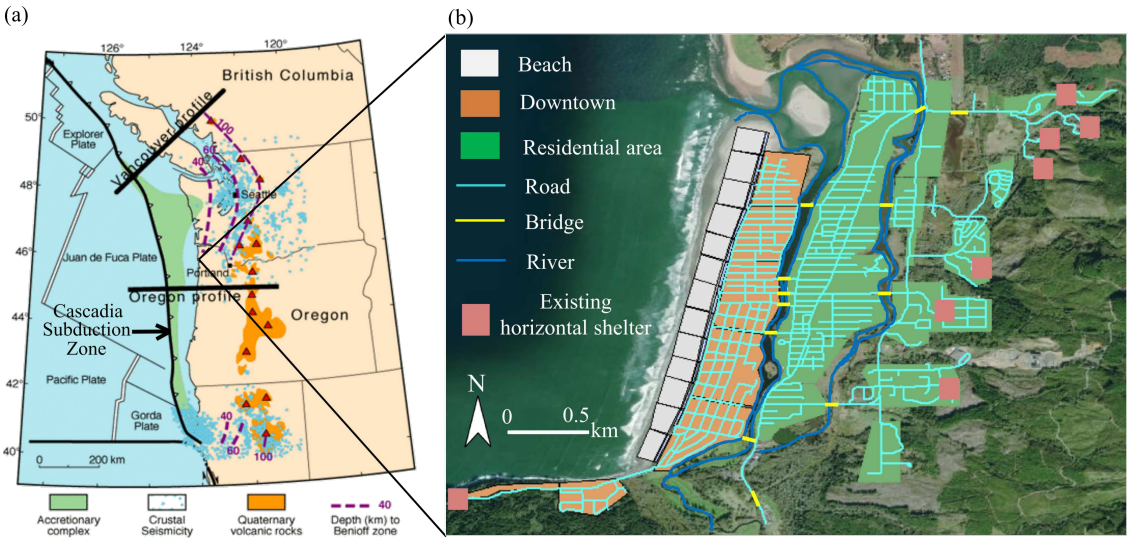


Figure 3.9: Illustration of (a) Cascadia Subduction Zone (CSZ) (USGS 2020a), and (b) Seaside, Oregon.

3.4.1 Study area

The coastal community Seaside, Oregon (shown in Fig. 3.9(b)) is selected as the study area, on which many tsunami evacuation studies have been focused (Wang et al. 2016; Mostafizi et al. 2017, 2019b). Seaside is regarded as one community with a high tsunami evacuation risk considering: (1) its high risk to the seismic and near-field tsunami hazards due to the proximity to the Cascadia Subduction Zone (CSZ, shown in Fig. 3.9(a)) (González et al. 2009; Priest et al. 2016; Mostafizi et al. 2017); (2) its high vulnerability to tsunami inundation due to the fairly flat topography with two rivers flowing through the city, the relatively far shelters (more than 1.5 km), and the bottlenecks in the transportation network (road network in this case) caused by the ten bridges over the two rivers (Mostafizi et al. 2017).

3.4.2 Agent-based tsunami evacuation model details

The agent-based model for tsunami evacuation simulation in Seaside, including evacuation environment, evacuation decision and behavior, and evacuation performance, will be discussed in the following sections. Also, the proposed improvements to each component will be described in detail.

Evacuation environment

We consider the seismic hazard and earthquake-induced tsunami generated from the 1000 km long CSZ. The CSZ stretches from northern Vancouver Island to Cape Mendocino in northern California. The last great seismic event on the CSZ is full-rupture and occurred on January 26, 1700, with a moment magnitude (M_w) estimated between 8.7 and 9.2, and a slip of 19 m (Satake 2003). The average return period for the full-length CSZ event is 530 years. Despite low levels of seismicity since the last megathrust earthquake, it was reported that partial rupture events on the north or south margins of the CSZ became more frequent (Goldfinger et al. 2012; Atwater and Griggs 2012; Park et al. 2017). There is a 9.0 M_w earthquake with about 10% probability of occurrence at the CSZ over a 35-year time frame (Goldfinger et al. 2012). In this research, the historical seismic event in 1700 is used as the hypothetical hazard scenario, under which $M_w = 9.0$ and the focal depth of 40 km are considered.

The road network consists of 700 nodes and 896 links (i.e., $n = 896$ roads and bridges). Fig. 3.10 shows the existing road network. The road cross-section standards corresponding to the federal functional classification of roads throughout Seaside (Clatsop County 2019) can be found in the typical design of streets in Clatsop County City of Seaside (2010). Table 3.2 summarizes the parameters used to determine the road widths occupied by the car and pedestrian for the existing road network (City of Seaside 2010). In the modeling of the pedestrian-vehicle interaction, it is assumed that one car is equivalent to ten pedestrians in terms of space.

Table 3.2: The parameters used to determine the road widths occupied by the car and pedestrian for the existing road network.

Functional class	w	w_{wmin}	w_w	w_r	n_l
Principle Arterial	12.80	4.49	5.49	2.75	2
Minor Arterial	10.97	2.66	3.66	2.75	2
Major Collector	10.36	2.66	3.66	2.75	2
Local Road	7.32	1.22	1.22	2.75	2

Following the approach in Lonergan et al. (2015), evacuation routes are identified based on the evacuation map (The Oregon Department of Geology and Mineral Industries 2013) and official

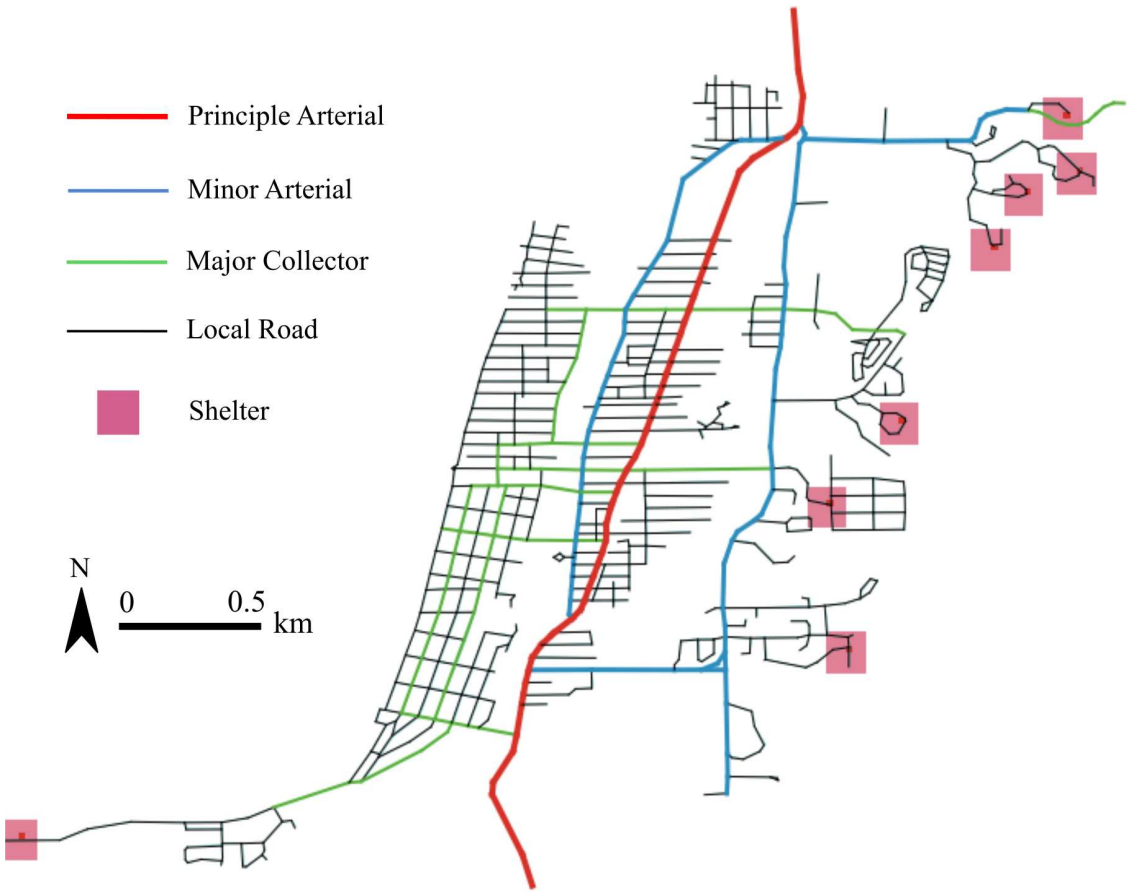


Figure 3.10: The existing road network in Seaside, Oregon.

shapefiles (Claptsop County 2008). In the evacuation map (The Oregon Department of Geology and Mineral Industries 2013), no exact evacuation routes are provided but only black arrows are used to indicate the evacuation direction. Evacuation routes are defined in the shapefiles (Claptsop County 2008), although the data might not be up-to-date. We identify the evacuation route by combining the evacuation direction with the evacuation routes from the shapefiles. Note that one additional evacuation route in the downtown is added that goes through the bridge over the river considering that the nearby evacuees would intuitively choose this route to go across the river (Neis et al. 2015). The identified evacuation routes are shown in Fig. 3.11.

Inspired by the evacuation map (The Oregon Department of Geology and Mineral Industries 2013) and the beat-the-wave evacuation map for tsunami hazards in Seaside (Priest et al. 2016),

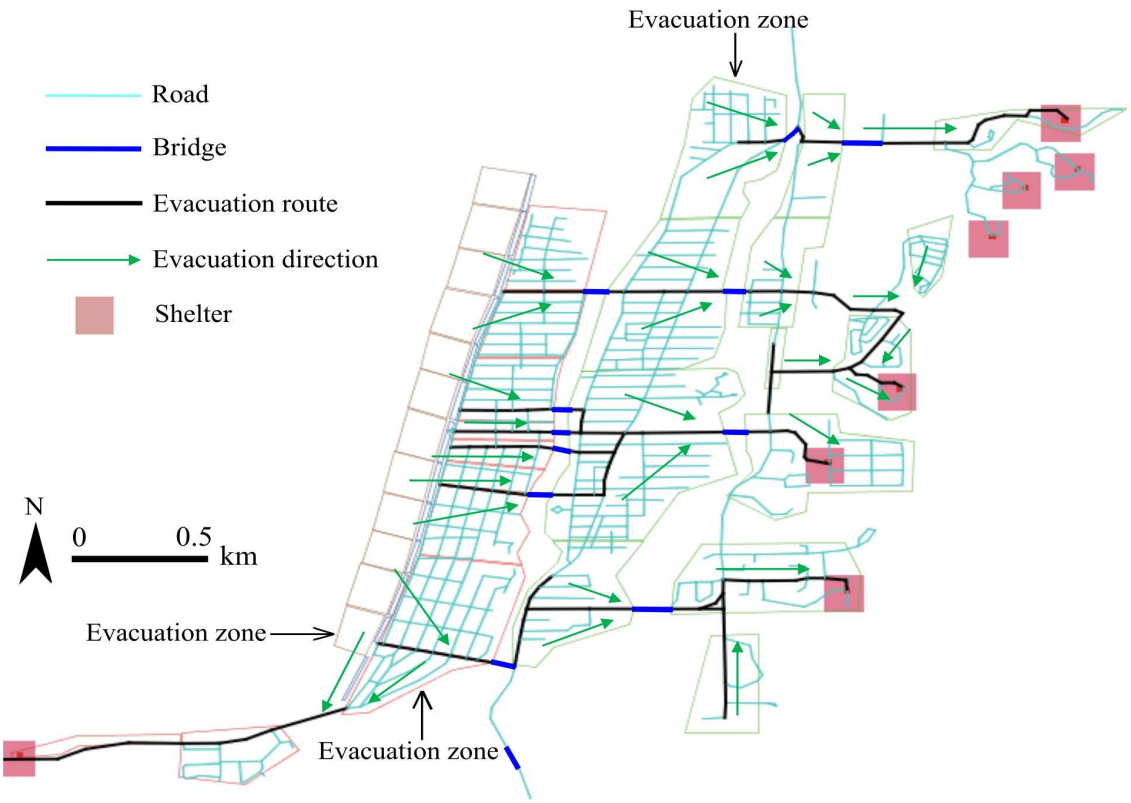


Figure 3.11: Tsunami evacuation routes and zones in Seaside, Oregon.

the evacuation zone and evacuation direction are created throughout the community (shown in Fig. 3.11) to determine the selection of the evacuation route by evacuees in each zone as well as the evacuation flow direction in the evacuation model. Note that in The Oregon Department of Geology and Mineral Industries (2013) no evacuation zone is provided and therefore the evacuation direction is not designed for any specific evacuation zone. In Priest et al. (2016), both evacuation zone and the corresponding evacuation direction are created where the evacuation zones have complex shapes (determined from the calculation of so-called least-cost distance). In the current study, both the evacuation route and corresponding evacuation direction are established, but they are established in a way that is different from The Oregon Department of Geology and Mineral Industries (2013) and Priest et al. (2016). In particular, from the point of view of capturing the more possible selection and use of the evacuation route, the current study takes into account the following considerations about the creation of the evacuation zone and use of the evacuation route: (1) the

region located between two main evacuation routes is divided into two evacuation zones such that the distance between each zone (centroid) and the adjacent route is close; (2) in each evacuation zone, the evacuees who decide to use evacuation routes will first move to the closest evacuation route and then follow the route to the shelter; (3) when the bridge on some route collapses, the evacuees who plan to use the evacuation route would search the shortest path for evacuation.

To consider the impact of the earthquake-induced damage to bridges and road blockage due to debris from damaged buildings on evacuation, the fragility functions of bridges and buildings in HAZUS (FEMA 2009) are used to estimate the probabilities for seismic damages to bridges and buildings, respectively. In HAZUS, spectral acceleration (S_a) and spectral displacement (S_d) are used as intensity measures in the fragility curves for bridges and buildings, respectively. Since S_d can be calculated when S_a and the structural period is known (FEMA 2009), here only S_a needs to be estimated for bridges and buildings using the corresponding fragility curves. Based on Stewart et al. (2015), the ground-motion prediction equations (GMPEs) in Campbell and Bozorgnia (2008) are selected to estimate the S_a at each bridge site and building site, respectively. According to HAZUS FEMA (2009), five damage states (i.e., none, slight, moderate, extensive, and complete) are defined for the bridge. Except for the bridges with complete damage, the reduction of traffic capacity of links due to the seismic damage is considered only for the car since evacuation by car is more likely to be affected by the damage of links compared to evacuation on foot. The residual traffic capacity of the bridge is assumed to be 100% (none/slight), 75% (moderate), 50% (extensive), and 0% (complete) of that without the seismic damage. The traffic capacity reduction of the damaged bridges for the car is modeled by reducing the jam density in the speed adjustment model.

For the shelters, we adopt the eight horizontal shelters outside the inundation zone identified by the Oregon Department of Geology and Mineral Industries (Priest et al. 2013), which are shown in Fig. 3.9(b). It is assumed that all the shelters can hold the evacuees that reach them.

We use the population density model in Mostafizi et al. (2017) to simulate the population distribution throughout the study area, which corresponds to the noontime of some weekends in the

summer. The evacuees including residents and tourists are distributed across the beach, downtown, and residential area with a proportion of $\rho_1 = 40\%$, $\rho_2 = 30\%$, and $\rho_3 = 30\%$, respectively. Both the populations on the beach and in the downtown are assumed to distribute following the normal distribution around the corresponding centroid of each region. The population is distributed uniformly throughout the residential area. Note that the population distribution throughout some sub-area (e.g., residential area) could be modeled through estimating the number of people that live in each building when the relevant information is available (Wang et al. 2021). As for the population size, the up-to-date residential population of Seaside is 6795 in 2018 according to U.S. Census (U.S. Census Bureau 2018); however, the net daytime residential population can decrease to around half of the population (Sleeter and Wood 2006) while the number of tourists can be up to 10,000 per day in the peak summer (Mostafizi et al. 2017), i.e., population mobility exists. We select $n_e = 5000$ that corresponds to the early summer to illustrate the tsunami evacuation simulation using the proposed agent-based model. The impact of population mobility on evacuation will be considered in evacuation risk assessment in Chapter 4.

To simulate the evacuation by car more realistically, one parking lot is placed beside each subregion of the beach, which is used to park for some of the evacuees on the beach (denoted as the pedestrian II). For the evacuation by car in the two regions other than the beach, cars with four evacuees per car are distributed throughout the regions considering the easier access to their cars for the evacuees in these two regions. The classification of different regions and corresponding population distributions are shown in Fig. 3.12.

Evacuation decision and behavior

For the modeling of the departure time described in Eq. (3.2), t_0 is considered to follow the uniform distribution on the interval [3, 10] (unit: min) for the local tsunami (U.S. Indian Ocean Tsunami Warning System Program (US IOTWS) 2007); τ and σ_t are considered to follow the uniform distribution on the interval [0, 5] (unit: min) and [1, 5], respectively.

In the modeling of the multimodal evacuation, the uncertainty in p_c is modeled by assuming it follows a truncated within (0, 1) normal distribution with mean μ_c and standard deviation σ_c. It is

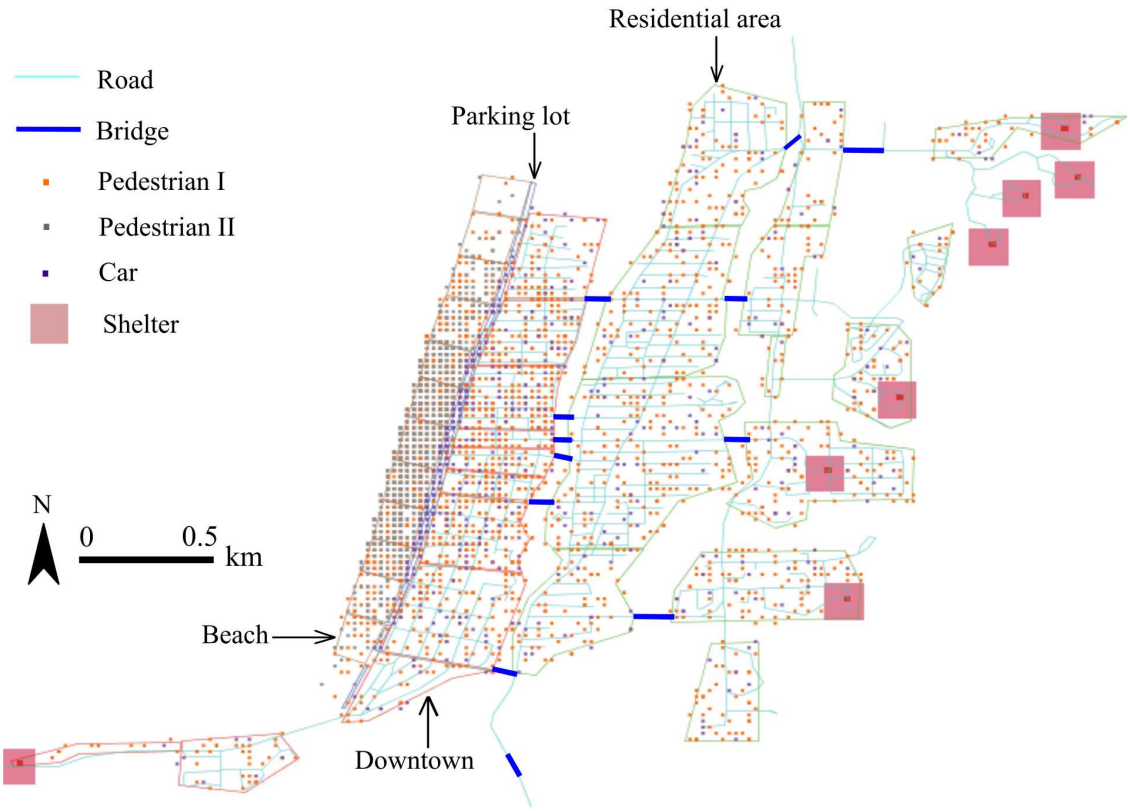


Figure 3.12: Population distribution in Seaside, Oregon at the noontime of some weekends in the summer.

further assumed that μ_c follows the uniform distribution on the interval [0, 1] and $\sigma_c = 0.15$. As for the evacuation by car, it is assumed that four passengers take one car. In the calculation of the pedestrian volume and car volume, one car is assumed to be equivalent to ten pedestrians in terms of space occupied.

The pedestrian speed v_p is considered to follow the truncated within (0.75, 3.83) (unit: m/s) normal distribution with uncertain mean μ_p and uncertain standard deviation σ_p. It is assumed that μ_p follows the uniform distribution on the interval [1.22, 2.68] (unit: m/s), where 1.22 m/s corresponds to the moderate pedestrian speed (Langlois et al. 1997) and 2.68 m/s the moderate running speed (Web Marketing Associates 2010). Due to the variability in the population distribution, σ_p might vary significantly. For example, σ_p is $0.05 \sim 0.4$ m/s in Yosritzal et al. (2018) and $0.18 \sim 0.78$ m/s in Fraser et al. (2014) for the walking speed. For the running speed, σ_p is 1.02 m/s in Fraser et al. (2014). Based on the above research, σ_p is considered to follow the uniform

distribution on the interval [0.05, 1] (unit: m/s). Note that the exact probability distributions considering the actual age groups (including residents and tourists) could be used to model v_p and the corresponding distribution parameters (i.e., μ_p and σ_p) when the data on the age group is available.

As for the evacuation path selection, it is assumed that a small proportion of evacuees (denoted p_f) have following behaviors and p_f is uniformly distributed on the interval [0.1, 0.3]. The proportion of evacuees that use the evacuation route (denoted p_r) follows the uniform distribution on the interval [0.3, 0.6]. The evacuees with a proportion of $p_s = 1 - p_f - p_r$ use the shortest path to evacuate.

To model the evacuation by car more realistically, instead of directly modeling the evacuees as car agents, the evacuation on foot before the evacuees reach their cars is also modeled. Essentially, the evacuees first walk to their cars at the assigned waking speeds, and then, the evacuation is modeled by the cars' movements once they arrive at their cars. For the maximum car speed limit in the well-known Greenshields' model that is used to simulate the car speed adjustment, here $v_{cm} = 40$, 35, 30, and 25 (unit: mph) for "Principle Arterial", "Minor Arterial", "Major Collector", and "Local Road" (Oregon Department of Transportation 2020), respectively; $\rho_{cm} = 200$ veh/km is considered for the links without traffic capacity reduction based on the study in Mostafizi et al. (2017, 2019b).

Evacuation performance

The fixed critical depth h_c is usually used to approximate the casualty in previous research, e.g., $h_c = 0.5$ m (Sugimoto et al. 2003), $h_c = 1$ m (Goto et al. 2012), or $h_c = 2$ m (Yeh 2014). To model the uncertainty in h_c for evacuation performance evaluation (i.e., casualty estimation), h_c is considered to follow a uniform distribution on [0.5, 2] (unit: m), which is applicable to both evacuation on foot and by car.

3.4.3 Evacuation simulation

We consider that the evacuation lasts for one hour starting from the occurrence of the earthquake. The tsunami evacuation simulation using the proposed agent-based model is implemented

in NetLogo (run from R using the package "RNetLogo" (Thiele 2014, 2017)). The proposed agent-based evacuation model is run with a time step of one second (i.e., 3600 time steps for each simulation).

Table 3.3: Key continuous uncertain model inputs in the tsunami evacuation simulation.

Input	Distribution	Parameter 1	Parameter 2
t_0	Uniform	3	10
t	Rayleigh	[0, 5]	[1, 5]
p_c	Truncated Gaussian	[0, 1]	0.15
$T_{1_{PA}}$	Uniform	1.00	1.53
$T_{2_{PA}}$	Uniform	2.30	4.19
$T_{1_{MA}}$	Uniform	0.59	0.97
$T_{2_{MA}}$	Uniform	1.64	3.14
$T_{1_{Mac}}$	Uniform	0.59	0.97
$T_{2_{Mac}}$	Uniform	1.53	2.79
$T_{1_{LR}}$	Uniform	0.27	0.38
$T_{2_{LR}}$	Uniform	0.54	1.04
v_p	Truncated Gaussian	[1.22, 2.68]	[0.05, 1]
p_f	Uniform	0.1	0.3
p_r	Uniform	0.3	0.6
h_c	Uniform	0.5	2

Table 3.3 presents the key continuous uncertain model inputs in the tsunami evacuation simulation, where $T_{1_{PA}}$, $T_{2_{PA}}$, $T_{1_{MA}}$, $T_{2_{MA}}$, $T_{1_{Mac}}$, $T_{2_{Mac}}$, $T_{1_{LR}}$, and $T_{2_{LR}}$ denote the thresholds in Eq. (3.4) and respectively correspond to the road class "Principle Arterial", "Minor Arterial", "Major Collector", and "Local Road". For uniform distribution, "Parameter 1" and "Parameter 2" correspond to the lower bound and upper bound, respectively. For Rayleigh distribution, "Parameter 1" and "Parameter 2" represent τ and σ_t, respectively. For Truncated Gaussian distribution, "Parameter 1" and "Parameter 2" are the mean and standard deviation of the corresponding normal distribution, respectively. p_c and v_p lie within (0,1) and (0.75,3.83) (unit: m/s), respectively. In addition, uncertain model inputs include those associated with seismic damages to bridges and buildings, intensity measures at bridge sites and building sites, and the location of the population.

In this example, one single simulation with 5000 evacuees is run, in which the mean value of each uncertain input is selected.

3.4.4 General tsunami evacuation process simulated using the proposed agent-based tsunami evacuation model

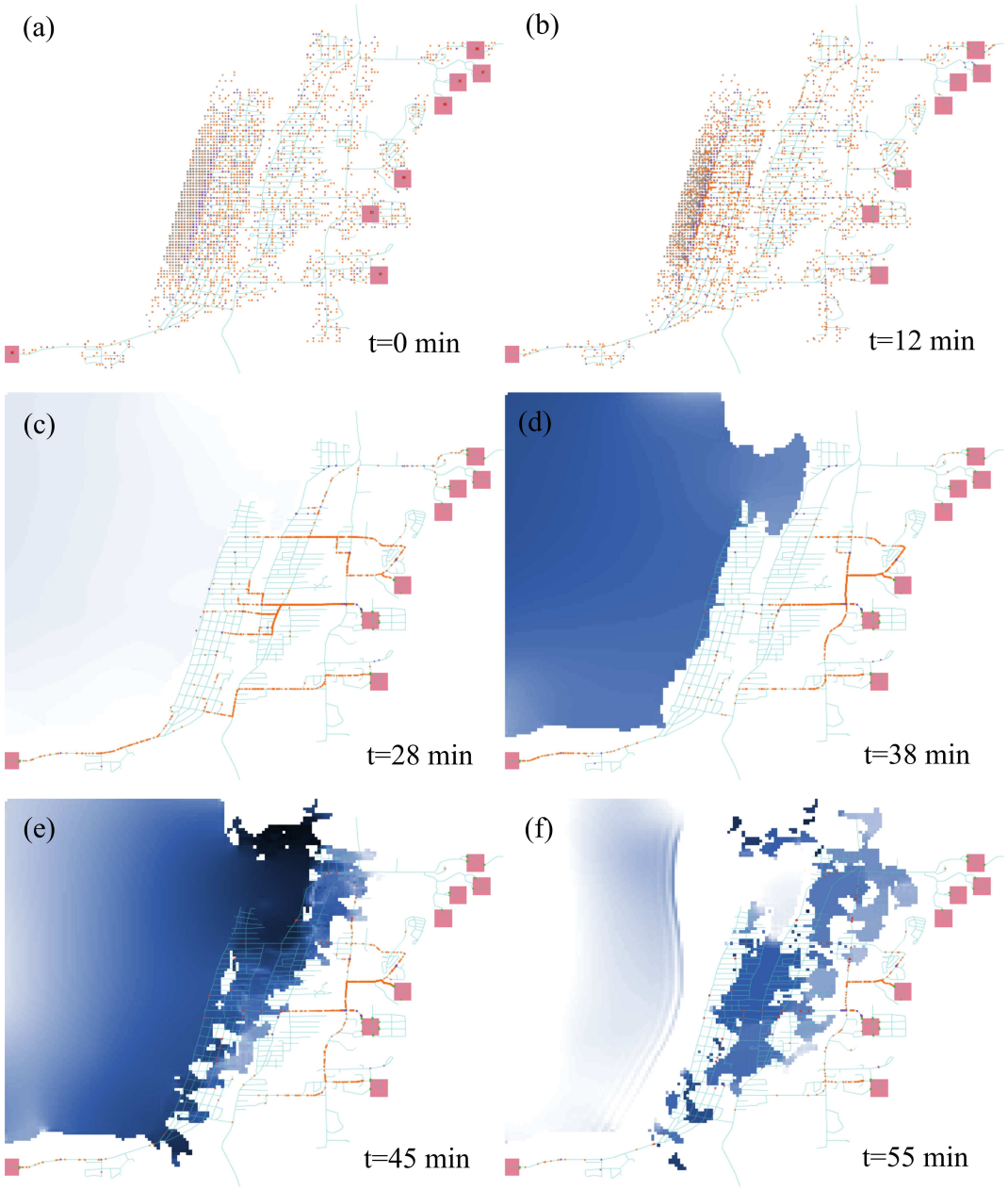


Figure 3.13: The general tsunami evacuation process simulated using the proposed agent-based tsunami evacuation model at (a) $t = 0$ min, (b) $t = 12$ min, (c) $t = 28$ min, (d) $t = 38$ min, (e) $t = 45$ min, and (f) $t = 55$ min.

The general tsunami evacuation process simulated using the proposed agent-based tsunami evacuation model is shown in Fig. 3.13. At the end of the initial strike of the earthquake (i.e., $t = 0$ min) shown in Fig. 3.13(a), the evacuees including pedestrians and cars are distributed throughout the community. The pedestrian I represented by the orange point evacuates on foot. The pedestrian II marked by the grey point is only distributed on the beach and first walks to the car in the parking lot, then evacuates by car. The car is represented by the violet point. Fig. 3.13(b) shows that many of the evacuees have started evacuation after 12 min. Around $t = 28$ min, shown in Fig. 3.13(c), the tsunami inundation almost goes across the beach. Most of the evacuees are on the way to their destinations, while some of the evacuees have arrived at the shelters, and these evacuees are represented by green points. Fig. 3.13(d) shows the tsunami starts to inundate the city after 38 min. The casualties represented by red points occur when the inundation depth exceeds the critical depth. Fig. 3.13(e) shows that the tsunami inundation crosses the Necanicum River and is moving further inland after 45 min when more evacuees become casualties. At $t = 55$ min, shown in Fig. 3.13(f), the tsunami inundation reaches the run-up limit and most of the evacuees reach the shelters.

3.5 Summary

An improved agent-based evacuation model is developed for more realistic tsunami evacuation simulation after introducing the benefits of the ABM over other modeling techniques (i.e., GIS, DEM, CA, and SD) and the limitations of existing agent-based models. The proposed model consists of the evacuation environment model (EEM), evacuation decision and behavior model (EBM), and evacuation performance model (EPM). Compared to existing agent-based models, the proposed model incorporates some typically neglected or simplified but important factors and mechanisms in evacuation, including (1) the traffic capacity is reduced by the bridge damage due to the earthquake or by the road blockage due to the debris from damaged buildings; (2) several different population sizes are used to model the population mobility and capture the non-linearity of tsunami evacuation; (3) a multimodal evacuation model is proposed that explicitly considers

the pedestrian speed variability, speed adjustment for both the pedestrian and car according to traffic density, and the pedestrian-vehicle interaction that is modeled by traffic stage transitions; (4) different evacuation path selections are considered, including following the evacuation route, searching the shortest path, and following behavior that is used to simulate the irrational behavior in the condensed time frame as well as the the interaction between individuals (pedestrians or cars); (5) in addition to the speed adjustment, following behavior, and pedestrian-vehicle interaction, the pedestrian could jump into the nearby car is used to model the interactions between evacuees; (6) the interactions between the evacuee and multi-hazard environment are modeled. The traffic capacity reduction of the damaged bridge would induce traffic congestion and hence slow down the evacuee's traveling speed, which would in turn impact the traffic congestion level of the damaged bridge. Evacuees would change direction when the traffic congestion occurs ahead. Pedestrians accelerate when they are told the inundation reaches the shoreline as well as when they see the inundation from some distance away; (7) various uncertainties associated with the evacuation such as that in seismic damages to bridges and road blockage due to debris from damaged buildings are explicitly considered. These improvements would better characterize the nature and dynamics of the evacuation system, model the individual-level interactions among evacuees, and the evacuees' interactions with the environment. The general tsunami evacuation process simulated using the proposed agent-based tsunami evacuation model was illustrated through the simulation of tsunami evacuation in Seaside, Oregon.

Chapter 4

Simulation-based tsunami evacuation risk assessment

4.1 Introduction

Tsunami evacuation risk assessment plays an important role in evacuation planning, e.g., determining the nature and level of response for risk mitigation (UNESCO 2007). To provide valuable information for effective evacuation planning, evacuation risk needs to be assessed accurately. There are significant sources of uncertainties associated with the tsunami evacuation, related to the multiple hazards (i.e., cascading hazards of earthquake and tsunami) (Park and Cox 2016; Muhammad et al. 2017), the population size and spatial distribution (Fraser et al. 2014; Mostafizi et al. 2017), and the evacuation decisions and behaviors of the population (Yazici 2010) (e.g., when to evacuate (Priest et al. 2016; Makinoshima et al. 2018), how to evacuate (on foot or by car, e.g., pedestrian speed (Fraser et al. 2014)), where to evacuate (using the evacuation route, searching the shortest path, or following behavior)). To accurately assess the tsunami evacuation risk (e.g., the expected proportion of the number of casualties to the population in the community within a given time frame), various uncertainties associated with the evacuation (including the aleatory and epistemic uncertainties) need to be quantified.

For the tsunami evacuation risk quantification in existing research, many uncertainties associated with the evacuation are neglected or the uncertainty quantification is simplified. The loss of life is usually estimated based on the run-up limit rather than the time-history of the tsunami inundation, i.e., not based on tsunami evacuation simulation. For example, the hazard assessment map was produced based on running the tsunami run-up scenario and casualties were calculated based on the coastal community's physical properties such as the water level for every building (El-Barmelgy and Hamed 2017). The casualty was estimated based on the time required for evac-

uation and the arrival time of the tsunami (Wood and Schmidtlein 2013; Okumura et al. 2017). Since the life loss is not estimated based on tsunami evacuation simulation, many uncertainties associated with the evacuation are neglected, especially those in evacuation decision and behavior such as departure time. For evacuation risk quantification based on tsunami evacuation simulation, typically some important uncertainties associated with the evacuation process are neglected. For example, the uncertainty in the seismic damage to the bridge is usually neglected. The pedestrian speed of the population and delay time were modeled by assigning deterministic values (Okumura et al. 2017), and associated uncertainties were neglected. Furthermore, uncertainty quantification is usually simplified by selecting the simplified probability model or neglecting the epistemic uncertainty (deterministic values instead of probability models are used). For example, the quantification of the uncertainty in the seismic damage was simplified by removing damaged bridges from the transportation network (Jacob et al. 2014; Mostafizi et al. 2017). The population density was modeled using the triangular distribution with a constant lower limit, upper limit, and mode in Post et al. (2009). The constant instead of uncertain scale parameter was used to define the Rayleigh distribution to model the departure time (Solís and Gazmuri 2017). A normal distribution with constant mean and the standard deviation was used to model the agent's speed while the variability was neglected (Makinoshima et al. 2018). The neglect of uncertainty in evacuation simulation and/or simplification of uncertainty quantification may lead to inaccurate risk quantification.

To address the above limitations in tsunami evacuation risk assessment, a generalized simulation-based framework is proposed for the quantification of evacuation risk. The framework can address complex evacuation models and uncertainty models (including the aleatory and epistemic uncertainties). In particular, the improved agent-based tsunami evacuation model introduced in Chapter 3 is incorporated in the framework to simulate the complex tsunami evacuation process. Then the tsunami evacuation risk is assessed by propagating the various uncertainties. Next, the framework is described in detail.

4.2 Proposed simulation-based framework for tsunami evacuation risk quantification

A generalized simulation-based framework (shown in Fig. 4.1) is proposed for the quantification of tsunami evacuation risk. The developed agent-based tsunami evacuation model is used to simulate the evacuation, and various uncertainties associated with the evacuation are explicitly considered in the framework. Imprecise probability models are used to quantify both the aleatory and epistemic uncertainties (Sankararaman and Mahadevan 2013; Hurtado 2013; Schöbi and Sudret 2019; Wei et al. 2019a,b), i.e., probability models are used to model the aleatory uncertainty in input random variables while epistemic uncertainty (for the selected probability model) is quantified through uncertainty in distribution parameters (i.e., hyperparameters for the distributions). Propagating all considered uncertainties leads to the quantification of evacuation risk.

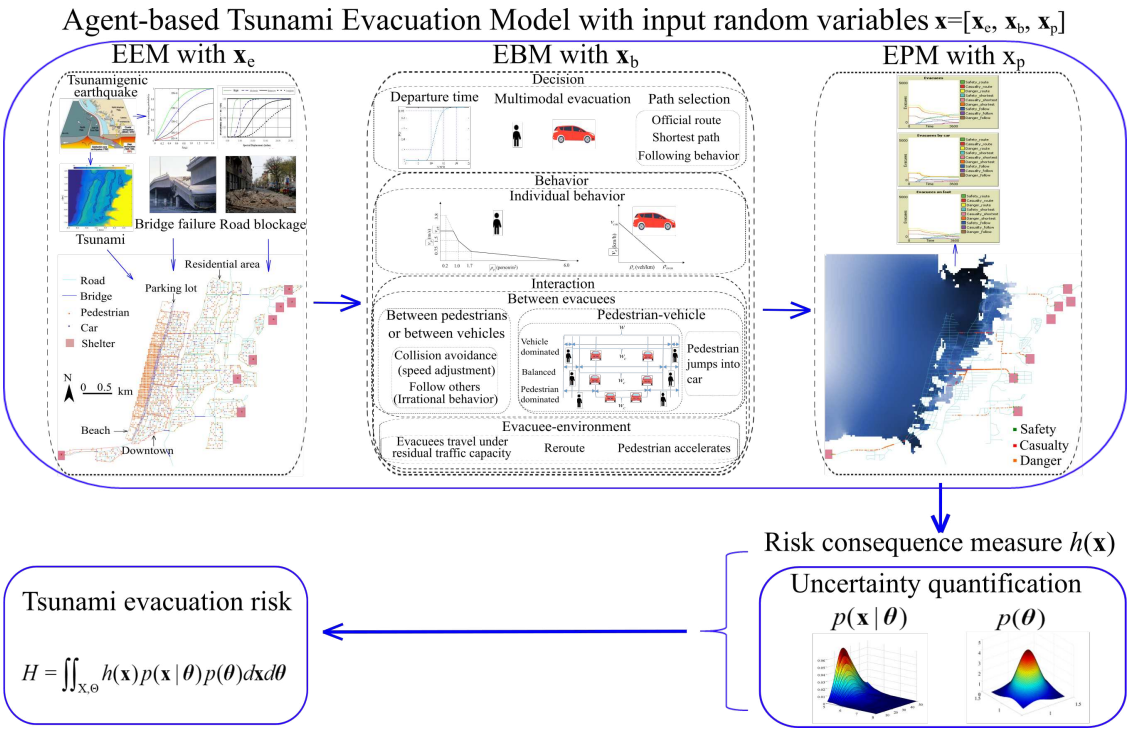


Figure 4.1: Framework for quantification of tsunami evacuation risk.

4.2.1 Uncertainty quantification

Let $\mathbf{x} = [\mathbf{x}_e, \mathbf{x}_b, \mathbf{x}_p] \in X$ represent all the input random variables in the space of X, where $\mathbf{x}_e$, $\mathbf{x}_b$, and $\mathbf{x}_p$ denote the input random variables in the evacuation environment model (EEM), evacuation decision and behavior model (EBM), and evacuation performance model (EPM), respectively. We can use the probability model $p(\mathbf{x}|\boldsymbol{\theta})$ to quantify the uncertainty in $\mathbf{x}$, which corresponds to the probability density function (PDF) for continuous variables or the probability mass function (PMF) for discrete variables. Here $\boldsymbol{\theta} = [\boldsymbol{\theta}_e, \boldsymbol{\theta}_b, \boldsymbol{\theta}_p] \in \boldsymbol{\Theta}$ represents distribution parameters that define the probability model $p(\mathbf{x}|\boldsymbol{\theta})$, where $\boldsymbol{\Theta}$ represents the space of possible values of $\boldsymbol{\theta}$. Similarly, the probability distribution $p(\boldsymbol{\theta})$ is used to quantify the uncertainty in $\boldsymbol{\theta}$ if $\boldsymbol{\theta}$ is uncertain. The uncertainties in $\boldsymbol{\theta}$ can be used to represent epistemic uncertainties in the probability models for $\mathbf{x}$. To quantify the tsunami evacuation risk, all the uncertainties in $\mathbf{x}$ and $\boldsymbol{\theta}$ (if any) need to be considered. These uncertainties include those associated with the multiple hazards (i.e., the seismic and tsunami hazards), the damages to the infrastructure (e.g., transportation network), the population size and spatial distribution, and the evacuation decisions and behaviors of the population (e.g., departure time), etc.

4.2.2 Risk consequence measure

Based on tsunami evacuation simulation, evacuation performance can be evaluated. Let $h(\mathbf{x})$ represent the performance measure of the evacuation system for given $\mathbf{x}$. We can define $h(\mathbf{x})$ as the risk consequence measure. Depending on the quantity of interest, metrics such as the evacuation time needed to get a certain proportion of the population in the community to the safety zone, the number of people evacuated within a certain time frame, and the number of casualty within a certain time frame could be selected as the evacuation risk consequence measure.

4.2.3 Risk quantification

When $h(\mathbf{x})$ corresponds to the risk consequence measure, propagation of the uncertainties in $\mathbf{x}$ then leads to the quantification of evacuation risk. The evacuation risk under the given value of the

distribution parameter $\boldsymbol{\theta}$ (i.e., conditional evacuation risk, denoted $H(\boldsymbol{\theta})$) can be written as

$$H(\boldsymbol{\theta}) = E_{\mathbf{x}|\boldsymbol{\theta}}[h(\mathbf{x})] = \int_X h(\mathbf{x}) p(\mathbf{x}|\boldsymbol{\theta}) d\mathbf{x} \tag{4.1}$$

where $E_{\mathbf{x}|\boldsymbol{\theta}}[.]$ denotes the expectation over the input random variables $\mathbf{x}$ and probability model $p(\mathbf{x}|\boldsymbol{\theta})$. This evacuation risk corresponds to the expected value of the selected risk consequence measure under the given value of $\boldsymbol{\theta}$.

When $\boldsymbol{\theta}$ is uncertain, further propagation of the uncertainties in $\boldsymbol{\theta}$ gives evacuation risk H

$$H = \iint_{X,\boldsymbol{\Theta}} h(\mathbf{x}) p(\mathbf{x}|\boldsymbol{\theta}) p(\boldsymbol{\theta}) d\mathbf{x} d\boldsymbol{\theta} \tag{4.2}$$

This evacuation risk corresponds to the expected value of the selected risk consequence measure.

4.3 Tsunami evacuation risk assessment

Using stochastic simulation (e.g., Monte Carlo simulation (MCS) (Robert and Casella 2004)) with N samples from some proposal density $q(\mathbf{x}, \boldsymbol{\theta})$, H is approximated as

$$\hat{H} = \frac{1}{N} \sum_{k=1}^{N} h(\mathbf{x}^k) \frac{p(\mathbf{x}^k|\boldsymbol{\theta}^k) p(\boldsymbol{\theta}^k)}{q(\mathbf{x}^k, \boldsymbol{\theta}^k)} \tag{4.3}$$

where $[\mathbf{x}^k, \boldsymbol{\theta}^k]$ represents the k^{th} sample of the input random variables and distribution parameters generated from $q(\mathbf{x}, \boldsymbol{\theta})$. As $N \to \infty$, $\hat{H} \to H$. However, Eq. (4.3) gives a good estimation for the risk integral for a relatively large N. The quality of the estimate can be assessed by the coefficient of variation (CoV) δ_{CoV}

$$\delta_{CoV} = \frac{1}{\sqrt{N}} \sqrt{\frac{\frac{1}{N} \sum_{k=1}^{N} h^2(\mathbf{x}^k) \frac{p^2(\mathbf{x}^k|\boldsymbol{\theta}^k) p^2(\boldsymbol{\theta}^k)}{q^2(\mathbf{x}^k, \boldsymbol{\theta}^k)}}{\hat{H}^2} - 1} \tag{4.4}$$

which is inversely proportional to $\sqrt{N}$. To improve the accuracy and efficiency for the estimate, a proper proposal density $q(\mathbf{x}, \boldsymbol{\theta})$ can be selected (e.g., corresponding to the idea of importance sam-

pling) (Robert and Casella 2004). Eq. (4.3) corresponds to direct MCS when the prior probability distribution $p(\mathbf{x}, \boldsymbol{\theta})$ is selected as $q(\mathbf{x}, \boldsymbol{\theta})$.

4.4 Illustrative example: Simulation-based tsunami evacuation risk assessment for Seaside, Oregon

The proposed framework is used for tsunami evacuation risk quantification for Seaside, Oregon. The details on Seaside and the proposed agent-based tsunami evacuation model can be found in Chapter 3 unless modifications are made, which will be presented in this application.

Since the computational time increases with the number of agents (or population size) and the number of simulations, to speed up the simulation, parallel computing is implemented on the Summit High-Performance Computing (HPC) system, a joint activity of Colorado State University (CSU) and the University of Colorado Boulder (CU). This allows us to run the evacuation model with a large number of agents as well as a large number of simulations for uncertainty propagation.

For the evacuation simulation, cases with different considerations of important factors and mechanisms are defined for comparison to investigate the impact of these factors and mechanisms on the tsunami evacuation risk as well as highlight the advantages of the proposed agent-based tsunami evacuation model. The factors and mechanisms include (1) seismic damage to bridges and debris on roads, (2) traffic information on the road blockage due to debris or bridge damage due to the earthquake, (3) car and pedestrian speed adjustment, (4) pedestrian-vehicle interaction, and (5) following behavior. The cases are listed in Table 4.1 where C0-C5 represent the six cases, "Yes" means considering the corresponding factor while "No" means neglecting the corresponding factor. C0 corresponds to the proposed agent-based tsunami evacuation model while other cases (i.e., C1-C5) neglect or simplify some important factors and mechanisms in the evacuation. Note that the pedestrian-vehicle interaction is invalid in C3 that neglects the car and pedestrian speed adjustment. Note the evacuation is assumed to occur at noontime of some weekend in summer except the nighttime scenario. The evacuation is considered to last one hour starting from the occurrence of the earthquake.

Table 4.1: Definition of simulation cases.

Cases	(1)	(2)	(3)	(4)	(5)
C0	Yes	Yes	Yes	Yes	Yes
C1	No	Yes	Yes	Yes	Yes
C2	Yes	No	Yes	Yes	Yes
C3	Yes	Yes	No	Yes	Yes
C4	Yes	Yes	Yes	No	Yes
C5	Yes	Yes	Yes	Yes	No

Under the simulation-based framework for risk quantification, for input random variables, $\mathbf{x}_e = [\mathbf{x}_{d_i}, \mathbf{x}_{IM_i}]$ with $i = 1, 2, ..., n_d$ and $\mathbf{x}_{d_i} = DS_j$ with $j = 1, 2, ..., 5$, where $\mathbf{x}_{d_i}$ represents the seismic damage to the bridge and building, n_d denotes the number of bridges and buildings, and $\mathbf{x}_{IM_i}$ is the intensity measure at each bridge site or building site; $\mathbf{x}_b = [t_0, t, p_c, T_{1_{PA}}, T_{2_{PA}}, T_{1_{MA}}, T_{2_{MA}}, T_{1_{Mac}}, T_{2_{Mac}}, T_{1_{LR}}, T_{2_{LR}}, v_p, p_f, p_r, p_s]$; $\mathbf{x}_p = [h_c]$. For distribution parameters, $\boldsymbol{\theta}_b = [\tau, \sigma_t, \mu_c, \mu_p, \sigma_p]$. The key continuous input random variables and associated distributions for C0-C5 can be found in Table 3.3 (for the daytime scenario), in which "Input" represents the key continuous input random variable and the uncertain "Parameter 1" or "Parameter 2" denotes the distribution parameter. For C5, due to no following behaviors, the proportions of the evacuees who follow the evacuation route or search the shortest path are considered to increase compared to C0-C4. More specifically, p_f = 0, $p_r \in [0.35\ 0.75]$ and p_s = 1 - p_r - p_f = 1 - p_r. Moreover, the thresholds that determine the traffic stage transitions (e.g., $T_{1_{PA}}$) are applicable for the cases expect C4.

All the six cases (i.e., C0-C5) are implemented under $n_e = 5000$ which is used to represent the population during the early summer. Considering the high population mobility in the study area as discussed in Section 3.4.2, C0 is also run under different population sizes (i.e., $n_e = 10,000$ and $n_e = 15,000$) to investigate the impact of the population size on the evacuation risk. Here, $n_e = 15,000$ is used to represent the population in peak summer, and $n_e = 10,000$ represents the population between the early summer and peak summer. Note that all the above simulations are run under the daytime scenario (i.e., noontime of some weekends). Besides, C0 is also run under the worst-case scenario for population (i.e., $n_e = 15,000$) and nighttime scenario to investigate the

impact of the time of day on the evacuation risk. Depending on the model input (e.g., population size), the runtimes for each simulation under different cases are different. However, overall the runtime for each simulation under C0 takes the longest time compared to other five cases (i.e., C1-C5), i.e., the runtime is up to 3, 10, and 24 hours of CPU time under $n_e = 5000$, $n_e = 10,000$, and $n_e = 15,000$, respectively.

Here, we use the casualty rate (i.e., the proportion of the number of casualties to the total population) in the community within a given time frame (no longer than one hour in this study) as the risk consequence measure $h(\mathbf{x})$ and three types of casualty rates are defined for the multimodal evacuation, i.e., the total casualty rate (TCR), pedestrian casualty rate (PCR), and car casualty rate (CCR). The TCR is calculated by total casualties including both casualties on foot and by car divided by the population. The PCR is the proportion of the casualties on foot to the population. The CCR is the proportion of the casualties by car to the population. In this context, the evacuation risk corresponds to the expected PCR, CCR, and TCR for the pedestrian, car, and total, respectively.

To assess evacuation risk, Eq. (4.3) is used with $q(\mathbf{x}, \boldsymbol{\theta}) = p(\mathbf{x}|\boldsymbol{\theta})p(\boldsymbol{\theta})$. $N = 2000$ tsunami evacuation simulations are used for each case under the corresponding scenario. The selection of $q(\mathbf{x}, \boldsymbol{\theta})$ and $N = 2000$ leads to high accuracy estimates for the expected total casualty rates (TCRs) at the end of the tsunami evacuation simulation (i.e., one hour), with δ_{CoV} below 2% for all cases.

As for results, Section 4.4.1 discusses the overall evacuation risk in terms of different risk measures (e.g., casualty rate) for C0-C5 under $n_e = 5000$. Section 4.4.2 investigates the impact of considered factors and mechanisms (i.e., corresponding to C0-C5) on tsunami evacuation risk under $n_e = 5000$. Section 4.4.3 examines the impact of population size (i.e., $n_e = 5000$, $n_e = 10,000$, and $n_e = 15,000$) on tsunami evacuation risk under C0 (i.e., the proposed agent-based model). Section 4.4.4 discusses the impact of the time of day (i.e., daytime and nighttime) on tsunami evacuation risk under $n_e = 5000$ under C0 (i.e., the proposed agent-based model). Note the evacuation risk is defined in terms of casualty rate (i.e., PCR, CCR, and TCR) in Section 4.4.2, Section 4.4.3, and Section 4.4.4.

4.4.1 Overall evacuation risk under different cases

This section investigates the overall probabilistic evacuation performance over time using the cases under $n_e = 5000$. The mean predictions of three important risk performance measures (i.e., the expected total danger rate (TDR), expected total safety rate (TSR), and expected total casualty rate (TCR)) and their variations over time are shown in Fig. 4.2(c). Note that "Danger" is defined as the situation in which evacuees are under the threat of a tsunami strike while "Safety" is the situation once evacuees reach shelters. The total rate includes contributions from the pedestrian and car. Similarly, we can define the expected danger rate, expected safety rate, and expected casualty rate for the pedestrian and car. Their variations are shown in Fig. 4.2(a) and Fig. 4.2(b), respectively.

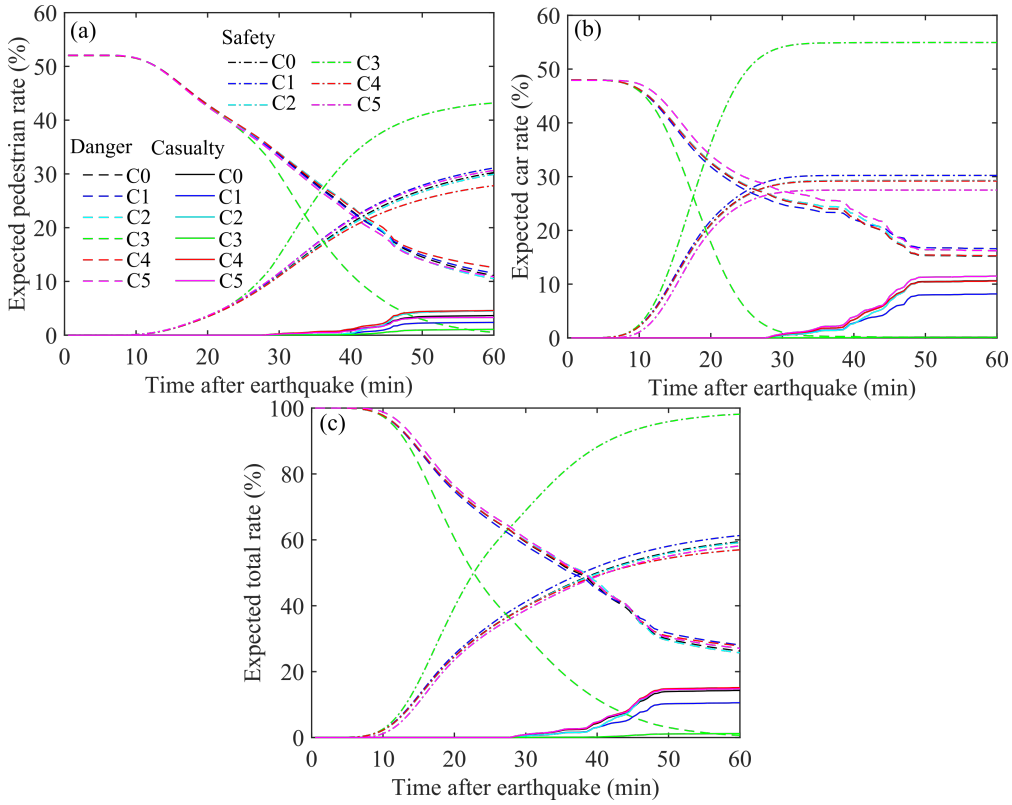


Figure 4.2: The variations of evacuation risk in terms of danger rate, safety rate, casualty rate over time under different cases, where (a) shows the expected pedestrian rate, (b) shows the expected car rate, and (c) shows the expected total rate.

From Fig. 4.2(c), overall the changes of the three rates over time under all six cases are consistent with the general tsunami evacuation process simulated using the proposed agent-based tsunami evacuation model discussed in Section 3.4.4. At $t = 0$ min, the TDR is 100% while the TSR and TCR are zero due to the definition that all evacuees are in danger facing the coming tsunami inundation. As time goes by, as expected the TDR decreases while the TSR and TCR increase. On average, after around 10 min, some of the evacuees would reach the shelter (i.e., reach safety), from which point on the TSR is not zero anymore and starts increasing. On the other hand, on average, before around 28 min, the TCR is still zero; afterwards, casualty starts occurring and the TCR starts increasing over time. Note that the TCR might reach the peak at some point before the end of the evacuation simulation and stop increasing. For the current simulations, on average, the TCR reaches the largest value (e.g., around 14% for C0) at around 50 min, which might correspond to the time when the tsunami inundation reaches the run-up limit. However, there might be evacuees still traveling towards the shelter through the road network between the run-up limit points and the shelter. Therefore, the TDR would keep decreasing with the increase of TSR until the end of the simulation.

From Fig. 4.2(a) and (b), overall the variation of the mean values of the three rates for the pedestrian and car show similar trends to the total rate. When comparing the results for the pedestrian and car, the following interesting observations are made. First, although the evacuation on foot and by car is almost half by half (based on the selection of the distribution for p_c in this example), the safety rates for the pedestrian and car show different variations over time. Around 10 min after the earthquake, both the pedestrian safety rate (PSR) and car safety rate (CSR) are not zero due to successful evacuation for both on foot and by car; however, the increase of the PSR is much slower than that of the CSR for the following 20 min, e.g., for C0, the PSR is only about 11.2% while the CSR is about 28.7% when $t = 30$ min. Between $t = 30$ min and $t = 60$ min, for C0, the PSR increases from around 11.2% to around 30.3%, which shows a much faster increase than the CSR that increases from around 28.7% to around 29.2%. With the increase of time, the PSR keeps increasing although the increase becomes slower while the CSR increases very slowly.

The above differences between the changes of the PSR and CSR should be attributed to different characteristics of evacuation on foot and by car. Compared to evacuation on foot, evacuation by car is more likely to cause severe traffic congestion as more cars are driving on the same link with the increase of time, which would reduce the car speed significantly and thus delay the evacuation. Therefore, the CSR would increase very fast when the cars can travel at free-flow speed before the occurrence of traffic congestion and would increase very slowly once there is traffic congestion.

In addition, due to the reasons that cause the difference in variation of the PSR and CSR, the variation of casualty rates for the pedestrian and car over time is also different. The variations will be discussed in detail in the next section.

Furthermore, due to the differences in variations of the safety rate and casualty rate for the pedestrian and car, the pedestrian danger rate (PDR) and car danger rate (CDR) also show different variations over time. For example, between 10 min and 30 min, the decrease of the PDR is much lower than that of the CDR while the opposite trend shows between 30 min and 40 min. Also, the PDR keeps decreasing till the end of the evacuation simulation while the CDR stops decreasing about 10 min before the end once both the safety rate and casualty rate stop increasing.

4.4.2 The impact of considered factors and mechanisms on tsunami evacuation risk

Under the population of 5000, the variations of evacuation risk in terms of casualty rate for the pedestrian, car, and total over time under all the six cases are shown in Fig. 4.3(a)-(c), respectively.

Pedestrian casualty rates (PCRs) Comparing the variation of PCRs among different cases shown in Fig. 4.3(a), the following differences can be observed.

(1) Overall, C1, C3, and C5 give lower PCRs while C3 gives the lowest PCR at the end of evacuation than C0 which incorporates all the considered important factors and mechanisms associated with evacuation. More specifically, the PCR is 3.6% for C0 while 2.4%, 1.1%, and 3.3% for C1, C3, and C5, respectively. Consideration of the seismic damage to bridges and the debris on

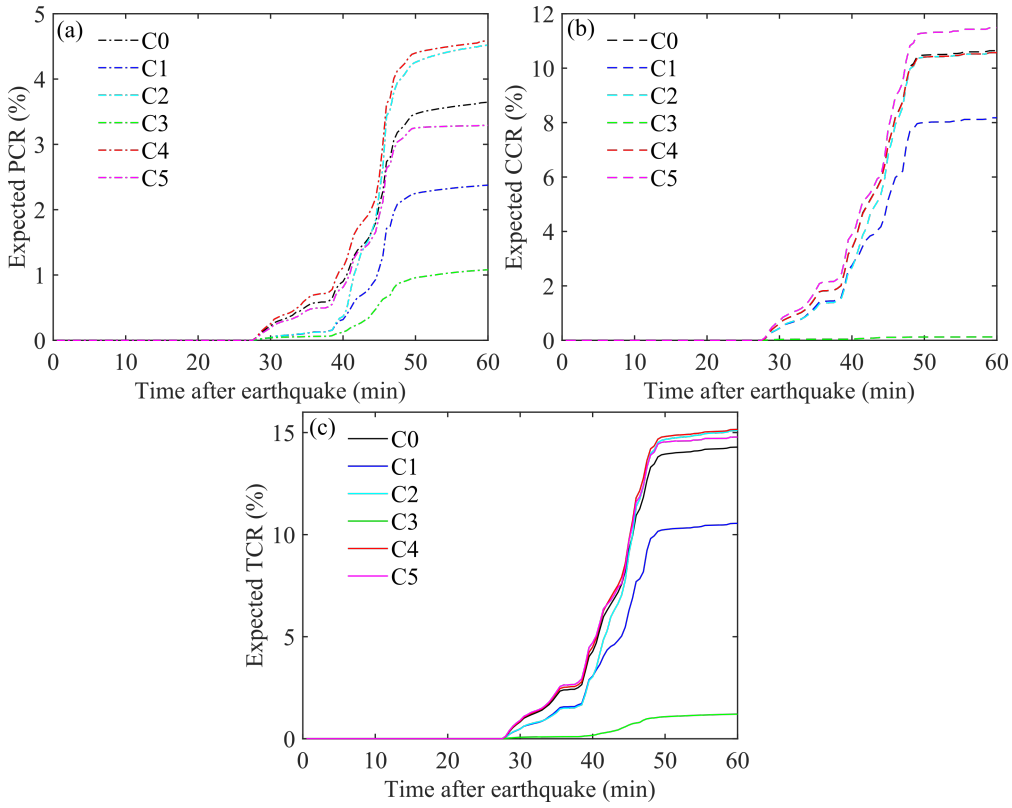


Figure 4.3: The variations of evacuation risk in terms of casualty rate for (a) pedestrian, (b) car, and (c) total over time under different cases.

roads from damaged buildings would lead to a reduction in the traffic capacity of the damaged or blocked link, which could slow down the evacuation and increase the casualty rate. However, C1 neglects these impacts and therefore underestimates the PCR. C3 neglects the speed adjustment and evacuees can evacuate at their preferred speed or free-flow speed by neglecting the potential speed reduction due to traffic congestion, which leads to a lower PCR. For C5, no pedestrians with the following behavior in evacuation means they either use the evacuation route or search the shortest path to evacuate. In this case, the pedestrian would evacuate efficiently rather than waste time searching the evacuation path when simply following others. Therefore, C5 results in a lower PCR.

(2) Compared to C0 (i.e.,3.6%), C2 and C4 give higher PCRs while C4 gives the highest PCR, i.e., 4.5% and 4.6%, respectively. For C2, when no traffic information on the road blockage and bridge damage is available, evacuees would have to reroute once when they find the road/bridge is

impassable. Compared to C0 in which the evacuees can avoid the above impassable road/bridge, searching the new evacuation path is likely to cause the evacuation delay and hence a higher casualty rate. For C4, neglecting the pedestrian-vehicle interaction means the pedestrian cannot take advantage of more road space if the pedestrian dominates the road when the pedestrian congestion is more likely to occur. Therefore, C4 gives a higher PCR.

(3) Based on the above discussions on the impacts of different factors and mechanisms associated with the evacuation on the PCR, the speed adjustment and pedestrian-vehicle interaction have higher impacts on the PCR in this case.

Car casualty rates (CCRs) Comparing the variation of CCRs among different cases shown in Fig. 4.3(b), the following observations can be made.

(1) Compared to the CCR for C0, which is 10.64%, the CCRs are lower for C1 (with the CCR of 8.2%) and C3 (with the CCR of only 0.1%), while the CCR for C4 (which is 10.57%) is close to that of C0. As discussed for the PCR, no evacuation delay is considered due to the traffic reduction caused by the seismic damage/debris and traffic congestion in C1 and C3, respectively. These neglects would also cause fewer casualties for evacuation by car. Note that C3 gives a very low CCR in this case, which significantly underestimates the CCR. The PCRs for C4 and C0 are very close for any given time after the earthquake. This can be explained by the way that pedestrian-vehicle interaction is modeled. Based on Eq. (3.4), pedestrian-vehicle interaction is considered by changing the road width that can be used by the car according to the traffic stage transition. However, based on the car speed-density model in Section 3.3.2, the change of road width would not affect the car speed. This is because the car speed is adjusted according to the car density some distance ahead on the same lane where the car density per lane is measured by the average number of cars that occupy some distance (usually one mile or one kilometer) on the lane and is not affected by the road width. Therefore, considering pedestrian-vehicle interaction or not does not affect the evacuation by car. The small difference of the CCR between C0 and C4 might be caused by that the pedestrian can jump into the nearby car when the pedestrian dominates the traffic stage.

(2) Compared to C0 (i.e., 10.64%), C5 gives a higher CCR and C2 gives a little lower CCR, i.e., 11.5% and 10.6%, respectively. Unlike evacuation on foot, evacuation by car by simply following others is more likely to cause traffic jams and hence delay the evacuation. Therefore, C5 gives a higher CCR. For C2, when the evacuation by car has to reroute once some link is impassable due to the road blockage or bridge failure, this delay might not affect the evacuation much due to the higher traveling speed. Ultimately, the CCR given by C2 is slightly lower than that by C0.

Comparison between PCRs and CCRs Comparing the PCR and CCR, the CCR is much higher than the PCR for all cases except C3. The highest PCR corresponding to C4 is only around 4.6% while the corresponding CCR for C4 is about 10.6%. These observations are based on the particular distributions of μ_c and p_c which are defined in Section 3.4.2. For the current selection, the average proportion of evacuation on foot or by car is around 50%, which can be seen in Fig. 4.2(a) and (b). The comparison indicates that evacuation by car might lead to higher evacuation risk than evacuation on foot. Note that for C3 the CCR (which is 0.1%) is much lower than the PCR (which is 1.1%). This is because evacuation by car is much faster than evacuation on foot when the potential traffic congestion is neglected for both the pedestrian and car.

Total casualty rates (TCRs) From Fig. 4.3(c), the following observations can be made regarding the TCRs.

(1) For all cases except C3, the variations of the mean of the TCRs show similar trends to CCRs while the variation of the mean of the TCR has a similar trend to the PCR for C3.

(2) Out of all cases, C3 has the lowest TCR (i.e., 1.2%), while C4 has the highest TCR (i.e., 15.2%). This is because C3 has the lowest casualty rate for both pedestrians and cars while C4 has the highest PCR and a relatively high CCR. Based on the above observation as well as the definitions of C3 and C4, neglecting the pedestrian speed adjustment might lead to underestimation of evacuation risk while neglecting pedestrian-vehicle interaction might lead to overestimation of evacuation risk.

(3) According to the definition of simulation cases, C0 corresponds to the proposed agent-based tsunami evacuation model while each of the other cases neglects one important factor/mechanism associated with tsunami evacuation. The TCR for C0 is around 14.3%. Treating C0 as the reference value, the overestimation is 0.8%, 0.9%, and 0.5% for C2, C4, and C5, respectively, while underestimation is 3.7% and 13.1% for C1 and C3, respectively. The smallest difference in the estimation of casualties still corresponds to around 25 casualties ($0.5\% \times 5000$), while the largest difference corresponds to around 654 casualties ($13.1\% \times 5000$). Note that the results would also depend on the population size, whose impact will be investigated and discussed in Section 4.4.3.

4.4.3 The impact of population size on tsunami evacuation risk

Based on the tsunami evacuation simulation using the proposed agent-based model (i.e., C0), this section investigates the impacts of population size on the evacuation risk in terms of the casualty rate. As mentioned earlier, three population sizes are considered in simulation, i.e., $n_e = 5000$, $n_e = 10,000$, and $n_e = 15,000$. The variations of evacuation risk in terms of casualty rate for the pedestrian, car, and total over time under the three selected population sizes are shown in Fig. 4.4.

Pedestrian casualty rates (PCRs) Overall, the variations of the PCRs over time for $n_e = 10,000$ and $n_e = 15,000$ show similar trends to that for $n_e = 5000$, i.e., initially the rate has a slow increase that lasts for a while (around 17 min), and then the rate has steep increase that only lasts for several minutes, after which the PCR almost does not increase anymore. One important observation from Fig. 4.4(a) is that for $n_e = 10,000$ and $n_e = 15,000$ the estimated PCRs are much higher than that of $n_e = 5000$. These differences can be explained by the fact that a larger population is more likely to cause more severe pedestrian congestion, which causes more casualties under the same tsunami inundation. The results verify the nonlinear nature of the evacuation. The comparisons highlight that simulations using smaller than actual population size may significantly underestimate the casualty rate.

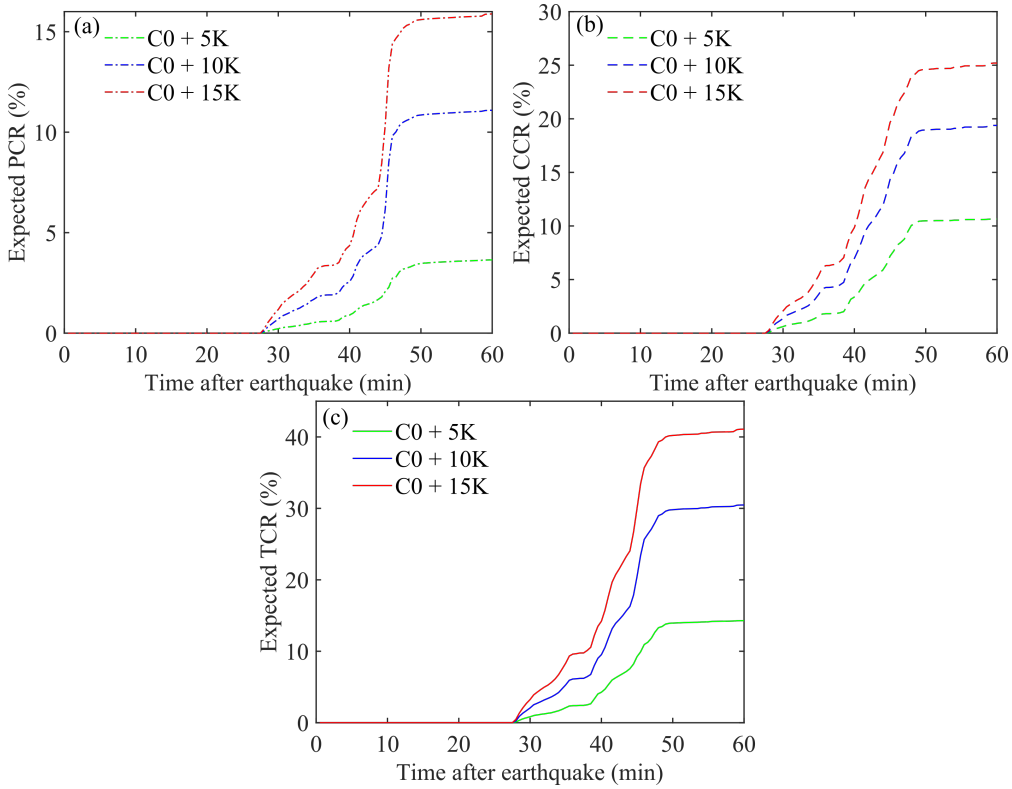


Figure 4.4: The variations of evacuation risk in terms of casualty rate for (a) pedestrian, (b) car, and (c) total over time under different population sizes.

Car casualty rates (CCRs) Overall, the variations of the CCRs over time for $n_e = 10,000$ and $n_e = 15,000$ show similar trends to that for $n_e = 5000$. In terms of the values of the CCRs, similar to the PCRs, for $n_e = 10,000$ and $n_e = 15,000$ the estimated CCRs are higher than that of $n_e = 5000$. This is because more car casualties occur for larger n_e due to more severe traffic congestion.

Comparison between PCRs and CCRs Comparing the casualty rates for the pedestrian and car, as the population size increases the PCR has a much larger relative increase than the CCR. The CCR is 10.6%, 19.4%, and 25.2% for $n_e = 5000$, 10,000, and 15,000, respectively, while the corresponding PCR is 3.6%, 11.1%, and 15.9%, respectively. This may be attributed to the fact that there might already be severe traffic congestion for $n_e = 5000$ and further increasing the population might not significantly increase the severity of traffic congestion. On the other hand, with a larger population, the pedestrian might face more severe pedestrian congestion.

Total casualty rates (TCRs) Stemming from increases in both PCRs and CCRs, as population size increases, the TCRs increase significantly, i.e., 14.3%, 30.5%, and 41.1% for $n_e = 5000$, 10,000, and 15,000, respectively. Therefore, for more accurate evacuation simulation and risk assessment, the actual population is recommended to be used. The estimation based on a smaller than actual population may lead to a significant underestimation of evacuation risk.

4.4.4 The impact of the time of day on tsunami evacuation risk

This section compares the evacuation risks between the daytime and nighttime scenarios to investigate the impact of the time of day on evacuation risk. For comparison, the same population size is considered for both scenarios, and the worst-case scenario for population $n_e = 15,000$ is selected. Compared to the daytime, due to many factors such as the low lighting conditions, being tired, etc. during the nighttime, evacuees may make different decisions and behave differently, e.g., more people have the following behavior (Jacob et al. 2014), late to start the evacuation, the pedestrian speed is slower (Aguilar et al. 2019), etc. Also, the population distribution across the three sub-areas (i.e., the beach, downtown, and residential area) would be different due to the difference of the time. This example aims to investigate the impact of the time on evacuation risk rather than model the night scenario, therefore only the main characteristics of the night scenario will be modeled.

The nighttime evacuation is assumed to occur during a summer festival and two possible worst nighttime scenarios (denoted Nighttime1 and Nighttime2) are defined in terms of different lighting conditions for comparison. The comparison of the lighting condition and its impact on evacuation between daytime and nighttime scenarios are summarized in Table 4.2. According to Jacob et al. (2014), two lighting conditions are considered to define Nighttime1 and Nighttime2. For both nighttime scenarios, it is assumed the street light fails due to the earthquake. The emergency lighting of 15 lux is available in the space of 30 m in Nighttime1 and the night with a full moon (lighting of 0.2 lux) is assumed for Nighttime2.

Table 4.2: The comparison of the daytime and nighttime scenarios.

Characteristics	Daytime	Nighttime1	Nighttime2
Lighting condition (lux)	direct sunlight	15	0.2
Sight distance-evacuee (m)	50	30	15
Sight distance-tsunami (m)	200	50	25
Preferred pedestrian speed (m/s)	v_{p_0}	$0.8v_{p_0}$	$0.5v_{p_0}$
ρ_{a_1}	1.2	1.1	1.1
ρ_{a_2}	1.4	1.3	1.2
p_f	$U(0.1, 0.3)$	$U(0.2, 0.4)$	$U(0.3, 0.5)$
p_r	$U(0.3, 0.6)$	$U(0.2, 0.5)$	$U(0.15, 0.45)$
ρ_1	0.4	0.1	0.1
ρ_2	0.3	0.5	0.5
ρ_3	0.3	0.4	0.4

Due to the poor visibility caused by the low lighting condition at night, the following differences are considered between the daytime scenario and Nighttime1: (1) the evacuee's sight distance (i.e., sight distance-evacuee in Table 4.2) decreases from 50 m to 30 m (Aguilar et al. 2019) and the distance within which the pedestrian can see the tsunami inundation (i.e., sight distance-tsunami in Table 4.2) decreases from 200 m to 50 m; (2) the effect of the poor visibility is also modeled by decreasing the preferred pedestrian speed (i.e., v_{p_0}) to 80% of that in daytime based on the study in Ouellette and Rea (1989). In the pedestrian speed-density model shown in Fig. 3.8, the three speeds, i.e., 0.75, 1.5, and 3.83 (unit: m/s) decrease to 0.6, 1.2, and 3.06 (unit: m/s); (3) the two scaling factors (scaling the preferred pedestrian speed in the pedestrian speed-density model, i.e., ρ_{a_1} and ρ_{a_2}) used to simulate the pedestrian's acceleration when the inundation reaches the shoreline as well as when they see the inundation from 50 m far away decrease, i.e., from 1.2 and 1.4 to 1.1 and 1.3, respectively; (4) due to smaller sight distance, more evacuees are considered to have following behaviors (Jacob et al. 2014) while less people use the evacuation route or search the shortest path to evacuate, i.e., $p_f \in U(0.2, 0.4)$, $p_r \in U(0.2, 0.5)$, and $p_s = 1 - p_f - p_r$.

Similarly, Nighttime2 has the following differences from the daytime scenario: (1) the evacuee's sight distance decreases from 50 m to 15 m (Aguilar et al. 2019) and the distance within which the pedestrian can see the tsunami inundation decreases from 200 m to 25 m; (2) the preferred pedestrian speed decreases to 50% of that in daytime based on the study in Ouellette and

Rea (1989). In the pedestrian speed-density model shown in Fig. 3.8, the three speeds, i.e., 0.75, 1.5, and 3.83 (unit: m/s) decrease to 0.375, 0.75, and 1.92 (unit: m/s); (3) the two scaling factors used to simulate the pedestrian's acceleration decrease from 1.2 and 1.4 to 1.1 and 1.2, respectively; (4) more evacuees have following behaviors (Jacob et al. 2014) while less people use the evacuation route or the shortest path to evacuate, i.e., $p_f \in U(0.3, 0.5)$, $p_r \in U(0.15, 0.45)$, and $p_s = 1 - p_f - p_r$.

In addition, the population distribution across the three sub-areas is different during the night, i.e., a larger proportion of evacuees are distributed in downtown and the residential area while fewer people are on the beach. The population proportion for both night scenarios is assumed to be 0.1, 0.5, and 0.4 on the beach, in the downtown, and in the residential area, respectively (i.e., $\rho_1 = 10\%$, $\rho_2 = 50\%$, and $\rho_3 = 40\%$).

The variations of evacuation risk in terms of casualty rate for the pedestrian, car, and total over time under the daytime and two nighttime scenarios are shown in Fig. 4.5.

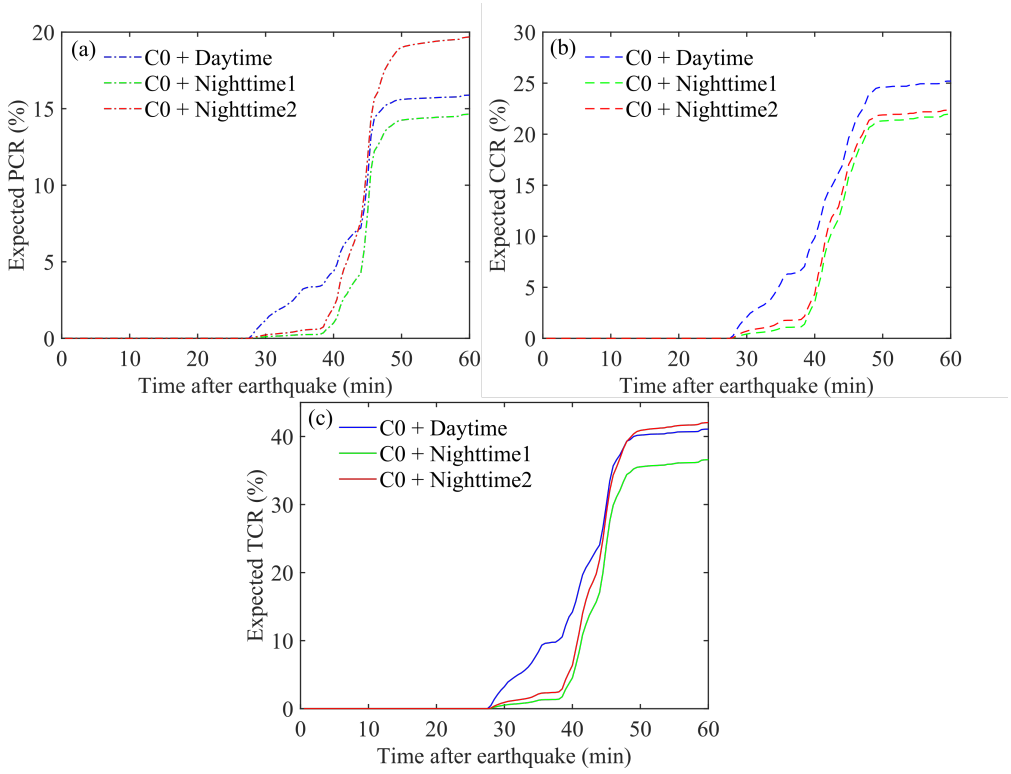


Figure 4.5: The variations of evacuation risk in terms of casualty rate for (a) pedestrian, (b) car, and (c) total over time under the daytime and two nighttime scenarios.

Pedestrian casualty rates (PCRs) Overall, as shown in Fig. 4.5(a), the variations of the PCRs over time for the nighttime scenarios show similar trends to that for the daytime scenario, i.e., initially the rate increases slowly and lasts for a while (around 12 min), and then increases fast but only lasts for several minutes, after which the PCR almost does not increase much. In particular, three important observations are: (1) Nighttime1 gives a lower PCR over time. For Nighttime1, the pedestrian speed is assumed to decrease (i.e., to 80% of that during daytime) due to the poor visibility at night, which would delay the evacuation on foot; however, the population is overall closer to the shelter, which would save the evacuation time for some pedestrians and hence decrease the casualty. Ultimately, the PCR for Nighttime1 is lower than the daytime scenario in this example; (2) The PCR for Nighttime2 is higher than Nighttime1, which should be attributed to the lower pedestrian speed for Nighttime2 due to the poorer visibility under the worse lighting condition; (3) Compared to the daytime scenario, Nighttime2 gives a lower PCR before around 45 min and gives a higher PCR after around 45 min. For Nighttime2, more pedestrians can reach the shelter due to the closer distance to the shelter in the short time after the inundation reaches the shoreline; however, as the tsunami inundates, more casualties are caused by the slow evacuation on foot for pedestrians who are initially far from the shelter. The comparisons show that the lighting condition at night can significantly affect the evacuation performance, which may cause more casualties than the daytime evacuation.

Car casualty rates (CCRs) Overall, the variations of the CCRs over time for the nighttime scenarios show similar trends to that for the daytime scenario (shown in Fig. 4.5(b)). In terms of the values of the CCRs, the estimated CCRs for Nighttime1 and Nighttime2 are lower than that for the daytime scenario. This is because evacuation by car is not assumed to be affected by the lighting condition at night due to the illumination of headlights. On the other hand, the population that evacuates by car is overall closer to the shelter during the night, which would save the evacuation time and result in fewer causalities.

Comparison between PCRs and CCRs Comparing the casualty rates for the pedestrian and car for the two nighttime scenarios, the CCRs for Nighttime1 and Nighttime2 are very close while the PCRs have a larger difference between Nighttime1 and Nighttime2. The CCR is 22.0% and 22.4% for Nighttime1 and Nighttime2, respectively, while the corresponding PCR is 14.6% and 19.7%, respectively. This is because different lighting conditions at night have a high impact on evacuation on foot but not on evacuation by car. Note that the CCRs for Nighttime1 and Nighttime2 are not the same. This should be attributed to the influence of the interactions between the pedestrian and car, i.e., pedestrian-vehicle interactions in terms of the traffic stage transition, the pedestrian can jump into the nearby car.

Total casualty rates (TCRs) Due to the differences of the PCRs and CCRs between the daytime and nighttime scenarios, as shown in Fig. 4.5(c), Nighttime1 has a lower TCR than the daytime scenario while the TCR for Nighttime2 is lower than the daytime scenario before around 48 min but is higher than the daytime scenario after around 48 min. This indicates the lighting condition can affect the evacuation behavior at night and the night evacuation might lead to more casualties than the daytime evacuation. For evacuation planning purposes, the worst nighttime scenario might be investigated to guide the evacuation planning. For more accurate night evacuation simulation and risk assessment, factors such as the lighting condition need to be taken into account.

4.5 Summary

A systematic simulation-based framework was proposed for the quantification of tsunami evacuation risk. Under the proposed simulation-based framework, the improved agent-based tsunami evacuation model is used for evacuation simulation in which various uncertainties (including the aleatory and epistemic uncertainties) associated with the evacuation are explicitly considered. Imprecise probability models are used to quantify both types of uncertainties, i.e., probability models are used to model the aleatory uncertainty in input random variables while the epistemic uncertainty (for the selected probability model) is quantified through the uncertainty in the distribution

parameter. The evacuation risk is quantified by propagating the uncertainties in input random variables and distribution parameters.

The proposed simulation-based framework was applied to the tsunami evacuation risk assessment in Seaside, Oregon. The variations of the overall evacuation risks over time in terms of the danger rate, safety rate, and casualty rate are consistent with the overall evacuation performance. Compared to the evacuation risk based on the simulations using the proposed agent-based model, neglect of important factors and mechanisms in evacuation might overestimate or underestimate the evacuation risk. The neglect of seismic damage to bridges and debris on roads from damaged buildings or speed adjustment might underestimate evacuation risk. The unavailability of the traffic information (i.e., on the bridge damage and road blockage) or the neglect of the pedestrian-vehicle interaction or the following behavior might overestimate evacuation risk. The evacuation risk would increase with the increase in population size. Evacuation risk is also impacted by the time of day when evacuation occurs and the night evacuation might result in a higher evacuation risk than the daytime evacuation.

Chapter 5

Sensitivity analysis of tsunami evacuation risk with respect to epistemic uncertainty

5.1 Introduction

Under the simulation-based framework proposed in Chapter 4, imprecise probability models are used to quantify the aleatory and epistemic uncertainties in tsunami evacuation risk quantification. The epistemic uncertainty is quantified through the uncertainty in the distribution parameters. For given value of distribution parameters, the corresponding evacuation risk can be assessed. Apparently, the epistemic uncertainty in the distribution parameters would lead to variability in the evacuation risk. Considering the epistemic uncertainty is reducible when additional data is available (Der Kiureghian and Ditlevsen 2009; González et al. 2009), evacuation risk could be more accurately assessed through the reduction of the epistemic uncertainty (Post et al. 2009; Jelínek et al. 2012), i.e., reduce the variability in the risk assessment. However, data collection (particularly the up-to-date data) typically requires many resources, especially for the complex tsunami evacuation process involving many physical, social, and psychological factors (Jelínek et al. 2012; Wood and Schmidtlein 2013; Alabdouli 2017). Therefore, the prioritization of data collection is crucial, i.e., where to devote limited resources to collecting more high-quality and important data. In this case, it is critical to identify the epistemic uncertainties that have higher impacts on the variability in the evacuation risk. For this purpose, sensitivity analysis can be used.

Sensitivity analysis examines how the uncertainty in the system input impacts the system output or performance quantity of interest (i.e., identification of the importance of system inputs) (Saltelli 2002). For sensitivity analysis, different global sensitivity measures have been proposed and used (Iooss and Lemaître 2015), mainly including variance-based sensitivity analysis such as Sobol' index (Homma and Saltelli 1996; Sobol 2001; Sudret 2008), entropy-based sensitivity in-

dices (Liu et al. 2004, 2006; Jia and Taflanidis 2014), and distribution based sensitivity indices (e.g., moment independent sensitivity indicator) (Borgonovo 2007; Liu and Homma 2009; Yun et al. 2018). Sobol' index is one of the most commonly used sensitivity measures, especially when we are interested in the sensitivity analysis in terms of variance of the output.

To examine the sensitivity of the variability in the evacuation risk to the epistemic uncertainty in the distribution parameters, the performance quantity of interest corresponds to some probabilistic performance (or risk), and the so-called risk sensitivity (Wang and Jia 2020a) can be defined. To the best of our knowledge, no research has been conducted on the full sensitivity analysis of tsunami evacuation risk to evaluate the impact of various epistemic uncertainties on the variability in the evacuation risk and identify those that have relatively high impacts. For risk sensitivity analysis with respect to the epistemic uncertainty in distribution parameters, compared to typical global sensitivity analysis, there is an additional layer of integration, corresponding to the risk integral for any given value of the distribution parameter (Tang et al. 2016; Nannapaneni and Mahadevan 2016; Chabridon and Gayton 2018; Au 2005). Direct estimation (e.g., using MCS) of the risk integral requires repeated evaluation of the system model. When combined with the computational challenges in evaluating the sensitivity index itself (e.g., Sobol' index), the overall computational effort for risk sensitivity analysis is even higher.

To address the above computational challenges, an augmented sample-based approach is proposed for efficient sensitivity analysis of tsunami evacuation risk with respect to the epistemic uncertainty in the distribution parameter. An augmented problem is first defined in the space of both distribution parameters and input random variables. Then samples are generated from a joint auxiliary density that is proportional to the integrand of the augmented risk integral. Based on the corresponding marginal samples, the marginal auxiliary densities for distribution parameters can be efficiently approximated using KDE. The marginal auxiliary density is then used to directly approximate the conditional expectations in Sobol' index, which are used to support the calculation of Sobol' indices. Using only one set of simulations, the augmented sample-based approach can estimate Sobol' index for all distribution parameters (including the first-order indices/main

effect and higher-order interactions). Then, the importance ranking of distribution parameters is identified based on the sensitivity index values.

As an illustrative example, the importance ranking of various distribution parameters associated with the tsunami evacuation risk of Seaside, Oregon is identified using the proposed augmented sample-based approach. The results can be used to guide the data collection prioritization for an effective epistemic uncertainty reduction, which can be further used for more accurate evacuation risk assessment, and more effective evacuation planning.

5.2 Sensitivity analysis of tsunami evacuation risk with respect to epistemic uncertainty

5.2.1 Sensitivity of tsunami evacuation risk to epistemic uncertainty

Let $\boldsymbol{\theta}$ denote the distribution parameters with $\boldsymbol{\theta} = [\theta_1, \ldots, \theta_i, \ldots, \theta_{n_\theta}] \in \boldsymbol{\Theta}$ where θ_i is the i^{th} distribution parameter and n_θ is the total number of the distribution parameter. For given value of $\boldsymbol{\theta}$, using evacuation risk measure and propagating the uncertainties in the input random variable $\mathbf{x}$, the corresponding evacuation risk can be established using Eq. (4.1) in Chapter 4, i.e., $H(\boldsymbol{\theta}) = E_{\mathbf{x}|\boldsymbol{\theta}}[h(\mathbf{x})] = \int_X h(\mathbf{x}) p(\mathbf{x}|\boldsymbol{\theta}) d\mathbf{x}$.

For sensitivity analysis of tsunami evacuation risk with respect to the epistemic uncertainty in distribution parameters, we are interested in how the uncertainty in each of the distribution parameters in $\boldsymbol{\theta}$ (i.e., θ_i) impacts the variability in evacuation risk $H(\boldsymbol{\theta})$. This is illustrated in Fig. 5.1 where μ_H and V_H represent the mean and variance of $H(\boldsymbol{\theta})$, respectively. Compared to typical global sensitivity analysis, for sensitivity analysis of tsunami evacuation risk, the output $H(\boldsymbol{\theta})$ corresponds to some probabilistic performance measure (i.e., evacuation risk). The evaluation of the probabilistic performance integral for a given value of $\boldsymbol{\theta}$ introduces another layer of integration (i.e., double-loop integration for calculation of global sensitivity measures, as will be shown later) and additional computational challenges besides the computational challenges of typical global sensitivity analysis. Note that when $h(\mathbf{x})$ corresponds to the indicator function $I_F(\mathbf{x})$, which takes

the value of 1 when the failure occurs where failure can be defined as when the evacuation performance does not meet some performance threshold (e.g., when casualty rate exceeds a certain threshold) and 0 otherwise, the evacuation risk $H(\boldsymbol{\theta})$ corresponds to the failure probability $P_F(\boldsymbol{\theta})$ (i.e., probability of having unacceptable evacuation performance). Sensitivity of evacuation risk then corresponds to the failure probability or reliability sensitivity. In terms of sensitivity measures, this research selects the commonly used variance-based measure, the Sobol' index. This selection is made considering (1) we are interested in investigating the sensitivity of the variability in evacuation risk to the epistemic uncertainty, and (2) among various variance-based sensitivity analysis methods, Sobol sensitivity analysis is regarded as one of the most general and powerful techniques (Brevault et al. 2013; Zhang et al. 2015) due to its advantages, e.g., converging to the exact relative contributions to the model inputs and their interactions to the output variability.

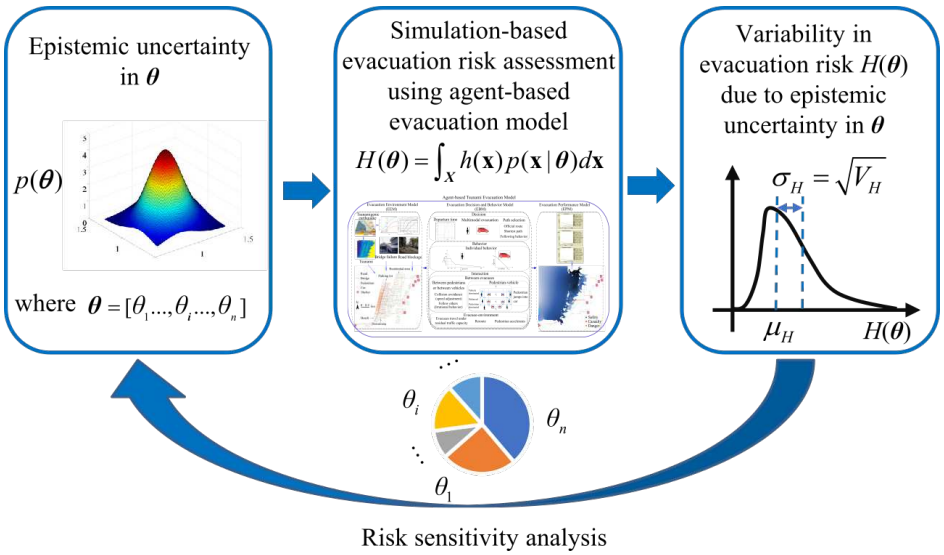


Figure 5.1: Illustration of sensitivity analysis of tsunami evacuation risk with respect to epistemic uncertainty.

5.2.2 Global sensitivity measure: Sobol' index

The first-order Sobol' index S_i for θ_i (also referred as the main effect of θ_i) is defined as (Sobol 2001)

$$S_i = \frac{V_i}{V_H} = \frac{E_i[\xi_i(\theta_i)^2] - \mu_H^2}{V_H} \tag{5.1}$$

where V_i represents the expected reduction in variance V_H due to fixing θ_i, and

$$\xi_i(\theta_i) = E_{\sim i}[H(\boldsymbol{\theta})|\theta_i] = \int_{\boldsymbol{\Theta}_{\sim i}} H(\boldsymbol{\theta}_{\sim i}, \theta_i) p(\boldsymbol{\theta}_{\sim i}|\theta_i) d\boldsymbol{\theta}_{\sim i} \tag{5.2}$$

where $\boldsymbol{\theta}_{\sim i}$ represents the remaining of the distribution parameter vector excluding θ_i. Here, the conditional density $p(\boldsymbol{\theta}_{\sim i}|\theta_i)$ is used to represent the most general case that the distribution parameters could be dependent (i.e., dependence between $\boldsymbol{\theta}_{\sim i}$ and θ_i). For example, the distribution parameters might be dependent when they are inferred from the same data for the random variables $\mathbf{x}$. When $\boldsymbol{\theta}_{\sim i}$ and θ_i are independent, $p(\boldsymbol{\theta}_{\sim i}|\theta_i)$ reduces to $p(\boldsymbol{\theta}_{\sim i})$. Here μ_H is equal to H that is expressed by Eq. (4.2), i.e., $\mu_H = E_{\boldsymbol{\theta}}[H(\boldsymbol{\theta})] = \int_{\boldsymbol{\Theta}} H(\boldsymbol{\theta}) p(\boldsymbol{\theta}) d\boldsymbol{\theta} = \iint_{X,\boldsymbol{\Theta}} h(\mathbf{x}) p(\mathbf{x}|\boldsymbol{\theta}) p(\boldsymbol{\theta}) d\mathbf{x} d\boldsymbol{\theta}$. V_H is given by

$$\begin{aligned} V_H &= E_{\boldsymbol{\theta}}[(H(\boldsymbol{\theta}) - \mu_H)^2] = \int_{\boldsymbol{\Theta}} H(\boldsymbol{\theta})^2 p(\boldsymbol{\theta}) d\boldsymbol{\theta} - \mu_H^2 \\ &= \int_{\boldsymbol{\Theta}} \left(\int_X h(\mathbf{x}) p(\mathbf{x}|\boldsymbol{\theta}) d\mathbf{x} \right)^2 p(\boldsymbol{\theta}) d\boldsymbol{\theta} - \mu_H^2 \end{aligned} \tag{5.3}$$

Besides the first-order Sobol' index, Sobol' index for higher-order interaction, as well as the total sensitivity index can be also defined (Homma and Saltelli 1996; Sobol 2001).

5.2.3 Computational challenges in the calculation of risk-based Sobol' indices

Plugging the expression for $\xi_i(\theta_i)$ in Eq. (5.2) into the term $E_i[\xi_i(\theta_i)^2]$ for the calculation of S_i leads to

$$E_i[\xi_i(\theta_i)^2] \;\; = \int_{\Theta_i} \left[\int_{X,\boldsymbol{\Theta}_{\sim i}} h(\mathbf{x}) p(\mathbf{x}|\boldsymbol{\theta}_{\sim i}, \theta_i) p(\boldsymbol{\theta}_{\sim i}|\theta_i) d\boldsymbol{\zeta} \right]^2 p(\theta_i) d\theta_i \tag{5.4}$$

where the integration in the bracket corresponds to the expanded version of $\xi_i(\theta_i) = E_{\sim i}[H(\boldsymbol{\theta})|\theta_i]$ and is with respect to $\boldsymbol{\zeta} = [\mathbf{x}, \boldsymbol{\theta}_{\sim i}]$. This is different from the typical sensitivity analysis where

the integration would be with respect to $\boldsymbol{\theta}_{\sim i}$ alone. Here to evaluate the conditional expectation $E_{\sim i}[H(\boldsymbol{\theta})|\theta_i]$, the integration with respect to $\mathbf{x}$ is additionally needed.

As can be seen, evaluation of every S_i requires knowledge of $E_i[\xi_i(\theta_i)^2]$, which involves a double-loop integration. The outer loop corresponds to the calculation of the expectation $E_i[\xi_i(\theta_i)^2]$ with respect to θ_i, and the inner loop corresponds to calculation of the conditional expectation $\xi_i(\theta_i) = E_{\sim i}[H(\boldsymbol{\theta})|\theta_i]$ or more specifically the expectation with respect to vector $[\mathbf{x}, \boldsymbol{\theta}_{\sim i}]$. To calculate Sobol' index for higher-order interaction, the integration in Eq. (5.4) needs to be repeated for different parameter combinations and parameter values. To evaluate the double-loop integral, the general approach is MCS (Sobol 2001). However, direct adoption of MCS entails significant computational burden, especially for systems with expensive evacuation models (i.e., calculation of $h(\mathbf{x})$ for given $\mathbf{x}$ is expensive, which is the case for the tsunami evacuation model) and a large number of inputs (n_x is large) and distribution parameters (n_θ is large).

5.3 Efficient sensitivity analysis of tsunami evacuation risk using the augmented sample-based approach

To address the above challenges, an augmented sample-based approach is proposed for efficient sensitivity analysis of tsunami evacuation risk with respect to the epistemic uncertainty in distribution parameters. The augmented sample-based approach extends on the sample-based approach in Jia and Taflanidis (2016) for efficient estimation of Sobol' index. The proposed augmented approach first defines an augmented problem in terms of $[\mathbf{x}, \boldsymbol{\theta}]$. Then, we define a joint auxiliary distribution $\pi(\mathbf{x}, \boldsymbol{\theta})$ with respect to $[\mathbf{x}, \boldsymbol{\theta}]$, which is proportional to the integrand of the augmented evacuation risk integral for μ_H,

$$\pi(\mathbf{x}, \boldsymbol{\theta}) = \frac{h(\mathbf{x})p(\mathbf{x}|\boldsymbol{\theta})p(\boldsymbol{\theta})}{\mu_H} \propto h(\mathbf{x})p(\mathbf{x}|\boldsymbol{\theta})p(\boldsymbol{\theta}) \tag{5.5}$$

The augmented sample-based approach relies on generating samples from the joint distribution $\pi(\mathbf{x}, \boldsymbol{\theta})$ to efficiently estimate the conditional expectation $\xi_i(\theta_i)$ and further the Sobol' index.

5.3.1 Calculation of first-order Sobol' indices

Based on the joint auxiliary PDF $\pi(\mathbf{x}, \boldsymbol{\theta})$, the marginal auxiliary distribution for $\boldsymbol{\theta}$ can be written as

$$\begin{aligned} \pi(\boldsymbol{\theta}) &= \int_X \pi(\mathbf{x}, \boldsymbol{\theta}) d\mathbf{x} \\ &= \frac{p(\boldsymbol{\theta}) \int_X h(\mathbf{x}) p(\mathbf{x}|\boldsymbol{\theta}) d\mathbf{x}}{H} \end{aligned} \tag{5.6}$$

Similarly, the marginal auxiliary density for θ_i, i.e., $\pi(\theta_i)$, can be established by integrating out $\mathbf{x}$ and $\boldsymbol{\theta}_{\sim i}$ (i.e., $\boldsymbol{\zeta}$),

$$\begin{aligned} \pi(\theta_i) &= \int_{X, \boldsymbol{\Theta}_{\sim i}} \pi(\mathbf{x}, \boldsymbol{\theta}) d\boldsymbol{\zeta} \\ &= \frac{p(\theta_i) \int_{X, \boldsymbol{\Theta}_{\sim i}} h(\mathbf{x}) p(\mathbf{x}|\boldsymbol{\theta}) p(\boldsymbol{\theta}_{\sim i}|\theta_i) d\boldsymbol{\zeta}}{\mu_H} \\ &= \frac{p(\theta_i)}{\mu_H} \xi_i(\theta_i) \end{aligned} \tag{5.7}$$

This means the conditional expectation $\xi_i(\theta_i)$ can be written as a function of two marginal PDFs for θ_i as

$$\xi_i(\theta_i) = \frac{\pi(\theta_i)}{p(\theta_i)} \mu_H \tag{5.8}$$

From the derivation of Eq. (5.7), it is clear that $\pi(\theta_i)$ corresponds to the marginal auxiliary density for θ_i of the joint auxiliary density $\pi(\mathbf{x}, \boldsymbol{\theta})$. Therefore, samples can be first generated from the joint auxiliary density $\pi(\mathbf{x}, \boldsymbol{\theta})$, and the θ_i component of the samples would correspond to samples from the marginal auxiliary density $\pi(\theta_i)$. Compared to directly sampling from $\pi(\boldsymbol{\theta})$ where the evaluation of $\pi(\boldsymbol{\theta})$ for each $\boldsymbol{\theta}$ requires evaluation of the integral $\int_X h(\mathbf{x}) p(\mathbf{x}|\boldsymbol{\theta}) d\mathbf{x}$, if we sample from the joint auxiliary density $\pi(\mathbf{x}, \boldsymbol{\theta})$, based on Eq. (5.5), to evaluate $\pi(\mathbf{x}, \boldsymbol{\theta})$ for given value of $[\mathbf{x}, \boldsymbol{\theta}]$, then only the evacuation model $h(\mathbf{x})$ needs to be evaluated, which is much more efficient than evaluating the integral $\int_X h(\mathbf{x}) p(\mathbf{x}|\boldsymbol{\theta}) d\mathbf{x}$.

To sample from $\pi(\mathbf{x}, \boldsymbol{\theta})$, first, a set of candidate samples $\{[\mathbf{x}^k, \boldsymbol{\theta}^k], k = 1, \ldots, N\}$ are generated from some joint proposal density $q(\mathbf{x}, \boldsymbol{\theta})$, and the corresponding $h(\mathbf{x})$ are evaluated, and then stochastic sampling algorithm is used to obtain n_π samples from the joint PDF $\pi(\mathbf{x}, \boldsymbol{\theta})$, denoted $\{[\mathbf{x}_\pi^k, \boldsymbol{\theta}_\pi^k], k = 1, \ldots, n_\pi\}$. The detailed stochastic sampling procedure is presented in Appendix A. More importantly, the stochastic sampling can be seamlessly integrated within the sample-based evaluation of the system risk by leveraging the information from the risk assessment (i.e., the candidate samples generated for $\{[\mathbf{x}^k, \boldsymbol{\theta}^k], k = 1, \ldots, N\}$ and the corresponding risk measure $h(\mathbf{x})$ calculated). Since these samples will be used within KDE to approximate the underlying density, independent samples are needed. Any stochastic sampling algorithms that can provide independent samples can be used, e.g., the standard accept-reject method (Robert and Casella 2004). To improve sampling efficiency and thus the performance of the proposed approach, an appropriate proposal density $q(\mathbf{x}, \boldsymbol{\theta})$ needs to be selected. To improve sampling efficiency, advanced stochastic sampling techniques can be used. For example, adaptive kernel sampling density (AKSD) has been proposed to build better proposal density with the explicit objective of maximizing the sampling efficiency (Jia et al. 2017). When the risk measure $h(\mathbf{x})$ corresponds to the indicator function $I_F(\mathbf{x})$, taking advantage of the property of indicator function (i.e., taking values of either 0 or 1), modified Metropolis-Hastings algorithm (Au and Beck 2003) and modified rejection sampling (Jia et al. 2017) have been used to reduce the number of unnecessary model evaluations during the sampling process. Also, for rare events or low failure probability, when directly generating samples is not efficient, sequentially and adaptively generating samples (e.g., in the context of subset simulation (Jia et al. 2017; Au and Beck 2003)) could significantly improve sampling efficiency as well. Since it is not the focus of this research, exactly which stochastic sampling algorithm to use will not be discussed here in detail.

Using Eq. (5.1) and Eq. (5.8), the first-order Sobol' index S_i can be written as

$$
\begin{aligned}
S_i &= \frac{\mu_H^2}{V_H}\left(\int_{\Theta_i}\left[\frac{\pi(\theta_i)}{p(\theta_i)}\right]^2 p(\theta_i)d\theta_i - 1\right) \\
&= \frac{\mu_H^2}{V_H}\left(\int_{\Theta_i}\left[\frac{\pi(\theta_i)}{p(\theta_i)}\right]\pi(\theta_i)d\theta_i - 1\right)
\end{aligned}
\tag{5.9}
$$

Based on the marginal samples from $\pi(\theta_i)$, kernel density estimation (KDE) (Karunamuni and Zhang 2008; Jia and Taflanidis 2016) (illustrated in Appendix B.1) can be used to efficiently approximate $\pi(\theta_i)$ for any value of θ_i (denoted $\tilde{\pi}(\theta_i)$) and then $\xi_i(\theta_i)$ through Eq. (5.8). To address bounded distribution parameters, which are frequently encountered in various engineering applications, instead of regular KDE, which has boundary bias problem for density with large weights near the boundaries, the boundary-corrected KDE in Jia and Taflanidis (2014, 2016) (see Appendix B.2) can be used to establish more accurate estimations of the density. Due to the curse of dimensionality for KDE and the estimation errors, in general, sample-based estimation of densities for higher dimensionality (e.g., larger than four) should be avoided (Jia and Taflanidis 2016).

Ultimately, the first-order Sobol' index S_i in Eq. (5.9) can be approximated by Monte Carlo Integration (MCI) as

$$
\hat{S}_i \approx \left(\frac{1}{n_\pi}\sum_{k=1}^{n_\pi}\frac{\tilde{\pi}(\theta_{\pi_i}^k)}{p(\theta_{\pi_i}^k)} - 1\right)\frac{\hat{\mu}_H^2}{\hat{V}_H} \tag{5.10}
$$

The coefficient of variation (CoV) for MCI approximation can be conveniently calculated and used as the statistical error of the estimator. As can be seen, the estimation accuracy of S_i relies on the accuracy of KDE. Since the accuracy of KDE improves as the number of samples increases, it is expected that using more samples (i.e., a larger value of n_π) would lead to a more accurate estimation of S_i. Based on Eq. (4.3), the unbiased estimator of $\mu_H = H$ can be established directly using MCI based on all the candidate samples from the proposal density $q(\mathbf{x}, \boldsymbol{\theta})$. As for V_H, it involves double-loop integration; direct estimation would involve first generating for example N_θ samples for $\boldsymbol{\theta}$ and then for each $\boldsymbol{\theta}$, generating for example N_x samples for $\mathbf{x}$ and evaluating the corresponding $h(\mathbf{x})$. It would require total of $N_\theta \times N_x$ model evaluations.

Instead of repeating the model evaluations as required by direct estimation of the double-loop integration, here the same set of simulations for the N candidate samples $\{[\mathbf{x}^k, \boldsymbol{\theta}^k], k = 1, \ldots, N\}$ and the corresponding N model evaluations $h(\mathbf{x})$ are used to efficiently estimate V_H. This approach uses the concept of importance sampling where the same proposal density is used to estimate the integral $\int_X h(\mathbf{x})p(\mathbf{x}|\boldsymbol{\theta})d\mathbf{x}$ under different $p(\mathbf{x}|\boldsymbol{\theta})$ through re-weighting the same set of samples (Wang and Jia 2019b, 2020b). The joint proposal density can be rewritten as $q(\mathbf{x}, \boldsymbol{\theta}) = q(\mathbf{x}|\boldsymbol{\theta})q(\boldsymbol{\theta})$. $q(\boldsymbol{\theta})$ can be used as proposal density for the outer loop (i.e., integration with respect to $\boldsymbol{\theta}$), and use $q(\mathbf{x}|\boldsymbol{\theta})$ as proposal density for the inner loop (i.e., integration with respect to $\mathbf{x}$). For given $\boldsymbol{\theta}$ value (e.g., $\boldsymbol{\theta} = \boldsymbol{\theta}^k$), the integral $H(\boldsymbol{\theta}^k) = \int_X h(\mathbf{x})p(\mathbf{x}|\boldsymbol{\theta}^k)d\mathbf{x}$ can be estimated using the candidate sample pairs of $\{[\mathbf{x}^j, \boldsymbol{\theta}^j], j = 1, \ldots, N\}$,

$$\hat{H}(\boldsymbol{\theta}^k) \approx \frac{1}{N}\sum_{j=1}^{N} h(\mathbf{x}^j)\frac{p(\mathbf{x}^j|\boldsymbol{\theta}^k)}{q(\mathbf{x}^j|\boldsymbol{\theta}^j)} \tag{5.11}$$

where $\mathbf{x}^j$ is generated according to proposal density $q(\mathbf{x}^j|\boldsymbol{\theta}^j)$. A special case would be $q(\mathbf{x}^j|\boldsymbol{\theta}^j) = q(\mathbf{x}^j)$ where the proposal density for $\mathbf{x}$ does not depend on $\boldsymbol{\theta}$. Using Eq. (5.11), the same candidate sample pairs of $\{[\mathbf{x}^j, \boldsymbol{\theta}^j], j = 1, \ldots, N\}$, can be used for evaluation of $H(\boldsymbol{\theta}^k)$ for different $\boldsymbol{\theta}^k$. In the end, using information in the same set of N simulations used for generating samples from the joint auxiliary density, the unbiased estimator of V_H can be established through the following equation,

$$\hat{V}_H \approx \frac{1}{N}\sum_{k=1}^{N}\left[\frac{1}{N}\sum_{j=1}^{N} h(\mathbf{x}^j)\frac{p(\mathbf{x}^j|\boldsymbol{\theta}^k)}{q(\mathbf{x}^j|\boldsymbol{\theta}^j)}\right]^2 \frac{p(\boldsymbol{\theta}^k)}{q(\boldsymbol{\theta}^k)} - \hat{\mu}_H^2 \tag{5.12}$$

In the end, Eq. (5.10) can be used to estimate S_i. Note that the statistical errors of the estimator $\hat{\mu}_H$ and $\hat{V}_H$ are assessed using the CoVs for the corresponding MCI approximations. The steps to efficiently calculate the first-order Sobol' index using the augmented sample-based approach is summarized in Fig. 5.2.

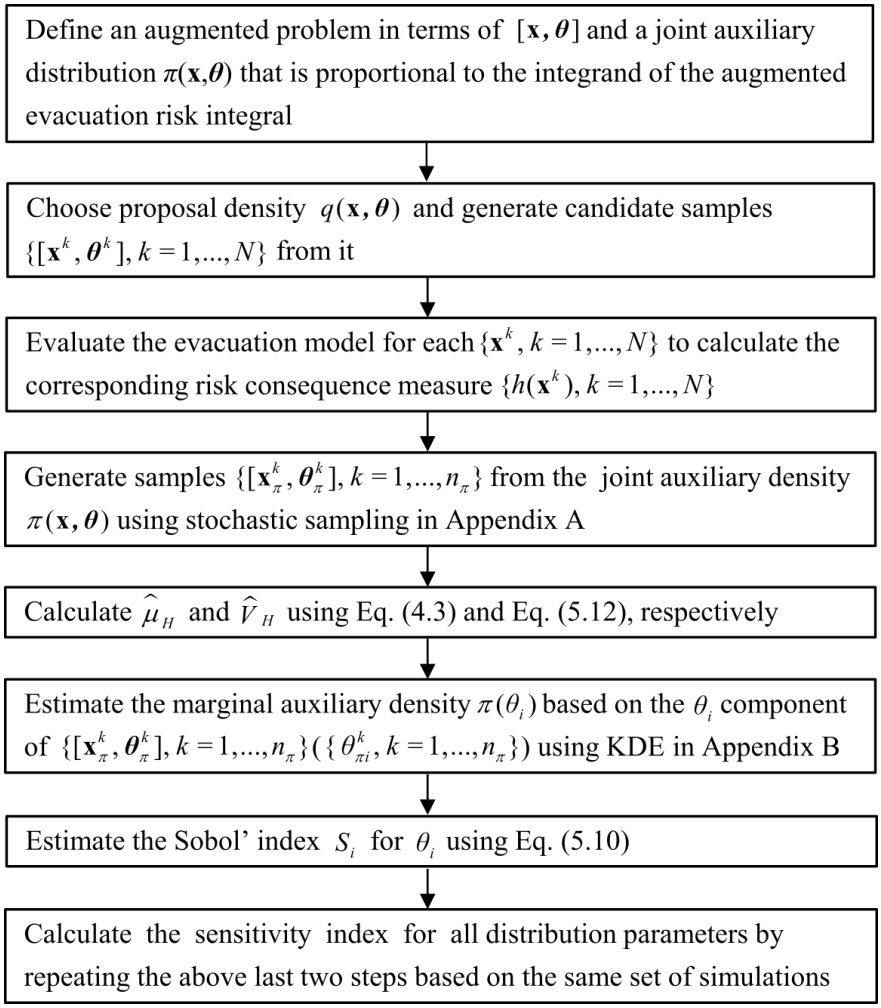


Figure 5.2: The steps to efficiently calculate the first-order Sobol' index using the augmented sample-based approach.

5.3.2 Calculation of higher-order Sobol' indices

Besides first-order sensitivity indices, using the same set of samples, the augmented sample-based approach can be directly used to estimate sensitivity indices for higher-order interactions. Let $S_{[ij]}$ represent the second-order sensitivity index for the interaction between θ_i and θ_j, and S_{ij} represent the joint second-order sensitivity index for the subset $\boldsymbol{\theta}_{ij} = [\theta_i, \theta_j]$. S_{ij} can be estimated using Eq. (5.10) by changing θ_{π_i} to $\boldsymbol{\theta}_{\pi_{ij}}$ and the KDE needs to use the corresponding multivariate KDE. More specifically, S_{ij} can be estimated by

$$\hat{S}_{ij} \approx \left(\frac{1}{n_\pi} \sum_{k=1}^{n_\pi} \frac{\tilde{\pi}(\boldsymbol{\theta}_{\pi_{ij}}^k)}{p(\boldsymbol{\theta}_{\pi_{ij}}^k)} - 1 \right) \frac{\hat{\mu}_H^2}{\hat{V}_H} \tag{5.13}$$

Based on the relationship $S_{[ij]} = S_{ij} - S_i - S_j$, $S_{[ij]}$ can be estimated by

$$\hat{S}_{[ij]} = \hat{S}_{ij} - \hat{S}_i - \hat{S}_j \tag{5.14}$$

Besides second-order interaction, other higher-order sensitivity indices can be established similarly (Jia and Taflanidis 2016).

As can be seen, by projecting the samples from $\pi(\mathbf{x}, \boldsymbol{\theta})$ to the subsets of interest, the corresponding Sobol' indices can be evaluated efficiently, including both first-order and higher-order indices. Compared to the direct evaluation of Sobol' index, which requires rerunning simulations for each index of interest, the augmented sample-based approach only requires one set of simulations or samples to estimate all sensitivity indices, corresponding to high efficiency. This high efficiency is important and desirable since the agent-based tsunami evacuation model is quite expensive to run (as discussed in Section 4.4). The accuracy and efficiency of the augmented sample-based approach in the evaluation of Sobol' index have been validated by several benchmark problems (Wang and Jia 2020a).

Once the sensitivity index (i.e., Sobol' index) values (including the first-order/main effect and higher-order interactions) are obtained, they can be used to compare the importance of each distribution parameter θ_i on the variability in the tsunami evacuation risk. Then, the importance ranking information can be used to guide the data collection prioritization for more effective epistemic uncertainty reduction and further for more accurate evacuation risk assessment, and more effective evacuation planning.

5.4 Illustrative example: Sensitivity analysis of tsunami evacuation risk with respect to epistemic uncertainty for Seaside, Oregon

We consider the example in Chapter 3; however, here uncertain population size and population proportions throughout different sub-areas with epistemic uncertainties are considered to

investigate the sensitivity analysis of tsunami evacuation risk with respect to various epistemic uncertainties. The epistemic uncertainty in the standard deviation of the population proportion that evacuates by car is also incorporated for a more comprehensive investigation. Table 5.1 presents the continuous input random variables $\mathbf{x}$ and associated parameters including uncertain ones (i.e., distribution parameters $\boldsymbol{\theta}$).

Table 5.1: Continuous input random variables and associated parameters in tsunami evacuation.

x_i	Distribution	Parameter 1	Parameter 2
t_0	Uniform	3	10
t	Rayleigh	[0, 5]	[1, 5]
n_e	Truncated Gaussian	[4000, 15,000]	[3000, 7000]
ρ_1	Truncated Gaussian	[0.2, 0.6]	[0.05, 0.25]
ρ_3	Truncated Gaussian	[0.25, 0.35]	[0.05, 0.25]
p_c	Truncated Gaussian	[0, 1]	[0.05, 0.25]
$T_{1_{PA}}$	Uniform	1.00	1.53
$T_{2_{PA}}$	Uniform	2.30	4.19
$T_{1_{MA}}$	Uniform	0.59	0.97
$T_{2_{MA}}$	Uniform	1.64	3.14
$T_{1_{Mac}}$	Uniform	0.59	0.97
$T_{2_{Mac}}$	Uniform	1.53	2.79
$T_{1_{LR}}$	Uniform	0.27	0.38
$T_{2_{LR}}$	Uniform	0.54	1.04
v_p	Truncated Gaussian	[1.22, 2.68]	[0.05, 1]
p_f	Uniform	0.1	0.3
p_r	Uniform	0.3	0.6
h_c	Uniform	0.5	2

For continuous input random variable x_i, n_e represents the population; ρ_1 and ρ_3 denote the population proportion on the beach and in the residential area, respectively. The population proportion in the downtown (denoted ρ_2) can be obtain using $\rho_2 = 1 - \rho_1 - \rho_3$. For the x_i following truncated Gaussian distribution, n_e, ρ_1, ρ_3, p_c, and v_p lie within (4000, 15,000), (0.2, 0.6), (0.25, 0.35), (0, 1), and (0.75, 3.83) (unit: m/s), respectively.

Here, $\boldsymbol{\theta}$ includes τ and σ_t that define the Rayleigh distribution to model t where $\tau \sim U(0, 5)$ represents the delay time after receiving the tsunami warning (unit: min) and $\sigma_t \sim U(1, 5)$ is the scale parameter, and the mean and standard deviation of the Gaussian distribution of n_e, ρ_1, ρ_3,

p_c, and v_p, i.e., μ_e and σ_e, μ_1 and σ_1, μ_3 and σ_3, μ_c and σ_c, μ_p and σ_p. Each of the above means and standard deviations follows the uniform distribution on the interval that is presented under "Parameter 1" and "Parameter 2".

In terms of evacuation risk consequence measure $h(\mathbf{x})$, two cases are considered. Case 1: $h(\mathbf{x})$ is defined as the total casualty rate (TCR) in the community within one hour and the risk $H(\boldsymbol{\theta})$ corresponds to the expected total casualty rate. Case 2:$h(\mathbf{x})$ is defined as the indicator function, i.e., $h(\mathbf{x}) = I_F(\mathbf{x})$, where $I_F(\mathbf{x}) = 1$ if the casualty rate exceeds a certain threshold and 0 otherwise, and the risk $H(\boldsymbol{\theta})$ corresponds to the failure probability $P_F(\boldsymbol{\theta})$ (i.e., the probability of the casualty rate exceeding a certain threshold).

5.4.1 Results and discussions: Case 1

To calculate the risk sensitivity indices, $n_\pi = 2000$ samples for $[\mathbf{x}, \boldsymbol{\theta}]$ are generated from the auxiliary PDF $\pi(\mathbf{x}, \boldsymbol{\theta})$ by selecting the the prior density as the proposal density (i.e., $q(\mathbf{x}, \boldsymbol{\theta}) = p(\mathbf{x}|\boldsymbol{\theta})p(\boldsymbol{\theta})$). This selection leads to a sampling efficiency of around 40%, i.e., around 5000 tsunami evacuation simulations are used to generate these auxiliary samples. Table 5.2 presents the sensitivity analysis results, including the first-order Sobol' indices for all distribution parameters and higher-order Sobol' indices for some cases of interest (greater importance). The results are the average values over 50 different runs where each run only involves repeating the stochastic sampling part (to generate the auxiliary samples) and does not require running additional evacuation simulations (i.e., still using the same set of 5000 simulations for the stochastic sampling). Note the coefficient of variation (CoV) for each MCI approximation in the estimation of Sobol' indices is below 1%.

Based on the first-order sensitivity results, μ_c has the greatest importance followed by μ_e and σ_t while other distribution parameters have much smaller importance. μ_c has greater importance indicates the epistemic uncertainty in μ_c has a higher impact on the variability in evacuation risk. Compared to evacuation on foot, evacuation by car is more likely to cause severe traffic congestion, which would delay the evacuation and cause more casualties. As μ_c increases (i.e., more cars and

Table 5.2: Sensitivity indices for the tsunami evacuation risk: Case 1.

Parameters	Indices	Parameters	Indices
First-order sensitivity indices			
τ	0.0021	σ_t	0.0133
μ_e	0.0415	σ_e	0.0026
μ_1	0.0057	σ_1	0.0025
μ_3	0.0037	σ_3	0.0019
μ_c	0.1446	σ_c	0.0047
μ_p	0.0031	σ_p	0.0032
Second-order sensitivity indices			
σ_t, μ_c	0.0198	μ_e, σ_e	0.0164
μ_1, σ_3	0.0150	μ_3, σ_c	0.0149
τ_t, μ_c	0.0147	σ_t, μ_3	0.0145
μ_e, μ_c	0.0143	σ_1, μ_3	0.0142
μ_c, σ_c	0.0138	μ_3, μ_c	0.0135
τ_t, μ_p	0.0132	μ_e, μ_1	0.0132
σ_1, μ_p	0.0131	μ_1, μ_p	0.0131
μ_3, σ_p	0.0127	μ_1, μ_3	0.0127
μ_c, σ_p	0.0126	μ_e, σ_p	0.0126
σ_e, σ_c	0.0125	τ_t, σ_3	0.0123

fewer pedestrians), the car casualty rate would increase and the pedestrian casualty rate would decrease. However, the increase of the car casualty rate is much larger than the decrease of the pedestrian casualty rate, which makes the total casualty rate increases significantly with an increase of μ_c (Wang and Jia 2021). On the contrary, the total casualty rate would decrease significantly with a decrease of μ_c (Wang and Jia 2021). The relatively greater importance of μ_e can be explained similarly, i.e., traffic congestion is sensitive to the population, which ultimately leads to the large sensitivity of the total casualty rate to the population. On one hand, the larger population (i.e., the larger value of μ_e) tends to induce more severe traffic congestion or even traffic jam, which would delay the evacuation and lead to a higher evacuation risk (Wang and Jia 2021). On the other hand, the smaller population results in a lower evacuation risk (Wang and Jia 2021). σ_t represents the spread of the distribution of the departure time, which could have a big impact on the evacuation. The overall evacuation performance (i.e., casualty rate) can be easily affected by the delay of evacuation (e.g., larger σ_t leads to more delays), especially under the near-field tsunami

that can reach the shoreline less than half an hour. Therefore, σ_t has a relatively high impact on the variability in evacuation risk as well.

As for the second-order sensitivity results, relatively strong interactions exist related to the distribution parameters corresponding to p_c, n_e, and t. For example, the strongest interaction is observed between μ_c and σ_t, which is even larger than the first-order index value for σ_t (i.e., $0.0198 > 0.0133$). As discussed in the first-order sensitivity results, μ_c and σ_t, respectively, have the largest and third-largest individual importance, and the strong interaction occurs related to them is anticipated. Another relatively strong interaction exists between μ_e and σ_e. This is because μ_e has the second-greatest importance individually as well as μ_e and σ_e correspond to the population size, which has a high impact on evacuation risk. Other top-ranked second-order sensitivity indices have very close values. For example, the Sobol' index value for the third-highest interaction $[\mu_1, \sigma_3]$ and 20^{th} interaction $[\tau_t, \sigma_3]$ is 0.0150 and 0.0123, respectively. This indicates these interactions have close importance in terms of their interaction on the variability in evacuation risk.

The above first-order and second-order sensitivity information (importance) can be used to prioritize the data collection for more effective epistemic uncertainty reduction, which can further support more accurate risk assessment and more effective evacuation planning. For example, the data collection on the distribution parameters corresponding to p_c especially μ_c has a top priority considering the epistemic uncertainty in μ_c dominates the variability in evacuation risk in this case. Besides μ_c and σ_c, the data on the distribution parameters associated with n_e and t are recommended to be collected in priority due to the individual importance of μ_e and σ_t, and the relatively strong interactions related to these parameters (i.e., μ_e, σ_e, τ and σ_t). Once sufficient data on the important distribution parameters are available, the epistemic uncertainty is expected to be reduced effectively and the evacuation risk would be assessed more accurately.

5.4.2 Results and discussions: Case 2

In this case, the performance threshold for failure is selected such that the average failure probability (i.e., μ_H) is around 10%. Similar to Case 1, the prior density is selected as the proposal

density to generate the candidate samples, which are then used to obtain the samples from $\pi(\mathbf{x}, \boldsymbol{\theta})$ through stochastic sampling. This leads to $n_\pi = 500$ samples being generated from around 5000 tsunami evacuation simulations with a sampling efficiency of 10% (i.e., equal to μ_H). Note that here no special effort is spent in building better proposal density that will lead to higher sampling efficiency; however, for small failure probability (i.e., μ_H is small), to reduce the total number of simulations, more advanced sampling techniques with well-designed proposal density can be used (e.g., using the approach in Jia et al. (2017)). Table 5.3 presents the first-order Sobol' indices for all distribution parameters and second-order Sobol' indices for some cases of interest (greater importance). The CoVs for all MCI approximations in the estimation of Sobol' indices are below 5%.

Table 5.3: Sensitivity indices for the tsunami evacuation risk: Case 2.

Parameters	Indices	Parameters	Indices
First-order sensitivity indices			
τ	0.0041	σ_t	0.0382
μ_e	0.0413	σ_e	0.0048
μ_1	0.0055	σ_1	0.0033
μ_3	0.0015	σ_3	0.0030
μ_c	0.3480	σ_c	0.0012
μ_p	0.0029	σ_p	0.0005
Second-order sensitivity indices			
σ_t, μ_c	0.0438	μ_e, μ_c	0.0413
μ_c, σ_c	0.0398	τ_t, μ_c	0.0226
μ_e, σ_e	0.0220	μ_1, μ_c	0.0190
σ_t, μ_e	0.0139	σ_1, μ_c	0.0125
σ_3, μ_c	0.0122	σ_e, μ_c	0.0115
μ_e, σ_p	0.0108	σ_t, μ_3	0.0104
σ_c, μ_p	0.0102	τ_t, σ_t	0.0097
σ_t, σ_c	0.0092	μ_e, σ_3	0.0092
σ_t, σ_3	0.0088	τ_t, σ_1	0.0088
σ_3, μ_p	0.0087	μ_c, σ_p	0.0082

The first-order sensitivity results show similar trends to Case 1, e.g., μ_c is the dominant distribution parameter followed by μ_e and σ_t while other distribution parameters are of negligible importance. However, the Sobol' index value for μ_c in Case 2 (i.e., 0.3480) is much larger than that

in Case 1 (i.e., 0.1446). Since the Sobol' index values for μ_e are close for both cases (i.e., 0.0413 in Case 2 and 0.0415 in Case 1), the much larger value of μ_c in Case 2 indicates even higher impact of μ_c compared to μ_e. This is because the relative importance of μ_c is enlarged in Case 2 due to the lower average tsunami evacuation risk ($\mu_H = 10\%$) than that in Case 1 ($\mu_H = 28.9\%$).

By looking at the second-order sensitivity results, some similarities to Case 1 can be found. For instance, most of the strong interactions are related to the distribution parameters corresponding to p_c, n_e, and t. In comparison to Case 1, the second-order sensitivity results in Case 2 demonstrate one interesting difference. In Case 2, μ_c dominates the strong interactions. For the ten strongest interactions (i.e., Sobol's index values between 0.0115 and 0.0438), eight of them are related to μ_c. This should be attributed to the dominance of the impact of the epistemic uncertainty in μ_c on the variability in evacuation risk.

Once the importance of all considered distribution parameters is identified based on the risk sensitivity analysis results, they can be used to guide the data collection prioritization for more effective epistemic uncertainty reduction. In this case, the efforts on the data collection are recommended to be put in the distribution parameters corresponding to p_c (especially μ_c) with a high priority rather than other distribution parameters considering the epistemic uncertainty in μ_c dominates the variability in the evacuation risk.

According to the calculation of the first-order Sobol' index for the distribution parameter θ_i, we know that the risk sensitivity with respect to θ_i can also be seen qualitatively from the comparison between $p(\theta_i)$ and $\pi(\theta_i)$. The larger difference between the two distributions indicates the greater importance of the distribution parameter. Fig. 5.3(a)-(d) show the samples for μ_c and μ_e from the corresponding marginal auxiliary densities (i.e., $\pi(\mu_c)$ and $\pi(\mu_e)$), the distributions approximated based on the corresponding samples using the boundary corrected KDE and the corresponding prior distributions (i.e., $p(\mu_c)$ and $p(\mu_e)$). As can be seen from Fig. 5.3(c), $\pi(\mu_c)$ changes significantly compared to $p(\mu_c)$, which clearly demonstrates why μ_c has a great importance. Similarly, the comparison between $\pi(\mu_e)$ and $p(\mu_e)$ (shown in Fig. 5.3(d)) demonstrates qualitatively the relatively great importance of μ_e. The difference between the marginal auxiliary distribution and

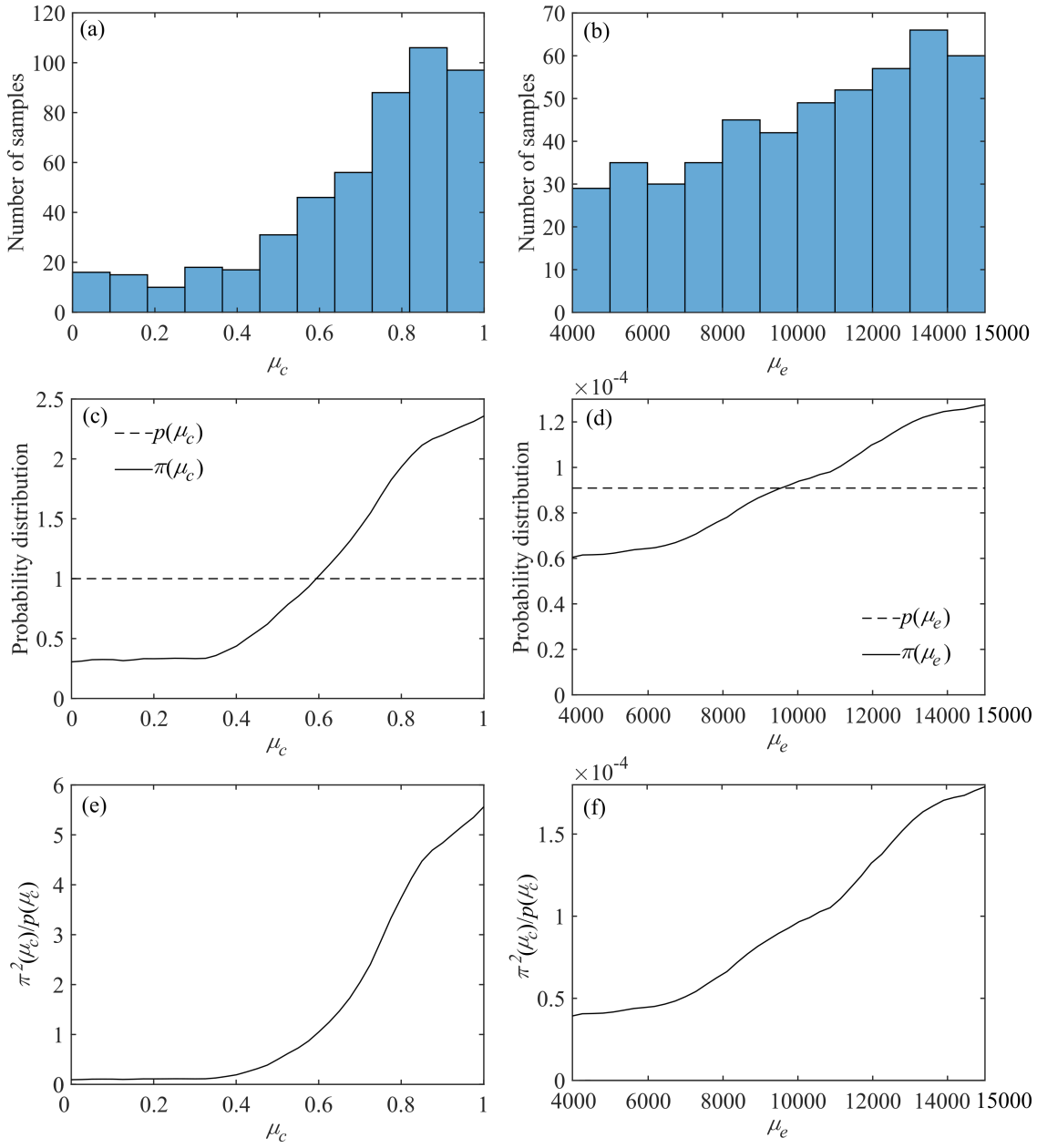


Figure 5.3: Illustration of (a) samples from $\pi(\mu_c)$, (b) samples from $\pi(\mu_e)$, (c) $\pi(\mu_c)$ estimated using boundary corrected KDE, (d) $\pi(\mu_e)$ estimated using boundary corrected KDE, (e) variation of the integrand $\pi^2(\mu_c)/p(\mu_c)$ in calculation of S_i for μ_c, and (f) variation of the integrand $\pi^2(\mu_e)/p(\mu_e)$ in calculation of S_i for μ_e. All results are for Case 2.

the corresponding prior distribution for μ_c is much larger than that for μ_e, meaning μ_c has a much greater importance than μ_e (as also verified by their sensitivity index values as shown in Table 5.3).

To provide an additional understanding of the sensitivity analysis results, Fig. 5.3(e) and Fig. 5.3(f), respectively, show the variation of the integrand in the calculation of the first-order

Sobol' index (i.e., S_i in Eq. (5.9)) for μ_c and μ_e. Fig. 5.3(e) shows that the integrand increases with μ_c, and it increases much faster under relatively large values of μ_c. Overall, the integrand has much larger values when μ_c is large. This indicates that relatively larger values of μ_c contribute more to the first-order sensitivity index value or the variability in the evacuation risk is more sensitive to the change of car use when a relatively large number of cars are used in the evacuation. Compared to the case when a relatively small number of cars are used, any change of the car number (either decrease or increase) could have a higher impact on the traffic congestion level when a relatively large number of cars are used. The larger variability in the traffic congestion level would ultimately lead to a larger variability in the casualty (evacuation risk) due to the evacuation delay caused by the traffic congestion. Fig. 5.3(f) for μ_e shows similar trends to Fig. 5.3(e) for μ_c, e.g., the integrand increases with μ_e and relatively larger values of μ_e contribute more to the variability in the evacuation risk.

5.5 Summary

This chapter investigated the sensitivity of tsunami evacuation risk with respect to various epistemic uncertainties in the distribution parameters where these parameters define the probability distributions of the input random variables in the proposed agent-based tsunami evacuation model. The variance-based sensitivity index, i.e., Sobol' index, was used as the sensitivity measure to quantify the importance of each distribution parameter and their interactions on the variability in the tsunami evacuation risk. An augmented sample-based approach was developed and used for the efficient calculation of the Sobol' index for all distribution parameters (including first-order and second-order indices) in the risk sensitivity analysis using only one set of simulations.

As an illustrative example, the sensitivity analysis of tsunami evacuation risk was efficiently performed for Seaside, Oregon under two different cases (i.e., different definitions of the risk measure) using the proposed augmented sample-based approach. The importance ranking of the distribution parameters associated with the evacuation process was identified for each case. The sensitivity analysis results show that the distribution parameters corresponding to the proportion of

the evacuees that use the car, population size, and departure time (especially the proportion of the evacuees that use the car) have greater importance than those associated with other input random variables. However, the exact importance ranking of various distribution parameters can vary with cases depending on the interested risk performance measure. The above risk sensitivity information on the importance of distribution parameters can be used to prioritize the data collection for an effective epistemic uncertainty reduction and further for a more accurate risk assessment, and more effective evacuation planning.

Chapter 6

Identification of critical risk factors using sensitivity analysis

6.1 Introduction

It is important to identify the critical risk factors that contribute more to the tsunami evacuation risk, which can be used to guide effective evacuation modeling and the search for effective risk mitigation strategies (Okumura et al. 2017). On one hand, for a more realistic simulation of the tsunami evacuation, many factors and mechanisms associated with the evacuation need to be considered and modeled as realistically as possible, especially important factors and mechanisms. Considering that critical risk factors have higher impacts on the evacuation risk, we can pay more attention to the modeling of the factors and mechanisms those closely related to critical risk factors for more effective modeling. On the other hand, after being informed about the level of evacuation risk by risk assessment, the decision-maker needs to know further about the relative contributions of different risk factors to the risk (i.e., importance ranking of risk factors or identification of critical risk factors). Such information can be used to guide the search for effective risk mitigation strategies, i.e., explore more effective risk-reduction strategies that are more associated with critical risk factors to achieve the acceptable risk level (Okumura et al. 2017).

As mentioned in Chapter 5, sensitivity analysis is typically used to examine the importance of the system input to the system output or performance quantity of interest (Saltelli 2002). Therefore, the sensitivity analysis can be performed to investigate the importance of various risk factors in affecting the evacuation risk. Under the simulation-based framework for the risk quantification proposed in Chapter 4, the input random variable with the aleatory uncertainty can represent the risk factor (e.g., the proportion of the evacuees that use the car, i.e., p_c). In this context, we are interested in identifying the importance of various input random variables in affecting the

evacuation risk to identify critical risk factors in tsunami evacuation. However, there has been limited research on sensitivity analysis associated with tsunami evacuation. Typically, they conduct the parametric study rather than perform full sensitivity analysis. The parametric study examines the sensitivity of the model output to the uncertainty of a single random variable while keeping other random variables constant each time (e.g., demographic-sensitivity analyses (Wood et al. 2015), model sensitivity to land cover and path direction (Schmidtlein and Wood 2015), model sensitivity to the individual random variable associated with the evacuation behavior (Fraser et al. 2014; Wang et al. 2016; Mostafizi et al. 2017, 2019b)). In this case, the parametric study can not take into account the uncertainty in other random variables. Moreover, repeating the analysis for different variables also entails significant computational challenges, which typically limits the parametric study to several selected cases/parameters.

To address the above limitations and computational challenges, the probabilistic sensitivity analysis in Taflanidis and Jia (2011) (which was proposed for identification of critical risk factors) is used to investigate the importance of various risk factors in affecting the evacuation risk, based on which critical risk factors are identified. To investigate the variation of the sensitivity of risk factors with the key distribution parameter, the augmented sample-based approach proposed in Chapter 5 is extended to efficiently perform the sensitivity analysis under different values of the distribution parameter. Because only one set of samples is needed, the approach has great efficiency and simultaneously provides sensitivity information for all input random variables under different given values of the distribution parameter.

The sensitivity analysis of the tsunami evacuation risk in Seaside, Oregon is performed using the augmented sample-based approach. The established sensitivity information can be used to guide effective evacuation modeling, and effective selection of candidate risk mitigation strategies and hence identification of more effective strategies (as shown later in Chapter 7).

6.2 Sensitivity analysis for identifying critical risk factors

The probabilistic sensitivity analysis in Taflanidis and Jia (2011) and Jia and Taflanidis (2014) is used to quantify the importance of risk factor (i.e., each input random variable in $\mathbf{x}$) in affecting the evacuation risk H. The probabilistic sensitivity analysis is defined by introducing an auxiliary PDF that is proportional to the integrand of evacuation risk integral, i.e., $\pi(\mathbf{x}) = \int_{\boldsymbol{\Theta}} h(\mathbf{x})p(\mathbf{x}|\boldsymbol{\theta})p(\boldsymbol{\theta})d\boldsymbol{\theta}/H$.

The sensitivity of the i^{th} input random variable x_i is quantified by the relative entropy that measures the difference between the marginal auxiliary distribution $\pi(x_i)$ and the prior probability distribution $p(x_i)$,

$$D\left(\pi(x_i) \parallel p(x_i)\right) = \int_{X_i} \pi(x_i) \log\left[\frac{\pi(x_i)}{p(x_i)}\right] dx_i \tag{6.1}$$

where $\pi(x_i) = \int_{X_{\sim i}} \pi(\mathbf{x}) d\mathbf{x}_{\sim i}$ and $p(x_i) = \int_{X_{\sim i}} p(\mathbf{x}) d\mathbf{x}_{\sim i}$, where $\mathbf{x}_{\sim i}$ represents the rest of $\mathbf{x}$ excluding x_i. The reason that such difference indicates the sensitivity of H with respect to x_i can be explained as follows. For the marginal distribution $\pi(x_i)$, based on definition, it can be expanded as $\pi(x_i) = \int_{X_{\sim i}} \pi(\mathbf{x}) d\mathbf{x}_{\sim i} = p(x_i) \iint_{X_{\sim i},\boldsymbol{\Theta}} h(\mathbf{x})p(\mathbf{x}_{\sim i}|\boldsymbol{\theta})p(\boldsymbol{\theta})\mathrm{d}\mathbf{x}_{\sim i}\mathrm{d}\boldsymbol{\theta}/H = p(x_i)H(x_i)/H$, where $H(x_i)$ represents the evacuation risk H when fixing x_i at particular value. Therefore, the ratio of $\pi(x_i)$ to $p(x_i)$ is directly related to the value of the evacuation risk H. This is why the difference between the marginal distribution $\pi(x_i)$ and the prior distribution $p(x_i)$ indicates the sensitivity of H with respect to x_i. Larger value of relative entropy indicates higher sensitivity/importance of the input random variable. However, it is challenging to directly evaluate $\pi(x_i)$ (e.g., use MCS), which corresponds to multi-dimensional integral. The above relative entropy can be efficiently calculated using the sample-based approach in Taflanidis and Jia (2011) and Jia and Taflanidis (2014), i.e., approximate $\pi(x_i)$ and $p(x_i)$ using kernel density estimation (KDE) based on the generated samples (i.e., n_π samples from $\pi(\mathbf{x})$). To obtain the samples from $\pi(\mathbf{x})$, the same sampling process as the augmented sample-based approach in Chapter 5 can be used. The only difference here is that we are interested in the marginal samples for $\mathbf{x}$ rather than marginal samples for $\boldsymbol{\theta}$.

For the sensitivity analysis of the discrete input random variable x_i, suppose x_i can take values in $\{\epsilon_j, j = 1, ..., m_i\}$, the relative entropy between $\Pi(x_i)$ and $P(x_i)$ can be expressed as (Jia et al. 2014; Wang and Jia 2020b)

$$D\left(\Pi(x_i) \parallel P(x_i)\right) = \sum_{j=1}^{m_i} \Pi(x_i = \epsilon_j) \log\left[\frac{\Pi(x_i = \epsilon_j)}{P(x_i = \epsilon_j)}\right] \tag{6.2}$$

where $\Pi(x_i = \epsilon_j)$ can be estimated by counting the number of samples that satisfy $x_i = \epsilon_j$ out of all n_π samples for x_i and dividing this number by n_π. Similarly, $P(x_i = \epsilon_j)$ can be estimated by counting the number of samples that satisfy $x_i = \epsilon_j$ out of all N samples for x_i and dividing this number by N.

6.3 Variation of the sensitivity of risk factors with key distribution parameters

The sensitivity analysis in Section 6.2 corresponds to the case when the uncertainties in the distribution parameters are fully propagated (assuming that the distribution parameters are uncertain). When there is less or no uncertainty in the distribution parameters or subsets of the distribution parameters (e.g., when there is good knowledge on the values of the distribution parameters, hence good knowledge on the distribution of the input random variables), how the sensitivity of the risk factors would vary also provides important insights on the overall sensitivity of the evacuation risk. Therefore, this section investigates the variation of sensitivity of risk factors with some key distribution parameters. Mathematically, we are interested in the sensitivity analysis under different values of some key distribution parameters.

Let $\boldsymbol{\theta}_s$ represent some key distribution parameters of interest, which is a subset of all distribution parameters $\boldsymbol{\theta}$. Note that $\boldsymbol{\theta}_s$ can be a scalar or vector. The evacuation risk under the given value of $\boldsymbol{\theta}_s$ (i.e., conditional evacuation risk) can be expressed as

$$H(\boldsymbol{\theta}_s) = \iint_{X,\boldsymbol{\Theta}_{\sim s}} h(\mathbf{x}) p(\mathbf{x}|\boldsymbol{\theta}_s, \boldsymbol{\theta}_{\sim s}) p(\boldsymbol{\theta}_{\sim s}|\boldsymbol{\theta}_s) d\mathbf{x} d\boldsymbol{\theta}_{\sim s} \tag{6.3}$$

where $\boldsymbol{\theta}_{\sim s}$ represents the rest of $\boldsymbol{\theta}$ excluding $\boldsymbol{\theta}_s$ in the space of $\boldsymbol{\Theta}_{\sim s}$.

Here the sensitivity analysis is used to quantify the importance of each input random variable x_i in affecting the conditional evacuation risk $H(\boldsymbol{\theta}_s)$. The sensitivity analysis is defined by introducing an auxiliary PDF $\pi(\mathbf{x}, \boldsymbol{\theta}_{\sim s}|\boldsymbol{\theta}_s)$ that is proportional to the integrand of the conditional evacuation risk integral. Then the marginal PDF $\pi(\mathbf{x}|\boldsymbol{\theta}_s)$ for $\mathbf{x}$ can be written as

$$\pi(\mathbf{x}|\boldsymbol{\theta}_s) = \frac{\int_{\boldsymbol{\Theta}_{\sim s}} h(\mathbf{x}) p(\mathbf{x}|\boldsymbol{\theta}_s, \boldsymbol{\theta}_{\sim s}) p(\boldsymbol{\theta}_{\sim s}|\boldsymbol{\theta}_s) d\boldsymbol{\theta}_{\sim s}}{H(\boldsymbol{\theta}_s)} \tag{6.4}$$

The sensitivity of the i^{th} input random variable x_i under the given value of $\boldsymbol{\theta}_s$ is quantified by the relative entropy between the marginal auxiliary distribution $\pi(x_i|\boldsymbol{\theta}_s)$ and the prior probability distribution $p(x_i|\boldsymbol{\theta}_s)$,

$$D\left(\pi(x_i|\boldsymbol{\theta}_s) \parallel p(x_i|\boldsymbol{\theta}_s)\right) = \int_{X_i} \pi(x_i|\boldsymbol{\theta}_s) \log\left[\frac{\pi(x_i|\boldsymbol{\theta}_s)}{p(x_i|\boldsymbol{\theta}_s)}\right] dx_i \tag{6.5}$$

where $\pi(x_i|\boldsymbol{\theta}_s) = \int_{X_{\sim i}} \pi(\mathbf{x}|\boldsymbol{\theta}_s) d\mathbf{x}_{\sim i}$ and $p(x_i|\boldsymbol{\theta}_s) = \int_{X_{\sim i}} p(\mathbf{x}|\boldsymbol{\theta}_s) d\mathbf{x}_{\sim i}$, where $x_{\sim i}$ represents the rest of $\mathbf{x}$ excluding x_i. Larger value of relative entropy indicates higher sensitivity/importance of the input random variable. However, it is challenging to directly evaluate $\pi(x_i|\boldsymbol{\theta}_s)$ (e.g., use MCS) for any given value of x_i, which corresponds to multi-dimensional integral. Therefore, direct evaluation of Eq. (6.5) is challenging for one input random variable, not to mention for all input random variables. When $\boldsymbol{\theta}_s$ takes some fixed value, the above relative entropy can be efficiently calculated using the sample-based approach in Taflanidis and Jia (2011) and Jia and Taflanidis (2014), i.e., approximate $\pi(x_i|\boldsymbol{\theta}_s)$ and $p(x_i|\boldsymbol{\theta}_s)$ using KDE based on the corresponding samples. However, here we are interested in sensitivity under different values of $\boldsymbol{\theta}_s$, for which direct application of the above sample-based approach would entail huge computational challenges due to the need to repeat the approach for different values of $\boldsymbol{\theta}$.

To address the above challenges, the augmented sample-based approach proposed in Chapter 5 is extended for efficient sensitivity analysis under any given value of $\boldsymbol{\theta}_s$. To estimate the relative entropy in Eq. (6.5) for x_i, conditional distributions $\pi(x_i|\boldsymbol{\theta}_s)$ and $p(x_i|\boldsymbol{\theta}_s)$ need to be estimated.

To facilitate this, an augmented problem is first defined in terms of $[\mathbf{x}, \boldsymbol{\theta}]$, in which $\boldsymbol{\theta}_s$ is artificially treated as uncertain with distribution $p(\boldsymbol{\theta}_s)$ over the domain of interest. Typically, uniform distribution is assumed for $\boldsymbol{\theta}_s$ for calculation convenience, since it has constant PDF value. Then, a set of candidate samples $\{[\mathbf{x}^k, \boldsymbol{\theta}^k], k = 1, \ldots, N\}$ are generated from some joint proposal density $q(\mathbf{x}, \boldsymbol{\theta})$, and the corresponding $h(\mathbf{x})$ are evaluated by running the evacuation simulation. Then, stochastic sampling algorithm (e.g., the accept-reject method (Robert and Casella 2004)) is used to obtain n_π samples from the joint PDF $\pi(\mathbf{x}, \boldsymbol{\theta})$, denoted $\{[\mathbf{x}_\pi^k, \boldsymbol{\theta}_\pi^k], k = 1, \ldots, n_\pi\}$. Note that although samples from the joint distribution $\pi(\mathbf{x}, \boldsymbol{\theta})$ are available, samples directly from the conditional distribution $\pi(x_i|\boldsymbol{\theta}_s)$ are not available. To make use of the samples, using the definition of conditional distribution (i.e., $\pi(x_i|\boldsymbol{\theta}_s) = \pi(x_i, \boldsymbol{\theta}_s)/\pi(\boldsymbol{\theta}_s)$), Eq. (6.5) is rewritten as

$$D\left(\pi(x_i|\boldsymbol{\theta}_s) \parallel p(x_i|\boldsymbol{\theta}_s)\right) = \int_{X_i} \frac{\pi(x_i, \boldsymbol{\theta}_s)}{\pi(\boldsymbol{\theta}_s)} \log\left[\frac{\pi(x_i, \boldsymbol{\theta}_s)}{\pi(\boldsymbol{\theta}_s) p(x_i|\boldsymbol{\theta}_s)}\right] dx_i \tag{6.6}$$

where $\pi(x_i, \boldsymbol{\theta}_s)$ is the joint auxiliary PDF for $[x_i, \boldsymbol{\theta}_s]$ and $\pi(\boldsymbol{\theta}_s)$ the marginal auxiliary PDF for $\boldsymbol{\theta}_s$. By projecting the joint samples to the space of $[x_i, \boldsymbol{\theta}_s]$, samples from $\pi(x_i, \boldsymbol{\theta}_s)$ can be established. Based on these samples, KDE can be used to establish an approximation, denoted $\tilde{\pi}(x_i, \boldsymbol{\theta}_s)$. In the end, the relative entropy for x_i conditional on any value of $\boldsymbol{\theta}_s$ can be calculated efficiently by

$$D\left(\pi(x_i|\boldsymbol{\theta}_s) \parallel p(x_i|\boldsymbol{\theta}_s)\right) = \int_{X_i} \frac{\tilde{\pi}(x_i, \boldsymbol{\theta}_s)}{\tilde{\pi}(\boldsymbol{\theta}_s)} \log\left[\frac{\tilde{\pi}(x_i, \boldsymbol{\theta}_s)}{\tilde{\pi}(\boldsymbol{\theta}_s) p(x_i|\boldsymbol{\theta}_s)}\right] dx_i \tag{6.7}$$

which can be calculated using numerical integration or MCI.

For the sensitivity analysis of the discrete input random variable x_i conditional on $\boldsymbol{\theta}_s$, suppose x_i can take values in $\{\epsilon_j, j = 1, ..., m_i\}$, the relative entropy between $\Pi(x_i|\boldsymbol{\theta}_s)$ and $P(x_i|\boldsymbol{\theta}_s)$ can be expressed as (Jia et al. 2014; Wang and Jia 2020b)

$$D\left(\Pi(x_i|\boldsymbol{\theta}_s) \parallel P(x_i|\boldsymbol{\theta}_s)\right) = \sum_{j=1}^{m_i} \Pi(x_i = \epsilon_j|\boldsymbol{\theta}_s) \log\left[\frac{\Pi(x_i = \epsilon_j|\boldsymbol{\theta}_s)}{P(x_i = \epsilon_j|\boldsymbol{\theta}_s)}\right] \tag{6.8}$$

To estimate $\Pi(x_i = \epsilon_j|\boldsymbol{\theta}_s)$ using the n_π samples from $\pi(\mathbf{x}, \boldsymbol{\theta}_s)$, Bayes' theorem is used in combination with KDE. Using Bayes' theorem, $\Pi(x_i = \epsilon_j|\boldsymbol{\theta}_s)$ can be written as

$$\Pi(x_i = \epsilon_j|\boldsymbol{\theta}_s) = \frac{\pi(\boldsymbol{\theta}_s|x_i = \epsilon_j)\Pi(x_i = \epsilon_j)}{\pi(\boldsymbol{\theta}_s)} \tag{6.9}$$

where $\Pi(x_i = \epsilon_j)$ can be estimated by counting the number of samples that satisfy $x_i = \epsilon_j$ out of all n_π samples for x_i and dividing this number by n_π. $\pi(\boldsymbol{\theta}_s|x_i = \epsilon_j)$ for any $\boldsymbol{\theta}_s$ can be estimated using KDE based on those marginal samples from $\pi(\boldsymbol{\theta}_s)$ that satisfy $x_i = \epsilon_j$. Therefore, using the same set of n_π samples, $\Pi(x_i = \epsilon_j|\boldsymbol{\theta}_s)$ can be estimated, which can be plugged into Eq. (6.8) to calculate the relative entropy for discrete input random variable x_i conditional any value of $\boldsymbol{\theta}_s$.

Overall, the sensitivity analysis under different values of some of the key distribution parameters of interest can be performed efficiently using the extended augmented sample-based approach, which only requires one set of samples/simulations and has great computational efficiency.

6.4 Illustrative example: Identification of critical risk factors using sensitivity analysis for Seaside, Oregon

The above two cases of sensitivity analysis are performed to identify critical risk factors associated with the tsunami evacuation in Seaside, Oregon. Previous studies have shown that the proportion of the evacuees that use the car for evacuation (i.e., p_c) has a high impact on evacuation performance. Therefore, for the sensitivity analysis under different values of the distribution parameter, we are interested in investigating how the probabilistic sensitivity with respect to input random variables varies with the mean value of p_c (i.e., μ_c). More specifically, the sensitivity analysis conditional on different values of the distribution parameter μ_c is considered, i.e., $\boldsymbol{\theta}_s = [\mu_c]$. Since we are interested in μ_c within [0, 1], θ is artificially treated as uncertain with uniform distribution on [0, 1] (i.e., $p(\mu_c) = 1$).

As for the evacuation simulation, the daytime scenario with 15,000 evacuees (i.e., $n_e = 15,000$, corresponding to the worst daytime scenario) under C0 (i.e., the proposed agent-based model) in Chapter 4 is considered for the two cases of sensitivity analysis. To obtain more insights, the sensitivity analysis in Section 6.2 is also performed under the daytime scenario with a population

size of $n_e = 5000$ and under the nighttime scenario (i.e., Nighttime1 defined in Section 4.4.4) with a population size of $n_e = 15,000$.

6.4.1 Sensitivity analysis

For each of the daytime and nighttime scenarios with 15,000 evacuees, around $n_\pi = 1200$ samples are generated from $\pi(\mathbf{x}, \boldsymbol{\theta})$ based on $N = 2000$ tsunami evacuation simulations. For the daytime scenario with 5000 evacuees, around $n_\pi = 600$ samples are generated from $\pi(\mathbf{x}, \boldsymbol{\theta})$ based on $N = 2000$ tsunami evacuation simulations. For each scenario, all the sensitivity results reported next are obtained efficiently using the corresponding set of 2000 simulations with low CoVs for all MCI approximations (i.e, below 1% for the cases with $n_e = 15,000$ and below 2% for the case with $n_e = 5000$) and the risk consequence measure corresponds to the total casualty rate (i.e., TCR) in the community within one hour.

The daytime scenario with 15,000 evacuees

The relative entropy values for continuous input random variables and the damage state of the top five ranked bridges are presented in Table 6.1. In the table, i_1, i_2,..., i_5 represents the link IDs for the top five ranked bridges; $T_{1_{PA}}$, $T_{2_{PA}}$, $T_{1_{MA}}$, $T_{2_{MA}}$, $T_{1_{Mac}}$, $T_{2_{Mac}}$, $T_{1_{LR}}$, and $T_{2_{LR}}$ denote the thresholds in Eq. (3.4) and, respectively, correspond to the road class "Principle Arterial", "Minor Arterial", "Major Collector", and "Local Road". Based on the relative entropy values for the individual input random variable, it is evident that the population proportion of evacuation by car p_c has the greatest importance followed by the proportion of the evacuees that use evacuation routes (i.e., p_r) as well as the top-ranked bridges while others have smaller influence. The group input random variables associated with p_c even have larger relative entropy values than p_c, e.g., 0.0469 for $[p_c, p_r]$ is larger than 0.0358 for p_c. The greater importance of car use is expected since it is more likely to cause traffic congestion and delay the evacuation when more people evacuate by car. Based on the importance ranking, p_c is the most critical risk factor, which can be used for guiding effective evacuation modeling and the selection of candidate risk mitigation strategies. For example, car use and associated aspects (e.g., speed adjustment for the car) need to be modeled as

realistically as possible. The evacuation by car should be discouraged in some cases (e.g., a large proportion of car use) or the road (especially the evacuation route) can be widened to alleviate the potential traffic congestion caused by car use in the evacuation.

Table 6.1: Relative entropy values for continuous input random variables and the damage states of the top five ranked bridges under the daytime scenario with 15,000 evacuees.

x_i or $[x_i, x_j]$	D	x_i or $[x_i, x_j]$	D	x_i or $[x_i, x_j]$	D
i_1	0.0029	p_f	0.0002	$T_{2_{LR}}$	0.0013
i_2	0.0028	p_s	0.0025	$[p_c, t_0]$	0.0401
i_3	0.0014	$T_{1_{PA}}$	0.0025	$[p_c, p_r]$	0.0469
i_4	0.0014	$T_{2_{PA}}$	0.0021	$[p_c, p_f]$	0.0419
i_5	0.0011	$T_{1_{MA}}$	0.0012	$[p_c, p_s]$	0.0461
p_c	0.0358	$T_{2_{MA}}$	0.0008	$[T_{1_{PA}}, T_{2_{PA}}]$	0.0099
t_0	0.0006	$T_{1_{Mac}}$	0.0011	$[T_{1_{MA}}, T_{2_{MA}}]$	0.0072
h_c	0.0004	$T_{2_{Mac}}$	0.0004	$[T_{1_{Mac}}, T_{2_{Mac}}]$	0.0065
p_r	0.0053	$T_{1_{LR}}$	0.0013	$[T_{1_{LR}}, T_{2_{LR}}]$	0.0058

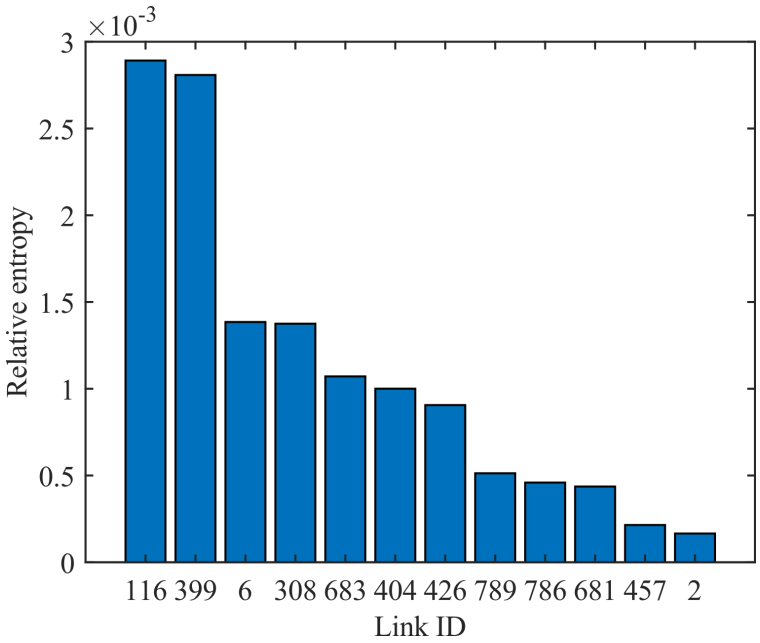


Figure 6.1: Relative entropy ranking for the damage state of bridges under the daytime scenario with 15,000 evacuees.

The relative entropy ranking (importance ranking) for the damage state of all the 12 bridges is shown in Fig. 6.1. Based on the relative entropy values, link 116 has the highest rank followed

by link 399 and other links while link 2 has the lowest rank. This means links 116 and 399 are more critical to evacuation risk than other bridges while link 2 is the least critical in this case. To have a better understanding of the above sensitivity analysis results, the relative entropy values of the damage state of all the 12 bridges with the link ID are shown in Fig. 6.2. On one hand, based on Fig. 6.2 and Fig. 3.9, links 116 and 399 located over one river form bottlenecks in the road network, and most of the evacuees would travel through these two bridges to the shelter. In this context, links 116 and 399 could be more critical to the tsunami evacuation and the corresponding seismic damages are more important to the evacuation risk. On the other hand, most of the evacuees would not use link 2 due to its location, and the seismic damage of link 2 would have the lowest impact on the evacuation risk. The above importance ranking of bridges can be used to guide the search for effective risk mitigation strategies, e.g., select critical bridges as the candidates to search the optimal bridge retrofit strategy such that evacuation risk is most effectively reduced.

The daytime scenario with 5000 evacuees

The relative entropy values for continuous input random variables and the damage state of the top five ranked bridges under the daytime scenario with 5000 evacuees are summarized in Table 6.2. Overall, the results show similar trends to the case with the relatively large population size (i.e., $n_e = 15,000$ shown in Table 6.1). For example, in terms of the importance of individual input random variable, the population proportion of evacuation by car p_c is the most important, followed by the proportion of the evacuees that use evacuation routes (i.e., p_r) and the top-ranked bridges while other input random variables are less important. Overall, the critical risk factors are similar under the two population sizes in this example.

The relative entropy ranking of the damage state of all the 12 bridges under the daytime scenario with 5000 evacuees is shown in Fig. 6.3. This ranking shows some similarities to the case with 15,000 evacuees, e.g., link 2 is the least important bridge. Under the two cases with different considered population sizes, however, the importance ranking of bridges are different. For example, links 399 and 116 are the most critical bridge under $n_e = 5000$ and $n_e = 15,000$, respectively. This is because the evacuation dynamics (e.g., change of the traffic congestion level on bridge link

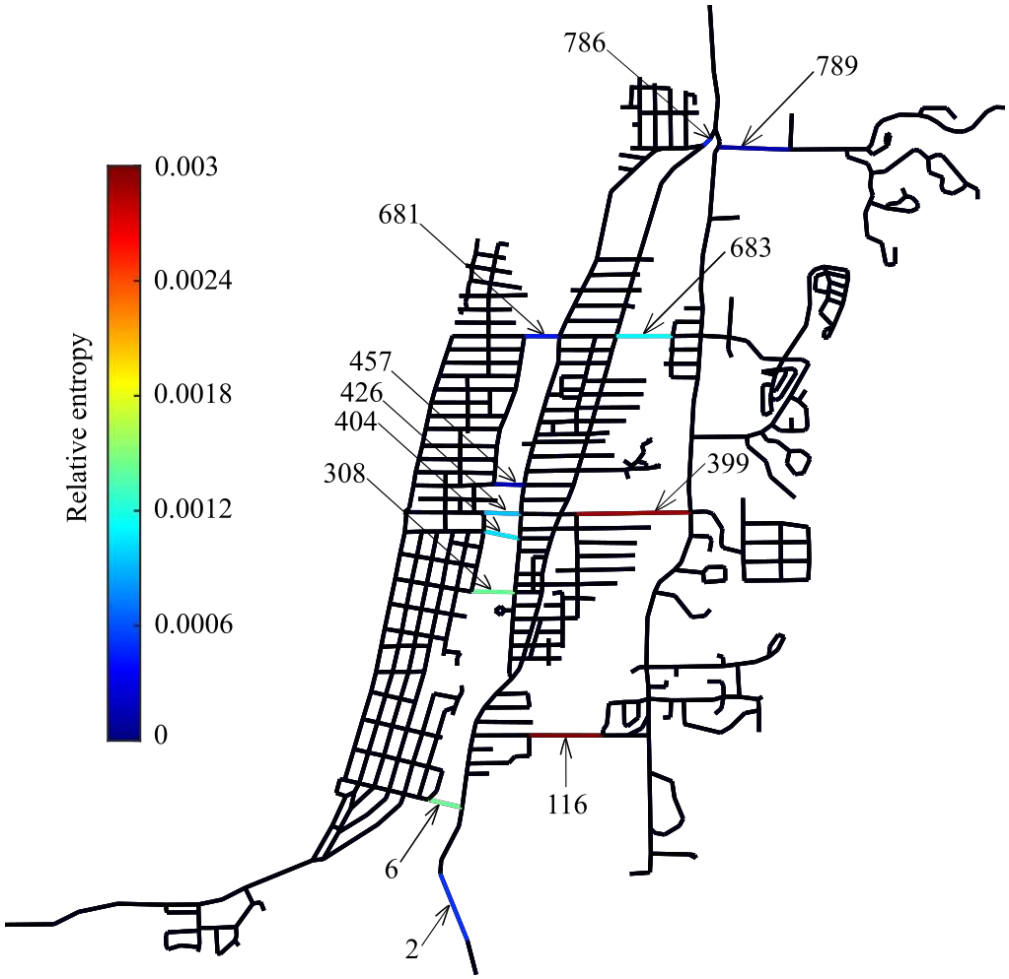


Figure 6.2: Relative entropy of the damage state of bridges under the daytime scenario with 15,000 evacuees.

Table 6.2: Relative entropy values for continuous input random variables and the damage states of the top five ranked bridges under the daytime scenario with 5000 evacuees.

x_i or $[x_i, x_j]$	D	x_i or $[x_i, x_j]$	D	x_i or $[x_i, x_j]$	D
i_1	0.0268	p_f	0.0025	$T_{2_{LR}}$	0.0062
i_2	0.0138	p_s	0.0163	$[p_c, t_0]$	0.4832
i_3	0.0086	$T_{1_{PA}}$	0.0080	$[p_c, p_r]$	0.4976
i_4	0.0064	$T_{2_{PA}}$	0.0076	$[p_c, p_f]$	0.4987
i_5	0.0062	$T_{1_{MA}}$	0.0090	$[p_c, p_s]$	0.4757
p_c	0.4609	$T_{2_{MA}}$	0.0063	$[T_{1_{PA}}, T_{2_{PA}}]$	0.0422
t_0	0.0044	$T_{1_{Mac}}$	0.0012	$[T_{1_{MA}}, T_{2_{MA}}]$	0.0271
h_c	0.0007	$T_{2_{Mac}}$	0.0113	$[T_{1_{Mac}}, T_{2_{Mac}}]$	0.0265
p_r	0.0280	$T_{1_{LR}}$	0.0025	$[T_{1_{LR}}, T_{2_{LR}}]$	0.0243

over time) would be different under the cases with different populations. Based on different im-

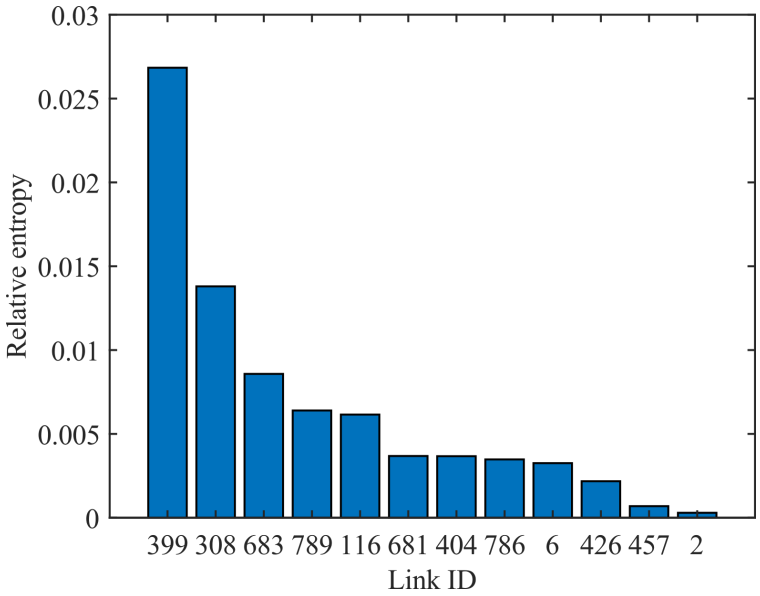


Figure 6.3: Relative entropy ranking for the damage state of bridges under the daytime scenario with 5000 evacuees.

portance rankings of bridges under the cases with different populations, different critical bridges may be retrofitted.

The nighttime scenario (Nighttime1) with 15,000 evacuees

The relative entropy values for continuous input random variables and the damage state of the top five ranked bridges under the nighttime scenario (Nighttime1) with 15,000 evacuees are presented in Table 6.3. The results show some similarities to the case under the daytime scenario with the same population size (shown in Table 6.1). For example, the population proportion of evacuation by car p_c has the greatest importance. Compare to the daytime scenario, however, the input random variables associated with the pedestrian-vehicle interaction (e.g., $T_{2_{MA}}$) instead of the proportion of the evacuees that use evacuation routes (i.e., p_r) have the relatively great importance following p_c. This indicates the critical risk factors may be different under the cases with different times of the day (i.e., daytime and nighttime).

The relative entropy ranking of the damage state of all the 12 bridges under the nighttime scenario (Nighttime1) with 15,000 evacuees is shown in Fig. 6.4. The sensitivity analysis results show some similarities to the case under the daytime scenario, e.g., link 2 has the smallest importance.

Table 6.3: Relative entropy values for continuous input random variables and the damage states of the top five ranked bridges under the nighttime scenario (Nighttime1) with 15,000 evacuees.

x_i or $[x_i, x_j]$	D	x_i or $[x_i, x_j]$	D	x_i or $[x_i, x_j]$	D
i_1	0.0052	p_f	0.0002	$T_{2_{LR}}$	0.0037
i_2	0.0025	p_s	0.0012	$[p_c, t_0]$	0.0657
i_3	0.0018	$T_{1_{PA}}$	0.0039	$[p_c, p_r]$	0.0514
i_4	0.0016	$T_{2_{PA}}$	0.0046	$[p_c, p_f]$	0.0521
i_5	0.0016	$T_{1_{MA}}$	0.0013	$[p_c, p_s]$	0.0514
p_c	0.0461	$T_{2_{MA}}$	0.0101	$[T_{1_{PA}}, T_{2_{PA}}]$	0.0174
t_0	0.0033	$T_{1_{Mac}}$	0.0101	$[T_{1_{MA}}, T_{2_{MA}}]$	0.0125
h_c	0.0001	$T_{2_{Mac}}$	0.0046	$[T_{1_{Mac}}, T_{2_{Mac}}]$	0.0190
p_r	0.0008	$T_{1_{LR}}$	0.0022	$[T_{1_{LR}}, T_{2_{LR}}]$	0.0070

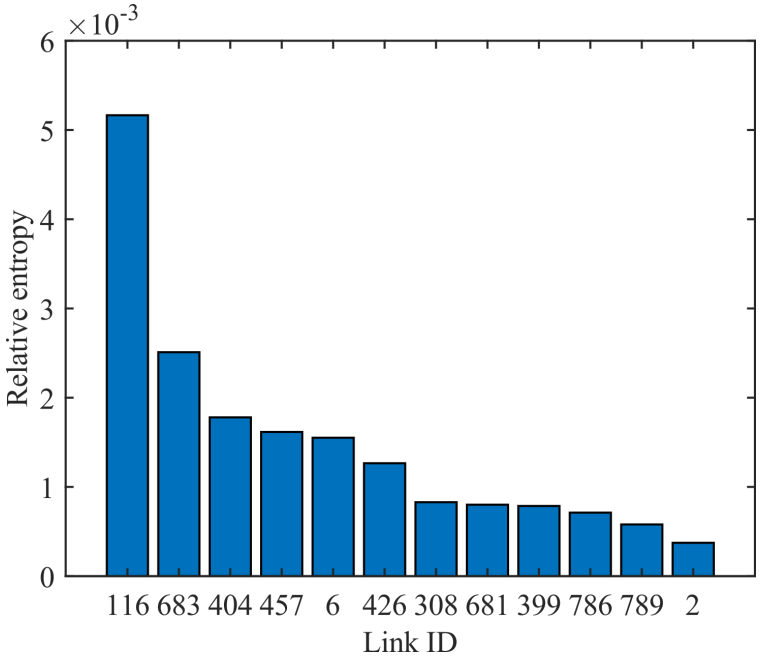


Figure 6.4: Relative entropy ranking for the damage state of bridges under the nighttime scenario (Nighttime1) with 15,000 evacuees.

However, the importance ranking of bridges under the nighttime scenario is different from that under the daytime scenario. For instance, under the nighttime scenario, the second most critical bridge is link 683 rather than link 399. Under the considered different times of the day, differences in the evacuation environment (e.g., lighting condition) and the evacuation behavior (e.g., pedestrian speed) exist. In this context, the evacuation dynamics (e.g., change of the traffic congestion level on bridge link over time) would be different, leading to different importance of the seismic damage of some bridge to the evacuation risk.

In summary, the population proportion of evacuation by car p_c has the greatest importance and overall the seismic damages of the top-ranked bridges have relatively great importance. These are true under the cases with different population sizes and with different times of the day. However, the importance ranking of risk factors (e.g., the seismic damage of the bridge) may be different under the cases with different population sizes and with different times of the day. The corresponding critical risk factors under the particular case need to be used when guiding effective modeling and selection of candidate mitigation strategies.

6.4.2 Variation of sensitivity of risk factors with the key distribution parameter

Based on $N = 2000$ tsunami evacuation simulations, around $n_\pi = 1200$ samples are generated from $\pi(\mathbf{x}, \boldsymbol{\theta})$. The augmented sample-based approach presented in Section 6.3 is applied to establish the probabilistic sensitivity information for $\mathbf{x}$ of interest under any given value of the distribution parameter μ_c. All the sensitivity results reported next are obtained efficiently using the same set of 2000 simulations with low CoVs for all MCI approximations (i.e., below 1%) and the risk consequence measure corresponds to the TCR in the community within one hour.

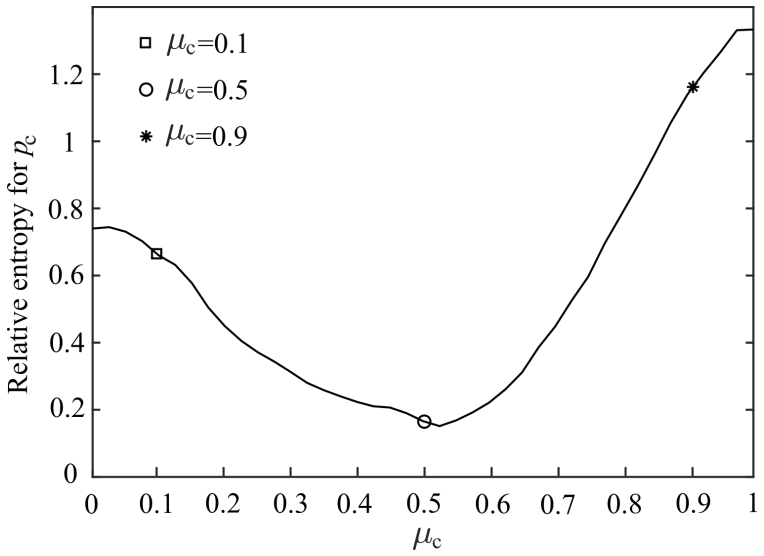


Figure 6.5: Relative entropy values for p_c conditional on different values of μ_c.

For the sensitivity results, overall under any given value of μ_c, p_c has the largest relative entropy value and thus greatest importance (the most critical), followed by the seismic damage of the top-ranked links while the continuous parameters other than p_c have relatively small relative entropy values. Considering its much larger value, the variation of the relative entropy for p_c as a function of μ_c is shown in Fig. 6.5 separately. While the relative entropy values for the continuous risk factors of interest other than p_c and the damage state of the top five ranked bridges are shown in Fig. 6.6 for three values of μ_c (i.e., 0.1, 0.5, and 0.9).

As μ_c increases, the variation of the relative entropy value for p_c shows a clear trend of first decreasing and then increasing. As μ_c (i.e., when $\mu_c < 0.5$) becomes smaller, more people evacuate on foot (i.e., smaller p_c) and the traffic congestion would get more severe for pedestrians, which leads to a faster increase in the casualty rate. Similarly, the traffic congestion would become more severe for cars and a faster increase would be caused in the casualty rate as μ_c becomes larger (i.e., when $\mu_c > 0.5$). This aligns with the first decreasing and then increasing relative entropy value and importance of p_c observed in Fig. 6.5. The fact that p_c has a much larger relative entropy value than other parameters indicates that p_c (i.e., car use) has much greater importance to evacuation risk than other parameters.

From Fig. 6.6, for input random variables other than p_c, the seismic damages of some bridges might have relatively large relative entropy values, which means evacuation risk is more sensitive to the seismic damages of those bridges than the other continuous input random variables (i.e., the ones other than p_c). Note that the relative entropy value corresponds to the seismic damage of the individual bridge and it is expected that the seismic damage of all bridges collectively would have a high impact on evacuation risk. For the continuous input random variables other than p_c, the relative entropy values are relatively small (e.g., the largest value is only 0.018 corresponding to p_r when $\mu_c = 0.9$). The importance ranking of these input random variables varies with the value of μ_c; however, overall p_r has relatively great importance. This information can be used for guiding evacuation risk mitigation, e.g., investigate the effectiveness of the evacuation route usage (i.e., p_r) and mitigate evacuation risk by using the evacuation route effectively.

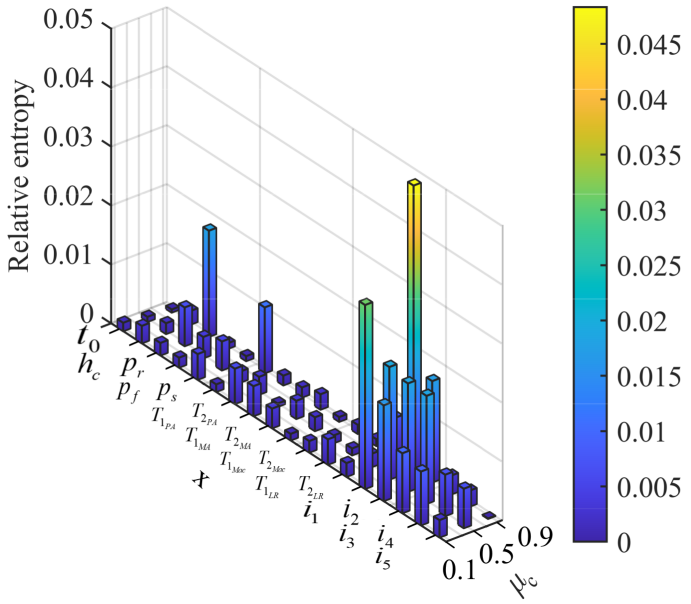


Figure 6.6: Relative entropy values for continuous input random variables of interest, and the damage state of the top five ranked bridges conditional on different values of μ_c.

As for the probabilistic sensitivity results of the seismic damage of bridges, overall, the top-ranked bridges correspond to larger relative entropy values than the continuous input random variables other than p_c as shown in Fig. 6.6; however, the importance ranking of bridges might be different under the different value of μ_c. The top five ranked bridges indices (i.e., i_1, i_2..., i_5) shown in Fig. 6.6 are reported in Table 6.4. Based on the sensitivity results, the importance ranking of bridges under the given value of μ_c could be identified to guide the selection of the optimal evacuation risk mitigation strategy (e.g., retrofit the critical bridges to reduce evacuation risk most effectively). The augmented sample-based approach can be used for such a purpose considering the high efficiency of establishing the probabilistic sensitivity information under any given value of μ_c using only one set of simulations.

Table 6.4: The link IDs for the top five ranked bridges corresponding to different μ_c values.

μ_c	i_1	i_2	i_3	i_4	i_5
0.1	786	404	399	308	426
0.5	789	6	681	308	404
0.9	789	6	457	308	681

The above sensitivity results (importance ranking of risk factors) can be used to guide effective evacuation modeling and the search for effective evacuation risk mitigation strategies. Considering the dominant importance of car use in the evacuation, for example, the modeling of car use and associated aspects (e.g., speed adjustment, pedestrian-vehicle interaction, etc.) need to be paid more attention to for more effective evacuation modeling. In the search for effective evacuation risk mitigation strategies, we can consider discouraging the large proportion of car use through tsunami-preparedness education to alleviate the potential traffic congestion and further reduce evacuation risk. The critical bridges (top-ranked) can be used as a candidate to search for effective evacuation risk mitigation strategies, i.e., which group of bridges to retrofit in priority such that evacuation risk is reduced most effectively.

6.5 Summary

Probabilistic sensitivity analysis was performed to identify critical risk factors associated with the tsunami evacuation. The variation of the sensitivity of risk factors with some key distribution parameters was also investigated. The augmented sample-based approach proposed for efficient sensitivity analysis of evacuation risk with respect to the epistemic uncertainty was extended to efficiently perform the sensitivity analysis.

Overall, the results showed that the proportion of the evacuees that use the car has the greatest importance, and the seismic damage of the top-ranked bridges as well as the proportion of the evacuees that use evacuation routes have relatively great importance while other risk factors have relatively small importance. However, the importance ranking of risk factors may be different under different cases, e.g., in terms of different population sizes and different times of the day. The sensitivity analysis results under different values of the key distribution parameter showed that the importance ranking of risk factors varies with car use. The critical risk factors identified by sensitivity analysis can be used to guide effective evacuation modeling and the selection of candidate risk mitigation strategies.

Chapter 7

Risk-informed evaluation of mitigation strategies

7.1 Introduction

For effective evacuation planning, pre-event mitigation is usually implemented to reduce the tsunami evacuation risk (UNESCO 2007). To effectively reduce the evacuation risk, effective or even optimal risk mitigation strategies need to be identified among potential strategies.

Various strategies being classified into different types have been proposed for mitigating tsunami risk in literature. For example, structural measures such as seawalls and breakwaters and non-structural measures of hazard map and evacuation were mainly discussed in Koshimura and Shuto (2015). In León and March (2016), strategies for coping with tsunami risk were summarized into three main types, including extensive civil-engineered defenses (e.g., breakwaters, sea gates, seawalls, control forests), land use and built environment measures (e.g., zoning, building codes and design recommendations), and emergency readiness systems (e.g., education, warning systems and especially population evacuation preparedness). In Aguirre-Ayerbe et al. (2018), four main strategies for risk reduction were presented, including prevention, preparedness strategies in the pre-event stage, emergency response, and recovery in the post-event phase. Many of the above strategies have been practiced for evacuation risk reduction around the world (Løvholt et al. 2019). For example, tsunami warning systems and evacuation-related education and exercise programs have become common since 2004. Evacuation routes and refuges are designed and applied in the U.S., Japan, and New Zealand. Tsunami defenses (breakwaters and coastal barriers) are widely implemented in Japan.

In terms of evaluation of the evacuation risk mitigation strategy, most of the research investigates a particular strategy. For example, road widening as a strategy to improve the road traffic condition in the evacuation was evaluated in Takada et al. (2013). Retrofitting critical bridges has been used to reduce the impact of seismic damage on the traffic capacity reduction (Mostafizi

et al. 2017). The effectiveness of the escape building for vertical evacuation has been evaluated in Haiqal et al. (2019). The suitable sites of vertical shelters were identified through geospatial, multi-criteria decision analysis in Wood et al. (2014). In addition to the above infrastructural strategies, a particular non-infrastructural strategy such as tsunami disaster education is widely recommended to be carried out for school children, their teachers and parents to better prepare for the potential tsunami evacuation. For example, the role of disaster education in the national tsunami hazard mitigation program was discussed in Dengler (2005). Tsunami disaster education was carried out for elementary school children and their parents to encourage the development of a family plan for tsunami evacuation (Katada and Kanai 2008). Pedagogical theories have been applied to help train teachers to teach disaster-related topics (Sharpe and Kelman 2011). The effectiveness of the curriculum-based disaster education program was evaluated in Adiyoso and Kanegae (2012). In Ronan et al. (2015), research on disaster preparedness for children and families was reviewed, with a focus on disaster preparedness and prevention education programs. Besides tsunami disaster education, the tsunami evacuation drill has been gaining more attention. The so-called "single-person drill" with emphasis on individual behaviors has been proposed to shift tsunami risk reduction from the community level to the individual level (Sun 2014). In Kawai et al. (2016), a tsunami evacuation drill system using motion hazard map and smart devices was introduced. The effectiveness of tsunami drills in guiding evacuation behavior was investigated after the onset of the Great East Japan Earthquake (Nakaya et al. 2018). A mobile application prototype was developed to be used as an educational tool in a drill exercise to enhance the traditional evacuation drill (Leelawat et al. 2018). Augmented reality technology has also been investigated to realize a game-based evacuation training system (Catal et al. 2020).

To identify more effective or even optimal risk mitigation strategies in a given area, the effectiveness of different candidate risk mitigation strategies needs to be evaluated quantitatively for comparison. When people select the candidate strategies to evaluate, typically they select the strategies based on feasibility but not necessarily based on quantitative analysis of whether the candidate strategies are promising or not in reducing the evacuation risk (Okumura et al. 2017;

Aguirre-Ayerbe et al. 2018). For the limited research on the evaluation of different types of evacuation risk mitigation strategies, most of them evaluate the strategies qualitatively or semi-quantitatively rather than quantitatively. For instance, three types of mitigation strategies were recommended in Priest et al. (2016) to establish optimal configurations, including bridge retrofit, street widening, and building tsunami refuges. However, these strategies were evaluated qualitatively rather than quantitatively. A method was proposed to prioritize the most suitable pre-event risk reduction measures based on the risk analysis and site-specific conditions (Aguirre-Ayerbe et al. 2018). However, the effectiveness of considered strategies was measured semi-quantitatively in terms of risk reduction, i.e., indicator-based (priority scores) rather than simulation-based.

In addition, the effectiveness of mitigation is typically not evaluated based on risk with systematic consideration of various uncertainties and hence the mitigation may not be robust to uncertainty. For instance, the effectiveness of road widening was evaluated in terms of a decrease in traffic congestion level in Takada et al. (2013). Different risk mitigation strategies such as vertical evacuation have been evaluated based on the reduction of risk defined in terms of the loss of life (Okumura et al. 2017). However, the risk was estimated based on the static model rather than dynamic evacuation simulation, i.e., estimate the mortality through simply comparing the arrival time of the tsunami and the time required for evacuation rather than running evacuation simulation under the time-history of tsunami inundation. In this case, many important uncertainties associated with the evacuation were neglected.

Furthermore, the effective mitigation for a particular type of strategy is usually identified by exhaustive enumeration, i.e., compare all combinations of mitigation design to identify the most effective one. This usually entails significant computational challenges due to the need to evaluate a large number of combinations of evacuation models, especially when the evacuation model is expensive to run. To devise more effective or optimal mitigation strategies, efficient algorithms are also needed.

To address the above limitations and challenges, risk-informed quantitative evaluation of different types of mitigation strategies (including infrastructural and non-infrastructural strategies)

is conducted to identify effective mitigation strategies that are also robust to uncertainties. Critical risk factors identified by sensitivity analysis are used to guide the effective selection of the candidate mitigation strategies. The evacuation risk under different candidate mitigation strategies is quantified and assessed using the proposed simulation-based framework, in which various uncertainties associated with the evacuation are explicitly quantified and the proposed agent-based model is used for tsunami evacuation simulation. The concepts of importance sampling and sample-based approach are used to efficiently evaluate the risk under different candidate strategies by leveraging existing simulations. Then, the effectiveness in the risk reduction of different candidate mitigation strategies is evaluated to identify more effective strategies. As an illustrative example, the risk-informed evaluation of mitigation strategies is conducted for the tsunami evacuation in Seaside, Oregon.

7.2 Sensitivity-based effective selection of candidate evacuation risk mitigation strategies

To reduce the tsunami evacuation risk, various mitigation strategies might be implemented, including the infrastructural and non-infrastructural strategies. For the infrastructural mitigation strategy, typically the existing infrastructure is modified to protect them from being damaged by the seismic and tsunami hazards or to improve the traffic condition, or new infrastructure is built such that evacuation risk is mitigated. The infrastructural mitigation strategy includes strategies such as building tsunami defenses such as seawalls and breakwaters (Koshimura and Shuto 2015; León and March 2016; Løvholt et al. 2019), building new bridges or retrofitting existing bridges (Mostafizi et al. 2017), widening road or evacuation route (Takada et al. 2013; Takabatake et al. 2017; Løvholt et al. 2019), and building shelters (vertical and horizontal) or retrofitting existing buildings as shelters (Raskin et al. 2011; Priest et al. 2016; Okumura et al. 2017; Løvholt et al. 2019). The non-infrastructural mitigation strategy involves the program or activity that aims to improve people's awareness of tsunami disaster and knowledge of tsunami evacuation. The non-infrastructural mitigation strategy involves tsunami warning system (León and March 2016; Løvholt et al. 2019),

tsunami preparedness education (Adiyoso and Kanegae 2012; León and March 2016; Aguirre-Ayerbe et al. 2018; Løvholt et al. 2019), evacuation drills (León and March 2016; Kawai et al. 2016; Oregon Office of Emergency Management 2017; Løvholt et al. 2019), and actual exercise (Murata et al. 2010; Løvholt et al. 2019).

To identity more effective ones among various mitigation strategies, some strategies can be selected as candidate strategies for evaluation and comparison rather than evaluating all the possible strategies. Candidate mitigation strategies can be effectively selected based on the critical risk factors associated with tsunami evacuation that are identified by sensitivity analysis in Chapter 6. As presented in the sensitivity analysis, critical risk factors that contribute more to evacuation risk have been identified. Evacuation risk would be reduced more effectively through the mitigation that targets those critical risk factors. More specifically, the strategy that is more closely related to the critical risk factor (directly or indirectly) is considered as the candidate strategy with a high priority. For instance, sensitivity analysis results in Chapter 6 have shown that car use is one of the critical risk factors and in general, more car use would lead to higher evacuation risk in the context of the considered example (especially when the proportion of evacuation by car is large). In this context, the strategy directly associated with car use such as discouraging the evacuation by car can be selected as the candidate non-infrastructural strategy. On the other hand, evacuation route widening (i.e., candidate infrastructural strategy) that is indirectly related to car use is also expected to mitigate evacuation risk, since the route widening can effectively alleviate the traffic congestion caused by car use (Takada et al. 2013). Note that the selection of risk mitigation strategies in a given area is usually influenced by coastal topographic characteristics and societal demands (Okumura et al. 2017). Here, we focus on the selection of candidate mitigation strategies based on critical risk factors and assume these candidate strategies meet criteria such as societal demands.

7.3 Risk-informed evaluation of mitigation strategies

Once candidate mitigation strategies are selected, the effectiveness of each strategy in terms of evacuation risk reduction needs to be evaluated for comparison to identify the more effective strategies. Fig. 7.1 illustrates the risk-informed evaluation of candidate mitigation strategies. Let H_0 represent the evacuation risk before mitigation and H_{s_i} denote the updated evacuation risk under the mitigation design of the i^{th} candidate strategy (denoted S_i). Then the risk reduction (denoted δH_i) can be calculated for each strategy, based on which the effectiveness of candidate mitigation strategies is evaluated. The more risk reduction (larger δH_i) means a more effective mitigation strategy. Note that one key step to evaluate the effectiveness of each candidate strategy is to calculate the evacuation risk under each strategy, i.e., calculation of H_{s_i}. Also, the optimal H_{s_i} might need to be identified under the i^{th} candidate strategy. The calculation of the evacuation risk under candidate mitigation strategies will be discussed next.

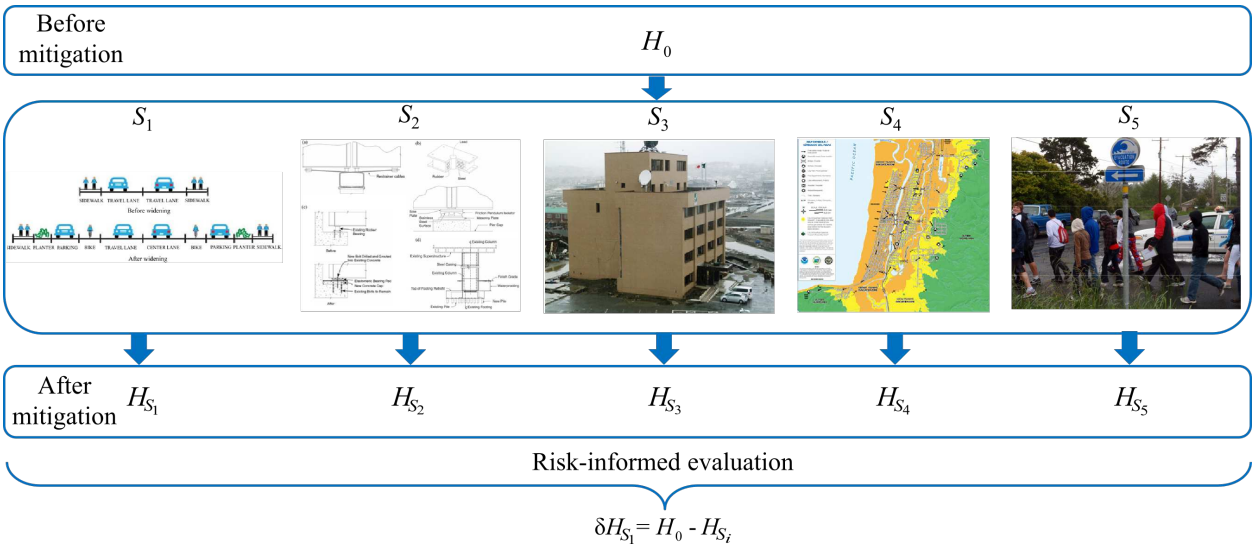


Figure 7.1: Illustration of risk-informed evaluation of candidate mitigation strategies. The sources of the figures are: S_1 (City of Seaside 2010), S_2 (Buckle et al. 2006), S_3 (Applied Technology Council 2019), S_4 (The Oregon Department of Geology and Mineral Industries 2013), and S_5 (Banse 2012).

7.3.1 Calculation of evacuation risk under the mitigation strategy by modifying the tsunami evacuation model

For some candidate mitigation strategies, the agent-based evacuation model developed in Chapter 3 needs to be modified to simulate the mitigation. This is usually applicable for the calculation of the evacuation risk under the infrastructural mitigation strategy. For example, to simulate evacuation route widening, the components of the evacuation model associated with the evacuation route need to be modified, such as the road width and the thresholds that are used to determine the traffic stage transition. Then, evacuation simulations are run using the updated model and the evacuation risk is estimated based on the new simulations using Eq. (4.3).

7.3.2 Calculation of evacuation risk under the mitigation strategy using existing simulations

Besides modifying the evacuation model and rerunning simulations, for some candidate mitigation strategies, the evacuation risk can be efficiently estimated based on the existing simulations, e.g., the simulations used for estimating the risk before mitigation (i.e., H_0). Typically, when the mitigation leads to a change in the value or distribution of the input random variables, the concepts of importance sampling (or reweighting samples) and sample-based approach can be leveraged to efficiently evaluate the updated risk using existing simulations. These two efficient computational approaches are introduced next in the context of calculation of updated evacuation risk under different mitigation strategies.

The evacuation risk under the candidate mitigation strategy (especially the non-infrastructural strategy) might be efficiently calculated based on the augmented sample-based approach that is developed for sensitivity analysis of evacuation risk with respect to the epistemic uncertainty in Chapter 5. For the non-infrastructural mitigation strategy, the critical risk factor typically corresponds to the continuous input random variables. For example, if discouraging car use in evacuation through tsunami evacuation drills is considered as the mitigation strategy, the critical risk factor corresponds to the population proportion that evacuates by car (i.e., $x_i = p_c$). In such

cases, the evacuation risk under any mitigation design corresponds to the conditional evacuation risk $H(x_i)$. The above conditional evacuation risk can be efficiently calculated using the proposed augmented sample-based approach. Here, the process in the context of risk mitigation is simply reviewed while the details can be found in Chapter 5.

For the risk mitigation under any given value of the critical risk factor represented by the continuous variable x_i (e.g., p_c), the corresponding evacuation risk $H(x_i)$ can be expressed by

$$H(x_i) = \iint_{X_{\sim i},\boldsymbol{\Theta}} h(\mathbf{x}_{\sim i}, x_i) p(\mathbf{x}_{\sim i}|\boldsymbol{\theta}) p(\boldsymbol{\theta}) d\mathbf{x}_{\sim i} d\boldsymbol{\theta} \tag{7.1}$$

where $\mathbf{x}_{\sim i}$ denotes the remaining of the input random variables excluding x_i.

This conditional evacuation risk can be estimated efficiently using the proposed augmented sample-based approach and KDE without the need to run additional evacuation simulations. More specifically, based on the joint auxiliary PDF $\pi(\mathbf{x}, \boldsymbol{\theta})$, the marginal auxiliary distribution for x_i can be written as

$$\begin{aligned} \pi(x_i) &= \iint_{X_{\sim i},\boldsymbol{\Theta}} \pi(\mathbf{x}, \boldsymbol{\theta}) \mathrm{d}\mathbf{x}_{\sim i} \mathrm{d}\boldsymbol{\theta} \\ &= \frac{p(x_i) \iint_{X_{\sim i},\boldsymbol{\Theta}} h(\mathbf{x}) p(\mathbf{x}_{\sim i}|\boldsymbol{\theta}) p(\boldsymbol{\theta}) \mathrm{d}\mathbf{x}_{\sim i} \mathrm{d}\boldsymbol{\theta}}{H} = \frac{p(x_i) H(x_i)}{H} \end{aligned} \tag{7.2}$$

Based on which, $H(x_i)$ can be written as

$$H(x_i) = \frac{\pi(x_i)}{p(x_i)} H \tag{7.3}$$

Then KDE or boundary-corrected KDE is used to efficiently estimate $\pi(x_i)$ based on the corresponding marginal samples for x_i. Since both H and $p(x_i)$ are available, the conditional risk for any value of x_i is efficiently estimated using

$$\hat{H}(x_i) = \frac{\tilde{\pi}(x_i)}{p(x_i)} \hat{H} \tag{7.4}$$

based on only one set of simulations (e.g., using the same simulations that are used to estimate the evacuation risk before mitigation, i.e., H_0).

Besides the above approach, when the mitigation only leads to a change in the distribution of the input random variables, the concept of importance sampling can be leveraged to efficiently evaluate the updated risk using existing simulations. One example is bridge retrofit. In such context, effective bridge retrofit strategies (e.g., which groups of bridges should be retrofitted in priority such that the evacuation risk can be reduced more) can be efficiently identified with minor computational efforts rather than rerun the evacuation model for each mitigation strategy (different combinations of bridges to retrofit). To achieve this, the tsunami evacuation risk under each mitigation strategy is assessed efficiently by reweighting existing samples using the concept of importance sampling (Wang and Jia 2019b, 2020b). Here, the key steps for the efficient update of evacuation risk are briefly described.

In the context of evacuation risk mitigation by retrofitting bridges (i.e., related to the seismic damage to bridges), the general form of evacuation risk (i.e., Eq. (4.2)) can be further expanded as

$$H = \iiiint_{X_d, X_{IM}, X_{\sim dIM}, \boldsymbol{\Theta}} h(\mathbf{x}) p(\mathbf{x_d}|\mathbf{x_{IM}}) p(\mathbf{x_{IM}}) p(\mathbf{x_{\sim dIM}}) p(\boldsymbol{\theta}) d\mathbf{x_d} d\mathbf{x_{IM}} d\mathbf{x_{\sim dIM}} d\boldsymbol{\theta} \tag{7.5}$$

where $\mathbf{x_d} = [x_{d_1}, ..., x_{d_i}, ..., x_{d_n}]$, and x_{d_i} represents the seismic damage for the i^{th} bridge out of n bridges in the transportation network; $\mathbf{x_{IM}} = [x_{IM_1}, ..., x_{IM_i}, ..., x_{IM_n}]$, and x_{IM_i} represents the intensity measure at the i^{th} bridge; $\mathbf{x_{\sim dIM}}$ denotes the input random variables excluding $\mathbf{x_d}$ and $\mathbf{x_{IM}}$. Here, $p(\mathbf{x_d}|\mathbf{x_{IM}})$ denotes the PMF for damage states conditional on given vector of intensity measures. For the i^{th} bridge, we have $p(x_{d_i}|x_{IM_i})$ under given intensity measure IM_i, and when considering n_D possible damage states, then $p(x_{d_i}|x_{IM_i}) = P(x_{d_i} = DS_j|x_{IM_i})$ where DS_j for any $j = 1, 2, ..., n_D$. And $p(\mathbf{x_{IM}}) = p(\mathbf{x_{IM}}|EQ)$ is the joint PDF for $\mathbf{x_{IM}}$ under the earthquake scenario EQ.

For mitigation planning purpose, suppose we want to retrofit m bridges out of the total n bridges. Let $\boldsymbol{r_m} = [r_1, ..., r_m]$ denotes the indices for the m selected bridges that will be retrofitted and $\mathbf{x_{dr}} = [x_{dr_1}, ..., x_{dr_m}]$ the corresponding vector of random damage states, and $\mathbf{x_{d\sim r}}$ represents

the rest of $\mathbf{x}$ excluding $\mathbf{x_{dr}}$. After retrofitting, the fragility of the corresponding bridges will change, i.e., $p(\mathbf{x_d}|\mathbf{x_{IM}})$ will change (e.g., to $p_s(\mathbf{x_d}|\mathbf{x_{IM}})$), and the marginal distribution for $\mathbf{x_d}$, i.e., $p(\mathbf{x_d})$ will change accordingly (e.g., to $p_s(\mathbf{x_d})$), which will affect the evacuation. The updated PDF $p_s(\mathbf{x_d})$ can be written as $p_s(\mathbf{x_d}) = \int_{X_{IM}} p_s(\mathbf{x_d}|\mathbf{x_{IM}})p(\mathbf{x_{IM}})d\mathbf{x_{IM}}$ where $p_s(\mathbf{x_d}|\mathbf{x_{IM}})$ can be further written as $p_s(\mathbf{x_d}|\mathbf{x_{IM}}) = p(\mathbf{x_{d\sim r}}|\mathbf{x_{IM\sim r}}) \prod_{j=1}^{m} p_s(x_{dr_j}|x_{IMr_j})$, i.e., only $p(x_{d_i}|x_{IM_i})$ for those retrofitted bridges need to be updated.

In the above context, the evacuation risk (denoted $H_{s_b}(\boldsymbol{r_m})$) under the candidate strategy defined by $\boldsymbol{r_m} = [r_1, ..., r_m]$ needs to be calculated for comparison. Using the existing samples $\{[\mathbf{x}^k, \boldsymbol{\theta}^k], k = 1 \dots N\}$ from the proposal density $q(\mathbf{x}, \boldsymbol{\theta})$ that are used to estimate the risk H_0, $H_{s_b}(\boldsymbol{r_m})$ can be efficiently estimated as

$$\hat{H}_{s_b}(\boldsymbol{r_m}) = \frac{1}{N} \sum_{k=1}^{N} \frac{h(\mathbf{x}^k) p(\mathbf{x}^k_{d\sim r}|\mathbf{x}^k_{IM\sim r}) p(\mathbf{x}^k_{IM}) p(\mathbf{x}^{\mathbf{k}}_{\sim \mathbf{dIM}}) p(\boldsymbol{\theta}^k)}{q(\mathbf{x}^k, \boldsymbol{\theta}^k)} \prod_{j=1}^{m} p_s(x^k_{dr_j}|x^k_{IMr_j}) \tag{7.6}$$

which can be further written as

$$\begin{aligned} \hat{H}_{s_b}(\boldsymbol{r_m}) =& \frac{1}{N} \sum_{k=1}^{N} \frac{h(\mathbf{x}^k) p(\mathbf{x}^k_{d}|\mathbf{x}^k_{IM}) p(\mathbf{x}^k_{IM}) p(\mathbf{x}^{\mathbf{k}}_{\sim \mathbf{dIM}}) p(\boldsymbol{\theta}^k)}{q(\mathbf{x}^k, \boldsymbol{\theta}^k)} \prod_{j=1}^{m} \frac{p_s(x^k_{dr_j}|x^k_{IMr_j})}{p(x^k_{dr_j}|x^k_{IMr_j})} \\ =& \frac{1}{N} \sum_{k=1}^{N} R(\mathbf{x}^k_d, \mathbf{x}^k_{IM}, \mathbf{x}^{\mathbf{k}}_{\sim \mathbf{dIM}}, \boldsymbol{\theta}^k) \prod_{j=1}^{m} \frac{p_s(x^k_{dr_j}|x^k_{IMr_j})}{p(x^k_{dr_j}|x^k_{IMr_j})} \end{aligned} \tag{7.7}$$

Because $R(\mathbf{x}^k_d, \mathbf{x}^k_{IM}, \mathbf{x}^{\mathbf{k}}_{\sim \mathbf{dIM}}, \boldsymbol{\theta}^k) = h(\mathbf{x}^k) p(\mathbf{x}^k_d|\mathbf{x}^k_{IM}) p(\mathbf{x}^k_{IM}) p(\mathbf{x}^{\mathbf{k}}_{\sim \mathbf{dIM}}) p(\boldsymbol{\theta}^k)/q(\mathbf{x}^k, \boldsymbol{\theta}^k)$ has been calculated for all $\{\mathbf{x}^k, \boldsymbol{\theta}^k\}$ when evaluating the initial evacuation risk H_0, to estimate $H_{s_b}(\boldsymbol{r_m})$ for different strategies $\boldsymbol{r}_m$, based on Eq. (7.7) only the ratio $p_s(x^k_{dr_j}|x^k_{IMr_j})/p(x^k_{dr_j}|x^k_{IMr_j})$ needs to be updated for all the selected bridges in $\boldsymbol{r}_m$. This ratio can be easily calculated for any selected strategy and does not involve any additional simulations of the evacuation model (i.e., calculation of $h(\mathbf{x}^k)$).

As for $\boldsymbol{r}_m$, the top m ranked bridges can be directly selected based on the importance ranking that is identified by sensitivity analysis. This way, we only need to update the evacuation risk one time, which is more efficient than estimating the risk for all combinations of any m out of n bridges. While individually each of the top m ranked bridges has a relatively high impact on evacuation risk, jointly the top m ranked bridges may not be the optimal combination. But since individually each of the top m ranked bridges is important, retrofitting these m bridges is expected to be relatively good as well, especially when the impact of the interaction between different bridges on evacuation risk is not strong. Considering the high efficiency of the reweighting approach, the optimal retrofit strategy might be searched by exhaustive enumeration when the number of combinations is not large.

7.4 Illustrative example: Risk-informed evaluation of different mitigation strategies for Seaside, Oregon

The risk-informed evaluation of different mitigation strategies is performed for Seaside, Oregon. As for the evacuation simulation, one existing scenario in Chapter 4 is considered to obtain the evacuation risk (i.e., H_0) before mitigation. The same set simulations are used to efficiently update the evacuation risk (i.e., H_{s_i}) for some strategies as presented in Section 7.3.2. Here, the daytime scenario with 15,000 evacuees corresponding to C0 in Chapter 4 is considered. For the mitigation simulation that needs to rebuild the agent-based evacuation model, the modifications on the evacuation model and/or simulation will be presented later. The details on the study area and evacuation simulation can be found in Chapter 4.

Here, the candidate mitigation strategies are effectively selected based on the critical risk factors identified by the sensitivity analysis in Section 6.4.1. The sensitivity analysis results showed that the proportion of evacuation by car (i.e., p_c) has the greatest importance followed by the proportion of evacuees who use the evacuation route (i.e., p_r), and followed by the seismic damages (corresponding to the damage sate, i.e., DS) of top-ranked bridges. Car use (i.e., p_c) dominates the evacuation risk, and this is because that car use tends to cause traffic congestion, which will

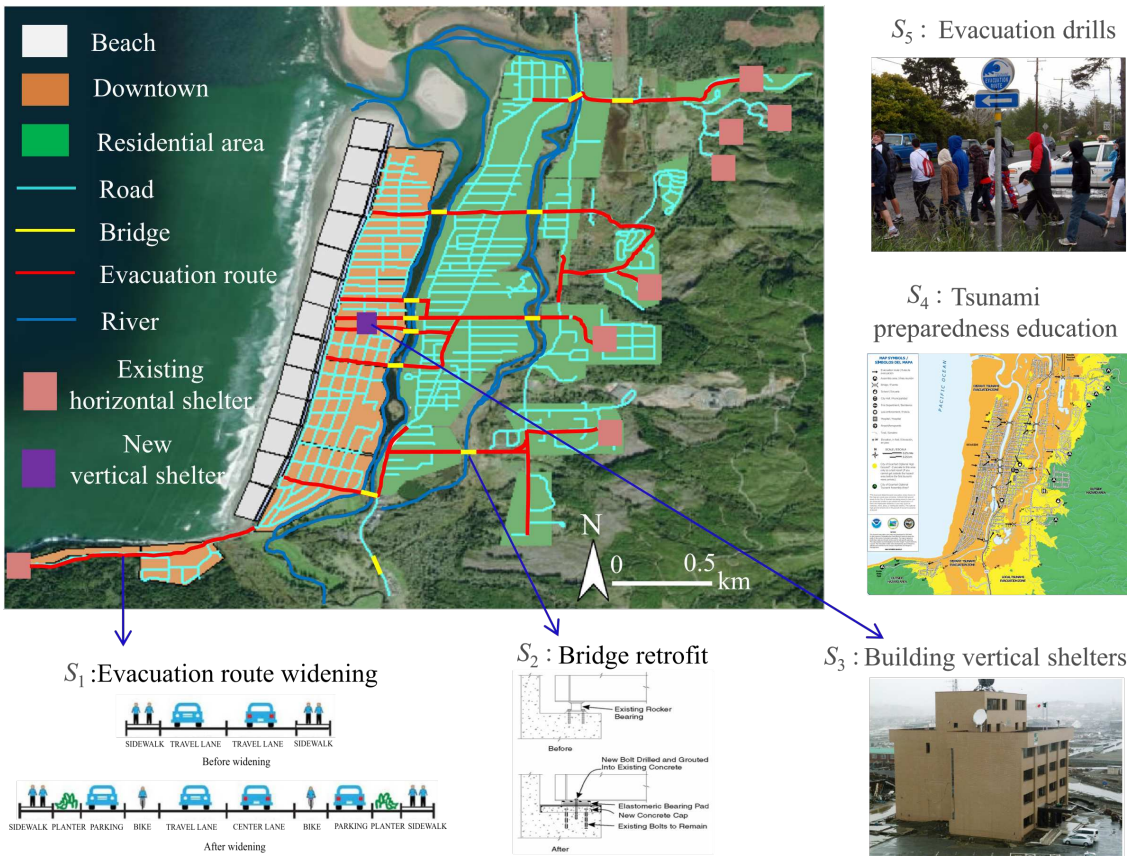


Figure 7.2: Illustration of the candidate evacuation risk mitigation strategies selected based on critical risk factors.

significantly delay the evacuation and increase casualty. Infrastructural and non-infrastructural countermeasures can be used to limit the evacuation by car and to help alleviate the potential traffic congestion (Takada et al. 2013). Two infrastructural countermeasures are considered here as candidates, including evacuation route widening and building a vertical shelter in the area with a high population density. Evacuation route widening aims to increase the road capacity and alleviate traffic congestion. Building vertical shelters is expected to decrease car use over long distances and reduce the potential traffic congestion. However, only infrastructural countermeasures might not solve the problem in the evacuation by car perfectly and it is necessary to consider non-infrastructural countermeasures (Takada et al. 2013). Therefore, discouraging car use in evacuation (lower value of p_c, which can be accomplished for example by evacuation drills) is selected as another candidate strategy. Due to the relatively great importance of the evacuation route usage

(i.e., p_r) to the evacuation risk, we consider the tsunami evacuation preparedness education aiming at increasing the effectiveness of the evacuation route usage as one candidate mitigation strategy. The seismic damage to bridges would reduce the traffic capacity and hence delay the evacuation. To reduce such impact caused by the seismic damage, bridge retrofit is considered as the candidate mitigation strategy. Ultimately, we select five candidate strategies including three infrastructural and two non-infrastructural strategies for evaluation in this example. The three infrastructural strategies are evacuation route widening (denoted S_1), bridge retrofit (denoted S_2), and building vertical shelters (denoted S_3). The two non-infrastructural strategies are tsunami preparedness education (denoted S_4) and evacuation drills (denoted S_5). The five candidate mitigation strategies are illustrated in Fig. 7.2. It is assumed that the above five candidate strategies satisfy the coastal topographic characteristics and societal demands in Seaside.

7.4.1 Candidate infrastructural mitigation strategies

Evacuation route widening (S_1)

It is assumed all existing evacuation routes (i.e., the ones designated on the evacuation map) are widened (illustrated in Fig. 7.2). The road class for the evacuation route does not change (shown in Fig. 3.10). The route width after being widened is set to be the same as that as designed in the Seaside transportation system plan (City of Seaside 2010). The parameters used to determine the road width of the evacuation routes occupied by the car or pedestrian after widening the evacuation route are presented in Table 7.1. In the modeling of pedestrian-vehicle interaction (see Eq. (3.4)), the thresholds used to determine the traffic stage on the widened evacuation routes are presented in Table 7.2. In the table, $T_{1_{PA}}$, $T_{2_{PA}}$, $T_{1_{MA}}$, $T_{2_{MA}}$, $T_{1_{Mac}}$, $T_{2_{Mac}}$, $T_{1_{LR}}$, and $T_{2_{LR}}$, respectively, correspond to the road class "Principle Arterial", "Minor Arterial", "Major Collector", and "Local Road". "Parameter 1" and "Parameter 2" correspond to the lower bound and upper bound of the uniform distribution, respectively. Note that the parameters used to determine the road widths occupied by the car and pedestrian for the existing transportation network (road network) can be found in Table 3.2. Let H_{s_1} denote the evacuation risk after widening evacuation routes. H_{s_1} is es-

timated based on the evacuation simulations using the modified agent-based evacuation model with evacuation routes being widened. The details on the risk assessment can be found in Chapter 4.

Table 7.1: The parameters used to determine the road widths of the evacuation routes occupied by the car and pedestrian after widening evacuation routes (shown based on the functional class of the evacuation route).

Functional class	w	w_{wmin}	w_w	w_r	n_l
Principle Arterial	17.68	3.99	5.49	2.75	3
Minor Arterial	15.85	7.53	8.53	2.75	2
Major Collector	14.63	6.32	7.32	2.75	2
Local Road	12.19	1.55	3.05	2.75	3

Table 7.2: The thresholds used to determine the traffic stage on widened evacuation routes.

Input	Distribution	Parameter 1	Parameter 2
$T_{1_{PA}}$	Uniform	0.59	0.97
$T_{2_{PA}}$	Uniform	1.78	3.61
$T_{1_{MA}}$	Uniform	1.69	2.47
$T_{2_{MA}}$	Uniform	3.39	5.94
$T_{1_{Mac}}$	Uniform	1.41	2.10
$T_{2_{Mac}}$	Uniform	2.95	5.24
$T_{1_{LR}}$	Uniform	0.23	0.47
$T_{2_{LR}}$	Uniform	0.84	1.51

Bridge retrofit (S_2)

There are 12 bridges in the road network in Seaside, and it is assumed to retrofit up to eight bridges (i.e., m ranges from one to eight) considering the limited resources (e.g., budget). The optimal strategy is identified by comparing all potential combinations of any m bridges (i.e., exhaustive enumeration) considering the relatively small number of combinations and the high efficiency of the reweighting approach for updating the evacuation risk for each combination (see Section 7.3.2). For the retrofitted bridge, its fragility curve is updated by scaling the median of the fragility of an as-built bridge (Padgett and DesRoches 2009). Here a scaling factor of 2.5 is used. H_{s_2} is used to represent the evacuation risk after the bridge retrofit. H_{s_2} is efficiently calculated using the reweighting approach presented in Section 7.3.2.

Building vertical shelters (S_3)

Previous studies on vertical evacuation (Raskin et al. 2011; Mostafizi et al. 2019a) show that the vertical shelter located in highly populated and vulnerable areas such as the center of downtown can be more effective in reducing casualty. In this example, one vertical shelter is considered to be built in the centroid of the downtown area with the highest population density in this area. It is assumed that only the evacuees using the shortest path on the beach and in the downtown will consider evacuating to this vertical shelter. Out of these evacuees, the proportion of the evacuees with such an action (denoted p_v) is considered to follow the uniform distribution on the interval [0,1]. Note that similar to the horizontal shelters no capacity limit is set for the vertical shelter and the shelter is assumed to be capable of withstanding the seismic and tsunami hazards. Let H_{s_3} represent the evacuation risk under building the vertical shelter. H_{s_3} is estimated based on the simulations using the modified agent-based evacuation model with the inclusion of the built vertical shelter.

7.4.2 Candidate non-infrastructural mitigation strategies

Tsunami preparedness education (S_4)

Tsunami preparedness education can be conducted in many forms such as visiting tsunami museums, recognizing evacuation routes, etc. (Adiyoso and Kanegae 2012). Considering the importance of the proportion of evacuees using the evacuation route (i.e., p_r) from the sensitivity analysis, here the tsunami preparedness education focuses on the effective use of the evacuation route. To better prepare people for effective use of the evacuation route in evacuation, we need to investigate the effectiveness of the route usage, i.e., estimate the evacuation risk conditional on p_r (denoted H_{s_4}) and search the optimal value of p_r that minimizes H_{s_4}. Note that H_{s_4} is efficiently calculated using the augmented sample-based approach presented in Section 7.3.2.

To investigate the variation of H_{s_4} with p_r, we artificially treat p_r as following a uniform distribution in the interval [0,1]. Then the augmented sample-based approach can be used to efficiently estimate H_{s_4} conditional on different values of p_r. The tsunami preparedness education

with respect to effective use of the evacuation route is expected to improve the evacuation through changing people's evacuation decisions (e.g., encourage more people to use the evacuation route). Correspondingly, the lower bound and upper bound for the proportion of evacuation with irrational behavior (following others, i.e., p_f) are reduced from 0.1 and 0.3 to 0 and 0.2, respectively. The proportion of evacuation using the shortest path is given by $p_s = 1 - p_r - p_f$.

Evacuation drills (S_5)

Disaster evacuation drills play an important role in training evacuees to respond properly in emergency (Leelawat et al. 2018). The people with tsunami evacuation drill experience are expected to make the decision and behave properly when a real tsunami arrives (Leelawat et al. 2018). Considering the dominant importance of the car use (i.e, p_c) to the evacuation risk based on sensitivity analysis, a tsunami evacuation drill can be designed such that evacuees can experience the evacuation delay caused by a large amount of car use as occurred in historical tsunami evacuations (Ohno et al. 2011; Murakami et al. 2014). Then, the proper evacuation mode (i.e., evacuation on foot or by car) can be recommended, e.g., encouraging evacuation on foot instead of by car.

To investigate the impact of car use on the evacuation risk, the variation of the evacuation risk with p_c (denoted H_{s_5}) will be examined. Based on the investigation, an optimal value of p_c under which the evacuation risk is minimum can be identified. Based on the simulations for estimating H_0, H_{s_5} is efficiently calculated using the augmented sample-based approach presented in Section 7.3.2.

7.5 Result and discussions

7.5.1 Risk mitigation by each candidate strategy

The risk mitigation (updated risk H_{s_i}) by each of the five candidate strategies is evaluated by comparing to the baseline H_0. Same as H_0, the expected PCR, CCR, and TCR are used as H_{s_i}.

To calculate the evacuation risk H_{s_1} for evacuation route widening and H_{s_3} for building vertical shelters, $N = 2000$ tsunami evacuation simulations with the selection of $q(\mathbf{x}, \boldsymbol{\theta}) = p(\mathbf{x}|\boldsymbol{\theta})p(\boldsymbol{\theta})$

are used for each case. Note that the evacuation is simulated by modifying the evacuation model that is described in Section 3.4.2. The selection of $q(\mathbf{x}, \boldsymbol{\theta})$ and $N = 2000$ leads to high accuracy estimates for the PCR, CCR, and TCR at the end of the evacuation simulation (i.e., one hour), with δ_{CoV} below 3% for both strategies.

For bridge retrofit, the updated risk H_{s_2} is efficiently calculated using the reweighting approach. The same $N = 2000$ samples for the estimation of H_0 are used. Such selection results in a below 5% δ_{CoV} for the estimate $\hat{H}_{s_2}$ (when all $m = 8$ bridges are retrofitted).

For tsunami preparedness education and evacuation drills, both the variation of H_{s_4} over p_r and the variation of H_{s_5} over p_c are efficiently calculated using the augmented sample-based approach. Based on the $N = 2000$ tsunami evacuation simulations used for estimating H_0, around $n_\pi = 1200$ samples are generated from $\pi(\mathbf{x}, \boldsymbol{\theta})$. All the risk results reported under S_4 and S_5 are obtained efficiently using the same set of 2000 simulations with low CoVs for all MCI approximations (i.e, below 2%).

Evacuation route widening (S_1)

The comparison of the variations of evacuation risk in terms of casualty rate for the pedestrian, car, and total over time before and after widening evacuation routes are shown in Fig. 7.3(a)-(c), respectively. Overall, the variations of the PCRs over time under route widening show similar trends to that without the evacuation route being widened (i.e., the baseline). However, the PCR becomes lower than the baseline (i.e., $12.2 < 15.9\%$) for evacuation route widening, which indicates route widening can effectively reduce the casualty for evacuation on foot. This is because route widening provides a much wider space for pedestrians to travel on most of the evacuation routes. Then route widening would effectively reduce the potential pedestrian congestion and ultimately improves the evacuation on foot. By comparing the CCRs before and after widening routes, the CCR when widening routes is only a little lower than the baseline (i.e., $24.1\% < 25.2\%$). Unlike evacuation on foot, evacuation by car is not impacted so much. This is because the increase of the number of lanes for the car would increase the traffic capacity for the route and alleviate the potential traffic congestion, which ultimately reduces the CCR. However, route widening only

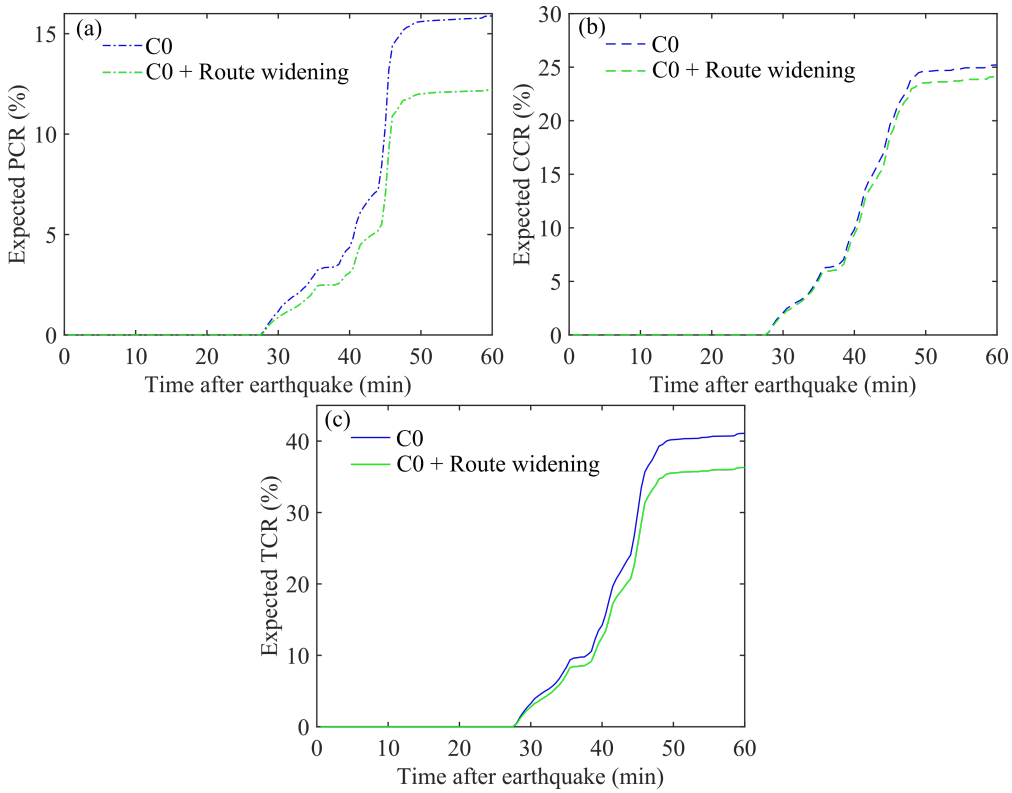


Figure 7.3: The variations of evacuation risk in terms of casualty rate for (a) pedestrian, (b) car, and (c) total over time before and after widening evacuation routes.

increases the number of lanes for the routes that are classified as road class of "Principle Arterial" and "Local Road" while for those that are classified as road class of "Minor Arterial" and "Major Collector", the number of lanes does not change (shown in Table 3.2 and Table 7.1). In this case, route widening does not reduce the CCR much. Due to the change of the PCR and CCR when widening routes, the TCR becomes lower compared to the baseline. Overall, route widening can effectively reduce the evacuation risk.

Bridge retrofit (S_2)

Fig. 7.4 shows the evacuation risk in terms of casualty rate for the pedestrian, car, and total when m ranges from 1 to 8, where the results under the optimal selection of m bridges are shown. Here the optimal selections are identified by comparing all potential combinations of m bridges. As expected, all the expected PCR, CCR, and TCR decrease with an increase of m, showing that as more bridges are retrofitted the evacuation risk reduces. For example, the TCR decreases from

41.1% to 17.5% when eight bridges are retrofitted. Another observation is the decrease of the expected PCR, CCR, or TCR becomes slower for a larger m. For example, the TCR decreases from 41.1% to 18.9% when $m = 7$ while only decreases from 18.9% to 17.5% when one more bridge is retrofitted ($m = 8$). When m is small, most of these m bridges are the most important to the road network. Retrofitting these m bridges would significantly reduce the impact of the traffic capacity reduction (caused by the seismic damage to these bridges) on the evacuation risk. As m increases, more bridges of less importance are retrofitted, which would have less impact on reducing the evacuation risk. Overall, the optimal bridge retrofit strategy can reduce the evacuation risk effectively.

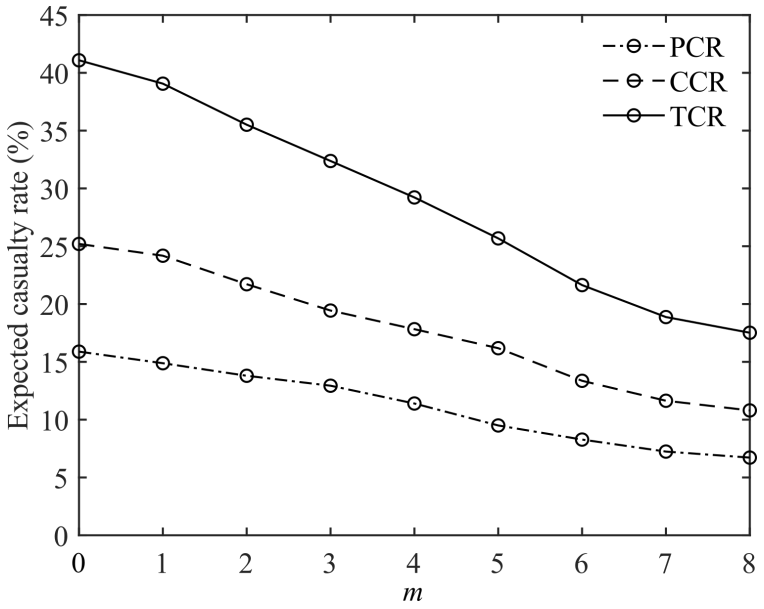


Figure 7.4: The evacuation risk in terms of casualty rate for the pedestrian, car, and total using the optimal bridge retrofit strategy with different m values.

Building vertical shelters (S_3)

The comparison of the variations of evacuation risk in terms of casualty rate for the pedestrian, car, and total over time before and after building vertical shelters are shown in Fig. 7.5(a)-(c), respectively. The comparison shows similar trends to that under evacuation route widening. For example, both the PCR and CCR are lower when building vertical shelters compared to the base-

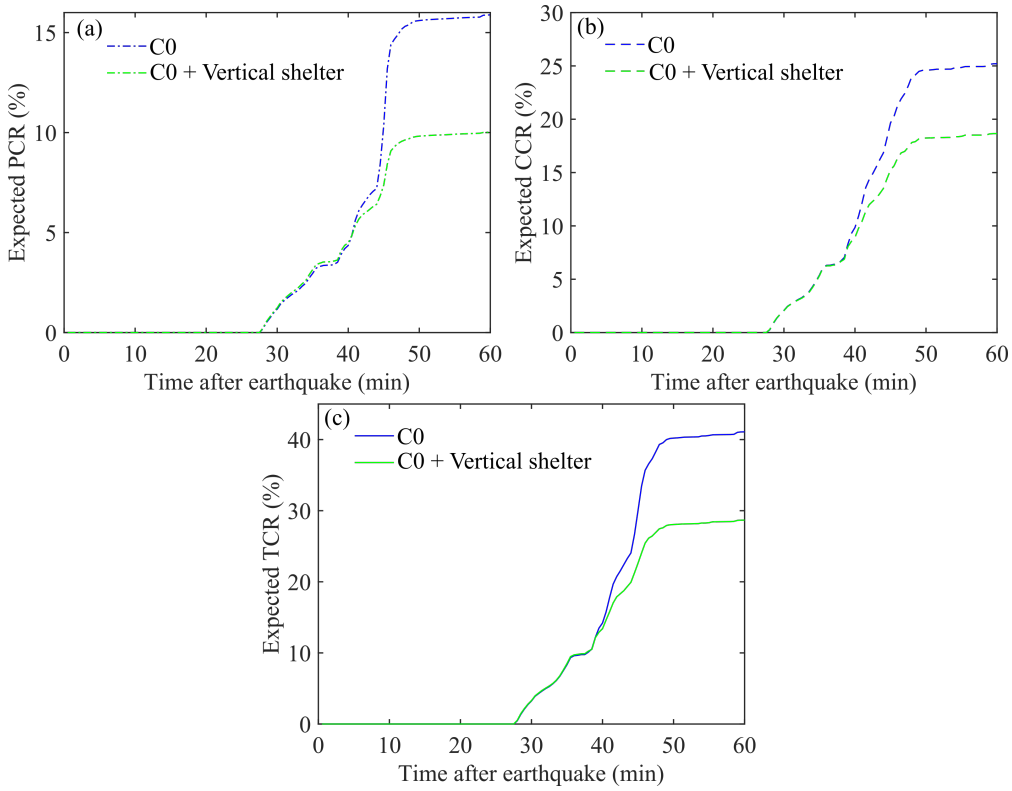


Figure 7.5: The variations of evacuation risk in terms of casualty rate for (a) pedestrian, (b) car, and (c) total over time before and after building vertical shelters.

line. Ultimately, the TCR becomes lower due to the reduction in the PCR and CCR when building vertical shelters. However, one big difference between building vertical shelter and route widening is the change of the CCR. For building vertical shelters, the CCR becomes much smaller than the baseline (i.e., $18.7\% < 25.2\%$). This is because evacuees can evacuate to the vertical shelter with a much smaller distance compared to evacuating to the horizontal shelters. The building of vertical shelters can have a big impact on the evacuation by car. The above comparisons indicate building vertical shelters can effectively improve the evacuation and reduce the evacuation risk.

Tsunami preparedness education (S_4)

Fig. 7.6 shows the variations of evacuation risk $H(p_r)$ for the pedestrian, car, and total over different values of p_r. As p_r increases, the PCR first decreases (from 19.3% to 14.4%) for most values of p_r (when p_r is smaller than around 0.8) and then does not change much for relatively large values of p_r (when p_r is larger than around 0.8). This means overall following the evacuation

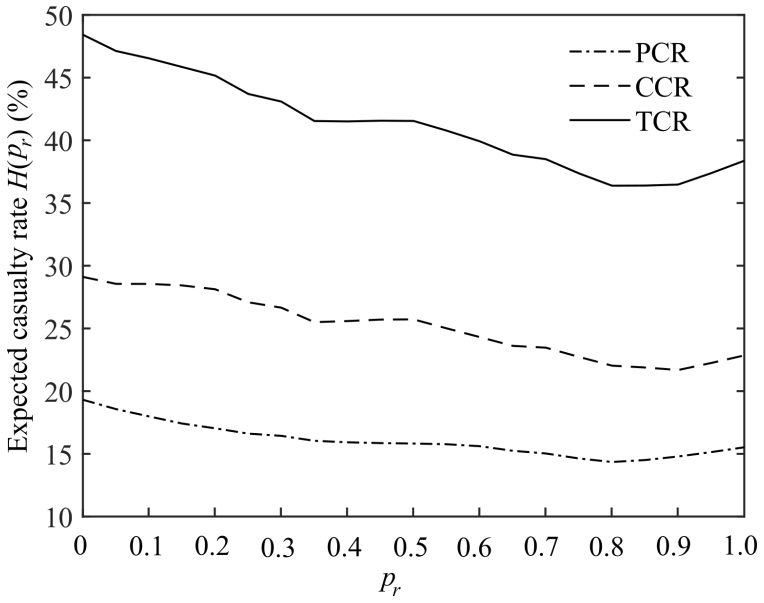


Figure 7.6: The variations of evacuation risk $H(p_r)$ as a function of p_r for the pedestrian, car, and total.

route could effectively reduce the PCR. Compared to using other roads that are overall narrower than the evacuation route, following the evacuation route is less likely to cause severe pedestrian congestion and hence fewer casualties due to the delay. However, note that the route usage would become less effective in the reduction of the PCR when most of the pedestrians use the route. This is because pedestrian congestion would occur or become more severe when most of the pedestrians select several evacuation routes, which would delay the evacuation on foot and may cause more casualties. The variation of the CCR with p_r shows a similar trend to the PCR, i.e., the casualty rate first decreases and then almost does not change much with the route usage. This indicates overall following the evacuation route could effectively reduce the CCR. The variation of the CCR should be attributed to a similar reason for the variation of the PCR with p_r. Compared to the PCR, however, the decrease of the CCR with the increase of p_r is larger. More specifically, as p_r increases from 0 to 1, the CCR decreases from 29.1% to 22.9% while the PCR decreases from 19.3% to 15.5%. Typically, evacuation by car tends to cause more severe traffic congestion than evacuation on foot. In this case, the alleviation of traffic congestion by following the evacuation route could improve the evacuation more significantly for evacuation by car than on foot. Due to the variations of the PCR and CCR with p_r, the TCR first decreases significantly and then increases

slightly as p_r increases. More specifically, the TCR first decreases from 48.4% to the minimum value of 36.4% when p_r is around 0.8, and then increases to 38.4% when all evacuees use the route (i.e., $p_r = 1$). Overall, the evacuation route usage can effectively reduce the TCR. From the perspective of improving the evacuation performance, evacuees are encouraged to evacuate by following the evacuation route.

Evacuation drills (S_5)

Fig. 7.7 shows the variations of evacuation risk $H(p_c)$ for the pedestrian, car, and total over different values of p_c. The PCR decreases from 45.0% to 0 as p_c increases from 0 to 1 (i.e., more car use). This decrease can stem from fewer pedestrians (i.e., the larger value of p_c) and/or less pedestrian congestion due to fewer pedestrians. To investigate the exact reason, another pedestrian casualty rate (denoted PCR_0) is also calculated and shown in Fig. 7.7, where PCR_0 is defined as the number of pedestrian casualties divided by the number of pedestrians (instead of by the total population like the PCR). Like the PCR, PCR_0 also decreases with the increase of p_c. Theoretically, since PCR_0 is defined by normalization with respect to the total number of pedestrians, as fewer people evacuate on foot (i.e., larger p_c), PCR_0 would not decrease if the pedestrian congestion is not alleviated. In this context, the decrease of PCR_0 indicates there is less pedestrian congestion when fewer people evacuate on foot, under which the evacuation on foot is less likely to be delayed due to pedestrian congestion. In this case, the decrease of the PCR with the increase of p_c also results from less pedestrian congestion and ultimately from fewer pedestrians.

The CCR increases as p_c increases, i.e., from 0 to 56.0% when p_c increases from 0 to 1, which means that the increase of car use would increase the CCR significantly. Similar to PCR_0, CCR_0 (i.e., the proportion of the number of casualties that evacuate by car to the number of the evacuees using cars) is calculated to investigate the reason for the variation of the CCR, i.e., whether it is due to the increase in the number of cars or due to the potentially more severe traffic congestion caused by more car use or due to both. CCR_0 first increases (i.e., from 0 to 58.6% when p_c is around 0.9) and then decrease a little (i.e., from 58.6% to 56.0%) as p_c increases. As more people evacuate by car, CCR_0 would not increase if the traffic congestion does not become more severe due to more

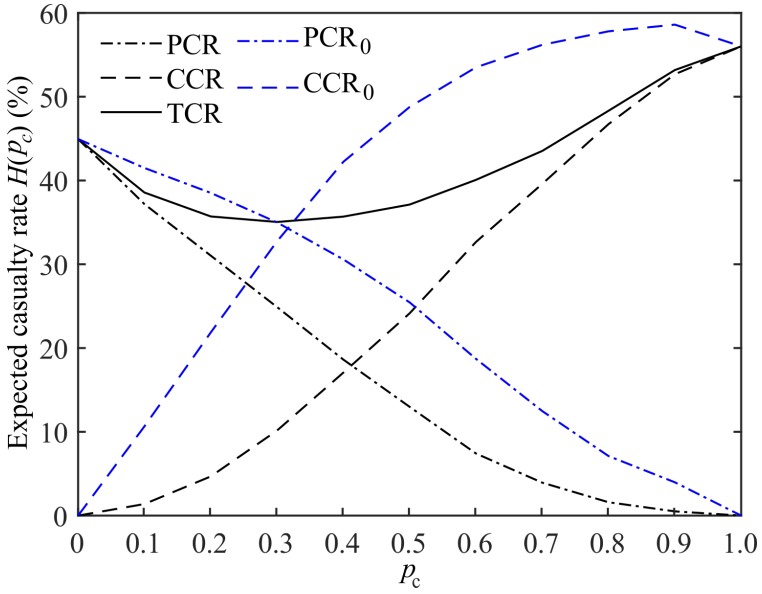


Figure 7.7: The variations of evacuation risk $H(p_c)$ as a function of p_c for the pedestrian, car, and total.

car use. In this context, the increase of CCR_0 indicates that more car use results in more severe traffic congestion, which delays the evacuation by car and causes more casualties. However, as more cars are used (i.e., $p_c > 0.9$), the congestion level would not increase so much, which would not delay the evacuation further. In this case, CCR_0 decreases a little with the increase of car use.

Due to the variations of the PCR and CCR with p_c, the TCR first decreases (i.e., from 45.0% to 35.0%) and then increases (i.e., from 35.0% to 56.0%) with the increase of p_c. This means more people evacuating on foot would cause more casualties when the car use is small (i.e., $p_c < 0.3$) and more casualties would result from evacuation by car when the car use is large (i.e., $p_c > 0.3$). Some value of p_c (optimal) leads to the minimum TCR, i.e., TCR$= 35.0\%$ is minimum when $p_c = 0.3$ in this example. This indicates that some optimal proportion of evacuation by car could lead to the minimum total evacuation risk.

7.5.2 Comparison of evacuation risk reductions for different strategies

Based on the total evacuation risk (i.e., expected TCR) at the end of evacuation simulation (i.e., one hour), the risk reductions by all five candidate strategies are compared. Considering that the evacuation risk varies with values of the critical risk factors for the non-infrastructural strategies,

the optimal value of the updated risk is used for comparison. The comparison of evacuation risk reductions for the candidate mitigation strategies is shown in Fig. 7.8.

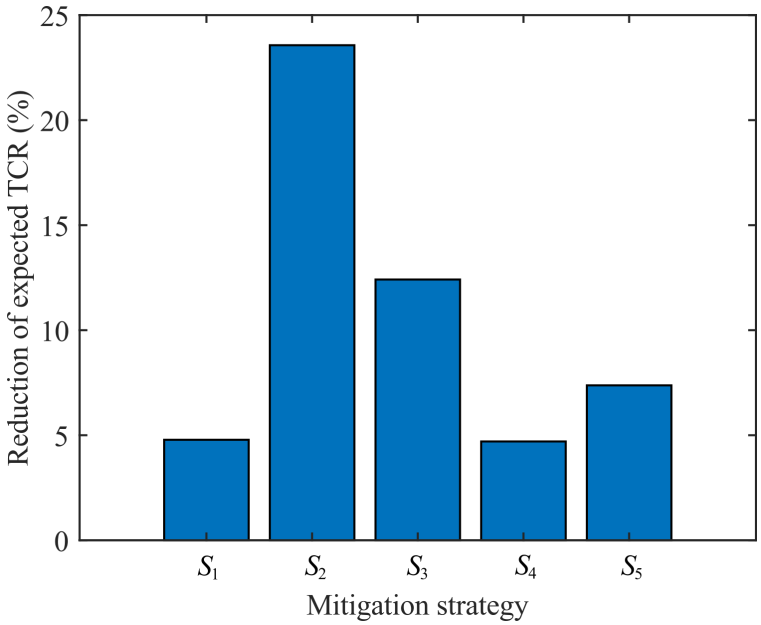


Figure 7.8: Comparison of evacuation risk reductions for considered mitigation strategies.

As can be seen, all five strategies can effectively reduce the expected TCR. However, different strategies demonstrate differences in the level of risk reduction. Bridge retrofit (S_2) leads to the maximum risk reduction (i.e., 23.6%) while the minimum risk reduction is given by the preparedness education (S_4) (i.e., 4.7%) in this example. The risk reductions by the other three strategies fall between these two extreme reductions. More specifically, building vertical shelters (S_3), evacuation drills (S_5), and route widening (S_1) result in a risk reduction of 12.4%, 7.4%, and 4.8%, respectively. Overall, bridge retrofit and building vertical shelters are more effective in risk reduction than the three other strategies in this case. To effectively reduce the evacuation risk, bridge retrofit and building vertical shelters can be implemented in priority if the resource is available. However, other strategies such as the two non-infrastructural ones (especially the evacuation drill) can also effectively reduce the evacuation risk. Therefore, the combinations of several mitigation strategies might be considered in evacuation planning.

7.6 Summary

The risk-informed evaluation of evacuation risk mitigation strategies was conducted to quantitatively identify more effective strategies. The candidate mitigation strategies (including infrastructural and non-infrastructural strategies) were selected based on the critical risk factors identified by sensitivity analysis. For each candidate strategy, the evacuation risk was either estimated based on modifying the proposed agent-based model and rerunning simulations or efficiently calculated using existing evacuation simulations. Based on the risk reduction, the effectiveness of each candidate strategy was evaluated and more effective strategies were identified.

As an illustrative example, the risk-informed evaluation of evacuation risk mitigation was conducted for Seaside, Oregon. Based on the critical risk factors identified by sensitivity analysis, five candidate mitigation strategies including the infrastructural strategy (i.e., route widening, bridge retrofit, and building vertical shelters) and non-infrastructural strategy (i.e., disaster preparedness education and evacuation drills) were considered. The evaluation of the effectiveness of the mitigation strategy showed that bridge retrofit can lead to more risk reduction followed by building vertical shelters, evacuation drills, and route widening while preparedness education in terms of effective use of the evacuation route results in the least risk reduction among the candidate strategies in this case. The above evaluation of the effectiveness can be used to guide effective evacuation planning.

Chapter 8

Conclusions and future directions

8.1 Conclusions

In this dissertation, simulation-based tsunami evacuation risk assessment and risk-informed mitigation were performed under a proposed generalized framework. The proposed framework integrated tsunami evacuation simulation, simulation-based evacuation risk assessment, sensitivity analysis of evacuation risk, and risk-informed mitigation. An improved agent-based model was first developed for more realistic tsunami evacuation simulation. A simulation-based framework that can address complex evacuation models and uncertainty (including aleatory and epistemic uncertainties) models was proposed for the quantification of evacuation risk. Then, sensitivity analysis of evacuation risk with respect to the epistemic uncertainty was performed to investigate the impact of various epistemic uncertainties on the variability in the risk. Sensitivity analysis was also performed to investigate the impact of various risk factors and associated uncertainties on the evacuation risk. Ultimately, risk-informed evaluation of different types of mitigation strategies was conducted to identify more effective strategies that are robust to uncertainties. Efficient sample-based approaches were developed to address the computational challenges in the risk assessment, sensitivity analysis, and risk mitigation. Using the proposed generalized framework, the simulation-based tsunami evacuation risk assessment and risk-informed mitigation were performed for Seaside, Oregon.

Chapter 2 proposed a generalized framework for simulation-based tsunami evacuation risk assessment and risk-informed mitigation. The framework was built layer by layer by integrating tsunami evacuation simulation, simulation-based evacuation risk assessment, sensitivity analysis of evacuation risk, and risk-informed evaluation of mitigation strategies. The tasks in subsequent chapters were conducted under this proposed framework, which can be used to support effective evacuation plan-making and management.

Chapter 3 developed an improved agent-based model for a more realistic tsunami evacuation simulation. The proposed model consists of the evacuation environment model (EEM), evacuation decision and behavior model (EBM), and evacuation performance model (EPM). Compared to existing agent-based models, the proposed model incorporates many of the typically neglected or simplified but important factors and mechanisms associated with the evacuation. For EEM, the traffic capacity reduction of the link due to bridge damage or debris from damaged buildings, the availability of traffic information on route passability, and the population mobility were all considered. For EBM, a multimodal evacuation model was proposed to concurrently consider the pedestrian speed variability, speed adjustment for both the pedestrian and car according to traffic density, and the pedestrian-vehicle interaction (which is modeled by traffic stage transitions). Different evacuation path selections were considered, including following the evacuation route, searching the shortest path, and following behavior. Different other aspects were also included to better simulate the complex evacuation decisions and behaviors. Also, various uncertainties associated with the evacuation were explicitly considered. These improvements would better characterize the nature and dynamics of the tsunami evacuation system, model the individual-level interactions among evacuees, and the evacuees' interactions with the environment. The tsunami evacuation process in Seaside, Oregon was investigated using the proposed agent-based tsunami evacuation model.

Chapter 4 proposed a simulation-based framework for the quantification of tsunami evacuation risk. Under the proposed simulation-based framework, the proposed agent-based tsunami evacuation model was used to simulate the evacuation and various uncertainties (including the aleatory and epistemic uncertainties) associated with the evacuation were considered. Imprecise probability models were used to quantify both types of uncertainties, i.e., probability models are used to model the aleatory uncertainty in input random variables while the epistemic uncertainty (for the selected probability model) is quantified through the uncertainty in the distribution parameter. The evacuation risk is quantified by propagating the uncertainties in input random variables and distribution parameters. Using the proposed simulation-based framework, the tsunami evacuation risk

in Seaside, Oregon was assessed and investigated under different scenarios in terms of different population sizes, different times of the day, etc.

Chapter 5 conducted the sensitivity analysis of the tsunami evacuation risk with respect to the epistemic uncertainty (so-called risk sensitivity analysis) to investigate the impact of the epistemic uncertainty on the variability in the risk. The variance-based sensitivity analysis (i.e., using Sobol' index as the sensitivity measure) was efficiently performed by a proposed augmented sample-based approach. The sensitivity indices for all distribution parameters (including both first-order main effects and higher-order interactions) were estimated based on only one set of simulations. The sensitivity analysis of tsunami evacuation risk with respect to the epistemic uncertainty was performed for Seaside, Oregon under two different risk definitions using the proposed augmented sample-based approach. The risk sensitivity analysis results (i.e., the importance of distribution parameters) can be used to prioritize the data collection for effective epistemic uncertainty reduction and further for more accurate risk assessment.

Chapter 6 performed the probabilistic sensitivity analysis to identify the critical risk factors that have high impacts on the evacuation risk. Sensitivity analysis was also performed to investigate the variation of the sensitivity of risk factors with some key distribution parameters. This sensitivity analysis was efficiently conducted using an augmented sample-based approach by extending the one proposed in Chapter 5. Sensitivity analysis of tsunami evacuation risk was performed to identify critical risk factors for Seaside, Oregon. The identified critical risk factors can be used to guide effective evacuation modeling and selection of candidate risk mitigation strategies.

Chapter 7 conducted a risk-informed evaluation of different candidate risk mitigation strategies (including infrastructural and non-infrastructural strategies) to identify more effective strategies that are robust to uncertainties. The candidate mitigation strategies were effectively selected based on the critical risk factors identified by sensitivity analysis in Chapter 6. For each candidate strategy, evacuation risk was either estimated based on evacuation simulations by modifying the proposed agent-based model or efficiently estimated based on existing simulations. Based on the risk reductions, the effectiveness of each candidate strategy was evaluated and more effec-

tive strategies were identified. The risk-informed evaluation of risk mitigation strategies including route widening, bridge retrofit, building vertical shelters, preparedness education, and evacuation drills was conducted for Seaside, Oregon. More effective mitigation strategies were identified, which can be used to guide effective evacuation planning.

8.2 Future directions

The proposed agent-based tsunami evacuation model incorporates many of the important factors and mechanisms in the evacuation with the goal to simulate the evacuation process more realistically. However, some assumptions on the evacuation decision and behavior were made due to the lack of empirical data from historical events, evacuation drills, etc. Also, people's evacuation behavior could be quite complex in the multi-hazard environment within the condensed time frame. The availability of empirical data could support to more realistically capture the complex evacuation behavior and model the evacuation process using the proposed evacuation model. This motivates the development of methodologies to collect data for the validation and training of the proposed evacuation model.

In addition, some potentially important factors and mechanisms other than the considered ones can be incorporated into the proposed evacuation model to more comprehensively investigate the complex evacuation behavior. For example, destructive tsunami waves/flow can carry debris (e.g., logs, vehicles, etc.) when the tsunami propagates inland. The tsunami debris can block the road and potentially place high impact loads on the pedestrian or car in evacuation. Depending on the direction of the tsunami, location of the shelters, and the evacuation routes (e.g., when evacuees are more likely to go through the inundation, while which is less likely to occur in the study area in this research), the road blockage due to water-borne debris may become important and may need to be explicitly modeled. The modeling of water-borne debris and its impact on the evacuation environment, behavior, and performance can be incorporated into the corresponding sub-model of the proposed evacuation model. In the EEM, the model for the generation of water-borne debris can be incorporated and the impact of the debris on the traffic capacity of the corresponding road

can be modeled (e.g., reduce the traffic capacity according to the level of the road blockage due to the tsunami debris). In the EBM, the modeling of the evacuation under the blocked road due to the tsunami debris can be incorporated, e.g., reroute when the road is heavily blocked by the tsunami debris. In the EPM, when approximating the evacuation performance (i.e., casualty) using the factors such as the evacuees' characteristics and flow characteristics, the impact loads on the pedestrian or car due to tsunami debris can be incorporated.

The generalized framework for simulation-based tsunami evacuation risk assessment and risk-informed mitigation was applied under one of the worst-case multi-hazard scenarios (i.e., historical event). The results on risk assessment and mitigation under such extreme scenarios could provide valuable information for evacuation planning and management. However, the proposed framework can be used to perform the simulation-based tsunami evacuation risk assessment and risk-informed mitigation under probabilistic multi-hazard scenarios, and guide effective evacuation planning and management accordingly. Furthermore, the proposed generalized framework can be extended to different regions or hazards (e.g., hurricane) or evacuations (e.g., building evacuation). These are all future research areas of interest.

The risk-informed evaluation of different types of risk mitigation strategies was conducted to identify more effective strategies. Due to the challenges of pricing some of the strategies (e.g., evacuation drills), the cost of each strategy was not taken into account in the evaluation. To provide more comprehensive information for decision-making, the cost-benefit analysis can be conducted for each strategy to identify more effective strategies considering that the resource (e.g., budget) for risk mitigation is usually limited. Also, the optimal combination of different strategies can be identified through optimization (e.g., optimizing the objective function in terms of the cost and benefit of each mitigation strategy) such that the evacuation risk can be reduced most effectively.

Bibliography

Abrahamson, N. A., Kuehn, N., Gülerce, Z., Gregor, N., Bozorgnia, Y., Parker, G. A., Stewart, J. P., Chiou, B., Idriss, I. M., Campbell, K., and Youngs, R. (2018). Update of the BCHydro Subduction Ground-Motion Model Using the NGA-Subduction Dataset. Technical report, Headquarters at the University of California, Berkeley, CA.

Abustan, M. S. B. H. (2013). *Numerical simulation of evacuation process in Malaysia by using Distinct-Element-Method based multi-agent model*. PhD thesis, Kyoto University.

Adachi, T. and Ellingwood, B. R. (2010). Comparative assessment of civil infrastructure network performance under probabilistic and scenario earthquakes. *Journal of Infrastructure Systems*, 16(1):1–10.

Adiyoso, W. and Kanegae, H. (2012). The effect of different disaster education programs on tsunami preparedness among schoolchildren in Aceh, Indonesia. *Disaster Mitigation of Cultural Heritage and Historic Cities*, 6:165–172.

Aguilar, L., Lalith, M., and Hori, M. (2017). Time critical mass evacuation simulation combining a multi-agent system and high-performance computing. In *Multi-agent Systems*, chapter 4, pages 69–91.

Aguilar, L., Wijerathne, L., Jacob, S., Hori, M., and Ichimura, T. (2019). Mass evacuation simulation considering detailed models: behavioral profiles, environmental effects, and mixed-mode evacuation. *Asia Pacific Management Review*, 24:114–123.

Aguirre-Ayerbe, I., Martínez Sánchez, J., Aniel-Quiroga, I., González-Riancho, P., Merino, M., Al-Yahyai, S., González, M., and Medina, R. (2018). From tsunami risk assessment to disaster risk reduction - the case of Oman. *Natural Hazards and Earth System Sciences*, 18:2241–2260.

Ahmad, S. and Simonovic, S. P. (2000a). Dynamic Modeling of Flood Management Policies. In *Proceedings of the 18th International Conference of the System Dynamics Society: Sustainability in the Third Millennium*, pages 6–10, Bergen, Norway.

Ahmad, S. and Simonovic, S. P. (2000b). System dynamics modeling of reservoir operations for flood management. *Journal of Computing in Civil Engineering*, 14(3):190–198.

Ahmad, S. and Simonovic, S. P. (2001). Modeling human behavior for evacuation planning: A system dynamics approach. In *Bridging the Gap: Meeting the World's Water and Environmental Resources Challenges*, pages 1–10, Orlando, Florida.

Alabdouli, K. (2017). Hypothetical Tsunami Scenarios and Evacuation Intention: A Case Study of Orange County, California. *Journal of Geography & Natural Disasters*, 7(3):1000212.

Anguelov, B. (2011). *Video Game Pathfinding and Improvements to Discrete Search on Grid-based Maps*. PhD thesis, University of Pretoria.

Applied Technology Council (2009). Vertical Evacuation from Tsunamis: A Guide for Community Officials. Technical report, Federal Emergency Management Agency, Washington, D.C.

Applied Technology Council (2019). Guidelines for Design of Structures for Vertical Evacuation from Tsunamis. Technical report, Federal Emergency Management Agency, Washington, D.C.

Astle, C. and Crooks, A. (2006). Principles and Concepts of Agent-Based Modelling for Developing Geospatial Simulations. Technical report, Centre for Advanced Spatial Analysis,University College London, London,UK.

Atwater, B. F. and Griggs, G. B. (2012). Deep-Sea Turbidites as Guides to Holocene Earthquake History at the Cascadia Subduction Zone-Alternative Views for a Seismic-Hazard Workshop. Technical report, U.S. Geological Survey, Reston, Virginia.

Au, S. K. (2005). Reliability-based design sensitivity by efficient simulation. *Computers & structures*, 83(14):1048–1061.

Au, S. K. and Beck, J. L. (2003). Subset Simulation and its Application to Seismic Risk Based on Dynamic Analysis. *Journal of Engineering Mechanics*, 129(8):901–917.

Australian Geographic (2011). The ten most destructive tsunamis in history. Released March 16, 2011. Available at: https://www.australiangeographic.com.au/topics/science-environment/2011/03/the-10-most-destructive-tsunamis-in-history/. Accessed September 4, 2020.

Banse, T. (2012). Coastal schools drill for tsunami, would rather relocate. Retrieved from https://www.knkx.org/post/coastal-schools-drill-tsunami-would-rather-relocate.

Benchekroun, S. and El Mouraouah, A. (2018). Tsunami evacuation plan for the city of Tangier-Morocco based on GIS tools. *Science of Tsunami Hazards*, 37(4):157–174.

Berariu, R., Fikar, C., Gronalt, M., and Hirsch, P. (2016). Training decision-makers in flood response with system dynamics. *Disaster Prevention and Management*, 25(2):118–136.

Bialynicki-Birula, I. and Bialynicka-Birula, I. (2005). *Modeling Reality: How Computers Mirror Life*. Oxford University Press, New York.

Billah, M., Sarker, S., and Ansary, M. A. (2018). Cyclone Evacuation Route Identification Using GIS for Coastal Communities in Mirzaganj Union, Patuakhali, Bangladesh.

Bonabeau, E. (2002). Agent-based modeling: Methods and techniques for simulating human systems. In *Proceedings of the National Academy of Sciences*, volume 99, pages 7280–7287, Irvine, CA.

Borgonovo, E. (2007). A new uncertainty importance measure. *Reliability Engineering and System Safety*, 92:771–784.

Brevault, L., Balesdent, M., Bérend, N., and Le Riche, R. (2013). Comparison of different global sensitivity analysis methods for aerospace vehicle optimal design. In *10th World Congress on Structural and Multidisciplinary Optimization, WCSMO-10*.

Buckle, I., Friedland, I., Mander, J., Martin, G., Nutt, R., and Power, M. (2006). Seismic Retrofitting Manual for Highway Structures : Part 1 – Bridges. Technical report, Turner-Fairbank Highway Research Center, McLean, VA.

Cabinet Office (2011). White paper on disaster management 2011- executive summary. Technical report, Tokyo, Japan.

Campbell, K. W. and Bozorgnia, Y. (2008). NGA ground motion model for the geometric mean horizontal component of PGA, PGV, PGD and 5% damped linear elastic response spectra for periods ranging from 0.01 to 10 s. *Earthquake Spectra*, 24(1):139–171.

Catal, C., Akbulut, A., Tunali, B., Ulug, E., and Ozturk, E. (2020). Evaluation of augmented reality technology for the design of an evacuation training game. *Virtual Reality*, 24(3):359–368.

Chabridon, V. and Gayton, N. (2018). Reliability-based sensitivity estimators of rare event probability in the presence of distribution parameter uncertainty. *Reliability Engineering and System Safety*, 178:164–178.

Cheng, J. C., Tan, Y., Song, Y., Mei, Z., Gan, V. J., and Wang, X. (2018). Developing an evacuation evaluation model for offshore oil and gas platforms using BIM and agent-based model. *Automation in Construction*, 89:214–224.

City of Seaside (2010). Seaside Transportation System Plan Volume I: Plan. Technical report, Seaside,Oregon.

Claptsop County (2008). Seaside ArcGIS Shapefiles. Released 2008. Available at: http://web.pdx.edu/˜jduh/seasidegis/shapefiles/main.php. Accessed September 4, 2020.

Clatsop County (2019). Oregon transportation map showing Federal Functional Classification of Roads City of Seaside. Released 2019. Available at: https://www.oregon.gov/odot/Data/Documents/City_Seaside.pdf. Accessed September 4, 2020.

CRATER (2005). *Coastal Risk Analysis of Tsunamis and Environmental Remediation (CRATER), evacuation routes tools ArcGIS® toolbox, user's manual*.

Cundall, P. A. and Strack, O. D. (1979). A discrete numerical model for granular assemblies. *Géotechnique*, 29:47–65.

Dalal, J., Mohapatra, P. K., and Mitra, G. C. (2007). Locating cyclone shelters: a case. *Disaster Prevention and Management*, 16(2):235–244.

De Silva, F. N. (2001). Providing spatial decision support for evacuation planning: a challenge in integrating technologies. *Disaster Prevention and Management*, 10(1):11–20.

De Silva, F. N. and Eglese, R. (2000). Integrating simulation modelling and GIS: spatial decision support systems for evacuation planning. *Journal of the Operational Research Society*, 51(4):423–430.

Dengler, L. (2005). The role of education in the national tsunami hazard mitigation program. *Natural Hazards*, 35:141–153.

Der Kiureghian, A. and Ditlevsen, O. (2009). Aleatory or epistemic? Does it matter? *Structural Safety*, 31:105–112.

Dewi, R. S. (2012). A-Gis Based Approach of an Evacuation Model for Tsunami Risk Reduction. *Journal of Integrated Disaster Risk Management*, 2(2):108–139.

Dunn, C. E. and Newton, D. (1992). Optimal routes in GIS and emergency planning applications. *Area*, 24(3):259–267.

El-Barmelgy, H. M. and Hamed, M. S. (2017). Tsunami risk assessment a mitigation planning tool. *International Journal of Development and Sustainability*, 6(9):1048–1065.

Elheishy, S. S., Saleh, A. A., and Asem, A. (2013). A Rough Set and GIS Based Approach for Selecting Suitable Shelters during an Evacuation Process. *Journal of Geographic Information System*, 5:1–12.

Fang, W., Yang, L., and Fan, W. (2003). Simulation of bi-direction pedestrian movement using a cellular automata model. *Physica A: Statistical Mechanics and its Applications*, 321(3-4):633–640.

FEMA (2009). Multi-hazard Loss Estimation Methodology-Earthquake Model. Technical report, Department of Homeland Security, Washington, D.C.

Feng, K., Li, Q., and Ellingwood, B. R. (2020). Post-earthquake modelling of transportation networks using an agent-based model. *Structure and Infrastructure Engineering*, pages 1–15.

Fletcher, E. J. (1998). The use of system dynamics as a decision support tool for the management of surface water resources. In *Proceedings of First International Conference on New Information Technologies for Decision-Making in Civil Engineering*, pages 909–920, Montreal, Canada.

Forrester, J. W. (1961). *Industrial dynamics*. The M.I.T. Press, Cambridge, MA.

Fraser, S. A., Wood, N. J., Johnston, D. M., Leonard, G. S., Greening, P. D., and Rossetto, T. (2014). Variable population exposure and distributed travel speeds in least-cost tsunami evacuation modelling. *Natural Hazards and Earth System Sciences*, 14:2975–2991.

Fujioka, M., Ishibashi, K., Kaji, H., and Tsukagoshi, I. (2002). Multi agent Simulation Model for Evaluating Evacuation Management System Against Tsunami Disaster. *Journal of Architecture and Planning (Transactions of AIJ)*, 67:231–236.

Gillespie, D. F., Robards, K. J., and Cho, S. (2004). Designing safe systems: Using system dynamics to understand complexity. *Natural Hazards Review*, 5(2):82–88.

Goldfinger, C., Nelson, C. H., Morey, a. E., Joel E, J., Patton, J., Karabanov, E., Gutierrez-Pastor, J., Eriksson, A., Gracia, E., Dunhill, G., Enkin, R., Dallimore, A., and Valiier, T. (2012). Turbidite event history—Methods and implications for Holocene paleoseismicity of the Cascadia subduction zone: U.S. Geological Survey Professional Paper 1661–F, 170 p, 64 figures, available at http://pubs.usgs.gov/pp/pp1661/f. Technical report.

González, F. I., Geist, E. L., and et al. Jaffe, B. (2009). Probabilistic tsunami hazard assessment at Seaside, Oregon, for near-and far-field seismic sources. *Journal of Geophysical Research: Oceans*, 114:C11023.

Goto, Y., Affan, M., Agussabti, Nurdin, Y., Yuliana, D. K., and Ardiansyah (2012). Tsunami evacuation simulation for disaster education and city planning. *Journal of Disaster Research*, 7(1):92–101.

Gotoh, H., Harada, E., and Andoh, E. (2012). Simulation of pedestrian contra-flow by multi-agent DEM model with self-evasive action model. *Safety Science*, 50(2):326–332.

Gotoh, H., Harada, E., Kubo, Y., and Sakai, T. (2004). Particle-system model of the behavior of crowd in tsunami flood refuge. *Coastal Engineering Journal*, 51:1261–1265.

Gotoh, H., Harada, E., Maruyama, Y., Takahashi, K., and Ohniwa, K. (2008). Contribution of Crowd Refuge Simulator to Town Planning against Tsunami Flood. *Coastal Engineering Journal*, 55:1371–1375.

Gotoh, H., Harada, E., and Ohniwa, K. (2009). Numerical simulation of coastal town planning against tsunami by DEM-base human behavior simulator. In *Proceedings of the Nineteenth (2009) International Offshore and Polar Engineering Conference*, pages 1248–1252, Osaka, Japan.

Greenshields, B. (1935). A Study of Traffic Capacity. In *Highway Research Board Proceedings*. National Research Council (USA), Highway Research Board.

Haiqal, M., Sari, L. H., Evalina, Z., and Hasibuan, P. (2019). A review of vertical evacuation on tsunami mitigation case. In *IOP Conference Series: Materials Science and Engineering*, volume 523, page 012061. IOP Publishing.

Helton, W. S., Kemp, S., and Walton, D. (2013). Individual differences in movements in response to natural disasters: tsunami and earthquake case studies. In *Proceedings of the Human Factors and Ergonomics Society*, volume 57, pages 858–862, Los Angeles, CA.

Homma, T. and Saltelli, A. (1996). Importance measures in global sensitivity analysis of nonlinear models. *Reliability Engineering & System Safety*, 52:1–17.

Hu, Y. (2017). Research Review of China Emergency Evacuation. *Advances in Economics, Business and Management Research*, 23:185–188.

Hurtado, J. E. (2013). Assessment of reliability intervals under input distributions with uncertain parameters. *Probabilistic Engineering Mechanics*, 32:80–92.

Imamura, F., Muhari, A., Mas, E., Pradono, M. H., Post, J., and Sugimoto, M. (2012). Tsunami disaster mitigation by integrating comprehensive countermeasures in Padang city, Indonesia. *Journal of Disaster Research*, 7(1):48–64.

Iooss, B. and Lemaître, P. (2015). A review on global sensitivity analysis methods. In *Uncertainty management in simulation-optimization of complex systems*, pages 101–122. Springer, Boston, MA.

Jacob, S., Aguilar, L., Wijerathne, L., Hori, M., Ichimura, T., and Tanaka, S. (2014). Agent Based Modeling and Simulation of Tsunami Triggered Mass Evacuation Considering Changes of Environment Due to Earthquake and Inundation. *Journal of Japan Society of Civil Engineers, Ser. A2 (Applied Mechanics (AM))*, 70(2):671–680.

Jelínek, R., Krausmann, E., González, M., Álvarez-Gómez, J. A., Birkmann, J., and Welle, T. (2012). Approaches for tsunami risk assessment and application to the city of Cádiz, Spain. *Natural Hazards*, 60:273–293.

Jia, G. (2014). *Kernel and Metamodel Based Methods for Analysis and Optimization of Systems Under Uncertainty*. PhD thesis, University of Notre Dame.

Jia, G., Gidaris, I., Taflanidis, A. A., and Mavroeidis, G. P. (2014). Reliability-based assessment/design of floor isolation systems. *Engineering Structures*, 78:41–56.

Jia, G. and Taflanidis, A. A. (2014). Sample-based evaluation of global probabilistic sensitivity measures. *Computers and Structures*, 144:103–118.

Jia, G. and Taflanidis, A. A. (2016). Efficient Evaluation of Sobol' Indices Utilizing Samples from an Auxiliary Probability Density Function. *Journal of Engineering Mechanics*, 142(5):04016012.

Jia, G., Taflanidis, A. A., and Beck, J. L. (2017). A New Adaptive Rejection Sampling Method Using Kernel Density Approximations and Its Application to Subset Simulation. *ASCE-ASME Journal of Risk and Uncertainty in Engineering Systems, Part A: Civil Engineering*, 3(2):D4015001.

Johnston, K. M. (2013). *Agent Analyst: Agent-Based Modeling in ArcGIS.* Esri Press, Redlands, California.

Jonkman, S. N., J. K. Vrijling, and Vrouwenvelder, A. C. W. M. (2008). Methods for the estimation of loss of life due to floods: a literature review and a proposal for a new method. *Natural Hazards*, 46:353–389.

Jumadi, Carver, S., and Quincey, D. (2017). A conceptual design of spatio-temporal agent-based model for volcanic evacuation. *Systems*, 5(4):53.

Kar, B. and Hodgson, M. E. (2008). A GIS-based model to determine site suitability of emergency evacuation shelters. *Transactions in GIS*, 12(2):227–248.

Karunamuni, R. J. and Zhang, S. (2008). Some improvements on a boundary corrected kernel density estimator. *Statistics and Probability Letters*, 78:499–507.

Katada, T. and Kanai, M. (2008). Implementation of tsunami disaster education for children and their parents at elementary school. *Solutions to Coastal Disasters 2008: Tsunamis*, pages 39–48.

Katada, T., Kuwasawa, N., Kanai, M., and Hosoi, K. (2004). Disaster Education for Owase citizen by using Tsunami Scenario Simulator and evaluation of that method. *Sociotechnica*, 2:199–208.

Kawai, J., Mitsuhara, H., and Shishibori, M. (2016). Tsunami Evacuation Drill System using Motion Hazard Map and Smart Devices. In *3rd International Conference on Information and Communication Technologies for Disaster Management (ICT-DM)*. IEEE.

Kirchner, A., Klüpfel, H., Nishinari, K., Schadschneider, A., and Schreckenberg, M. (2003a). Simulation of competitive egress behavior: comparison with aircraft evacuation data. *Physica A: Statistical Mechanics and its Applications*, 324(3-4):689–697.

Kirchner, A., Nishinari, K., and Schadschneider, A. (2003b). Friction effects and clogging in a cellular automaton model for pedestrian dynamics. *Physical review E*, 67(5):056122.

Kita, E., Hara, A., and Ye, Q. (2015). Traffic network design for disaster evacuation by cellular automata simulation. *Proceedings-2014 2nd International Symposium on Computing and Networking, CANDAR 2014*, pages 487–490.

Kiyono, J., Miura, F., and Takimato, K. (1996). Simulation of emergency evacuation behavior in a disaster by using distinct element method. In *Proceedings of civil engineering conference*, volume 537, pages 233–244.

Kiyono, J., Miura, F., and Yagi, H. (1998). Simulation of evacuation behavior in a disaster by distinct element method. In *Proceedings-Japan Society of Civil Engineers*, pages 365–378. Doboku Gakkai.

Koshimura, S. and Shuto, N. (2015). Response to the 2011 Great East Japan Earthquake and Tsunami disaster. *Philosophical Transactions of the Royal Society A: Mathematical, Physical and Engineering Sciences*, 373:20140373.

Kwan, M. P. and Lee, J. (2005). Emergency response after 9/11: the potential of real-time 3D GIS for quick emergency response in micro-spatial environments. *Computers, Environment and Urban Systems*, 29:93–113.

Lämmel, G. (2011). *Escaping the Tsunami : Evacuation Strategies for Large Urban Areas*. PhD thesis, Technical University of Berlin.

Langlois, J. A., Keyl, P. M., Guralnik, J. M., Foley, D. J., Marottoli, R. A., and Wallace, R. B. (1997). Characteristics of older pedestrians who have difficulty crossing the street. *American Journal of Public Health*, 87(3):393–397.

Langston, P. A., Masling, R., and Asmar, B. N. (2006). Crowd dynamics discrete element multi-circle model. *Safety Science*, 44:395–417.

Leelawat, N., Suppasri, A., Latcharote, P., Abe, Y., Sugiyasu, K., and Imamura, F. (2018). Tsunami evacuation experiment using a mobile application: A design science approach. *International Journal of Disaster Risk Reduction*, 29:63–72.

León, J. and March, A. (2016). An urban form response to disaster vulnerability: Improving tsunami evacuation in Iquique, Chile. *Environment and Planning B: Planning and Design*, 43(5):826–847.

Li, J., Yang, L., and Zhao, D. (2005). Simulation of bi-direction pedestrian movement in corridor. *Physica A: Statistical Mechanics and its Applications*, 354:619–628.

Li, Y., Chen, M., Dou, Z., Zheng, X., Cheng, Y., and Mebarki, A. (2019a). A review of cellular automata models for crowd evacuation. *Physica A: Statistical Mechanics and its Applications*, 526:120752.

Li, Y., Hu, B., Zhang, D., Gong, J., Song, Y., and Sun, J. (2019b). Flood evacuation simulations using cellular automata and multiagent systems -a human-environment relationship perspective. *International Journal of Geographical Information Science*, 33(11):2241–2258.

Lind, N., Hartford, D., and Assaf, H. (2004). Hydrodynamic models of human stability in a flood. *Journal of the American Water Resources Association*, 40:89–96.

Liu, H., Chen, W., and Sudjianto, A. (2004). Probabilistic Sensitivity Analysis Methods for Design under Uncertainty. In *10th AIAA/ISSMO Multidisciplinary Analysis and Optimization Conference*, page 4589.

Liu, H., Chen, W., and Sudjianto, A. (2006). Relative Entropy Based Method for Probabilistic Sensitivity Analysis in Engineering Design. *Journal of Mechanical Design*, 128:326–336.

Liu, Q. and Homma, T. (2009). A new computational method of a moment-independent uncertainty importance measure. *Reliability Engineering and System Safety*, 94:1205–1211.

Lonergan, C., Hedley, N., and Clague, J. J. (2015). A visibility-based assessment of tsunami evacuation signs in Seaside, Oregon. *Natural Hazards*, 78:41–59.

Loth, C. and Baker, J. W. (2013). A spatial cross-correlation model of spectral accelerations at multiple periods. *Earthquake Engineering and Structural Dynamics*, 42:397–417.

Løvholt, F., Fraser, S., Salgado-Gálvez, M., Lorito, S., J., S., and F., R. (2019). Global trends in advancing tsunami science for improved hazard and risk understanding. *Contributing Paper to GAR19*, pages 1–50.

Lumbroso, D. M., Simm, J. D., Davison, M., White, K. D., and Durden, S. (2017). Use of Agent-Based Modelling to Validate Hurricane Evacuation Planning. In *Coastal Structures and Solutions to Coastal Disasters 2015: Resilient Coastal Communities.*, pages 321–329, Reston, VA.

Ma, J., Liu, S., Wang, W., Lin, P., and Lo, S. (2012). A GIS-based Micro-simulation Queue Model for Vehicle Evacuation. *Journal of Risk Analysis and Crisis Response*, 2(3):178–187.

Makinoshima, F., Imamura, F., and Abe, Y. (2018). Enhancing a tsunami evacuation simulation for a multi-scenario analysis using parallel computing. *Simulation Modelling Practice and Theory*, 83:36–50.

Mallick, B. (2014). Cyclone shelters and their locational suitability: An empirical analysis from coastal Bangladesh. *Disasters*, 38(3):654–671.

Manley, M. and Kim, Y. S. (2012). Modeling emergency evacuation of individuals with disabilities (exitus): An agent-based public decision support system. *Expert Systems with Applications*, 39:8300–8311.

Mas, E., Koshimura, S., Imamura, F., Suppasri, A., Muhari, A., and Adriano, B. (2015). Recent Advances in Agent-Based Tsunami Evacuation Simulations: Case Studies in Indonesia, Thailand, Japan and Peru. *Pure and Applied Geophysics*, 172:3409–3424.

Mas, E., Suppasri, A., Imamura, F., and Koshimura, S. (2012). Agent-based Simulation of the 2011 Great East Japan Earthquake/Tsunami Evacuation: An Integrated Model of Tsunami Inundation and Evacuation. *Journal of Natural Disaster Science*, 34(1):41–57.

Mauro, M. D., Lees, M., and Megawati, K. (2014). Pedestrian-Vehicles Interaction During Evacuation: Agent-Based Hybrid Evacuation Modelling of Southeast Asian Cities. In *Pedestrian and Evacuation Dynamics 2012*, pages 435–443.

McGuire, R. K. (2001). Deterministic vs. probabilistic earthquake hazards and risks. *Soil Dynamics and Earthquake Engineering*, 21(5):377–384.

Mostafizi, A., Wang, H., Cox, D., Cramer, L. A., and Dong, S. (2017). Agent-based tsunami evacuation modeling of unplanned network disruptions for evidence-driven resource allocation and retrofitting strategies. *Natural Hazards*, 88:1347–1372.

Mostafizi, A., Wang, H., Cox, D., and Dong, S. (2019a). An agent-based vertical evacuation model for a near-field tsunami: Choice behavior, logical shelter locations, and life safety. *International Journal of Disaster Risk Reduction*, 34:467–479.

Mostafizi, A., Wang, H., and Dong, S. (2019b). Understanding the Multimodal Evacuation Behavior for a Near-Field Tsunami. *Transportation Research Record*, 2673:480–492.

Muhammad, A., Goda, K., Alexander, N. A., Kongko, W., and Muhari, A. (2017). Tsunami evacuation plans for future megathrust earthquakes in Padang, Indonesia, considering stochastic earthquake scenarios. *Natural Hazards and Earth System Sciences*, 17:2245–2270.

Munadi, K., Nurdin, Y., Dirhamsyah, M., and Muchalil, S. (2012). Multiagent based Tsunami Evacuation Simulation: A Conceptual Model. In *Proceedings of the Annual International Con-*

ference, Syiah Kuala University-Life Sciences & Engineering Chapter, volume 2, pages 254–259, Banda AcehIndonesia.

Murakami, H., Yanagihara, S., Goto, Y., Mikami, T., Sato, S., and Wakihama, T. (2014). Study on casualty and tsunami evacuation behavior in Ishinomaki City-questionnaire survey for the 2011 great east Japan Earthquake. In *10th U.S. National Conference on Earthquake Engineering: Frontiers of Earthquake Engineering*, Anchorage, Alaska.

Murata, S., Imamura, F., Katoh, K., Kawata, Y., Takahashi, S., and Takayama (2010). *Tsunami: to survive from tsunami*. World Scientific, Singapore.

Nakaya, N., Nemoto, H., Yi, C., Sato, A., Shingu, K., Shoji, T., Sato, S., Tsuchiya, N., Nakamura, T., Narita, A., Kogure, M., Sugawara, Y., Yu, Z., Gunawansa, N., Kuriyama, S., Murao, O., Sato, T., Imamura, F., Tsuji, I., Hozawa, A., and Tomita, H. (2018). Effect of tsunami drill experience on evacuation behavior after the onset of the Great East Japan Earthquake. *International Journal of Disaster Risk Reduction*, 28:206–213.

Nannapaneni, S. and Mahadevan, S. (2016). Reliability analysis under epistemic uncertainty. *Reliability Engineering and System Safety*, 155:9–20.

Neis, H., Pempus, H., Wright, P., and Nolte, K. (2015). Up and Out 2. Technical report, The Portland Urban Architecture Research Laboratory, Portland, OR.

Nishinari, K., Sugawara, K., Kazama, T., Schadschneider, A., and Chowdhury, D. (2006). Modelling of self-driven particles: Foraging ants and pedestrians. *Physica A: Statistical Mechanics and its Applications*, 372:132–141.

Ohno, S., Takagi, A., Kurauchi, F., Demura, Y., and Ohsaki, T. (2011). Database Construction of Newspaper Article about Evacuation Behavior from Tsunami in the Great East Japan Earthquake. pages 61–66.

Okumura, N., Jonkman, S. N., Esteban, M., Hofland, B., and Shibayama, T. (2017). A method for tsunami risk assessment: a case study for Kamakura, Japan. *Natural Hazards*, 88:1451–1472.

Oregon Department of Transportation (2020). Speed Zone Manual. Technical report, Statewide Project Delivery Branch–Engineering & Technical Services Branch Traffic-Roadway Section, Salem, Oregon.

Oregon Office of Emergency Management (2017). Tsunami Evacuation Drill Guidebook. Technical report, Oregon Office of Emergency Management, Salem, Oregon.

Ouellette, M. J. and Rea, M. S. (1989). Illuminance requirements for emergency lighting. *Journal of the Illuminating Engineering Society*, 18(1):37–42.

Padgett, J. E. and DesRoches, R. (2009). Retrofitted bridge fragility analysis for typical classes of multispan bridges. *Earthquake Spectra*, 25(1):117–141.

Palmer, R. N., Keyes, A. M., and Fisher, S. (1993). Empowering stakeholders through simulation in water resources planning. In *Proceedings of the 20th anniversary conference: Water management in the'90s. A time for innovation*.

Pan, X., Han, C. S., Dauber, K., and Law, K. H. (2007). A multi-agent based framework for the simulation of human and social behaviors during emergency evacuations. *AI and Society*, 22:113–132.

Park, H. and Cox, D. T. (2016). Probabilistic assessment of near-field tsunami hazards: Inundation depth, velocity, momentum flux, arrival time, and duration applied to Seaside, Oregon. *Coastal Engineering*, 117:79–96.

Park, H., Cox, D. T., and Barbosa, A. R. (2017). Comparison of inundation depth and momentum flux based fragilities for probabilistic tsunami damage assessment and uncertainty analysis. *Coastal Engineering*, 122:10–26.

Peng, M., Peng, Y., and Chen, H. (2014). Post-seismic supply chain risk management: A system dynamics disruption analysis approach for inventory and logistics planning. *Computers and Operations Research*, 42:14–24.

Péroche, M., Leone, F., and Gutton, R. (2014). An accessibility graph-based model to optimize tsunami evacuation sites and routes in Martinique, France. *Advances in Geosciences*, 38:1–8.

Post, J., Wegscheider, S., Mück, M., Zosseder, K., Kiefl, R., Steinmetz, T., and Strunz, G. (2009). Assessment of human immediate response capability related to tsunami threats in Indonesia at a sub-national scale. *Natural Hazards and Earth System Science*, 9:1075–1086.

Priest, G. R., Stimely, L. L., Wood, N. J., Madin, I. P., and Watzig, R. J. (2016). Beat-the-wave evacuation mapping for tsunami hazards in Seaside, Oregon, USA. *Natural Hazards*, 80:1031–1056.

Priest, G. R., Witter, R. C., and Zhang, Y. J. (2013). Tsunami Animations, Time Histories, and Digital Point Data for Flow Depth, Elevation, and Velocity for the South Coast Project Area, Curry County, Oregon. Technical report, Department of Geology and Mineral Industries.

Qiu, F. and Hu, X. (2010). Modeling group structures in pedestrian crowd simulation. *Simulation Modelling Practice and Theory*, 18:190–205.

Rahman, N. A., Harada, E., and Gotoh, H. (2014). DEM-based Group Behaviour Model and Its Impact in Tsunami Evacuation Simulation. *Journal of Natural Sciences Research*, 4:1–10.

Raskin, J., Wang, Y., Boyer, M., Fiez, T., Moncada, J., Yu, K., and Yeh, H. (2011). An evacuation building project for Cascadia earthquakes and tsunamis. *Obras y proyectos*, 9:11–22.

Robert, C. P. and Casella, G. (2004). *Monte Carlo Statistical Methods*. New York, 2nd edition.

Roess, R. P., Prassas, E. S., and McShane, W. R. (2011). *Traffic engineering*. Pearson, NJ: Prentice Hall, 4th edition.

Ronan, K. R., Alisic, E., Towers, B., Johnson, V. A., and Johnston, D. M. (2015). Disaster Preparedness for Children and Families: a Critical Review. *Current Psychiatry Reports*, 17:58.

Sahal, A., Leone, F., and Péroche, M. (2013). Complementary methods to plan pedestrian evacuation of the French Riviera's beaches in case of tsunami threat: graph-and multi-agent-based modelling. *Natural Hazards and Earth System Sciences*, 13(7):1735–1743.

Saltelli, A. (2002). Sensitivity analysis for importance assessment. *Risk Analysis*, 22(3):579–590.

Sankararaman, S. and Mahadevan, S. (2013). Separating the contributions of variability and parameter uncertainty in probability distributions. *Reliability Engineering and System Safety*, 112:187–199.

Satake, K. (2003). Fault slip and seismic moment of the 1700 Cascadia earthquake inferred from Japanese tsunami descriptions. *Journal of Geophysical Research*, 108(B11):2535.

Schelling, T. C. (1971). Dynamic models of segregation. *The Journal of Mathematical Sociology*, 1:143–186.

Schmidtlein, M. C. and Wood, N. J. (2015). Sensitivity of tsunami evacuation modeling to direction and land cover assumptions. *Applied Geography*, 56:154–163.

Schöbi, R. and Sudret, B. (2019). Global sensitivity analysis in the context of imprecise probabilities (p-boxes) using sparse polynomial chaos expansions. *Reliability Engineering and System Safety*, 187:129–141.

Schultz, M., Lehmann, S., and Fricke, H. (2007). A discrete microscopic model for pedestrian dynamics to manage emergency situations in airport terminals. In *Pedestrian and Evacuation Dynamics 2005*, pages 369–375, Berlin, Heidelberg.

Shahabi, K. and Wilson, J. P. (2014). CASPER: Intelligent capacity-aware evacuation routing. *Computers, Environment and Urban Systems*, 46:12–24.

Sharpe, J. and Kelman, I. (2011). Improving the disaster-related component of secondary school geography education in England. *International Research in Geographical and Environmental Education*, 20(4):327–343.

Shendarkar, A., Vasudevan, K., Lee, S., and Son, Y. j. (2008). Crowd simulation for emergency response using BDI agents based on immersive virtual reality. *Simulation Modelling Practice and Theory*, 16:1415–1429.

Simonovic, S. P. and Ahmad, S. (2005). Computer-based model for flood evacuation emergency planning. *Natural Hazards*, 34:25–51.

Simonovic, S. P. and Fahmy, H. (1999). A new modeling approach for water resources policy analysis. *Water Resources Research*, 35(1):295–304.

Simonovic, S. P., Fahmy, H., and El-Shorbagy, A. (1997). The Use of Object-Oriented Modeling for Water Resources Planning in Egypt. *Water Resources Management*, 11:243–261.

Singh, H., Arter, R., Dodd, L., Langston, P., Lester, E., and Drury, J. (2009). Modelling subgroup behaviour in crowd dynamics DEM simulation. *Applied Mathematical Modelling*, 33:4408–4423.

Sipper, M. and Tomassini, M. (1998). An Introduction to Cellular Automata. *Bio-inspired Computing Machines*, 3:49–58.

Sleeter, R. and Wood, N. (2006). Estimating daytime and nighttime population density for coastal communities in Oregon. In *44th Urban and Regional Information Systems Association Annual Conference*, British Columbia.

Smith, S. K. and Mccarty, C. (2009). Fleeing the storm(s): an examination of evacuation behavior during florida's 2004 hurricane season. *Demography*, 46(1):127–145.

SMS Tsunami Warning (2018). Tsunamis in our history. Retrieved from https://www.sms-tsunami-warning.com/pages/tsunami-history#.X0aEK8hKi.

Sobol, I. M. (2001). Global sensitivity indices for nonlinear mathematical models and their Monte Carlo estimates. *Mathematics and Computers in Simulation*, 55:271–280.

Solís, I. A. and Gazmuri, P. (2017). Evaluation of the risk and the evacuation policy in the case of a tsunami in the city of Iquique, Chile. *Natural Hazards*, 88:503–532.

Stern, E. and Sinuany-Stern, Z. (1989). A behavioral-based simulation model for urban evacuation. In *Papers of the Regional Science Association*, volume 66, pages 87–103.

Stewart, J. P., Douglas, J., Javanbarg, M., Bozorgnia, Y., Abrahamson, N. A., Boore, D. M., Campbell, K. W., Delavaud, E., Erdik, M., and Stafford, P. J. (2015). Selection of ground motion prediction equations for the global earthquake model. *Earthquake Spectra*, 31(1):19–45.

Sudret, B. (2008). Global sensitivity analysis using polynomial chaos expansions. *Reliability Engineering and System Safety*, 93:964–979.

Sugimoto, T., Murakami, H., Kozuki, Y., Nishikawa, K., and Shimada, T. (2003). A human damage prediction method for tsunami disasters incorporating evacuation activities. *Natural Hazards*, 29:585–600.

Sun, Y. (2014). *Action Research to Promote Tsunami Risk Reduction: Ethnographic Approaches to Disaster Education and Tsunami Evacuation*. PhD thesis, Kyoto University.

Suppasri, A., Shuto, N., Imamura, F., Koshimura, S., Mas, E., and Yalciner, A. C. (2013). Lessons Learned from the 2011 Great East Japan Tsunami: Performance of Tsunami Countermeasures, Coastal Buildings, and Tsunami Evacuation in Japan. *Pure and Applied Geophysics*, 170:993–1018.

Taflanidis, A. A. and Jia, G. (2011). A simulation-based framework for risk assessment and probabilistic sensitivity analysis of base-isolated structures. *Earthquake Engineering & Structural Dynamics*, 40(14):1629–1651.

Takabatake, T., Shibayama, T., Esteban, M., and Ishii, H. (2018). Advanced casualty estimation based on tsunami evacuation intended behavior: case study at Yuigahama Beach, Kamakura, Japan. *Natural Hazards*, 92:1763–1788.

Takabatake, T., Shibayama, T., Esteban, M., Ishii, H., and Hamano, G. (2017). Simulated tsunami evacuation behavior of local residents and visitors in Kamakura, Japan. *International Journal of Disaster Risk Reduction*, 23:1–14.

Takada, K., Fujiu, M., Ohara, M., and Onomura, K. (2013). Development of Traffic Simulation for Tsunami Evacuation-Case Study for Kesennuma city. In *Proceedings of the Eastern Asia Society for Transportation Studies*, volume 9.

Tamaki, T., Yasue, S., and Kita, E. (2004). Traffic simulation using stochastic velocity model and CA. *Transaction of Information Processing Society in Japan*, 45:858–869.

Tang, Z.-C., Lu, Z., Wang, P., Xia, Y., Yang, P., and Wang, P. (2016). Efficient numerical simulation method for evaluations of global sensitivity analysis with parameter uncertainty. *Applied Mathematical Modelling*, 40(1):597–611.

The Oregon Department of Geology and Mineral Industries (2013). Tsunami Evacuation Map Seaside & Gearhart, Oregon. Released June 3, 2013. Available at: https://www.oregongeology.org/pubs/tsubrochures/SeasideGearhartEvacBrochure-6-3-13_onscreen.pdf. Accessed September 4, 2020.

Thiele, J. C. (2014). R Marries NetLogo: Introduction to the RNetLogo Package. *Journal of Statistical Software*, 58(2):1–41.

Thiele, M. J. C. (2017). Package 'RNetLogo'. Retrieved from https://cran.r-project.org/web/packages/RNetLogo/.

Titov, V. V. and González, F. I. (1997). Implementation and testing of the method of splitting tsunami (MOST) model. Technical report, NOAA/Pacific Marine Environmental Laboratory, Seattle, WA.

Toyama, M. C., Bazzan, A. L., and Silva, R. D. (2006). An agent-based simulation of pedestrian dynamics: from lane formation to auditorium evacuation. In *Proceedings of the fifth international joint conference on Autonomous agents and multiagent systems*, pages 108–110.

Tsushima, H., Hirata, K., Hayashi, Y., Tanioka, Y., Kimura, K., Sakai, S., Shinohara, M., Kanazawa, T., Hino, R., and Maeda, K. (2011). Near-field tsunami forecasting using offshore tsunami data from the 2011 off the Pacific coast of Tohoku Earthquake. *Earth, Planets and Space*, 63(7):821–826.

Turner, A. and Penn, A. (2002). Encoding natural movement as an agent-based system: an investigation into human pedestrian behaviour in the built environment. *Environment and Planning B: Planning and Design*, 29:473–490.

UNESCO (2007). Tsunami risk assessment and mitigation for the Indian Ocean: knowing your tsunami risk–and what to do about it. IOC Manual and Guides No. 52.

U.S. Census Bureau (2018). 2018 Census. Retrieved from https://www.census.gov/.

U.S. Indian Ocean Tsunami Warning System Program (US IOTWS) (2007). Tsunami Warning Center Reference Guide supported by the United States Agency for International Development and partners. Technical report, Bangkok, Thailand.

USGS (2020a). Cascadia Subduction Zone. Retrieved from https://www.usgs.gov/media/images/cascadia-subduction-zone-1.

USGS (2020b). Life of a tsunami. Available at: https://www.usgs.gov/media/images/life-a-tsunami-2. Accessed September 4, 2020.

USGS (2020c). What is it about an earthquake that causes a tsunami? Available at: https://www.usgs.gov/faqs/what-it-about-earthquake-causes-a-tsunami?qt-news_science_products=0#qt-news_science_products. Accessed September 4, 2020.

Usuzawa, H., Imamura, F., and Shuto, N. (1997). Development of the method for evacuation numerical simulation for tsunami events. In *Annual Meeting of the Tohoku Branch Technology Research Conference, Japan Society of Civil Engineers*, pages 430–431.

Vallarta Daily News (2017). Massive earthquake hits Mexico, possible tsunami. Retrieved from https://www.vallartadaily.com/mexico-possible-tsunami/.

Varas, A., Cornejo, M. D., Mainemer, D., Toledo, B., Rogan, J., Muñoz, V., and Valdivia, J. A. (2007). Cellular automaton model for evacuation process with obstacles. *Physica A: Statistical Mechanics and its Applications*, 382:631–642.

Wang, H., Mostafizi, A., Cramer, L. A., Cox, D., and Park, H. (2016). An agent-based model of a multimodal near-field tsunami evacuation: Decision-making and life safety. *Transportation Research Part C: Emerging Technologies*, 64:86–100.

Wang, W., van de Lindt, J. W., Cutler, H., Rosenheim, N., Koliou, M., Lee, J. S., and Calderon, D. (2021). Community resilience assessment of an EF-5 Tornado using the IN-CORE modeling environment. In *Life-Cycle Civil Engineering: Innovation, Theory and Practice*, pages 394–398. CRC Press.

Wang, Z. and Jia, G. (2019a). Non-parametric stochastic subset optimization for reliability-based importance ranking of bridges in transportation networks. *Applied Mathematical Modelling*, 76:348–361.

Wang, Z. and Jia, G. (2019b). Stochastic Sampling for Efficient Seismic Risk Assessment of Transportation Network. In *13th International Conference on Applications of Statistics and Probability in Civil Engineering, ICASP13*, pages 1–8, Seoul, South Korea.

Wang, Z. and Jia, G. (2020a). Augmented sample-based approach for efficient evaluation of risk sensitivity with respect to epistemic uncertainty in distribution parameters. *Reliability Engineering and System Safety*, 197:106783.

Wang, Z. and Jia, G. (2020b). Efficient sample-based approach for effective seismic risk mitigation of transportation networks. *Sustainable and Resilient Infrastructure*, 5(6):349–364.

Wang, Z. and Jia, G. (2021). Efficient tsunami evacuation risk assessment and probabilistic sensitivity analysis using augmented sample-based approach. *International Journal of Disaster Risk Reduction (Under review)*.

Weatherill, G. A., Silva, V., Crowley, H., and Bazzurro, P. (2015). Exploring the impact of spatial correlations and uncertainties for portfolio analysis in probabilistic seismic loss estimation. *Bulletin of Earthquake Engineering*, 13:957–981.

Web Marketing Associates (2010). Boston marathon race results 2010. Retrieved from http://www.marathonguide.com.

Wei, P., Song, J., Bi, S., Broggi, M., Beer, M., Lu, Z., and Yue, Z. (2019a). Non-intrusive stochastic analysis with parameterized imprecise probability models: I. Performance estimation. *Mechanical Systems and Signal Processing*, 124:349–368.

Wei, P., Song, J., Bi, S., Broggi, M., Beer, M., Lu, Z., and Yue, Z. (2019b). Non-intrusive stochastic analysis with parameterized imprecise probability models: II. Reliability and rare events analysis. *Mechanical Systems and Signal Processing*, 126:227–247.

Wijerathne, M. L. L., Melgar, L. A., Hori, M., Ichimura, T., and Tanaka, S. (2013). HPC enhanced large urban area evacuation simulations with vision based autonomously navigating multi agents. *Procedia Computer Science*, 18:1515–1524.

Wilensky, U. (2001). Modeling nature's emergent patterns with multi-agent languages. In *Proceedings of EuroLogo 2001*, pages 1–16, Linz, Austria.

Wilson, R. D. and Cales, B. (2008). Geographic Information Systems, Evacuation Planning and Execution. *Communications of the IIMA*, 8(4):13–30.

Wood, N., Jones, J., Schelling, J., and Schmidtlein, M. (2014). Tsunami vertical-evacuation planning in the U . S . Pacific Northwest as a geospatial, multi-criteria decision problem. *International Journal of Disaster Risk Reduction*, 9:68–83.

Wood, N., Jones, J., Schmidtlein, M., Schelling, J., and Frazier, T. (2016). Pedestrian flow-path modeling to support tsunami evacuation and disaster relief planning in the U.S. Pacific Northwest. *International Journal of Disaster Risk Reduction*, 18:41–55.

Wood, N. J., Jones, J., Spielman, S., and Schmidtlein, M. C. (2015). Community clusters of tsunami vulnerability in the US Pacific Northwest. *Proceedings of the National Academy of Sciences of the United States of America*, 112(17):5354–5359.

Wood, N. J. and Schmidtlein, M. C. (2013). Community variations in population exposure to near-field tsunami hazards as a function of pedestrian travel time to safety. *Natural Hazards*, 65:1603–1628.

Yazici, M. A. (2010). *Introducing uncertainty into evacuation modeling via dynamic traffic assignment with probabilistic demand and capacity constraints*. PhD thesis, The State University of New Jersey.

Yeh, H. (2010). Gender and Age Factors in Tsunami Casualties. *Natural Hazards Review*, 11(1):29–34.

Yeh, H. (2014). Tsunami hazard and casualty estimation model. In *Tenth US National Conference on Earthquake Engineering*, Anchorage, Alaska.

Yosritzal, Kemal, B. M., Purnawan, and Putra, H. (2018). An observation of the walking speed of evacuees during a simulated tsunami evacuation in Padang, Indonesia. *IOP Conference Series: Earth and Environmental Science*, 140:012090.

Yu, Y. and Song, W. (2007). Cellular automaton simulation of pedestrian counter flow considering the surrounding environment. *Physical Review E*, 75(4):046112.

Yuan, W. and Tan, K. H. (2009). Cellular automata model for simulation of effect of guiders and visibility range. *Current Applied Physics*, 9:1014–1023.

Yuan, W. and Tan, K. H. (2011). A model for simulation of crowd behaviour in the evacuation from a smoke-filled compartment. *Physica A: Statistical Mechanics and its Applications*, 390:4210–4218.

Yun, W., Lu, Z., Jiang, X., and Zhang, L. (2018). Borgonovo moment independent global sensitivity analysis by Gaussian radial basis function meta-model. *Applied Mathematical Modelling*, 54:378–392.

Zarboutis, N. and Marmaras, N. (2004). Searching efficient plans for emergency rescue through simulation: the case of a metro fire. *Cognition, Technology & Work*, 6:117–126.

Zhang, X.-Y., Trame, M. N., Lesko, L. J., and Schmidt, S. (2015). Sobol sensitivity analysis: a tool to guide the development and evaluation of systems pharmacology models. *CPT: pharmacometrics & systems pharmacology*, 4(2):69–79.

Zhao, D., Yang, L., and Li, J. (2006). Exit dynamics of occupant evacuation in an emergency. *Physica A: Statistical Mechanics and its Applications*, 363:501–511.

Zheng, X., Zhong, T., and Liu, M. (2009). Modeling crowd evacuation of a building based on seven methodological approaches. *Building and Environment*, 44:437–445.

Zsifkovits, M. and Pham, T. S. (2017). Modelling and parameterizing pedestrian behaviour in public places: a review. *International Journal of Simulation Modelling*, 16(4):630–643.

Appendix A

Stochastic sampling

In the proposed sample-based approaches, e.g., in Chapter 5, samples are required to be generated from a joint auxiliary PDF $\pi(\mathbf{x}, \boldsymbol{\theta})$ that is proportional to the integrand of the risk integral,

$$\pi(\mathbf{x}, \boldsymbol{\theta}) = \frac{h(\mathbf{x})p(\mathbf{x}|\boldsymbol{\theta})p(\boldsymbol{\theta})}{H} \propto h(\mathbf{x})p(\mathbf{x}|\boldsymbol{\theta})p(\boldsymbol{\theta}) \tag{A.1}$$

Samples from $\pi(\mathbf{x}, \boldsymbol{\theta})$ can be generated using a stochastic sampling algorithm such as the accept–reject algorithm (Robert and Casella 2004). If directly running accept-reject algorithm, it works as follows. First, some joint proposal density $q_s(\mathbf{x}, \boldsymbol{\theta})$ is selected, e.g., selected the same as the prior distributions $q_s(\mathbf{x}, \boldsymbol{\theta}) = p(\mathbf{x}|\boldsymbol{\theta})p(\boldsymbol{\theta})$ or using techniques such as adaptive kernel sampling density (AKSD) (Jia et al. 2017). Then, independent samples are generated as follows,

(1) Simulate candidate sample $[\mathbf{x}^k, \boldsymbol{\theta}^k]$ from $q_s(\mathbf{x}, \boldsymbol{\theta})$, and u^k from uniform (0,1).

(2) Accept $[\mathbf{x}^k, \boldsymbol{\theta}^k]$, if

$$\frac{h(\mathbf{x}^k)p(\mathbf{x}^k|\boldsymbol{\theta}^k)p(\boldsymbol{\theta}^k)}{M \cdot q_s(\mathbf{x}^k, \boldsymbol{\theta}^k)} > u^k; \text{where } M > \max\left[\frac{h(\mathbf{x}^k)p(\mathbf{x}^k|\boldsymbol{\theta}^k)p(\boldsymbol{\theta}^k)}{q_s(\mathbf{x}^k, \boldsymbol{\theta}^k)}\right] \tag{A.2}$$

(3) Return to (1) otherwise.

The above process is repeated until the required number of samples $\{[\mathbf{x}_\pi^k, \boldsymbol{\theta}_\pi^k], k = 1, \ldots, n_\pi\}$ are obtained. The sampling efficiency can be calculated as the number of trials required to obtain one sample but ultimately determined by the selection of proposal density $q_s(\mathbf{x}, \boldsymbol{\theta})$ (Robert and Casella 2004) and M.

The above stochastic sampling can be seamlessly integrated within the sample-based evaluation of the system risk in Eq. (4.3) as shown in Fig. A.1. More specifically, from the risk assessment, there are already N candidate samples $\{[\mathbf{x}^k, \boldsymbol{\theta}^k], k = 1, \ldots, N\}$ generated with the corresponding risk measure $h(\mathbf{x})$ calculated. Such information can be directly used in the stochastic sampling to

generate samples from $\pi(\mathbf{x}, \boldsymbol{\theta})$. In particular, for all the candidate samples, check the following condition

$$\frac{h(\mathbf{x}^k)p(\mathbf{x}^k|\boldsymbol{\theta}^k)p(\boldsymbol{\theta}^k)}{M \cdot q_s(\mathbf{x}^k, \boldsymbol{\theta}^k)} > u^k \tag{A.3}$$

If it is satisfied, then the sample $[\mathbf{x}^k, \boldsymbol{\theta}^k]$ is accepted as a sample from $\pi(\mathbf{x}, \boldsymbol{\theta})$. In the end, a total of n_π samples are generated.

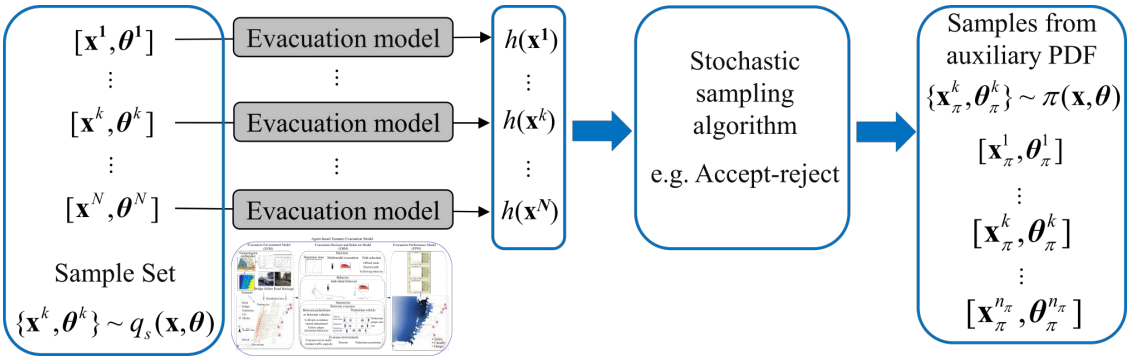


Figure A.1: Integration of stochastic sampling with risk assessment to generate samples from $\pi(\mathbf{x}, \boldsymbol{\theta})$.

Appendix B

Kernel density estimation

In the estimation of the conditional risk, Sobol' index, and relative entropy using the proposed simulation-based approaches in this research, kernel density estimation (KDE) is used to efficiently approximate the marginal auxiliary density based on the marginal samples.

B.1 Regular KDE

Based on samples, a non-parametric approximation to the underlying PDF can be obtained using KDE. This is established by centering over each of the samples, a smooth, symmetric Kernel with some chosen bandwidth, defining the spread of the Kernel (the region over each sample that the Kernel ultimately impacts). For example, consider the scalar distribution parameter θ with corresponding PDF $\pi(\theta)$, based on n_π samples $\{\theta^k\}, k = 1, \ldots, n_\pi$ from $\pi(\theta)$, the KDE approximation of $\pi(\theta)$ can be established as

$$\tilde{\pi}(\theta) = \frac{1}{n_\pi} \sum_{k=1}^{n_\pi} \frac{1}{w^{opt}} K\left(\frac{\theta - \theta^k}{w^{opt}}\right) \tag{B.1}$$

where $K(.)$ is the chosen kernel (e.g., Gaussian kernel or Epanechnikov kernel), w^{opt} is the bandwidth parameter. The regular KDE for an example $\pi(\theta)$ is illustrated in Fig. B.1, where the samples from $\pi(\theta)$ is shown in Fig. B.1(a) and the approximation established by regular KDE (i.e., KDE without boundary correction) is shown in Fig. B.1(b).

B.2 Boundary corrected KDE

The regular KDE underestimates the PDF values near the boundaries, especially when the PDF has large values near the boundaries. As can be seen in Fig. B.1, it is obvious that regular KDE significantly underestimates the PDF values near the boundaries. To address this, boundary

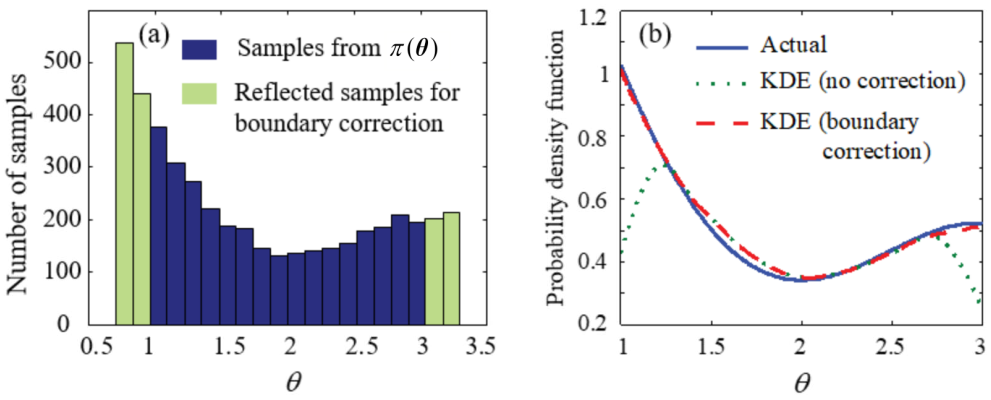


Figure B.1: Illustration of KDE and boundary corrected KDE (Jia 2014)

corrected KDE instead of regular KDE is used for a more accurate estimation of the relevant PDFs as well as the conditional risk, Sobol' index, and relative entropy.

A boundary corrected KDE based on reflection of samples is adopted (Karunamuni and Zhang 2008). However, the one in Karunamuni and Zhang (2008) is for scalar variable. To address the need of KDE for multivariate variables, the boundary corrected KDE in Karunamuni and Zhang (2008) was extended in Jia and Taflanidis (2016) to accommodate multivariate variables. The boundary corrected KDE for multivariate variables in Jia and Taflanidis (2016) is briefly described next. Consider a m-dimensional multivariate variable represented by $\boldsymbol{\theta} = [\theta_1, \ldots, \theta_i, \ldots, \theta_m]$ with corresponding joint PDF $\pi(\boldsymbol{\theta})$, based on n_π samples $\{\boldsymbol{\theta}^k\}, k = 1, \ldots, n_\pi$ from $\pi(\boldsymbol{\theta})$, the multivariate boundary corrected KDE can be established as follows. The correction is implemented for each component of the $\boldsymbol{\theta}$ vector independently, and the joint PDF for the entire vector is obtained by the product kernel rule, which is a common methodology for developing multivariate KDEs. This ultimately leads to the following KDE expression (Jia and Taflanidis 2016)

$$\tilde{\pi}(\boldsymbol{\theta}) = \frac{1}{n_\pi} \sum_{k=1}^{n_\pi} \prod_{i=1}^{m} \left\{ \frac{1}{w_i^{opt}} \left[K\left(\frac{\theta_i - \theta_i^k}{w_i^{opt}} \right) + K\left(\frac{\theta_i - \theta_i^l + g(\theta_i^k - \theta_i^l)}{w_i^{opt}} \right) + K\left(\frac{-\theta_i + \theta_i^u + g(-\theta_i^k + \theta_i^u)}{w_i^{opt}} \right) \right] \right\} \tag{B.2}$$

where $g(.)$ is a function to facilitate the reflection of samples in the boundary, θ_i^l and θ_i^u are the lower and upper bounds of θ_i, respectively. For example, in Fig. B.1(a), the samples in green correspond to the reflected samples for correction near both boundaries (i.e., regions near the lower

and upper bounds). Compared to regular KDE, the boundary corrected KDE has two additional terms. The second and third term within the brackets in Eq. (B.2) are introduced for addressing reflection to the left and right, respectively, boundary for θ_i, and can be neglected for unbounded parameters. More details about selection of $g(.)$ can be found in Karunamuni and Zhang (2008). For $K(.)$ the Epanechnikov kernel is chosen here which has been shown to provide optimal results for many applications whereas the bandwidth is chosen based on the recommendation in Jia and Taflanidis (2016), leading to

$$\begin{aligned} K(t) &= \tfrac{3}{4}(1-t^2) \quad \text{if} \quad -1 \le t \le 1 \\ &= 0 \qquad\qquad \text{else} \end{aligned} \tag{B.3}$$

$$w_i^{opt} = \left[25(\frac{3}{5})^{2-m}(2\sqrt{\pi})^m\right]^{1/(m+4)} \left[\frac{4}{(m+2)n_s}\right]^{1/(m+4)} \sigma_i \tag{B.4}$$

where σ_i corresponds to the standard deviation for the samples $\{\theta_i^k\}$ for θ_i. As can be seen from Fig. B.1(b), the boundary corrected KDE (i.e., using Eq. (B.2) with $m = 1$ for scalar variable) gives much closer approximation of the actual PDF near the boundaries while regular KDE significantly underestimates the PDFs values near the boundaries.